

ÉCOLE DOCTORALE SCIENCES ET TECHNOLOGIES
Unité de Recherche de Science du Sol (INRA)

THÈSE présentée par :
Cédric LAVEUF

Soutenance publique le : **7 avril 2009**

pour obtenir le grade de : **Docteur de l'université d'Orléans**

Discipline/ Spécialité : Science du Sol

**Les terres rares et le zinc comme
traceurs des processus pédogénétiques :
application à une séquence de sols issue
de calcaires minéralisés**

THÈSE dirigée par :

Mme Sophie CORNU

Chargée de Recherche, INRA Science du Sol, Orléans

RAPPORTEURS :

Mme Aline DIA

M. Guilhem BOURRIE

Directrice de Recherche, Géosciences, CNRS, Rennes

Directeur de Recherche, INRA Géochimie des Eaux et des Sols,
Aix-en-Provence

JURY :

M. Ary BRUAND

Professeur, ISTO, Université d'Orléans

Président du jury

Mme Aline DIA

M. Guilhem BOURRIE

Directrice de Recherche, Géosciences, CNRS, Rennes

Directeur de Recherche, INRA Géochimie des Eaux et des Sols,
Aix-en-Provence

Mme Anne-Véronique

WALTER-SIMMONNET

Mme Sophie CORNU

M. Farid JUILLLOT

Maître de Conférences, Université de Franche-Comté, Besançon

Chargée de Recherche, INRA Science du Sol, Orléans

Maître de Conférences, Université Paris 7

*La phrase la plus excitante en science,
celle annonciatrice de nouvelles découvertes,
n'est pas " Eureka ! " mais " Tiens, c'est drôle ".*

Isaac Asimov

Remerciements

Voilà sans doute les lignes qui, bien que les plus plaisantes, me sont aussi les plus difficiles à formuler. J'espère qu'elles exprimeront convenablement ma gratitude à toutes les personnes qui ont contribué, à quelque niveau que ce soit, à l'achèvement de ce travail collectif signé en mon nom. J'espère surtout n'oublier aucun de vous... Au cas où, merci à toutes et tous de m'avoir agréablement accompagné et grandement aidé au cours de ces quelques années inoubliables.

En premier lieu, je tiens à remercier la Région Centre et l'INRA pour leur soutien financier sans lequel rien n'aurait été possible, de même que Guy Richard et Paolo Vasconcelos pour leur accueil au sein de l'unité de Science du Sol de l'INRA d'Orléans et du Department of Earth Sciences of the University of Queensland.

Aux deux rapporteurs, Aline Dia et Guilhem Bourrié, qui ont accepté d'évaluer cette thèse au côté d'Anne-Véronique Walter et d'Ary Bruand : recevez toute ma reconnaissance pour votre compétence et nos échanges constructifs.

Je sais infiniment gré avant tout à Sophie Cornu et Farid Juillot : plus qu'un encadrement, et je reprendrai tes mots, Sophie, car je les estime tout-à-fait adéquats, ce fut un compagnonnage scientifique au cours duquel vous avez su former l'apprenti-chercheur que j'étais en chercheur à part entière. Merci à vous deux pour... tellement de choses... votre implication avant tout, votre disponibilité sans faille, vos conseils toujours judicieux, votre confiance envers mes capacités, votre soutien quand j'en doutais, votre recul et votre expérience quand j'en étais trop sûr... bref, pas loin de mille mercis ! Et tant que j'y suis, merci d'avance pour ce qui suivra, je n'en doute pas.

Merci également aux membres du comité de pilotage pour leurs conseils avisés lors de nos discussions annuelles, j'ai nommé Anne Probst, Philippe Négrel, Jean-Luc Potdevin, Alain Meunier et Guy Richard. Je remercie aussi tout particulièrement Denis Baize qui a su partager avec enthousiasme ses connaissances pédologiques (notamment des sols des plateformes sinémuriennes, mais pas seulement), que cela soit lors de sorties sur le terrain, lors des réunions qui ont ponctué ce travail ou encore lors de mes nombreuses visites dans son bureau...

Avant de passer au gros des troupes ayant pris part à la bataille et ayant contribué à cette victoire, je remercie tous les propriétaires et exploitants de m'avoir laissé faire des petits trous un peu partout, et particulièrement Jean-Pierre Diot pour l'accès à la parcelle de Savigny-en-Terre-Plaine.

Comment oublier cette première journée de terrain sous la neige à sonder des sols gelés en compagnie de Jean Chrétien et Dominique Meunier ? Merci à tous deux de m'avoir accompagné dans la découverte des sols de Côte d'Or, en plus des nombreuses données qu'ils ont eu l'amabilité de fournir, tout comme Alain de Cuyper et Bertrand Laroche.

Mes connaissances géologiques limitées m'ont permis de bénéficier des recommandations de Jean-Pierre Garcia et Christophe Petit, ainsi que de l'expérience d'identification des roches de Jean-Louis Dommergues et René Mouterde. Merci pour votre aide précieuse. Je remercie ici également Mathieu Rué de m'avoir initié à l'archéologie et invité à observer de magnifiques coupes et profils (promis, j'essaierai de tirer quelque chose des données !).

Un immense obrigado à "Bebeto" Luiz Roberto Guimaraes Guilherme pour son aide, ses conseils, et la bonne humeur brésilienne insufflée dans notre bureau. Le mystère des mesures de potentiel redox sur le terrain reste à élucider...

Toute ma reconnaissance à Bernard Renaux qui a toujours répondu présent pour m'accompagner sur le terrain (et au gîte...), porter mes quintaux d'échantillons jusqu'à la voiture et sonder, même si tu n'en avais pas le droit ! Merci encore pour les analyses granulométriques et pour ta mémorable démonstration d'effraction de pick-up de service par la lunette arrière (les portes qui se verrouillent toutes seules à 19 heures, c'est pas drôle...).

Merci à Philippe Berché, alias "Mouloud", maître ès pelleuse qui a lui aussi activement participé aux sorties terrain, notamment à la principale, lors de l'été 2006 qui fut si chaud. Et non, les trous pour le densimètre ne sont pas des latrines...

Je remercie aussi Catherine Pasquier pour les relevés topographiques qu'elle a réalisés, aidée de Pierre Courtemanche, et pour toutes les cartes que je lui ai demandées par la suite, parfois à la dernière minute.

Question GPS, outre Catherine, j'ai aussi régulièrement mais alternativement dérangé Sébastien Lehmann (l'empailleur de maison), Matthieu Mouclier (qu'est même pas venu à ma soutenance !) et Céline Ratier (je suis sûr que ma voix de crooner à travers le mur te manque...).

Je remercie les acupuncteurs du sol, Guillaume Giot et Pierre Courtemanche (le bricoleur qui a toujours une bonne idée pour résoudre les problèmes techniques) pour les mesures de résistivité électrique.

Pour toutes les sections polies, les lames minces, pour toutes ses explications en microscopie et pour sa participation aux sorties de terrain, un grand merci à Christian Le Lay. PS : pense juste à vérifier qui est dans les toilettes avant de crier « Sortez, haut les mains, police ! »...

Des centaines de kilos de terre... Quartages, broyages, tamisages, sédimentations, analyses DRX et ATP-ADT... sans Olivier Josière, je n'aurais pas tous ces résultats disponibles...

Et sans Michel Hardy pour m'aider à les interpréter, je ne les aurais pas exploités pleinement...

J'ai aussi ramené plein de morceaux de calcaire de Bourgogne dont Hervé Gaillard et Joëlle Davy ont eu la gentillesse de mesurer les densités après les découpes de Christian (c'est dur, hein, le sinémurien !).

Environ 1 m³ d'échantillons liquides ! Heureusement qu'Adeline Besnault et Emmanuelle Raimbault m'ont aidé à analyser ces milliers de solutions...

Mille mercis à Joël Daroussin, le maestro minutieux et consciencieux d'ArcInfo, pour tout ce travail sur la représentation 3D sous ArcGis, et surtout pour le fichier de suivi sans lequel je ne pourrais pas en faire grand-chose !

Mes remerciements aussi à Sacha Desbourdes, l'infographe qu'on prend plaisir à déranger pour tout... ou rien... juste pour l'entendre râler, puis discuter... PS : quand on parle d'un tiers à quelqu'un, toujours vérifier les liens entre eux avant...

Ne crois pas que si j'ai un problème en statistique, tu pourras y échapper, même si je ne suis plus là. Tu restes le boss, Hocine Bourenmane...

Je sais gré à Lydie Leforestier des accès au séparateur magnétique, à la microsonde et à la micro-polisseuse, les deux nôtres s'enflammant parfois spontanément les veilles de séance microsonde...

Je remercie Jérôme Rose pour les analyses par micro-fluorescence des lames calcaires. Pas évident de positionner les zones à distance...

Un ticket GLPI de remerciements aux PRI Alain Couturier, Eric Velluet, Bernard Renaux et Gérard Yart pour le bon fonctionnement de l'informatique.

Un grand merci aux filles du bocal, Monique Soler, Magalie Marolleau et Marie-Pierre Poussineau, pour leur admirable gestion de l'administratif auquel je ne comprends toujours pas grand-chose...

Du respect pour les documentalistes du centre, Karine Robineau et Franck Rogeon qui dégottent un article en deux temps trois mouvements ou qui arrivent à retrouver un M. Wang en Chine. Scotché !

Pour le temps qu'ils m'ont consacré, leurs relectures, leurs inestimables conseils lors des réunions tout au long de ces années, notamment lors des dernières répétitions de la soutenance, je suis très reconnaissant à Isabelle Cousin, Anatja Samouëlian, Dominique King et Frédéric Darboux.

Je remercie encore Odile Duval qui a su faire preuve de patience en attendant la version définitive de ce manuscrit et qui m'a grandement aidé pour la mise en forme (appelée parfois « Word of Warcraft » ou « guerre des nerfs »).

Que les vieux sages Marcel Jamagne et Michel Isambert reçoivent toute ma gratitude pour leur assistance et le partage chaleureux de leurs expériences.

Merci à Anthony Frison, jumeau de thèse, pour l'inversion des données de résistivité. Finalement, t'auras signé la biérataise avant moi. Bonne route à toi...

Bonne chance à Marie-Pierre Lefebvre, la prochaine qui devra la signer, keep cool MP3 !... et à celles et ceux qui suivent, Laurence Quénard (qui a eu le malheur de partager mon bureau sur la fin) et Marion Tétégan, ou qui ont failli mais se sont rattrapés avant (et très bien même ! Bravo à toi, Maud Seger, qui a eu encore plus de malheur en partageant mon appart').

Merci aux anciens qui ont montré la voie, Céline Collin Bellier (Mademoiselle !), Arlène Besson (encore une ex-coloc' désespérée...) et David Montagne (durs les mois de février hein ?).

Enfin, infiniment merci à mes proches qui m'ont toujours soutenu tout au long de ces années (particulièrement pour le pot de soutenance !). À mes parents qui m'ont toujours laissé suivre mon chemin, même s'il est parfois semé d'embûches et de désillusions mais aussi rempli d'espérances. À ma sœur et à mon frère qui sont restés curieux de mes travaux, malgré mes difficultés à les leur expliquer, et qui j'espère sont fiers de leur petit frère. À Céline (pardon, Madame !) qui, ayant déjà enduré l'épreuve de la thèse, a patiemment subi ma mauvaise humeur, mon stress, les réveils nocturnes, et qui a amoureuxment su me reconforter et m'épauler (mollo l'épaule, hein...).

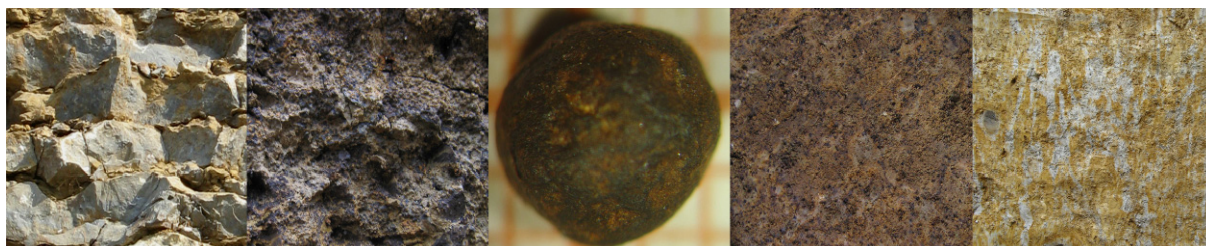
Sommaire



<i>Chapitre 1. Introduction générale</i>	7
<i>Chapitre 2. Matériels et Méthodes</i>	12
<i>Chapitre 3. Potentialité du zinc comme traceur des différents processus pédogénétiques</i>	25
<i>Chapitre 4. Potentialité des terres rares comme traceurs des différents processus pédogénétiques</i>	43
<i>Chapitre 5. Reconstruction des matériaux parentaux</i>	86
<i>Chapitre 6. Impact des processus sur la redistribution des terres rares</i>	115
<i>Chapitre 7. Conclusions générales et Perspectives</i>	157
<i>Bibliographie</i>	163
<i>Annexes</i>	194
<i>Table des matières</i>	223
<i>Liste des figures</i>	231
<i>Liste des tableaux</i>	242

Chapitre 1

Introduction générale



1.1. Enjeux scientifiques et objectifs de la thèse

La succession des processus pédogénétiques au cours du temps est à l'origine de flux de matière et d'énergie gouvernant l'organisation tridimensionnelle de la couverture pédologique (Runge, 1973 ; Huggett, 1975 ; Rasmussen et Tabor, 2007). Il est généralement admis qu'un sol est un système qui tend spontanément vers un état "d'équilibre" avec son environnement (Ruellan, 1971 ; Chesworth, 1973 ; Duchaufour et Souchier, 1977 ; Pedro, 1987).

En conséquence, tout changement dans l'environnement du sol modifie son comportement (Boulaine, 1980 ; Pedro, 1987), c'est-à-dire les processus pédogénétiques, et en conséquence les flux de matière et d'énergie qui lui sont associés.

Très tôt, les contraintes anthropiques ont été reconnues comme entraînant des modifications importantes de l'environnement du sol (Jenny, 1941 ; Bidwell et Hole, 1965 ; Yaalon et Yaron, 1966). Ces contraintes peuvent être directes, telles les pratiques agricoles ou d'aménagement du territoire, ou indirectes, tel le changement climatique (Cattle *et al.*, 1994 ; Quideau, 1996 ; Langhor, 2001 ; Richard *et al.*, 2001 ; Caravaca *et al.*, 2002 ; Lima *et al.*, 2002 ; Chantigny, 2003 ; Montagne, 2006 ; Sivakumar et Stefanski, 2007).

Néanmoins, les conséquences pédogénétiques des forçages anthropiques demeurent mal comprises et n'ont été que rarement quantifiées (Richter et Markewitz, 2001 ; Montagne, 2006). Pour cause, l'impact anthropique se surimpose à l'évolution naturelle du sol et il n'est pas aisé de faire la part entre les deux (Cornu, 2005 ; Montagne *et al.*, 2007). De plus, des travaux plus ou moins récents montrent que la pédogenèse, généralement considérée comme continue dans le temps et lente par rapport à l'échelle de temps humaine, est certainement plus réactive que ce l'on pense (Cornu *et al.*, 1995 ; Montagne, 2006 ; Cornu *et al.*, 2008) et que les sols peuvent réagir aux modifications de leur environnement par des régimes régies par des seuils ou par des événements exceptionnels (Boulaine, 1978 ; Boulaine, 1980 ; Ruellan, 1983 ; Chadwick et Chorover, 2001), si bien que l'extrapolation d'une observation actuelle à une échelle de temps supérieure à celle de l'observation peut être hasardeuse.

Il apparaît ainsi que pour comprendre et protéger la ressource non-renouvelable à l'échelle humaine qu'est le sol, il est nécessaire de connaître le fonctionnement naturel passé et actuel des sols, de façon à comprendre comment l'homme interfère avec celui-ci (Ruellan, 1971), et d'envisager de le modéliser pour prédire et quantifier son fonctionnement futur (Hoosbeek et Bryant, 1992 ; Cornu *et al.*, 2008 ; Minasny *et al.*, 2008 ; Samouelian et Cornu, 2008). V.V. Dokuchaev fût le premier à postuler que les sols sont la mémoire de leur histoire et de leur genèse. Ce postulat a ensuite été formalisé par ses successeurs selon la formule "facteurs → processus → traits" schématisant qu'un trait pédologique est la mémoire du processus pédogénétique qui l'a créé et des principales caractéristiques environnementales au cours de la pédogenèse (Rode, 1961 ; Yaalon, 1971 ; Jenny, 1994 ; Pomel, 2008). C'est sur ce constat, sans doute le plus important en pédologie (Yaalon, 1983), que s'appuient les pédologues pour retracer l'histoire d'un sol.

Ainsi, pour aider à la compréhension de l'état actuel d'un sol et à modéliser son état futur, **l'objectif de mon travail a été de tenter d'élaborer une démarche permettant de retracer et de quantifier l'évolution pédogénétique passée d'un sol.**

1.2. Démarche envisagée

La démarche pédologique classique consiste à rechercher, étudier et interpréter les caractères pédologiques témoins des processus à différents niveaux d'étude, puis à reconstruire leur chronologie, conjointement avec les facteurs de l'environnement qui ont contribué à constituer et à modifier l'état actuel d'un sol (Joffe, 1949 ; Bridges, 1972 ; Cruickshank, 1972 ; Buol *et al.*, 1973 ; Duchaufour et Souchier, 1977 ; Gavaud, 1977 ; Foth, 1991 ; Brady et Weil, 2001). La quantification des flux engendrés par ces processus s'appuie sur l'étude des éléments chimiques majeurs constituant les différentes phases minéralogiques solides, à travers l'interprétation croisée des analyses chimiques et physiques des différents traits pédologiques et de leurs stocks actuels par rapport à leurs stocks initiaux (Brimhall et Dietrich, 1987 ; Hoosbeek et Bryant, 1992 ; Minasny *et al.*, 2008). Néanmoins, les éléments majeurs sont présents dans de nombreux minéraux (Sposito, 1989). En conséquence, ils ne sont pas spécifiquement mobilisés par un processus unique, ce qui complique la déconvolution du rôle des différents processus sur la pédogenèse. Cet aspect limite souvent la quantification à une interprétation intégrée des flux.

Au cours de la pédogenèse, les éléments traces sont aussi libérés avec les éléments majeurs lors de l'altération des phases minérales primaires (Alloway, 1990). L'affinité de ces éléments traces libérés pour les différentes phases minéralogiques et organiques détermine leur devenir géochimique à long terme (McBride, 1994). En effet, ils peuvent être préférentiellement soit incorporés dans le réseau cristallin de différentes phases minérales secondaires (minéraux argileux, oxy-hydroxydes de fer et de manganèse, phosphates, etc.), soit adsorbés ou complexés à la surface des minéraux ou des matières organiques. Enfin d'autres éléments traces sont plutôt évacués par la solution du sol d'un horizon de sol vers un autre ou vers les autres compartiments de l'environnement (plante, nappe phréatique, etc.).

Les études pédologiques visent généralement à comprendre et quantifier ce comportement des éléments traces au cours des processus pédogénétiques pour répondre des problématiques environnementales (Hartemink *et al.*, 2001). Notre but ici n'est pas de répondre directement à des problématiques environnementales, mais de comprendre et quantifier la pédogenèse. Pour cela, **notre démarche consiste dans un premier temps à étudier, en complément de la démarche classique, les comportements physiques et chimiques de certains éléments traces au cours de différents processus pédogénétiques, pour, dans un second temps, inverser la démarche et utiliser les comportements physiques et chimiques spécifiques de ces éléments traces vis-à-vis de processus particuliers comme traceurs pour différencier et quantifier ces processus.**

1.3. Choix des traceurs

Les techniques actuelles rendant accessibles à l'analyse un grand nombre d'éléments chimiques présents en faibles concentrations dans les sols, le choix des traceurs est vaste. Parmi ceux disponibles, j'ai sélectionné sur la base de leur mobilité relative et de leurs comportements géochimiques vis-à-vis de certains processus de la pédogenèse, le zinc et les terres rares.

La mobilité du zinc au cours de la pédogenèse dépend beaucoup de sa spéciation initiale (Jacquat *et al.*, 2004 ; Voegelin *et al.*, 2004 ; Jacquat *et al.*, 2005 ; Voegelin *et al.*,

2005 ; Kretzschmar *et al.*, 2006). Une fois en solution, le zinc se lie – par adsorption ou précipitation – aux phyllosilicates, aux hydrotalcites zincifères, aux oxydes, aux carbonates ou à la matière organique (Garcia-Rizo *et al.*, 1999 ; Manceau *et al.*, 2000 ; Scheinost *et al.*, 2002 ; Juillot *et al.*, 2003 ; Isaure *et al.*, 2005 ; Voegelin *et al.*, 2005 ; Kretzschmar *et al.*, 2006 ; Dère *et al.*, 2007). La répartition quantitative du zinc dans ces différentes phases est liée notamment à la disponibilité des éléments majeurs lors de la précipitation de certaines de ces phases, au pH du sol, à la minéralogie et à d'autres paramètres mal identifiés (Iwasaki *et al.*, 1993 ; Chowdhury *et al.*, 1997 ; Juillot, 1998 ; Delmas-Gadras, 2000 ; Wu *et al.*, 2000 ; Buatier *et al.*, 2001 ; Catlett *et al.*, 2002 ; Jacquat *et al.*, 2004 ; Voegelin *et al.*, 2004). La présence du zinc dans des minéraux mobilisés par des processus différents peut donc se révéler intéressante pour son utilisation comme traceur des processus pédogénétique.

Les lanthanides, ou terres rares (ou en anglais REEs pour Rare Earth Elements), constituent une famille de 14 éléments qui présentent des propriétés chimiques voisines (Henderson, 1984 ; Tyler, 2004 ; Hu *et al.*, 2006). Néanmoins, certaines terres rares ou certains groupes de terres rares présentent des affinités plus spécifiques vis-à-vis de certains minéraux ou processus physico-chimiques, induisant alors des fractionnements entre elles ou eux. Cette spécificité des terres rares justifie leur étude en tant que groupe. Depuis que les techniques d'analyse des terres rares se sont développées dans les années 1980, ces éléments sont utilisés dans de nombreuses disciplines, notamment en géologie et en hydrologie, où elles servent de traceurs de genèse, d'origine, de processus géochimiques entre autres (Piper, 1974 ; Courtois et Hoffert, 1977 ; Zouita, 1986 ; Grandjean *et al.*, 1987 ; Goldstein et Jacobsen, 1988 ; Walter, 1991 ; Grandjeanlécuyer *et al.*, 1993 ; Johannesson *et al.*, 1997 ; Ding *et al.*, 1998 ; Moukadiri et Pin, 1998 ; Leleyter *et al.*, 1999 ; Tachikawa *et al.*, 1999 ; Dia *et al.*, 2000 ; Ling et Liu, 2001 ; Bentahila *et al.*, 2002 ; Picard *et al.*, 2002 ; Chen *et al.*, 2003 ; Yuan *et al.*, 2003 ; Li *et al.*, 2004 ; Nelson *et al.*, 2004 ; Yokoo *et al.*, 2004 ; Négrel *et al.*, 2006). Malgré le potentiel de traçage mis en évidence dans ces disciplines, les terres rares demeurent très peu utilisées en pédologie, alors même que leur origine dans les sols est majoritairement héritée des matériaux parentaux par rapport aux apports anthropiques (Hu *et al.*, 2006). La question se pose donc de savoir si ces éléments et notamment leurs fractionnements chimiques, peuvent être utilisés en pédogenèse comme traceurs de processus pédogénétiques.

1.4. Organisation de l'étude

Pour mettre au point une méthodologie d'étude utilisant des traceurs des processus pédogénétiques, un site modèle a été choisi. Le **chapitre 2** justifie le choix de ce site modèle et présente son contexte géologique et pédologique, ainsi que les prélèvements réalisés et les expérimentations mises en place.

Le **chapitre 3** consiste en une étude détaillant le comportement du zinc au cours de la pédogenèse, permettant d'identifier les processus pédogénétiques que cet élément pourrait permettre de tracer dans le contexte pédo-géologique du site étudié.

Le **chapitre 4** expose en deux parties la potentialité des terres rares comme traceurs des processus pédogénétiques. La première partie de ce chapitre est consacrée à une étude bibliographique sur le potentiel de l'utilisation des fractionnements en terres rares pour tracer les processus pédogénétiques. Dans une deuxième partie, une méthodologie innovante d'utilisation des terres rares comme traceurs des processus pédogénétiques est proposée.

D'abord mise au point sur le même site que pour le zinc, cette méthodologie a ensuite été validée et améliorée sur un second site.

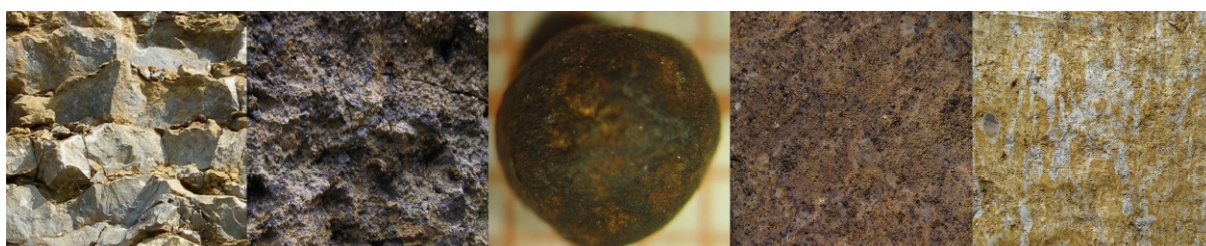
La quantification des flux passés d'éléments exigeant la connaissance de leurs stocks initiaux, le **chapitre 5** propose une méthodologie pour reconstituer les matériaux parentaux altérés. Cette première étape est cruciale pour pouvoir ensuite calculer des bilans de masse dans un contexte de matériau parental hétérogène.

Sur ces bases, j'étudie ensuite dans le **chapitre 6** l'impact des différents processus qui interviennent successivement dans ce contexte pédologique sur la mobilisation des terres rares. J'aborderai ainsi dans un premier temps le processus pédogénétique de décarbonatation afin d'estimer le devenir des terres rares une fois en solution dans le système sol. Dans un second temps, j'utiliserai les terres rares pour tracer les cycles de précipitation/dissolution des oxydes ferro-manganiques au cours de la pédogenèse.

Enfin, une conclusion générale en **chapitre 7** présente un bilan des résultats obtenus et ouvre des perspectives.

Chapitre 2

Matériels et Méthodes



De façon à étudier le potentiel du zinc et des terres rares comme traceurs des processus pédogénétiques, j’ai choisi de me positionner dans un cas d’école, soit un site présentant les caractéristiques suivantes :

- (i) des concentrations en zinc et en terres rares dans les sols élevées, pour ne pas être confronté à des difficultés analytiques ;
- (ii) des sols présentant une pédogénèse bien différenciée, afin que les fractionnements en zinc et en terres rares soient prononcés, c’est-à-dire, dans un contexte de climat tempéré, des sols âgés ;
- (iii) des sols ayant subi une succession de processus pédogénétiques de natures différentes, afin d’avoir accès au plus grand nombre de processus pédogénétiques possibles.

Les sols développés dans la formation calcaire d’âge sinémurien *sensu largo (s.l.)* sur les bordures Nord et Est du Massif du Morvan remplissent ces conditions et ont donc été choisis (Figure 1). Ces sols couvrent environ 8 100 hectares dans l’Yonne et 29 000 hectares en Côte d’Or (Baize et Chrétien, 1994). Deux sites ont été étudiés : l’un à Pouilly-en-Auxois (Côte d’Or), à la limite Sud de la dépression liasique de l’Auxois-Nord, et l’autre à Savigny-en-Terre-Plaine (Yonne), au cœur de la dépression liasique de la Terre-Plaine, soit

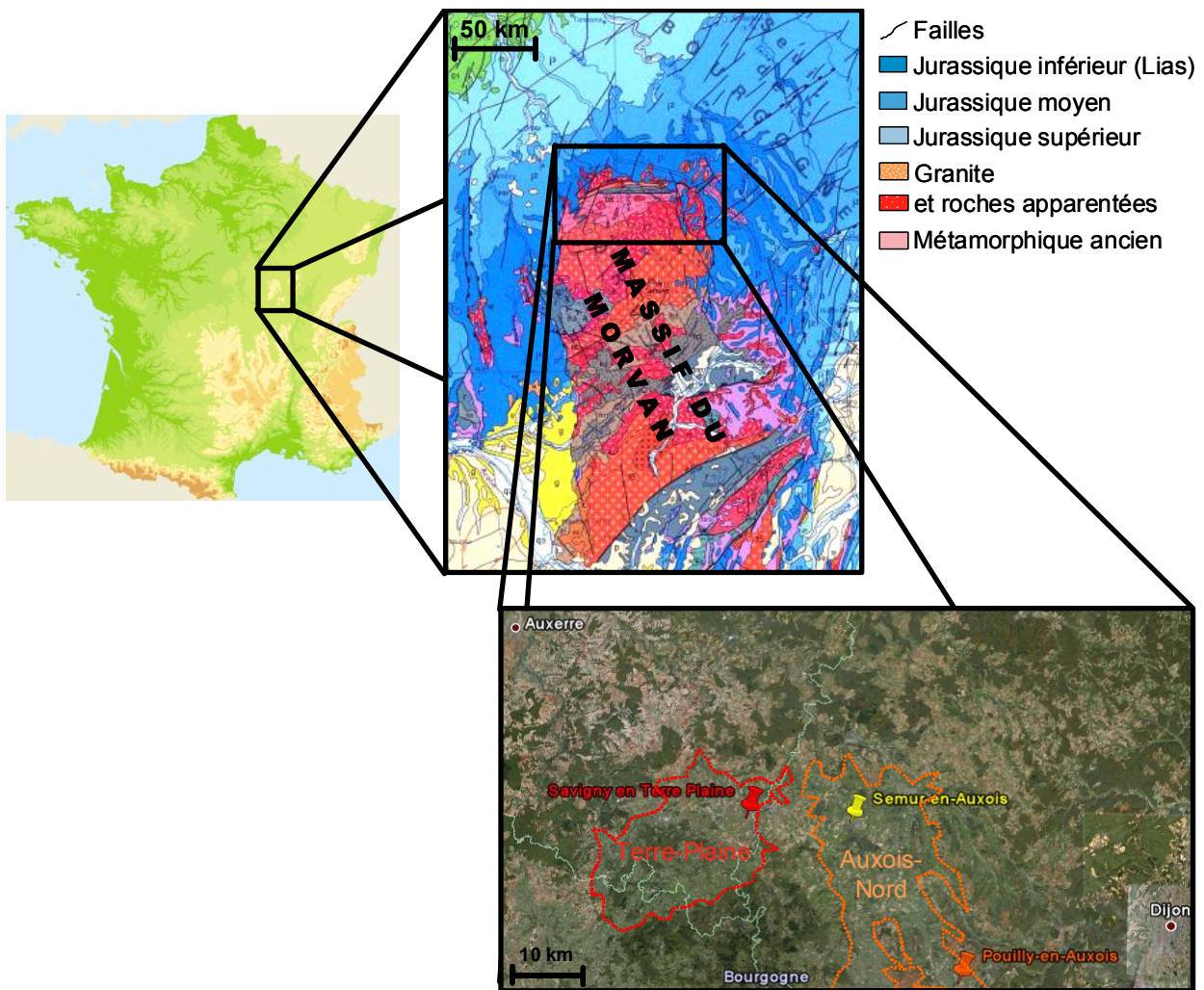


Figure 1. Localisation des deux sites d’études en Bourgogne sur le pourtour liasique du Massif granitique du Morvan – Savigny-en-Terre-Plaine (Yonne) et Pouilly-en-Auxois (Côte d’Or) – ainsi que de Semur-en-Auxois, ville du stratotype de la formation d’âge sinémurien.

respectivement à l'Est et au Nord du Massif du Morvan (Figure 1).

Je présenterai tout d'abord successivement le contexte géologique et le contexte pédologique. Les différences entre les solums échantillonnés sont ensuite décrites (descriptions pédologiques complètes disponibles en Annexe 1), ainsi que le régime hydrique particulier de ces sols – puis les prélèvements et les analyses réalisés.

2.1. Genèse de la formation calcaire d'âge sinémurien et principales caractéristiques

Le pourtour du socle granitique du Massif du Morvan a été recouvert de dépôts sédimentaires, principalement au cours du Lias ($-199,6 \pm 0,6$ à $-175,6 \pm 2,0$ millions d'années ; Figure 1). Le pendage moyen des couches liasiques est de 2 % dans une direction moyenne située vers le centre du Bassin sédimentaire de Paris, c'est-à-dire entre le Nord-Nord-Ouest et le Nord-Ouest (Mégny, 1960).

Les nombreuses failles qui hachent cette région (Figure 1) ont permis la remontée de fluides hydrothermaux chargés en divers éléments (Collenot, 1876-1877 ; Mégny, 1960 ; Renaud, 1961 ; Couchot *et al.*, 1963 ; Scolari, 1964 ; BRGM, 1967, 1968 ; Clair, 1987 ; Forest-Bize, 2000 ; Sizaret, 2002). Cet hydrothermalisme, débuté dès le Keuper ($-228,0 \pm 2,0$ à $-199,6 \pm 0,6$ millions d'années), s'est poursuivi jusqu'au Sinémurien ($-196,5 \pm 1,0$ à $-189,6 \pm 1,5$ millions d'années), dernier sous-étage dont les strates ont ainsi été métamorphosées en différents lieux (Collenot, 1873, 1878-1879). Lors des périodes interglaciaires qui débutent dès la fin du Pliocène ($-5,332 \pm 0,005$ à $-1,806 \pm 0,005$ millions d'années), les retraits des glaciers du Morvan ont progressivement et successivement érodé les dépôts marneux tendres postérieurs au Sinémurien (Carixien, Domérien...). Plus résistante à l'érosion, en raison de sa compacité, de sa dureté (Mégny, 1960 ; Clair, 1987) et de sa silicification métamorphique hydrothermale (Collenot, 1873) qui la lie fortement dépôts sous-jacents, la formation calcaire d'âge sinémurien *s.l.* a ainsi été mise à nu.

Le stratotype de la formation calcaire d'âge sinémurien *s.l.* a été décrit par Alcide Dessalines d'Orbigny (vers 1849-1850) à Semur-en-Auxois en Côte d'Or (Figure 1). Cette formation se compose d'une alternance de bancs calcaires à surface ondulée de faible puissance (quelques centimètres à 80 cm), irrégulièrement séparés par de minces interlits marneux (quelques millimètres à quelques centimètres ; Figure 2). Calcaire et



Figure 2. Coupe du calcaire d'âge sinémurien (Vic de Chassenay, Yonne), mettant en évidence l'alternance des bancs calcaires gris-bleutés et des interlits marneux ocres.

marnes sont d'origines détritiques (Collenot, 1873, 1878-1879 ; Mousterde, 1952 ; Le Calvez et Lefavrais-Raymond, 1961 ; Clair, 1987).

Les bancs calcaires sont cristallins, compacts, durs, gris-bleutés plus ou moins foncés, avec des taches ferrugines, et bioclastiques très riches en gryphées, d'où sa dénomination de "calcaire à gryphées" (Figure 3 ; Collenot, 1873, 1878-1879 ; Mousterde, 1952 ; Le Calvez et Lefavrais-Raymond, 1961 ; Clair, 1987). L'uniformité minéralogique des bancs calcaires d'âge sinémurien *s.l.* permet de reconnaître cet étage (Collenot, 1873). Elle se caractérise par des teneurs élevées en carbonates, par une association kaolinite/illite (Mangin *et al.*, 1961), et par une minéralisation phosphatée. D'après Forest-Bize (2000), cette minéralisation phosphatée est caractérisée par la présence de fluorapatite comme forme minérale dominante.

La partie supérieure de la formation calcaire d'âge sinémurien *s.l.* (que je nommerai par la suite strates lotharingiennes, en référence à l'ancienne appellation "Lotharingien" de cette partie du sous-étage Sinémurien) est moins cristalline et comporte plus de nodules phosphatés et de fossiles que la partie inférieure datant du Sinémurien *sensu stricto* (Collenot, 1873, 1878-1879 ; Mousterde, 1952 ; Mégrien, 1960 ; Clair, 1987 ; Forest, 1995 ; Forest-Bize, 2000). Le passage aux strates lotharingiennes se reconnaît lorsque *Gryphæa arcuata* cède la place à *Gryphæa obliqua*, puis à *Gryphæa cymbium* (Figure 3 ; Mousterde, 1952 ; Guérin *et al.*, 1961). Sur la bordure orientale, le passage aux strates lotharingiennes est marqué par un niveau super-condensé riche en nodules phosphatés (Mousterde, 1952). Ces nodules de 1 à 2 cm de diamètre, blancs-jaunâtres et tendres (Figure 4), représentent la forme la plus commune de la minéralisation phosphatée dans les séries condensées du



Figure 3. A droite, gryphées arquées (*Gryphæa arcuata*) affleurant à la surface d'un banc du calcaire d'âge sinémurien, dit calcaire à gryphées. A gauche, de bas en haut, coupe d'une gryphée arquée enchâssée dans le calcaire, photos de gryphées arquée et cymbium (présente dans la partie supérieure de la formation calcaire d'âge sinémurien) mettant en évidence leurs différences morphologiques.

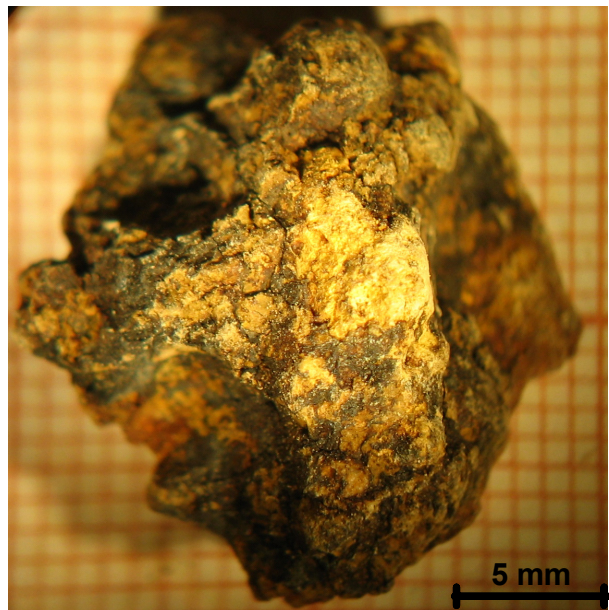


Figure 4. Photographie d'un nodule phosphaté isolé de sa matrice.

Lias (Forest, 1995 ; Forest-Bize, 2000). La présence de ce niveau super-condensé tend à disparaître vers l'Ouest et avec l'éloignement au Massif du Morvan (Mouterde, 1952 ; Forest-Bize, 2000). Par ailleurs, plus on va vers l'Est, plus les strates lotharingiennes sont détritiques, marneuses, rouille, fines et irrégulières (Collenot, 1873, 1878-1879 ; Mouterde, 1952).

La puissance de la formation calcaire d'âge sinémurien *s.l.* varie selon sa localisation. A proximité immédiate du Massif du Morvan, du fait de la nature côtière de ces sédiments (Collenot, 1873), elle est peu épaisse, variant de 4 mètres à plus de 11 mètres (Collenot, 1873, 1878-1879 ; Mouterde, 1952 ; Le Calvez et Lefavrais-Raymond, 1961 ; Clair, 1987). Dans l'Auxois, la formation calcaire d'âge sinémurien *s.l.* présente une puissance totale de 8 à 11 mètres et contient le niveau super-condensé à nodules phosphatés caractéristique de la base des strates lotharingiennes. Dans la Terre-Plaine, la formation calcaire d'âge sinémurien *s.l.* a une puissance totale de 6 à 10 mètres (Mouterde, 1946, 1952). Cette région a subi une érosion plus intense que l'Auxois, ce qui a permis la mise à nu de la formation calcaire d'âge sinémurien *s.l.* sur des étendues continues plus vastes (BRGM, 1968).

La puissance des strates lotharingiennes augmente globalement vers l'Est. Totalement absentes par endroits, ces strates peuvent atteindre environ 4 mètres (Collenot, 1873, 1878-1879 ; Mouterde, 1946, 1952 ; Le Calvez et Lefavrais-Raymond, 1961 ; Clair, 1987 ; Forest, 1995 ; Forest-Bize, 2000). Dans l'Auxois, elles ont une puissance de 3 à 4 mètres (Collenot, 1873, 1878-1879 ; Cayeux, 1939 ; Clair, 1987 ; Forest, 1995 ; Forest-Bize, 2000). La formation calcaire d'âge sinémurien *s.l.* est souvent surmontée par les marnes datant du Carixien, voire du Domérien (BRGM, 1967 ; Clair, 1987). Dans la Terre-Plaine, du fait de l'érosion, les strates lotharingiennes ne dépassent pas, quand elles sont présentes, une puissance de 1 mètre environ (Cayeux, 1939 ; Mouterde, 1946, 1952 ; Forest, 1995 ; Forest-Bize, 2000) ; le plus souvent elles sont absentes (Mégny, 1960). Elles contiennent rarement le niveau à nodules phosphatés (Cayeux, 1939 ; Mouterde, 1946, 1952 ; Forest, 1995 ; Forest-Bize, 2000).

2.2. Contexte pédologique

Les couvertures pédologiques sont issues de l'altération autochtone de la formation calcaire d'âge sinémurien *s.l.* dans la Terre-Plaine, et peut-être également de l'altération des marnes datant du Carixien, voire du Domérien dans l'Auxois (Baize et Chrétien, 1994 ; Drouin, 2003 ; Laveuf *et al.*, 2008, cf. Chapitre 4.2.1.).

Ces couvertures pédologiques s'organisent schématiquement selon une toposéquence d'érosion (Figure 5 ; Baize, 1993 ; Baize et Chrétien, 1994 ; Chrétien, 1995).

En haut de pente, les sols complets (non tronqués) présentent des horizons supérieurs LE ou A, et E, limono-argileux de teintes claires, puis des horizons Bgd dégradés avec des marques d'hydromorphie (AFES, 1995 ; Figure 5).

En milieu de pente, les sols marron se caractérisent par l'absence des horizons limono-argileux, totalement érodés, avec pour conséquence la mise en surface de l'horizon B (AFES, 1995), qui n'est pas dégradé (Figure 5). En bas de pente, les Terres Noires, fortement érodées, sont des sols superficiels de moins de 50 cm d'épaisseur, très argileux, se limitant à l'horizon dit à bouillie noire (BN), voire à l'horizon B concrétionné (noté Bc) sus-jacent (Figure 5 ; Baize, 1993 ; Baize et Chrétien, 1994 ; Chrétien, 1995).

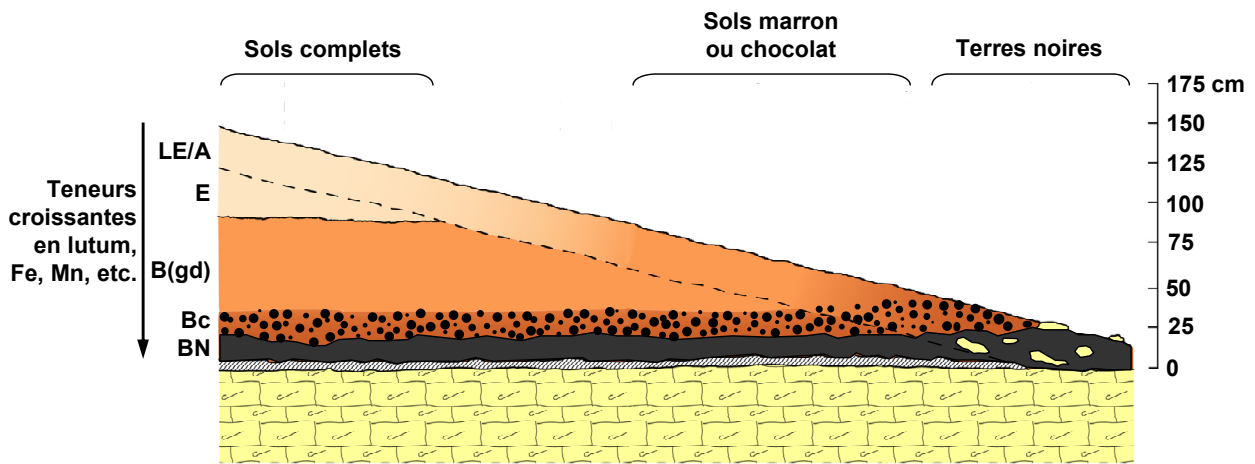


Figure 5. Toposéquence de sols d'érosion sur les plateaux calcaires sinémuriens d'après Baize et Chrétien (1994).

Les sols de cette toposéquence se caractérisent par leur abondance en fer et en manganèse, du fait de la minéralisation de la formation calcaire (Baize et Chrétien, 1994). Ces éléments se rencontrent sous forme de :

- (i) « plombs de chasse », petits nodules ferro-manganiques subsphériques de couleur gris-foncée à noire, de 50 μm à 5 mm de diamètre (Figure 6), formés par précipitation du fer et du manganèse dans un matériau argileux à faible drainage interne ; ces nodules Fe-Mn se trouvent en forte densité dans l'horizon Bc (horizon B concrétionné ; Figure 5) et sont également présents dans tous les horizons sus-jacents ;
- (ii) fins enduits et revêtements noirs très abondants sur les faces des agrégats de la plupart des horizons, notamment des horizons Bc et Bgd ;
- (iii) « bouillie noire » (BN), horizon argileux, plastique, onctueux, avec des accumulations ferro-manganiques noires diffuses, qui ne contient généralement pas de "plombs de chasse". Cet horizon se caractérise par une forte humidité permanente, due au contact direct avec le calcaire d'âge sinémurien *s.l.* relativement imperméable (Figure 5). Cet horizon est parfois épais de quelques centimètres seulement – et semble assez uniformément noir – mais il est plus fréquemment épais de un à quelques décimètres – et alors hétérogène, juxtaposant aux accumulations ferro-manganiques noires des passées jaunegrisâtres.

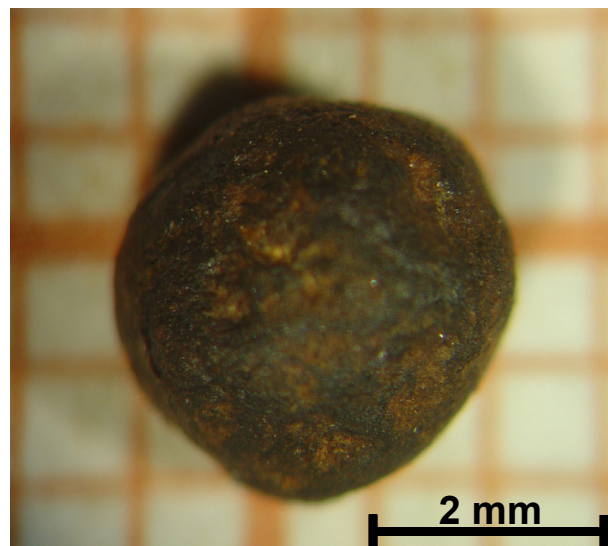


Figure 6. Photographie d'un nodule ferro-manganique prélevé dans l'horizon Bc d'un solum complet (Pouilly-en-Auxois, Côte d'Or).

Ces solums présentent aussi des teneurs élevées en argiles, composées d'illite et kaolinite héritées de la formation calcaire d'âge sinémurien *s.l.*, mais également de minéraux argileux gonflants riches en vermiculite et en smectite (Baize et Chrétien, 1994 ; Chrétien, 1995).

Ces sols se sont formés sous l'action des processus successifs suivants : décarbonatation de la formation calcaire d'âge sinémurien *s.l.*, processus redox primaires (formation des nodules ferro-manganiques), processus redox secondaires (dégradation morphologique), lessivage et en parallèle, évolution minéralogique des argiles (Baize et Chrétien, 1994 ; Chrétien, 1995 ; Laveuf *et al.*, 2008, cf. Chapitre 4.2.1.). Seuls les sols complets ont subi l'ensemble des processus, les sols marron et les Terres Noires n'ayant pas subi de redox secondaires (absence de dégradation) ou de lessivage aussi intense que dans les sols complets (Baize et Chrétien, 1994).

2.3. Description des solums échantillonnés

Un profil complet sous forêt a été échantillonné dans l'Auxois, ainsi que les trois types de sols le long d'une toposéquence d'érosion sous culture dans la Terre-Plaine. Les trois fosses échantillonnées en Terre-Plaine sont positionnées le long d'un transect et notées FSC pour Fosse Sol Complet, FSM pour Fosse Sol Marron et FTN pour Fosse Terre Noire (Figure 7).

Le positionnement de ces trois fosses a été décidé après l'analyse structurale de la toposéquence, permettant de déterminer les limites des trois types de sol et leurs solums les plus représentatifs (Figure 7).

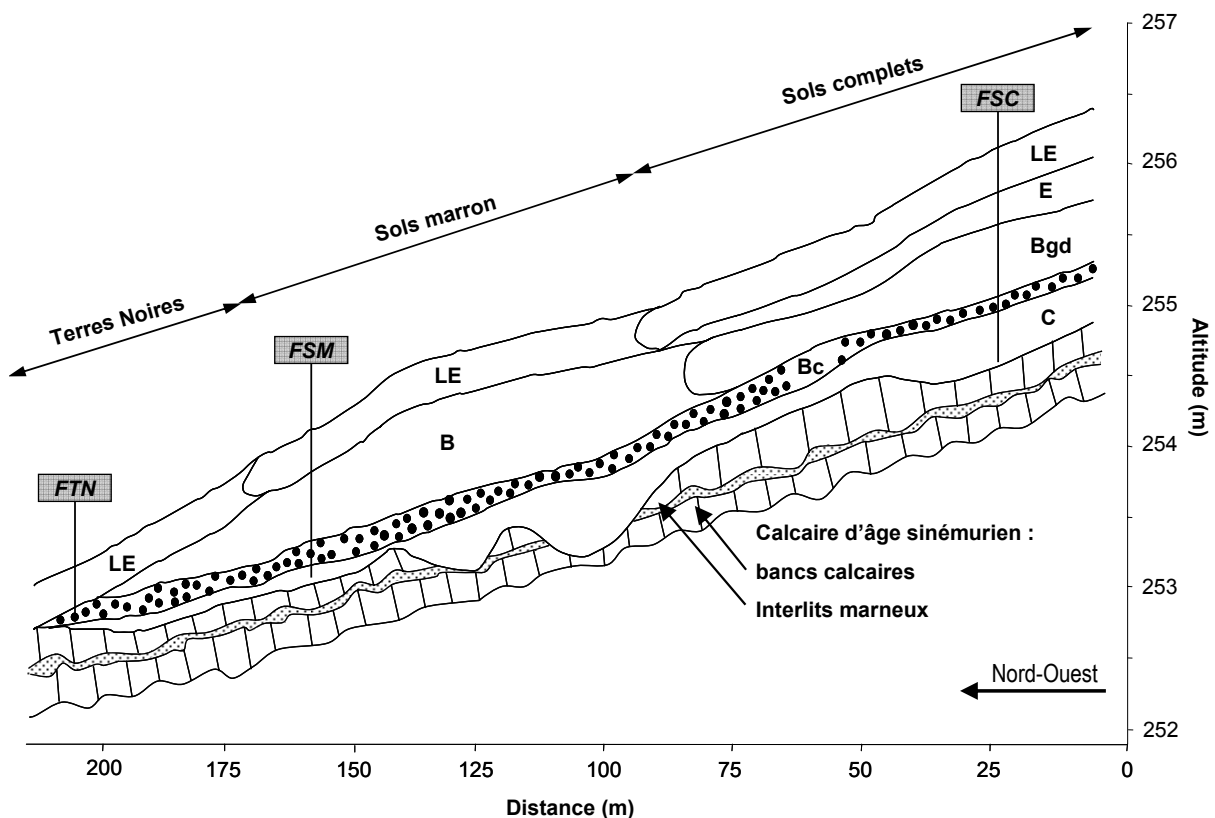


Figure 7. Succession d'horizons dans la toposéquence de Savigny-en-Terre-Plaine (Yonne) avec la localisation des trois fosses les plus représentatives des trois types de sols le long de la pente.

Seuls les sols complets ont été étudiés dans la mesure où ils présentent la succession de processus pédogénétiques la plus complète. Ainsi seules les principales caractéristiques différenciant les profils des sols complets sont présentées ici. Les descriptions pédologiques détaillées de tous les sols échantillonnés sont présentées en [Annexe 1](#).

Les sols complets des sites de l'Auxois et de la Terre-Plaine présentent les mêmes principaux horizons de référence (LE, E, Bgd, Bc et C). Cependant, ces solums diffèrent par les aspects suivants :

- (i) l'horizon de référence de surface, A ou LE, du fait de différents modes d'occupation ([Figure 8](#)) ;
- (ii) leur épaisseur : le solum de l'Auxois est plus profond que celui de la Terre-Plaine, 175 cm contre 140 cm, respectivement ([Figure 8](#)). Cela implique qu'une plus grande épaisseur de matériaux parentaux a été nécessaire pour former le solum de Pouilly-en-Auxois ;
- (iii) la présence d'un horizon à nodules de phosphates dans l'Auxois ([Figure 8](#)), lié à l'incorporation du banc de nodules phosphatés de la base des strates lotharingiennes dans la formation de ce solum plus épais ;
- (iv) l'épaisseur de leur horizon Bc, plus épais dans l'Auxois qu'en Terre-Plaine ([Figure 8](#)).

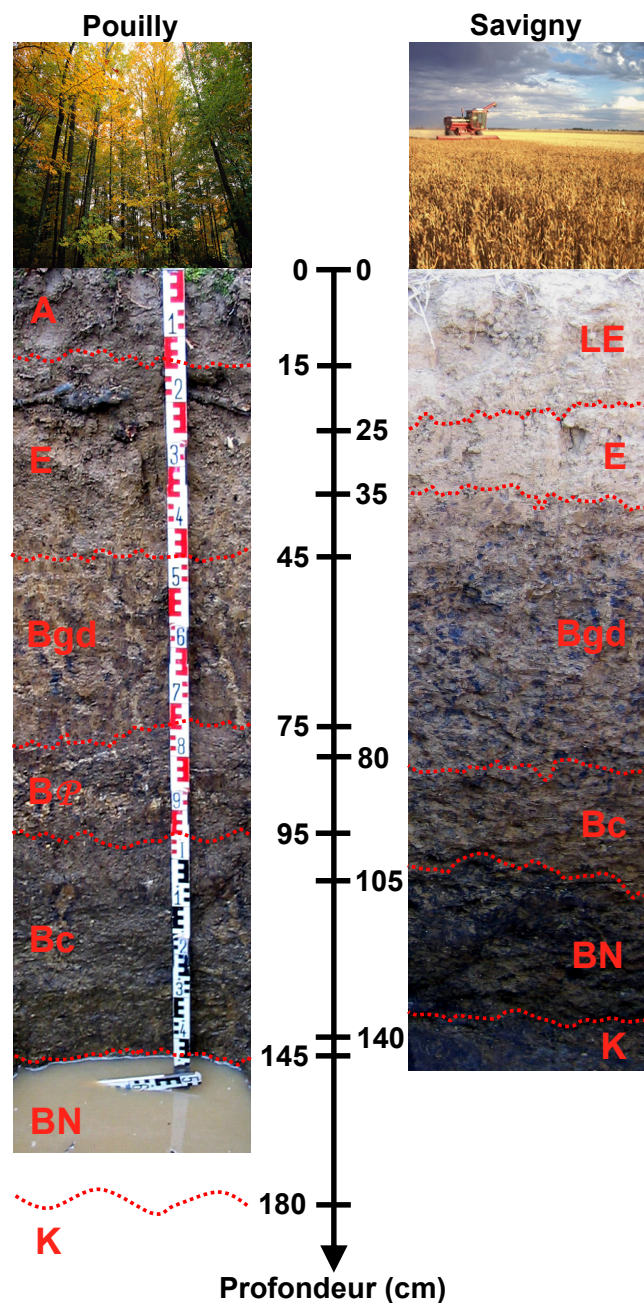


Figure 8. Profil des sols complets de Pouilly-en-Auxois (gauche) et de Savigny-en-Terre-Plaine (droite).

2.4. Régime hydrique de la toposéquence de la Terre-Plaine

Les petites régions pédologiques naturelles de la Terre-Plaine et de l'Auxois constituent des dépressions humides à cause de (i) l'imperméabilité des plates-formes structurales que sont les calcaires d'âge sinémurien (Collenot, 1873 ; Mégnién, 1960) et (ii) de la pluviométrie annuelle importante du Haut-Morvan (1 600 à 2 000 mm/an suivant les sommets ; Breton et Rouveroux, 1972). On observe ainsi un chevelu hydrographique dense dans ces régions (Mégnién, 1960). La fissuration du calcaire d'âge sinémurien par endroits permet toutefois à l'eau de percoler comme le met en évidence la présence de niveaux de source au contact des niveaux calcaréo-marneux datant de l'Hettangien ($-199,6 \pm 0,6$ à $-196,5 \pm 1$ millions d'années ; Mégnién, 1960 ; BRGM, 1967). Des études montrent que le débit des cours d'eau n'a cessé de baisser depuis le début du Moustérien (vers -300 000 années ; Mégnién, 1960), montrant que ces régions étaient auparavant soumises à de plus forts événements hydriques qu'actuellement.

Pour comprendre le régime hydrique des toposéquences développées sur la formation calcaire d'âge sinémurien découlant de ce contexte hydrique global, j'ai suivi le niveau de la nappe perchée sur le site de Savigny-en-Terre-Plaine lors de périodes hydriques contrastées. Les niveaux ont ainsi été relevés en avril 2006, juillet 2006, novembre 2006 et février 2007, dates correspondant respectivement à la période de début de ressuyage des sols, à la période la plus sèche, aux premiers événements pluvieux importants répétés suivant l'été, et à une période de fort engorgement des sols (Figure 9).

En juillet 2006, l'ensemble de sols était ressuyé avec une humidité résiduelle en fond de fosse dans les sols complets plus profonds (Figure 9). De nombreuses fentes de retrait, larges et profondes, s'étaient formées.

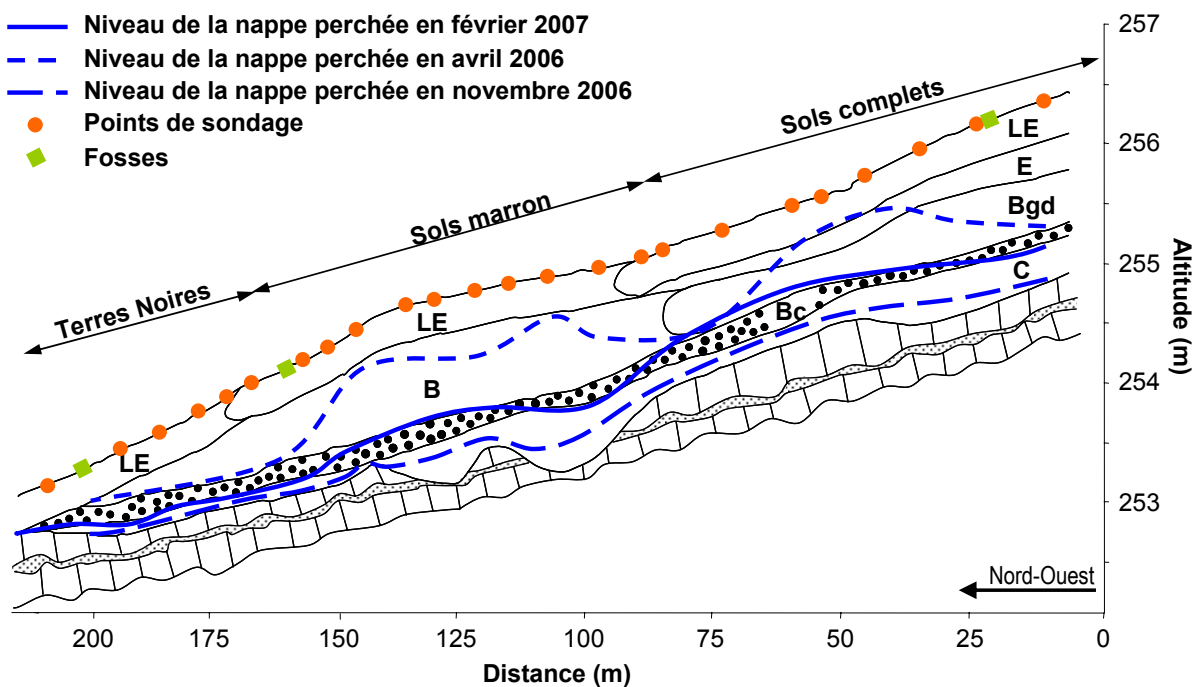


Figure 9. Niveaux de la nappe perchée le long de la toposéquence de Savigny-en-Terre-Plaine (89) en avril 2006, novembre 2006 et février 2007 avec les points de sondage et l'emplacement des fosses. La nappe étant absente en juillet 2006, elle n'est pas mentionnée dans la figure.

Le relevé du niveau de la nappe en novembre 2006 a suivi la première succession importante d'événements pluvieux de l'automne ([Annexe 2](#)). Une nappe au contact du calcaire d'âge sinémurien était présente tout au long de la toposéquence, alors que les horizons de surface restaient secs ([Figure 9](#)). Ceci était probablement lié à la présence des fentes de retrait qui permet un transfert rapide de l'eau vers l'horizon C à bouillie noire. D'après les relevés de février 2007 et avril 2006, cette nappe perchée serait présente dans l'horizon C à bouillie noire tout au long de l'hiver et ne disparaîtrait qu'à la fin du printemps ([Figure 9](#)). Ainsi, l'horizon C à bouillie noire est le siège d'une hydromorphie constante de l'automne à l'été et reste même humide au cours de l'été, induisant vraisemblablement des conditions réductrices prolongées. Dans les Terres Noires, la nappe perchée n'est apparue qu'à partir de février d'après nos relevés ([Figure 9](#)), le ressuyage y est rapide, et les battements de nappe plus limités qu'en amont, si bien que l'horizon C à bouillie noire y est moins développé.

Les relevés de novembre 2006 et avril 2006 ont montré que durant cette période, l'horizon Bc est gorgé d'eau ([Figure 9](#)). Sur l'année hydrologique, l'horizon Bc est ainsi le siège d'un battement de nappe à l'origine de l'alternance de conditions réductrices et oxydantes, conditions connues pour être favorables à la formation de nodules Fe-Mn ([McKenzie, 1989](#) ; [Khan et Fenton, 1994](#) ; [Zhang et Karathanasis, 1997](#)). Cela laisserait supposer que les nodules Fe-Mn sont toujours en formation.

En plein hiver, une seconde nappe, perchée, est présente dans l'horizon Bgd et les sols sont engorgés dès la surface ([Figure 9](#)). Cette nappe perchée est sans doute responsable des phénomènes de dégradation observés dans les horizons supérieurs des profils complets.

2.5. Echantillonnage

Des fosses ont été creusées au niveau du sol complet de Pouilly-en-Auxois et des trois types de sol de la toposéquence de Savigny-en-Terre-Plaine ([Figure 7](#)). Les prélèvements présentés dans le [Tableau 1](#) ont été réalisés pour chacune des quatre fosses.

Tableau 1. Echantillonnage des sols et des matériaux parentaux des différents solums sur les sites de l’Auxois et de la Terre-Plaine.

	Pouilly-en-Auxois (Côte d’Or)	Savigny-en-Terre-Plaine (Yonne)
Solums échantillonnés	Sol complet	Sol complet (FSC) Sol marron (FSM) Terre Noire (FTN)
Echantillons de sols	Vrac tous les ~10 cm tout en respectant les horizons Blocs de sol non perturbés pour la confection de lames minces (Kubienna, 1938)	
Densité apparente des sols	Prélèvements par cylindre dans les différents horizons en triplicata	
Echantillons de matériaux parentaux	Une strate calcaire d’âge sinémurien sous-jacente Une strate calcaire d’âge lotharingien et trois strates calcaires d’âge sinémurien dans une tranchée 200 m au Sud	Une strate calcaire d’âge sinémurien sous-jacente dans FSC (C1) Deux strates calcaires d’âge sinémurien sous-jacentes dans FSM (C2 et C3) Deux strates calcaires d’âge sinémurien (C4 et C5) et un interlit marneux sous-jacents dans FTN
Densité apparente des matériaux parentaux	-	Prélèvement puis mesure par densitomètre à membrane dans le lit marneux

2.6. Analyses

Pour comprendre les processus pédogénétiques et leur impact sur la mobilisation des éléments majeurs et des traceurs (zinc et terres rares), l’évolution des phases minérales et de la localisation (spéciation au sens large) des éléments majeurs et des traceurs associés à ces phases a été étudiée des matériaux parentaux aux horizons de surface. Les matériaux pédologiques et géologiques ainsi considérés sont :

- (i) les matériaux parentaux (bancs calcaires et interlits marneux), leurs résidus de décarbonatation, mais aussi la fraction totale de l’horizon C ;
- (ii) les nodules Fe-Mn ;
- (iii) les fractions granulométriques 0-2 μm ; 2-5 μm , 5-10 μm et 10-50 μm ou la fraction <50 μm selon les horizons.

Sur ces matériaux, les différentes analyses reportées sur la [Figure 10](#) ont été réalisées.

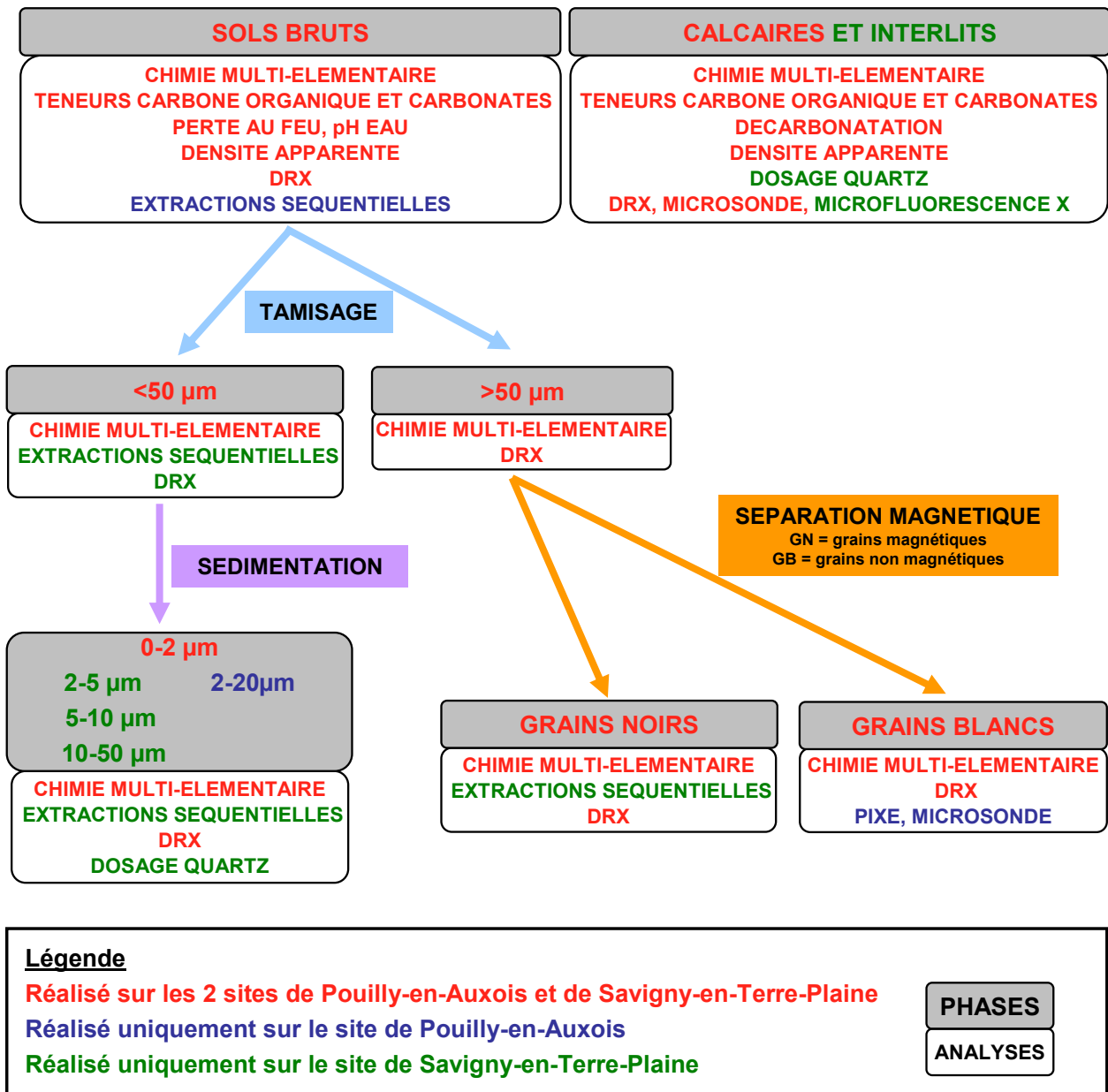


Figure 10. Démarche d’analyse minéralogique et chimique des échantillons de sols sur les deux sites d’étude de Pouilly-en-Auxois et de Savigny-en-Terre-Plaine.

La démarche analytique choisie couple des fractionnements physiques (tamisage, sédimentation, séparation magnétique) avec des fractionnements chimiques (extractions séquentielles, décarbonatation). Les différentes fractions obtenues ont été analysées minéralogiquement (diffraction des rayons X, analyses thermo-pondérales et analyses thermo-différentielles) et chimiquement (analyses multi-élémentaires). La spéciation des traceurs dans les matériaux parentaux a été déterminée par microscopie optique et microscopie électronique à balayage couplée à des micro-analyses par EDS (Energy Dispersive X-ray Spectroscopy) et par des analyses par microsonde, par PIXE (Proton-Induced X-ray Emission) et par microfluorescence X.

Afin de réaliser des bilans de masse, les densités apparentes ont été mesurées après séchage à 105°C par la méthode des cylindres pour les horizons de sol et au densitomètre à

membrane pour les lits marneux. Les densités apparentes des différents échantillons calcaires ont été mesurées par déplacement de volume au pétrole sur au moins trois blocs d'un même échantillon.

Des protocoles d'extractions séquentielles différents ont été utilisés pour les différentes fractions étudiées et pour les deux sites ([Tableau 2](#)).

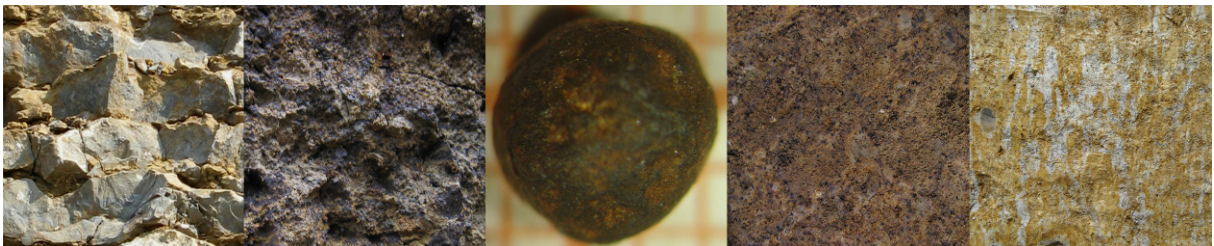
Tableau 2. Schéma d'extraction séquentielle des différentes fractions de sol des sites de l'Auxois et de la Terre-Plaine.

Site	Pouilly-en-Auxois (Côte d'Or)		Savigny-en-Terre-Plaine (Yonne)		
	Solum(s)	Sol complet	Sol complet Sol marron Terre Noire	Sol complet	Sol complet Sol marron Terre Noire
Horizons	LE, E, Bgd, C	B \mathcal{P} , Bc	Tous les horizons	LE, Bc, C	Bc
Fractions	brutes	<50 μm	<50 μm	0-2 μm 2-5 μm 5-10 μm 10-50 μm	Grains noirs (nodules Fe-Mn)
Extraction des éléments...					
échangeables	X	X			
adsorbés et/ou liés aux carbonates	X	X	X	X	
liés aux oxydes de manganèse	X	X	X	X	X
liés à la matière organique labile	X	X	X	X	
liés aux oxydes de fer amorphes	X	X	X	X	X
liés aux oxydes de fer cristallisés	X	X	X	X	X
liés à la matière organique résistante et aux sulfures	X	X			
liés aux silicates	X	X	X	X	X

En effet, les extractions réalisées sur les échantillons du site de l'Auxois montraient que les éléments échangeables et liés à la matière organique résistante et aux sulfures représentaient des quantités négligeables de fer, manganèse et zinc (cf. [Chapitre 3](#)). J'ai donc décidé de ne pas appliquer ces étapes lors des extractions séquentielles réalisées sur les échantillons du site de la Terre-Plaine ([Tableau 2](#)). Par ailleurs, les teneurs en carbonates et en carbone organique dans les grains noirs étaient inférieures aux limites de détection des analyses réalisées par le Laboratoire d'Analyse des Sols de l'INRA d'Arras (cf. [Chapitre 6](#)). En conséquence, les étapes correspondant à ces deux phases n'ont pas été incluses dans le protocole d'extraction séquentielle des grains noirs. Enfin, les grains noirs consistant principalement en des concrétions ferro-manganiques, ils présentent des teneurs élevées en oxy-hydroxydes de fer et de manganèse, nécessitant un plus grand nombre de répétition des étapes extrayant ces phases (cf. [Chapitre 6](#)). Le détail opératoire des extractions séquentielles est décrit au fur et à mesure de leurs besoins dans les chapitres qui suivent.

Chapitre 3

**Potentialité du zinc comme traceur
des différents processus pédogénétiques**



L'objectif de ce chapitre est de déterminer le potentiel du zinc à tracer les processus pédogénétiques. Pour cela, j'ai envisagé l'impact des différents processus sur la mobilisation du zinc.

Ce travail est rédigé sous forme d'un article en anglais publié dans PEDOSPHERE. Il présente une étude des risques environnementaux à long terme inhérents aux fortes concentrations en zinc, équivalentes à celles de certains sites pollués. Pour répondre à cette problématique, nous évaluons la redistribution quantitative du zinc par les différents processus, depuis son stock initial jusqu'à son stock actuel dans les différents phases minéralogiques et organiques.

Ainsi, bien que le but premier de cette étude soit environnemental, la compréhension du comportement du zinc dans ce solum au cours de la pédogenèse me permet de tirer des conclusions sur sa potentialité à tracer certains des processus identifiés.

3.1. Comportement du zinc au cours de la pédogenèse

PEDOSPHERE 2009, 19(3): 292-304 (doi:10.1016/S1002-0160(09)60120-X)

Running Title: ZINC FATE THROUGH PEDOGENESIS

Zinc Redistribution in a Soil Developed from Limestone During Pedogenesis ^{*1}

C. LAVEUF^{1,*2}, S. CORNU¹, D. BAIZE¹, M. HARDY¹, O. JOSIERE¹, S. DROUIN², A.
BRUAND² and F. JUILLOT³

¹INRA, UR0272 Science du Sol, Centre de recherche d'Orléans, 45075 Orléans cedex 2 (France)

²ISTO, UMR 6113, CNRS – Université d'Orléans, 45071 Orléans cedex 2 (France)

³IMPMC, UMR CNRS 7590, Universités Paris 6 et 7, IPGC, 75252 Paris cedex 05 (France)

(Received November 20, 2008; revised March 23, 2009)

ABSTRACT

The long-term redistribution of Zn in a naturally Zn-enriched soil during pedogenesis was quantified based on mass balance calculations. According to their fate, parent limestones comprised three Zn pools: bound to calcite and pyrite-sphalerite grains, bound to phyllosilicates and bound to goethite in the inherited phosphate nodules. Four pedological processes, *i.e.*, carbonate dissolution, two stages of redox processes and eluviation, redistributed Zn during pedogenesis. The carbonate dissolution of limestones released Zn bound to calcite into soil solution. Due to residual enrichment, Zn concentrations in the soil are higher than those in parent limestones. Birnessite, ferrihydrite and goethite dispersed in soil horizon trapped high quantities of Zn during their formation. Afterwards, primary redox conditions induced the release of Zn and Fe into soil solution, and the subsequent individualization of Fe and Mn into Zn-rich concretions. Both processes and subsequent aging of the concretions formed induced significant exportation of Zn through the bottom water table. Secondary redox conditions promoted the weathering of Fe and Mn oxides in cements and concretions. This process caused other losses of Zn through lateral exportation in an upper water table. Concomitantly, eluviation occurred at the top of the solum. The lateral exportation of eluviated minerals through the upper water table limited illuviation. Eluviation was also responsible for Zn loss, but this Zn bound to phyllosilicates was not bioavailable.

Key Words: carbonate dissolution, eluviation, long-term, redox, speciation

^{*1} Project supported by the "GDR TRANSMET" Program of the Centre National de la Recherche Scientifique (CNRS), France.

^{*2} Corresponding author. E-mail: laveuf@orleans.inra.fr.

Although Zn is an essential nutrient for living organisms, this element exhibits a well-established toxic nature for fauna and flora at high concentrations in soils. Studies dealing with the geochemical behaviour of Zn focused particularly on polluted soils, because numerous human activities lead to accumulations of Zn in soils, which can represent an environmental hazard in some cases (Salomons *et al.*, 1995). However, some soils developed on natural geochemical anomalies display concentrations of Zn as high as those of polluted soils (Kabata-Pendias and Pendias, 2001), but to our knowledge, no Zn toxicity for plants was recorded on these large cropping areas (Nicolini, 1990). The fate of Zn in soils depends not only on its total concentration, since its potential mobility and bioavailability are governed by its speciation and location in relationship to roots, and by its rate of release into the soil solution.

As a general rule, geogenic trace elements including Zn are believed to be less mobile than those of anthropogenic origin, but few empirical datasets published support this hypothesis. In this study we tested the hypothesis that the lower mobility of geogenic Zn in soils relative to anthropogenic Zn was due to differences in speciation. The present work aimed at quantifying the long-term redistribution of Zn due to different pedological processes during the pedogenesis of a soil developed on natural geochemical anomalies. The approach consisted in determining the speciation *sensu largo* of Zn, *i.e.*, its repartition within the different solid components, both in the parent material and in the solum. Information on the speciation of Zn was cross-linked with mass balance calculations according to the Brimhall approach in order to estimate the fluxes of Zn due to each pedological process identified (Brimhall *et al.*, 1991).

MATERIALS AND METHODS

Studied site and samples

The studied site, located 2.5 km southward of Pouilly-en-Auxois (Burgundy, France), consists in a thick and old forested solum, which developed from limestones dated from the Sinemurian and Lotharingian (upper Sinemurian). The Sinemurian-aged limestone is 5- to 10-m thick and consists of hard and compact crystalline grey-blue limestone layers irregularly intercalated with thin soft marled beds. The overlying Lotharingian-aged limestone is 1- to 3-m thick and consists of a grey-blue matrix with brown-rust coloured inclusions and of a bed of pluricentimetric phosphate nodules corresponding to marine fossils at its bottom. Mineralization events due to hydrothermal fluids rising along fault lines during the Lias epoch (Baize and Chrétien, 1994) are responsible for their high contents of Zn.

The studied solum is composed of the succession of horizons described in Table I. The limit with the unweathered and impermeable Sinemurian-aged limestone undulates between 170- and 180-cm depth. The abundant phosphate nodules in the BP-horizon were inherited from the bed of phosphate nodules at the bottom of the Lotharingian-aged limestone. Consequently, the overlying horizons derived from the autochthonous weathering of the Lotharingian-aged limestone, whereas the underlying ones derived from the autochthonous weathering of the Sinemurian-aged limestone. Indeed, Baize and Chrétien (1994) assessed the autochthony of these soils by petrography coupled with geochemical and mineralogical analyses, avoiding significant contribution of loess deposits in the studied area. The soil horizons identified were sampled on the whole width of a pit, once when homogenous or all 10 cm when an evolution with depth was evidenced.

TABLE I

Characteristics of the soil horizons (from top to bottom) in the studied solum

Horizon	Soil depth cm	Characteristic
A	0-(10-15)	Yellowish brown (10YR5/4), with few small black Fe-Mn concretions
E	(1--15)-45	Yellowish brown (10YR5/6 to 4/4), depleted in clay particle-size fractions, with few small black Fe-Mn concretions at the top (E1), more numerous ones at the bottom (E2)
Bd	4--(75-80)	Ochre (10YR4/4), irregularly bleached and degraded, with small black numerous Fe-Mn concretions and few small phosphate nodules
Bc	(75-80)-95	Compact, with numerous Fe-Mn concretions and abundant big white soft phosphate nodules (1 to 2 cm)
BP	95-145	Ochre (10YR4/4 to 5/4), with few phosphate nodules and abundant black Fe-Mn concretions that are ovoid-shaped, hard, from various sizes (less than 0.5 to more than 5 mm) and discordant with the matrix of the horizon
C	145-(170-180)	Ochre (10YR5/6), clay-rich, developed in a water table, with rare Fe-Mn concretions

The Lotharingian-aged limestone (abbreviated L, excluding the bed of phosphate nodules at its bottom) was sampled in a road trench, 800 meters southward of the studied pit where it is completely weathered. One sample of the Sinemurian-aged limestone (abbreviated S) was taken at the bottom of the pit (S1) and three additional ones from different strata on the same road trench (S2, S3 and S4).

Analyses on soil samples

Bulk density of each soil horizon was determined in triplicate by the cylinder method after drying at 105 °C. Pedological analyses were performed at the Laboratoire d'Analyse des Sols ([LAS](#), Arras, France): pH was determined according to the standard protocol NF ISO 10390; CaCO₃ according to NF ISO 10693 (calcimetry); organic matter (OM) obtained by multiplying by 1.73 the organic carbon measured according to NF ISO 10694. Total major elements were analyzed at the Service d'Analyse des Roches et des Minéraux ([SARM](#), Vandoeuvre-lès-Nancy, France) by ICP-AES and Zn by ICP-MS after LiBO₂ fusion. Results being in the range of those reported by [Baize and Chrétien \(1994\)](#) ([Table II](#)), the studied solum is thus representative of those encountered in the studied area.

TABLE II

 Main pedological characteristics, total Fe, Mn, P and Zn concentrations and volumetric strain (ϵ) of the different soil horizons

Horizon	Depth cm	pH _{water}	Base saturation %	CaCO ₃		Organic matter			Zn mg kg ⁻¹	ϵ %
				g kg ⁻¹		Fe	Mn	P		
A	0-10	5.7	36	1.2	53	40 [§]	2.3 [□]	1.7 [#]	129 ⁺	-85.1
E1	20-30	5.8	42	0	25	47 [§]	2.3 [□]	1.3 [#]	146 ⁺	-86.0
E2	35-45	5.5	42	0	11	60 [§]	3.5 [□]	1.7 [#]	189 ⁺	-83.2
Bd1	50-60	5.8	67	0	9	78 [§]	8.3 [§]	4.2 [#]	315 ⁺	-79.9
Bd2	60-70	-	-	-	-	89 [§]	9.2 [§]	3.8 [#]	337 ⁺	-80.0
BP	80-90	6.3	77	2.7	6	94 [§]	14 [§]	61 ⁺	772 ⁺	-
Bc1	105-115	-	-	-	-	86 [§]	16 [§]	15 ⁺	508 ⁺	-82.9
Bc2	115-125	7.0	86	1.2	8	83 [§]	12 [§]	8.0 ⁺	475 ⁺	-80.7
Bc3	125-135	-	-	-	-	86 [§]	12 [§]	9.0 ⁺	481 ⁺	-80.3
Bc4	135-145	-	-	-	-	90 [§]	15 [§]	9.0 ⁺	515 ⁺	-80.2
C	145-170	7.9	100	22	11	90 [§]	8.0 [§]	4.4 ⁺	919 ⁺	-82.4

§, +, #, □ Analytical error of 2%, 5%, 10%, and 15%, respectively.

The A-, E1-, Bd1-, BP-, Bc2- and C-soil samples were wet-sieved at 500, 200 and 50 μm in deionized water, without preliminary treatments. The remaining fractions ($< 50 \mu\text{m}$) were further fractionated by sedimentation in deionized water according to Stokes law. The particle-size fractions obtained were: 0–2, 2–20, 20–50, 50–200, 200–500 and $> 500 \mu\text{m}$. Organic fragments were removed from the fractions $> 500 \mu\text{m}$ by water flotation before total chemical analysis of the remaining mineral fractions. For the BP- and all Bc-horizons, all phosphate nodules and Fe-Mn concretions larger than 1 mm were manually sorted. All fractions (particle-size fractions, soil-phosphate nodules and Fe-Mn concretions) were analyzed for Fe, Mn, Al, Si and Zn at the [SARM](#) as described above.

X-ray diffraction (XRD) analyses on powder were performed on bulk samples, 2–20 μm fractions, soil-phosphate nodules and Fe-Mn concretions, with 2θ ranging from 0° to 75° and a counting time of 1 s/ 0.02° . XRD analyses on natural, glycoled and heated oriented slides were performed on 0–2 μm particle-size fractions, with 2θ ranging from 0° to 47° and a counting time of 20 s/ 0.02° . All diffraction data were obtained using $\text{CuK}\alpha$ radiation (45 kV, 30 mA).

Since the solum is rich in Fe and Mn ([Table II](#)), the chosen 8-step procedure of sequential extractions, adapted from [Hall et al. \(1996\)](#) and [Cornu et al. \(2006\)](#), focused particularly on the extraction of Fe and Mn oxides. Extractions were performed in triplicate on 1 g of the bulk sample ground to 50 μm for the A-, E1-, Bd1- and C-horizons and on 1 g of the fraction $< 50 \mu\text{m}$ for the BP- and Bc2-horizons, under permanent shaking and at ambient temperature, if not specified.

Step 1 was a single extraction with 10 mL of a solution of NaNO_3 0.1 mol L^{-1} (analytical reagent, AR, Chem-Lab) for 120 min; step 2 a single extraction with 20 mL of a solution of CH_3COONa 1 mol L^{-1} (ultra pure, UP, Chem-Lab) adjusted to pH 5.5 with CH_3COOH 99%–100% (UP, Chem-Lab) for 360 min; step 3 twofold extraction with 20 mL of a solution of $\text{NH}_2\text{OH}\cdot\text{HCl}$ 0.1 mol L^{-1} (AR, Chem-Lab)/ HCl 0.1 mol L^{-1} (UP, Prolabo Normatom) at pH 2.0 for 30 min; step 4 a single extraction with 10 mL of a solution of $\text{Na}_4\text{P}_2\text{O}_7$ 0.1 mol L^{-1} (AR, Prolabo Merck) at pH 10 for 90 min; step 5 twofold extraction with 20 mL of a solution of $\text{NH}_2\text{OH}\cdot\text{HCl}$ 0.25 mol L^{-1} (AR, Chem-Lab)/ HCl 0.25 mol L^{-1} (UP, Prolabo Normatom) at pH 1.5 and 60 $^\circ\text{C}$ for 120 min; step 6 twofold extraction with 30 mL of a solution of $\text{NH}_2\text{OH}\cdot\text{HCl}$ 1 mol L^{-1} (AR, Chem-Lab)/ CH_3COOH 99%–100% at 25% (UP, Chem-Lab) at pH 1.0 and 90 $^\circ\text{C}$ for 180 min, then 90 min; step 7 a single extraction with 750 mg of KClO_3 (AR, Chem-Lab) and 15 mL of a solution of HCl 12 mol L^{-1} (AR, Chem-Lab) for 30 min, then another extraction with 10 mL of a solution of HNO_3 4 mol L^{-1} (UP, Chem-Lab) at 90 $^\circ\text{C}$ for 20 min.

The residual fraction of step 7 was analyzed for Fe, Mn and Zn at the [SARM](#). After each step, a rinse with 20 mL of MilliQ[®] water was performed for 1 h. The extraction and rinse solutions were centrifuged at $10\,800 \times g$ and filtered through a 0.2- μm pore-size membrane in cellulose acetate. Blanks were realized following the same procedures. Filtrates were acidified to 1% with HNO_3 65% (UP, Chem-Lab) if necessary and individually stored at 4 $^\circ\text{C}$ before analyses for Fe, Mn and Zn by spectroscopic flame atomic absorption. All values of Fe, Mn and Zn for extraction results discussed hereafter were corrected from those measured in the blanks that were near or below the limits of detection. Differential XRD was performed following [Schulze \(1981\)](#), in order to determine the minerals dissolved during sequential extractions: bulk samples and residues from extractions were analyzed on powder with 2θ ranging from 36° to 48° and a counting time of 50 s/ 0.02° .

A decimetric soil monolith was sampled in the BP-horizon with a Kubiena box. Two

thin sections ($45 \times 60 \text{ mm}^2$, $25 \text{ }\mu\text{m}$ thick) containing typical phosphate nodules were realized. They were observed with a scanning electron microscope (SEM, Cambridge Stereoscan 90B), and analyzed for Fe and Zn with a microprobe (Cameca SX50; with a beam voltage of 15 keV, a beam current of 12 nA and a counting time of 10 s for Fe and 30 s for Zn) and by proton induced X-ray emission (PIXE; vertical Van de Graaff accelerator HV-KN-3000; with a proton beam energy of 3 MeV and a beam current ranging from 1 to 200 μA on a $30 \times 60 \text{ }\mu\text{m}^2$ area).

Analyses on limestone samples

Limestone-phosphate nodules (S2P) were separated from carbonated matrix (S2M) in sample S2. Unweathered parts of all limestone samples were selected and analyzed for Fe, Mn, Al, Si, Ca, P and Zn at the [SARM](#) and for CaCO_3 at the [LAS](#). Bulk density of each limestone sample was determined in triplicate on three different pieces (sizes of about $5 \times 5 \times 5 \text{ cm}^3$) by volume displacement in kerosene after drying at $40 \text{ }^\circ\text{C}$. Unweathered limestone samples (L, S1, S2M) and limestone-phosphate nodules (S2P) were roughly ground. About 10 g of each sample were put in closed batches with 30 mL of MilliQ[®] water and placed onto a magnetic agitator at room temperature. pH was monitored along the experiment. A solution of HCl 1 mol L^{-1} was introduced, regulating the flow in order to maintain $\text{pH} > 5$ and to avoid the alteration of Fe oxides and of phyllosilicates. The limestone residues from carbonate dissolution were analyzed for Fe, Mn, Al, Si, Ca, P and Zn at the [SARM](#) and for CaCO_3 at the [LAS](#). X-ray diffraction (XRD) analyses on powder were performed on the limestone residues, with 2θ ranging from 0° to 75° and a counting time of $8 \text{ s}/0.02^\circ$. Surface-indurated sections (25 mm in diameter, 5 mm thick) of samples S2M, S3, S4 and L were prepared and analyzed with a microprobe for Ca, P, F, Si, Al, Fe, Mn, and of 30 s for S and Zn as described above.

Mass balance calculations

Current stocks of Zn, Al, Si, Fe and Mn were calculated for each soil horizon. Element fluxes, $m_{j,hor}$, were computed for each soil horizon with the procedure and detailed equations of [Brimhall et al. \(1991\)](#) modified by [Egli and Fitze \(2000\)](#), on the basis of the volumetric strain ε , *i.e.*, the soil volume change through time ([Table II](#)), and of the mass-transport function $\tau_{j,hor}$, *i.e.*, the mass fraction of element j gained or lost from the weathered product compared to its initial mass in the parent material. Zirconium, relatively immobile in soils ([Brimhall et al., 1991](#)), was used as immobile element.

The choice of the parent material used as a reference is of prime importance in these calculations. The studied solum formed from two different limestones. The A-, E1-, E2-, Bd1- and Bd2-horizons were issued from the weathering of the Lotharingian-aged strata. Their reference was thus the L limestone. The four Bc-horizons were issued from the weathering of Sinemurian-aged strata, since located just beneath the BP-horizon, and contain small phosphate nodules. The S2M limestone was sampled just beneath the bed of phosphate nodules at the bottom of the L limestone and contains also small phosphate nodules. The S2M limestone was thus the reference for the Bc-horizons. The C-horizon overlies the S1 limestone. This limestone was thus the reference for the C-horizon. Initial stocks of Zn, Al, Si, Fe and Mn in these parent materials were finally calculated.

Mass balance calculations were not performed on the BP-horizon, because the occurrence of pluricentimetric phosphate nodules seriously impeded precise volumetric strain

calculations. Errors on calculations were estimated by the classical mathematical methodology of the total differential equations, using the analytical errors given by the [SARM](#) for chemical concentrations and the experimental standard deviations for bulk densities.

RESULTS AND DISCUSSION

Zinc location in the parent materials

Limestones L, S1 and S2M mainly consisted of calcite and displayed low concentrations of Zn ([Table III](#)). The stock percentages released into solution during dissolution from the Sinemurian- and Lotharingian-aged limestones were about 15% and 40% for Zn, 10% and 15% for Fe, and 85% and 95% for Mn, respectively, indicating that these elements were bound to calcite ([Table III](#)).

TABLE III

Chemical composition of the bulk samples of the Lotharingian and Sinemurian aged-limestones, their residues from carbonate dissolution and their estimated calcite contents derived from the previous data

Sample	Abbreviation ^{a)}	Fraction considered	CaCO ₃	Ca	Fe	Mn	P	Zn
			%	g kg ⁻¹				mg kg ⁻¹
Lotharingian limestone	aged- L	Bulk	87.2 ^{b)}	339 [§]	23.7 [§]	1.9 [□]	4.0 [#]	38 [#]
		Residue	-	14.4 ⁺	164 [§]	0.9 [□]	14.4 ⁺	169 ⁺
		Calcite ^{○)}	-	387	3.1	2.1	2.4	19
Sinemurian limestone	aged- S1	Bulk	88.0 ^{d)}	350 [§]	10.3 [§]	2.3 [□]	5.6 ⁺	11 [#]
		Residue	-	292 [*]	81 [§]	0.44 [□]	45 ⁺	62 ⁺
		Calcite ^{c)}	-	387	0.9	2.6	0.5	4.4
	S2M	Bulk	68.3 ^{b)}	322 [§]	9.5 [§]	1.9 [□]	1.8 [#]	77 ⁺
		Residue	-	302 [§]	22.9 [§]	1.9 [□]	3.3 [#]	189 ⁺
		Calcite ^{c)}	-	377	3.3	1.9	1.1	25.0
	S2P	Bulk	27.8 ^{b)}	352 [§]	53 [§]	1.3 [□]	92 ⁺	1179 ⁺
		Residue	-	91.8 [§]	62 [§]	1.2 [□]	123 ⁺	1327 ⁺
		Calcite ^{c)}	-	375	31.2	1.5	11.1	795

§, +, #, □ Analytical error of 2%, 5%, 10%, and 15%, respectively.

^{a)}S2M stands for carbonated matrix and S2P for phosphate nodules in sample S2; ^{b)}Determined by the loss of mass after experimental carbonate dissolution in batch experiment; ^{c)}Calculation of the concentration in the calcite determined thanks to carbonate dissolution experiment; ^{d)}Measured by calcimetry.

XRD analyses revealed that, apart from some remaining calcite, limestone residues consisted of quartz, phyllosilicates (predominantly kaolinite, illite and interstratified for all samples, plus chlorite for S3), apatite (for S1, S4 and L), pyrite and sphalerite (for S3 and S4). Microprobe analyses provided evidences for the association of low concentrations of Zn and Fe together with Si and Al, of low concentrations of Zn with Ca, P and F, and of high concentrations of Fe and Zn with S. This was interpreted as the occurrence of Zn and Fe in phyllosilicates, of Zn in apatite and of small grains of mixed pyrite (FeS₂) and sphalerite (ZnS).

Calcite was the main Mn-bearing phase. It suggests the occurrence of a solid solution with some rhodocrosite (MnCO₃; [Lee et al., 2002](#)). Calcite was a non-negligible Zn- and Fe-bearing phase, even if these elements were mainly bound to phyllosilicates and, to a lesser extend, to pyrite/sphalerite grains.

Soil-phosphate nodules were significant Zn-bearing phases as they represented 10% (in

average) and 84% of the > 500 µm fractions of the Bc- and BP-horizons, respectively (Figs. 1 and 2). Although soil-phosphate nodules exhibited a slightly higher porosity than the limestone-phosphate nodules (S2P), both showed a very similar chemical and mineralogical composition (Table III, Fig. 3). Pedogenesis thus poorly influences phosphate nodules, which are mainly inherited. At the micrometer scale, the structure of phosphate nodules was highly heterogeneous. Zones with different grey levels were observed by SEM (Fig. 3). Microprobe and PIXE analyses gave low concentrations of Zn (several hundreds mg kg⁻¹) in the zones of fluorapatite matrix (Fig. 3). On the opposite, much higher concentrations of Zn (several thousands mg kg⁻¹), as well as Fe, were detected in the zones with very bright grey levels (Fig. 3). Goethite being the only Fe-bearing mineral identified on XRD spectra, these bright grey zones probably consist of goethite with high concentrations of Zn and are responsible for the high quantities of Zn in the phosphate nodules.

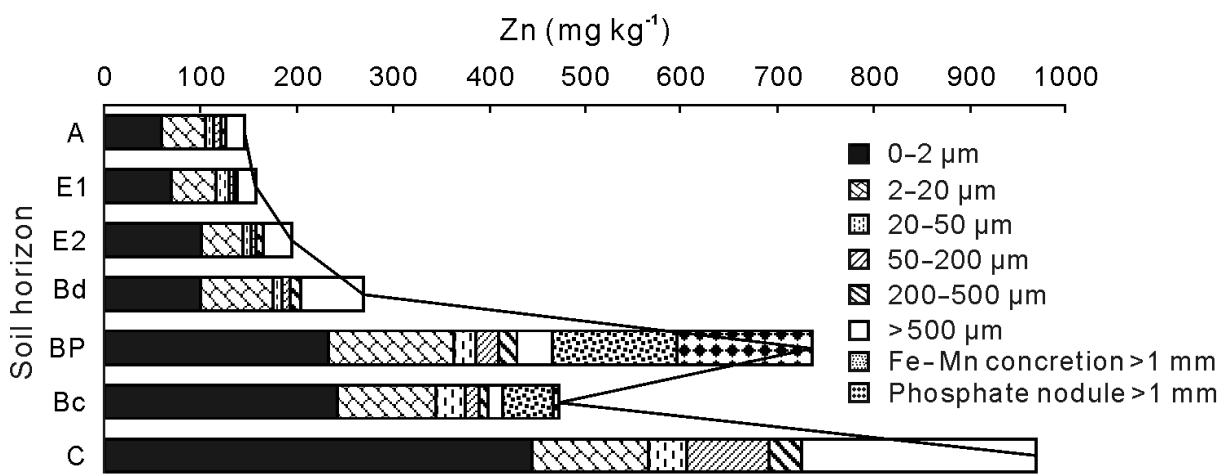


Fig. 1 Zinc particle-size distribution in the different soil horizons.

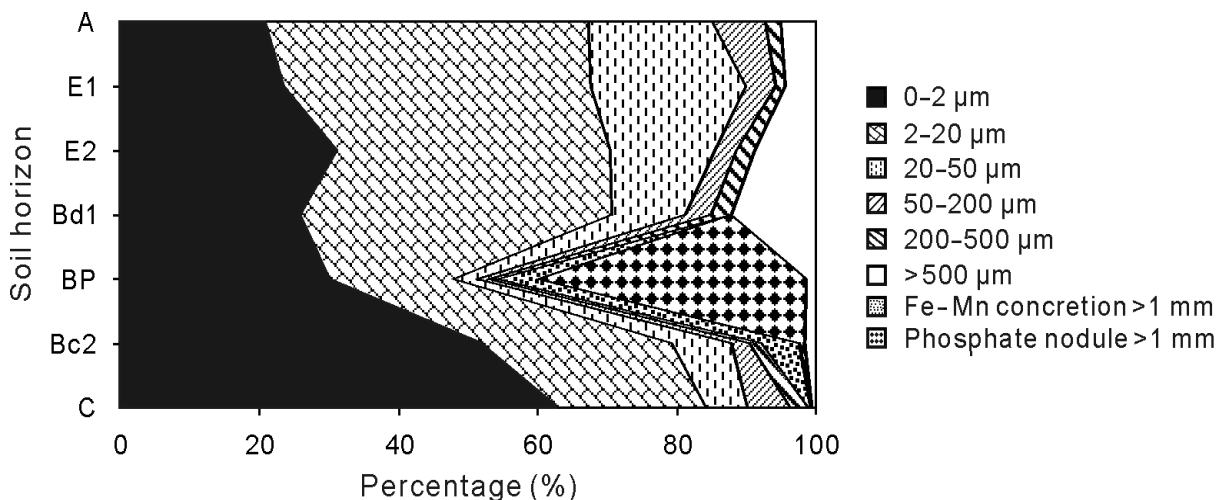


Fig. 2 Particle-size distribution in the solum.

Zinc redistribution along the solum during soil evolution

Zinc in the bulk soil samples increased with depth (Fig. 1), notably in the C-horizon, with a peak in the BP-horizon due to the abundance of Zn-rich phosphate nodules (Figs. 2 and 3). In order to estimate the impact of pedological processes on Zn redistribution at the solum scale, the fluxes of Zn were quantified with mass balance calculations. Because redox processes mobilize Fe and Mn, whereas eluviation/illuviation processes mobilize Si and Al, the fluxes of Fe, Mn, Si and Al were also quantified.

The volumetric strain ranged from 80% to 86% according to the horizon considered (Table II). These values were consistent with the amounts of CaCO₃ in the limestones compared to those remaining in the soil horizons (Tables II and III), which indicates realistic results of mass balance calculations.

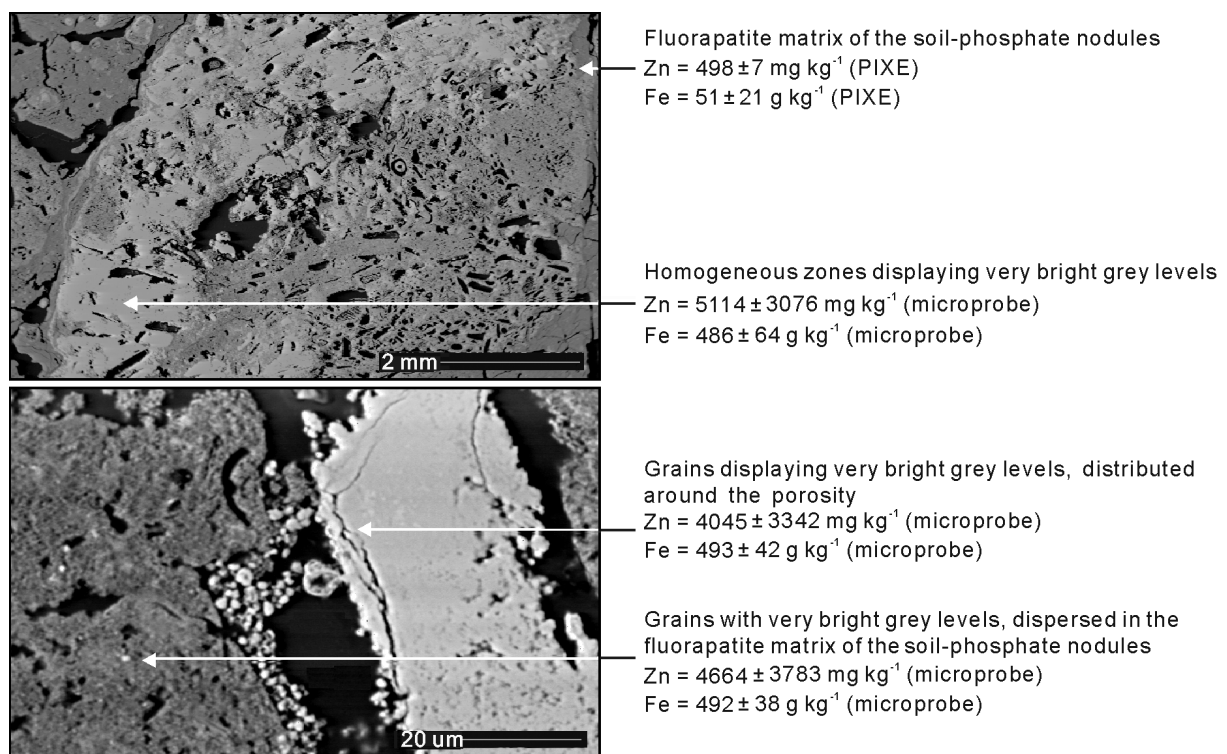


Fig. 3 Scanning electron microscope pictures (in the backscattered electron mode) of the phosphate nodules of the BP-horizon and associated average concentrations of zinc and iron, analyzed by microprobe and proton induced X-ray emission (PIXE), of the fluorapatite matrix and the zones with very bright grey level. Average concentration of zinc in the phosphate nodules of the BP-horizon is 928.6 mg kg⁻¹.

Since similar trends were observed for Si and Al on the one hand, and for Fe and Mn on the other hand, only results concerning Al, Fe and Zn are shown in Fig. 4. These results indicate that important fluxes of Al (Si), Fe (Mn) and Zn occurred during pedogenesis, compared to their initial stocks in the respective parent limestones (Fig. 4). About one third of the initial Al (Si) stock was lost during the formation of the A- and E-horizons. These fluxes were roughly equal to those entering the underlying horizons (Fig. 4). About three quarters of the initial Fe (Mn) stock were lost during the formation of the A- to Bd-horizons. The formation of both the Bc- and C-horizons did not induce any net fluxes. It thus seems that the losses of Fe (Mn) recorded

in the A- to Bd-horizons correspond to exportations out of the solum, while a redistribution occurred in the Bc- and C-horizons since the positive flux in the Bc-horizon balances the negative one in the C-horizon (Fig. 4). Except for the Bd-horizon, all fluxes of Zn were significant according to uncertainties calculated. About the half of the initial stock of Zn was lost during the formation of the A- to Bd-horizons. Zinc fluxes leaving the A- to Bc-horizons were roughly equal to the high one entering the C-horizon (Fig. 4).

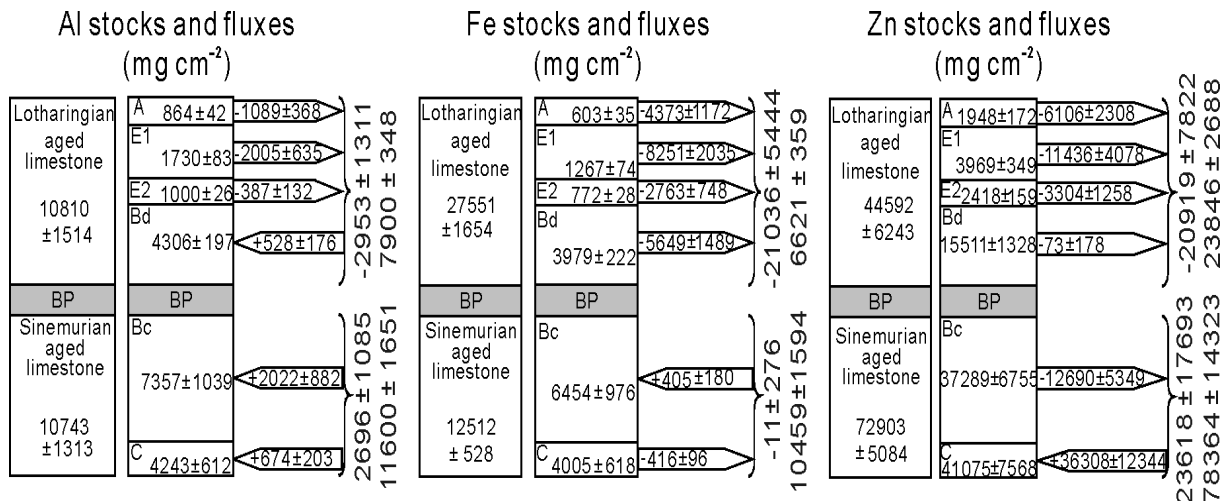


Fig. 4 Al, Fe and Zn stocks and fluxes in and from the different soil horizons, estimated by mass balance calculations following the method of [Brimhall et al. \(1991\)](#) modified by [Egli and Fitze \(2000\)](#) using Zr as invariant.

Finally, the A- and E-horizons were systematically depleted in all elements. At the solum scale, Fe (Mn) was lost, while Zn and Al (Si) were not (Fig. 4). Mass balance calculations do not explain the high concentration and input of Zn in the C-horizon. It may for instance be due to an important heterogeneity in the composition of the parent limestone or to lateral gains through the water table.

Impact of the different pedological processes on the redistribution of zinc

Validation of solid phases extracted by each extraction step and location of Zn Quantities of Fe, Mn and Zn extracted at each extraction step of the procedure are shown in Fig. 5. Recovery rates ranged from 87% to 94% for Fe, 79% to 98% for Mn and 93% to 112% for Zn, which were acceptable for sequential extractions ([Quevauviller, 1998](#)).

Although extractions are not fully selective of a specific mineral phase, results remain informative when discussed with respect to the main solid phase(s) extracted during each step of the chosen procedure. Step 1 enables the extraction of the exchangeable Zn ([Gupta and Aten, 1993](#)), whereas step 2 enables the extraction of Zn sorbed and/or bound to carbonates ([Han and Banin, 1995](#)). These two first steps released almost negligible quantities of Zn, except in the C-horizon where about 10 mg kg⁻¹ of Zn were extracted during step 2 (Fig. 5).

Step 3 enables the extraction of Mn oxides ([Hall et al., 1996](#)), but also apatite ([Land et al., 1999](#)). The major part of Mn (68% to 94%), and only a few percentage of total Fe, were extracted during this step along the studied solum (Fig. 5). This step also released less than 10% of total Zn from the A- to Bc2-horizons and up to 30% Zn to the C-horizon (Fig. 5). In addition,

microprobe and PIXE analyses of the phosphate nodules of the BP-horizon detected only small quantities of Zn in the fluorapatite matrix (Fig. 3). The contribution of apatite to the quantities of Zn extracted during step 3 is therefore limited, although not totally excluded, and Zn extracted during step 3 was thus mainly released by Mn oxides. According to Manceau *et al.* (1997) who studied the Fe-Mn concretions of these soils, Mn oxides occur as birnessite that sorbs Zn, as also shown in polluted soils (Isaure *et al.*, 2005).

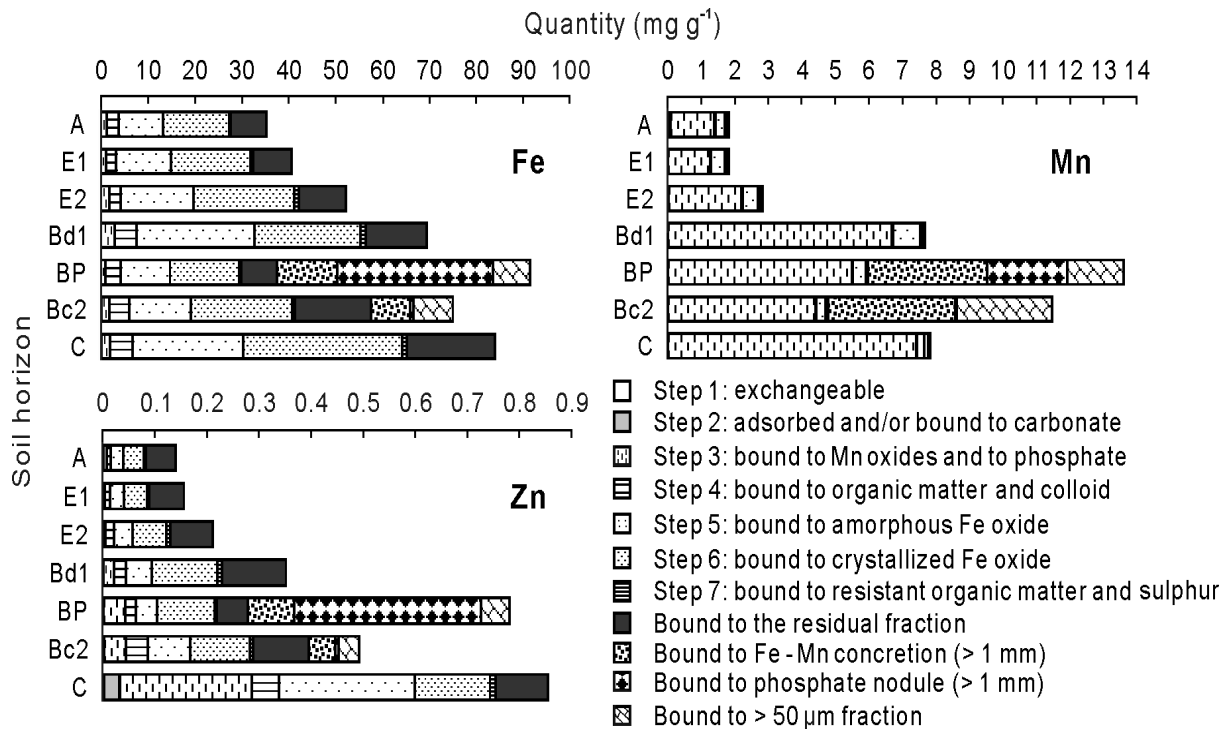


Fig. 5 Quantities of Fe, Mn and Zn extracted by sequential extractions along the solum. Sequential extractions were carried out on the < 50 μm fractions for the BP- and Bc2-horizons and on the bulk samples for the other soil horizons.

Step 4 enables the extraction of Zn bound to OM (Benitez and Dubois, 1999), although sodium pyrophosphate also acts as a dispersive agent on small hydrated Fe oxide colloids (Jeanroy *et al.*, 1984). Iron quantities extracted during step 4 were small, but non-negligible (Fig. 5). Considering the OM contents of the studied solum (Table II) and a mean concentration of Fe in plants of 300 mg kg⁻¹ (Angelone and Bini, 1992), the maximum quantity of Fe bound to OM should be 20 mg kg⁻¹ soil. Since at least 2 g Fe kg⁻¹ soil were extracted during step 4 (Fig. 5), it mainly corresponded to colloidal losses and not to extraction of OM. This assumption is heightened by the increase with depth of Fe extracted during step 4 (Fig. 5), while the OM contents decreased (Table II). This evolution with depth is not consistent with a complexation of Fe with OM, all the more that Fe has a weak affinity for soil OM (Burt *et al.*, 2003). Therefore, the small Zn extracted during step 4 (Fig. 5) were also probably related to dispersion of Zn-bearing Fe colloids rather than to oxidative destruction of OM.

Steps 5 and 6 enable the extraction of amorphous and crystalline Fe oxides, respectively (Hall *et al.*, 1996). The high quantities of Fe (61% to 71%) extracted during these steps suggest that this element mainly occurred as Fe oxides in the studied solum (Fig. 5). This was confirmed by the differential XRD spectra, which showed peaks of small intensities attributed

to goethite and a very broad peak stretching from 0.21 to 0.38 nm attributed to ferrihydrite (Schulze, 1981). The quantities of Zn extracted during steps 5 and 6 ranged from 45% to 70% of total Zn depending on the depth, which suggests a significant association of Zn with amorphous and crystalline Fe oxides (Fig. 5). Such a strong affinity of Zn for Fe oxides was already observed in polluted soils (Manceau *et al.*, 2000; Isaure *et al.*, 2005).

Step 7 enables the extraction of Zn bound to resistant OM and sulphides (Hall *et al.*, 1996). Quantities of Fe, Mn and Zn extracted during step 7 were low (Fig. 5). It confirms the lower affinity of Zn for OM than for Fe oxides, already shown in polluted soils (Burt *et al.*, 2003).

Finally, the residual fraction consisted of quartz and of phyllosilicates according to XRD spectra. The significant residual quantities of Fe (19% to 28% of total Fe) and Zn (12% to 43% of total Zn) were thus bound to phyllosilicates (Fig. 5). These latter minerals are important Fe- and Zn-bearing minerals in this solum, either through inclusion within their lattice or sorption at their surface and/or in their interlayer region (Manceau *et al.*, 2000).

Sequential extractions finally showed that Zn is located in two main phases in the studied old solum: Fe and Mn oxides for the largest part and phyllosilicates. This Zn location results from successive pedological processes: carbonate dissolution, two stages of alternation of redox conditions, evolution of phyllosilicates, and eluviation/illuviation, as evidenced by Baize and Chrétien (1994). These pedological processes are responsible for the differentiation of the solum into horizons that are representative of a given pedological process: C-horizon for carbonate dissolution, Bc-horizon for primary redox processes, Bd-horizon for secondary redox conditions, and E- and A-horizons for eluviation, the BP-horizon being mainly inherited. In the following paragraphs, the fate of Zn during pedogenesis or how the different pedological processes act on the redistribution of Zn in the involved horizons is discussed.

Redistribution of Zn by carbonate dissolution. The first process involved in the soil formation is the carbonate dissolution of the calcite matrix of the parent limestones. Despite its low concentrations in Zn, Fe and Mn, the large volume of calcite dissolved during the process implies high releases of Zn, Fe and Mn into soil solution (Tables II and III). Carbonate dissolution still occurs in the C-horizon, as it is incomplete (Table II). Results suggest that, once released into soil solution, Fe and Mn subsequently precipitated as birnessite, ferrihydrite and goethite in the C-horizon (Fig. 5). The high amounts of Zn in Mn oxides and amorphous Fe oxides of the C-horizon indicate that, once precipitated, these newly formed phases bound a significant fraction of the dissolved Zn (Fig. 5). This assumption is supported by the strong enrichment of Zn into birnessite and ferrihydrite in the C-horizon (Table IV), which is favoured by its high pH value due to the persistence of carbonates (Table II) (Uygur and Rimmer, 2000). Once released into soil solution, geogenic Zn is thus trapped in the same solid phases like anthropogenic Zn in some polluted calcareous or pseudogley soils (Isaure *et al.*, 2005).

TABLE IV

Extraction ratios of Fe in step 6 versus step 5 and of Zn/Mn for step 3 and Zn/Fe for steps 5 and 6

Horizon	Step 6/step 5 (Fe)	Zn/Mn (step 3)	Zn/Fe (step 5)	Zn/Fe (step 6)
	%			
A	1.47	3.9	2.6	2.8
E1	1.44	2.6	2.2	2.7
E2	1.39	2.2	2.3	3.1
Bd1	0.90	3.0	2.0	5.5
BP	1.39	7.7	3.8	7.5
Bc2	1.64	9.7	6.3	5.3
C	1.44	34.2	11.0	4.3

Redistribution of Zn by primary redox processes

The second process involved in soil formation is a past succession of redox cycles supposed to have formed the Fe-Mn concretions in the Bc- and BP-horizons (Baize and Chrétien, 1994). Indeed, the > 500 µm fractions of the Bc2- and BP-horizons contain 70% and 13% of Fe-Mn concretions, respectively (Fig. 2). The Fe-Mn concretions consist of goethite, birnessite (Manceau *et al.*, 1997) and traces of ferrihydrite. They hold significant quantities of Zn (Figs. 1 and 5). Since the parent limestones are free of ferruginous oolites, Fe-Mn concretions are not inherited and have thus a pedological origin. The C-horizon, because of more permanent reductive conditions, displays only rare Fe-Mn concretions (Fig. 2). Once the pedological process established, its impact on Zn and Zn-bearing solid phases is examined. Thus the origin of Fe, Mn and Zn inside the concretions, the incorporation of Zn during their formation, and their evolution through time and related consequences on Zn fate are successively discussed.

Reductive cycles that occurred in the BP- and Bc-horizons induced the releases of Fe and Mn, due to the dissolution either of Fe oxides dispersed within the soil matrix or of pyrite-sphalerite (FeS₂-ZnS) grains observed in the Sinemurian-aged limestone. The C-horizon also underwent redox conditions and is thus probably another source of Fe and Mn into soil solution.

Once in soil solution, Mn, Fe and Zn are transferred from centimetric to decimetric scale and concentrate as concretions (Zhang and Karathanasis, 1997). This transfer occurred from the C- to the Bc-horizons during temporary elevations of the water table, as suggested by the Fe and Mn fluxes exiting the C-horizon equal to those entering the Bc-horizon (Fig. 4). This assumption is supported by the concentric organization of Fe-Mn concretions in alternating rings of Mn or Fe oxides (Latrille *et al.*, 2001). The formation of Fe-Mn concretions was also favored by the saturation of the adsorbing complex by Ca²⁺ in the Bc-horizon (Table II), which prevented the sorption of Fe ions and thus facilitated the individualization of Fe compounds (Bottner, 1972). From the C- to the Bc-horizons, the quantities of Mn extracted by step 3 decreased (Fig. 5). This result is consistent with a concentration of birnessite in the Fe-Mn concretions at the expense of the birnessite dispersed in the matrix. The Fe-Mn concretions display an association of Zn-enriched areas with Mn-enriched ones (Manceau *et al.*, 1997; Latrille *et al.*, 2001), surely due to the strong affinity of Zn for the surface of birnessite (Lanson *et al.*, 2002). In addition, the significant decrease from the C- to the BP-horizons of the Zn/Mn ratio in step 3 (Table IV) and the flux of Zn exiting the Bc-horizon (Fig. 4), possibly reflect a loss of Zn during the dissolution of the dispersed birnessite and the subsequent reconcentration of Mn in the Fe-Mn concretions.

Once formed, the Fe-Mn concretions undergo aging process. Indeed, the goethite/ferrihydrite ratio (indicated by the Fe ratio of step 6/step 5) increased from the C- to the

Bc2-horizons (Table IV). The decrease of the Zn/Fe ratio in step 5 from the C- to the BP-horizons, concomitant with the increase of the same ratio in step 6 (Table IV), is consistent with a release of Zn during the process of transformation of the ferrihydrite into goethite (Kaur *et al.*, 2006). Despite the oldness of this solum, this transformation is still incomplete, probably because high concentrations of elements such as Zn or Mn slow down the kinetics of this reaction (Cornell and Giovanoli, 1987).

We thus show that if Fe and Mn oxides are the main phases scavenging Zn from soil solution, as already found in some polluted soils (Manceau *et al.*, 2000; Isaure *et al.*, 2005), the subsequent aging of these oxides induces Zn losses in the environment.

Redistribution of Zn by secondary redox processes The third process involved in soil formation is a second stage of redox conditions. They result from the occurrence of the very compact BP-horizon, which hinders water percolation (by field observations), hence the formation of a temporary perched water table in the Bd-horizon and preferential lateral water flow. This temporary water table leads to the reductive dissolution of oxide cements, macroscopically proven by the bleached zones in the Bd-horizon, and to the weathering of Fe-Mn concretions. Moreover, the desaturation of the adsorbing complex induces a decrease in pH (Table II) that favors the destruction of oxide cements. From the BP- to the E-horizons, Fe losses occurred (Fig. 4), due to a net decrease in Fe-Mn concretions resulting from their weathering. From the Bd- to the E-horizons, the quantities of Fe and Mn bound to ferrihydrite, goethite and birnessite decreased (Fig. 5). The quantities of Mn occurring as birnessite was divided by three from the Bd1- to the E2-horizons, those of Fe as ferrihydrite by two, while those of Fe as goethite decreased only from the E2- to E1-horizons (Fig. 5). Thus, Mn was lost in a greater proportion and before Fe, in agreement with the relative sensibility of the different oxides to redox conditions. In addition, the quantities of Zn bound to these oxides decreased similarly from the Bd- to the E-horizons (Fig. 5), while exported fluxes of Zn increased (Fig. 4). Since the BP-horizon induced a preferential lateral water flow and according to mass balance calculations (Fig. 4), Fe, Mn and Zn released into soil solution by the current dissolution of Fe and Mn oxides were mainly exported laterally.

Redistribution of Zn due to the evolution of phyllosilicates and eluviation/illuviation Zinc was largely bound to the 0–2 and 2–20 μm fractions (Fig. 1) and to the residues from sequential extractions (Fig. 5). Phyllosilicates are thus important Zn-bearing phases. The quantities of Zn bound to the 0–2 μm fraction decreased toward soil surface (Fig. 1), together with the 0–2 μm fraction (Fig. 2), which can be due to an evolution of the composition of the phyllosilicates and/or eluviation of the 0–2 μm fraction.

Illite, vermiculite, smectite, chlorite, interstratified phyllosilicates, and mainly kaolinite occurred in the 0–2 μm fractions of the solum (Fig. 6). Chlorite occurred only in the 0–2 μm fraction of the A- and E-horizons as shown by the peak at 1.41 nm (Fig. 6), which probably results from the physical breakdown of chlorite in the 2–20 μm fractions of the A- and E-horizons (Hardy *et al.*, 1999). The relative proportion of phyllosilicates of the 0–2 μm fraction evolved with depth (Fig. 6), whatever the parent limestones of the soil horizon considered. However, the mineralogical evolution of phyllosilicates is apparently restricted to a small proportion, thus can not significantly affect the redistribution of Zn.

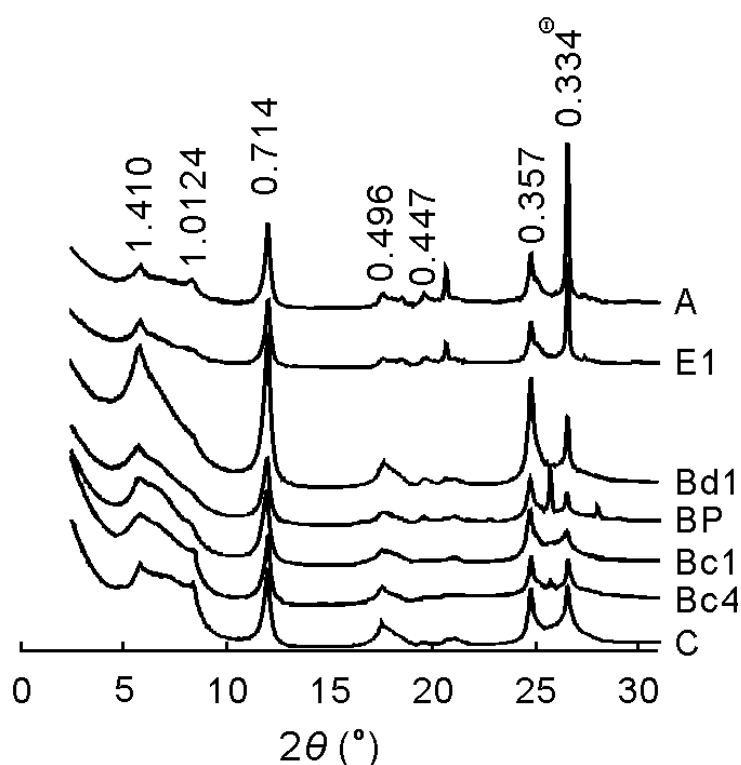


Fig. 6 X-ray diffraction spectra of the natural oriented slides of the 0–2 μm fractions for the different soil horizons. Intensities of (001) quartz peaks ($^{\circ}$) are normalized to that of the A-horizon. Interreticular distances (in nm) are reported for main peaks.

Oxide cements were not dissolved before particle-size analyses, but [Baize and Chrétien \(1994\)](#) showed that the decrease in the quantities of the 0–2 μm fraction toward soil surface is maintained after acidic dissolution of oxide cements. It proves that this evolution results from an eluviation of 0–2 μm fractions from the A- to E-horizons and not from its cementation into 2–20 μm fractions. Indeed, the sufficient desaturation of the adsorbing complex in the A- and E-horizons facilitates the transfer of fine particle-size constituents ([Table II](#)) ([Bottner, 1972](#)). Besides, significant Al (Si) losses occurred in the A- and E-horizons ([Fig. 4](#)). Moreover, from the Bd1- to the A-horizons, the peak intensity ratio of phyllosilicates to quartz decreased in bulk samples and 0–2 μm fractions (from 2.1 to 0.5; [Fig. 6](#)), concomitant with an increase of Si/Al ratio in the residual fraction from extractions (from 3.6 to 6.5). Losses of Al and Si actually arise from the eluviation of phyllosilicates from the A- and E-horizons, while quartz is relatively enriched. Consequently, the decrease in the quantities of Zn bound to 0–2 μm fractions surely results from the eluviation of 0–2 μm fractions from the A- and E-horizons. This also explains the decreases in Zn quantities and concentrations bound to phyllosilicates from the Bd- to the A-horizon ([Fig. 5](#)). Except quartz, all mineral phases of the 0–2 μm ([Fig. 6](#)) and 2–20 μm fractions, *i.e.*, phyllosilicates, Fe oxides (goethite and ferrihydrite) and apatite, likely contain significant amounts of Zn. Therefore, eluviation, together with secondary redox processes that dissolve oxide cements as previously mentioned, is responsible for the losses of Fe, Mn and Zn observed in the A- and E-horizons ([Fig. 4](#)).

At last, the eluviated phyllosilicates can either be accumulated within the solum or lost. Mass balance calculations showed only small enrichments of Al and Si in the Bd-horizon relative to losses recorded from the overlying A- and E-horizons ([Fig. 4](#)). Besides, the thin argilans in the Bd-horizons observed by petrography exhibit a restricted illuviation. Since the

compact underlying BP-horizon induces a preferential lateral water flow, the eluviated phyllosilicates are mainly transferred laterally outside of the solum. Since phyllosilicates are important Zn-bearing minerals (Fig. 5), the illuviation in the Bd-horizon, even if restricted, may nevertheless balance losses of Zn induced by the ongoing secondary redox process leading to significant losses of Fe and Mn (Fig. 4). This could explain the lack of Zn flux from or into the Bd-horizon.

CONCLUSIONS

Four pedological processes (*i.e.*, carbonate dissolution, two stages of redox processes and eluviation) contributed to the redistribution of Zn, which occur in three main pools in the parent limestones according to their fate: the easily and highly mobilized pool of Zn released into soil solution, *i.e.*, dispersed in calcite, mobilized as soon as carbonate dissolution begins, and bound to pyrite-sphalerite grains, mobilized when redox conditions become enough oxidative; the pool of Zn with a lower and rather physical mobility, *i.e.*, bound to potentially eluviated phyllosilicates; and the non-mobilized pool of Zn, *i.e.*, bound to goethite phases in the inherited phosphate nodules. Due to residual enrichment, Zn concentrations in the soil were higher than those in parent limestones. Birnessite, ferrihydrite and goethite dispersed in soil horizon trapped high quantities of Zn during their formation, but non-negligible quantities exited the solum through a bottom water table. Afterwards, primary redox conditions induced the release of Zn and Fe into soil solution, then individualization of Fe and Mn into Zn-rich concretions. Both processes and subsequent aging of the concretions formed induced significant exportation of Zn through the bottom water table. Thus even if oxides are the main phases scavenging Zn from the soil solution, the subsequent evolution and aging of these oxides induce Zn losses in the environment. Secondary redox conditions, as well as ongoing desaturation, promoted the weathering of Fe and Mn oxides in cements and concretions. This process caused other losses of Zn through lateral exportation in an upper water table. Concomitantly, lateral eluviation occurred at the top of the solum. Eluviation was also responsible for Zn loss, but this Zn bound to phyllosilicates is not bioavailable.

Combined approaches including mass balance allow better quantification of the impact of different pedological processes on the long-term fate of Zn in soils. However, further work is required to assess the role of each pedological process on Zn redistribution. A mass balance calculation of Zn related to each process may eventually fill in this gap. Moreover, the kinetic of the release of Zn over a long time is crucial, since environmental hazards depend on how slow or fast the release is.

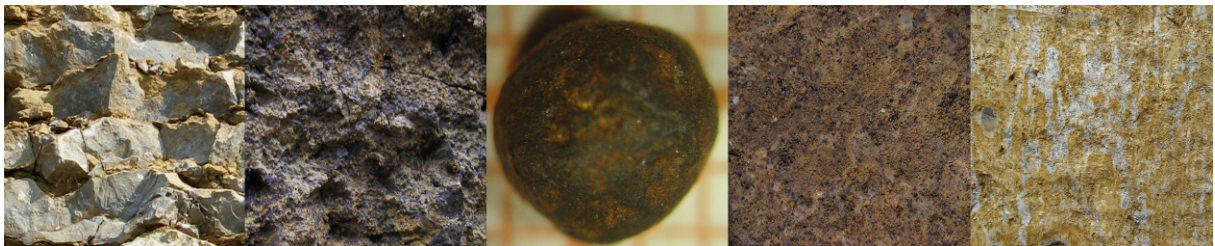
3.2. Conclusions sur la potentialité du zinc pour tracer des processus pédogénétiques

L'étude de la mobilité du zinc au cours de la pédogenèse montre que la fraction libérée dans la solution du sol après dissolution des minéraux primaires est majoritairement reprise dans les oxydes de fer et de manganèse qui se forment au cours des conditions redox. Par ailleurs, le zinc est aussi présent en forte proportion dans les phyllosilicates principalement hérité des matériaux parentaux. La pédogenèse n'induit pas de modification sensible des teneurs en zinc dans ceux-ci. En conséquence, comme le zinc se trouve à la fois dans les oxydes ferro-manganiques et les phyllosilicates, il est difficile, sur la base de cet élément, de déconvoluer l'impact des différents processus, notamment dans les horizons où ces deux phases sont mobilisées en même temps.

C'est pourquoi ce traceur ne m'a pas semblé idéal. Je me suis alors concentré dans la suite de ce travail sur les terres rares. Ces éléments, moins classiques que le zinc, ont par ailleurs été peu exploités jusqu'alors en pédogenèse.

Chapitre 4

**Potentialité des terres rares comme traceurs
des différents processus pédogénétiques**



L'objectif de ce chapitre est de déterminer le potentiel des terres rares à tracer les processus pédogénétiques.

Pour cela, dans une première partie, nous avons envisagé l'impact de différents processus d'altération et de pédogenèse sur le fractionnement des terres rares par une étude bibliographique, sous forme d'un article en anglais soumis à *Geoderma*. Les données accessibles dans différentes disciplines sur les propriétés physiques et chimiques des terres rares, sur leur mobilisation au cours de différents processus physiques et chimiques, sur leur spéciation dans divers environnements, et sur leur origine dans les sols ont été compilées. Elles permettent d'émettre des hypothèses sur l'impact de différents processus pédogénétiques sur le devenir des terres rares dans les sols.

Par ailleurs, l'utilisation des terres rares repose sur le choix d'un matériau de référence utilisé pour normaliser les concentrations en terres rares, du fait de l'abondance très contrastée des différentes terres rares dans les matériaux géologiques. Ainsi, je propose dans la seconde partie de ce chapitre une méthodologie de normalisation des terres rares développée pour mettre en évidence l'impact des différents processus pédogénétiques sur leurs mobilisations et fractionnements.

4.1. Etude bibliographique de l'impact de différents processus d'altération et de pédogenèse sur le fractionnement des terres rares

Potentiality of Rare Earth Elements as Tracers of Pedogenetic Processes: A Review ^{*1}

C. LAVEUF¹ and S. CORNU¹

¹INRA, UR0272 Science du Sol, Centre de recherche d'Orléans, CS 40001 Ardon, 45075 ORLEANS Cedex 2 (France). E-mail: laveuf@orleans.inra.fr

ABSTRACT

This review aims at considering the use of REEs to trace pedogenetic processes, in order to quantify the respective contribution of the successive processes on pedogenesis.

We first consider the origins and contents of REEs in soils, to assess their natural occurrence, and tackle their common graphic data presentation and data use. We review subsequently the impact of the different pedogenetic processes on the fate of REEs in soils: from their release into soil solution by primary mineral (heavy minerals, phosphates, silicates, and carbonates) dissolution during weathering, to their fixation on- or into main REE-bearing secondary minerals (clay minerals, Fe-Mn-oxides, and carbonates), then their mobilization by plant recycling and organic matter, and finally the impact of lessivage and redox processes on their fractionation.

We conclude that REEs, much more than other trace elements, can interestingly trace the considered processes that are encountered in a large diversity of non-polluted soils arising from diverse parent materials. Weathering generally fractionates REEs and accounts for a significant part of the variation in the initial REE stock of the soils. Plant recycling induces a weak mobilization of REEs and their accumulation in topsoil. Lessivage can be traced using the MREE-enrichment and the Eu-anomaly of the clay minerals. Redox processes can be traced by the Ce-anomaly caused by the precipitation of cerium on Mn-oxides. To use REEs as tracers of pedogenetic processes, we recommend a high characterization of the REE-bearing minerals, a clever choice of reference(s) for normalization and the use of mass balance calculations.

Key Words: lanthanides, lessivage, pedological carbonates, redox processes, weathering

^{*1} Corresponding author. Tel.: +33 2 38 41 78 00. Fax: +33 2 38 41 78 69. E-mail address: laveuf@orleans.inra.fr (C. Laveuf)

1. Introduction

Soils form through the evolution of parent materials undergoing supergene conditions, with a set of physical, chemical and biological processes (Alloway, 1990), whose different combinations define different pedogenetic routes.

In order to preserve soils in the frame of soil sustainability and climate change, Man needs to identify and quantify the impact of the successive processes on soil evolution (Hoosbeek and Bryant, 1992). Classically, major elements and mineralogy are used in soil science to achieve this objective. As several pedogenetic processes mobilise the same major elements, it is, however, generally difficult to quantify the different pedogenetic processes on the sole basis of these data. Other tracers have to be identified.

Rare Earth Elements (REEs) include the elements of the group IIIB of the periodic table, *i.e.* the 14 natural elements of the lanthanide series (La to Lu). They are naturally widespread as a group in the environment (Henderson, 1984) and exhibit remarkable chemical properties. Technical improvements in chemical analytical tools in the last two decades allow REEs to be analysed in routine (Crock and Lichte, 1982; Lalonde and Dalton, 1982; Gladney and Bower, 1985; Cao *et al.*, 2000). Thus, they have been progressively used as proxies in different disciplines in earth sciences, such as hydrology, geochemistry or geology, notably to trace origin and processes. For instance, among processes, REEs trace hydrothermal events (Ling and Liu, 2002 and references therein), diagenesis (Picard *et al.*, 2002) or the way of formation of different materials (*e.g.* Addy, 1979; Watson and Green, 1981; Frietsch and Perdahl, 1995; Yuan *et al.*, 2003a; Yuan *et al.*, 2003b). They were more rarely used as tracers in pedogenesis (Aide and Smith-Aide, 2003).

REEs have a common electronic configuration with 6 shells, large ionic radii, a 3+ oxidation state and an electronegativity close to those of Ca, Na or Sr, but lower than those of the transition elements of the periodic table (Table 1). REEs thus form preferentially ionic bindings than covalent ones (Henderson, 1984) and are lithophile elements (Goldschmidt, 1937; Bernat, 1975). These similar chemical and physical properties confer them a close behaviour in the environment (Henderson, 1984; Tyler, 2004b; Hu *et al.*, 2006b).

However, the progressive filling of the 4f orbit leads to slight variations in their behaviour in natural systems: their ionic radius decreases, while their electronegativity increases from La to Lu (Table 1), and their coordination numbers range from 6 to 11 according on the REE or group of REEs considered (Table 2; Henderson, 1984; Kanazawa and Kamitani, 2006). For this reason, two or three groups of REEs are generally distinguished: light REEs (LREEs), heavy REEs (HREEs) and sometimes middle or medium REEs (MREEs) (Henderson, 1984). This distinction varies according to the authors, the science fields, the environment studied, etc, so that attention must be paid to the REEs included in these groups. Generally, studies assign LREEs from La to Pr or Nd, MREEs from Pr or Nd to Dy or Ho and HREEs from Dy or Ho to Lu. At last, unlike other REEs, Eu and Ce are encountered in two oxidation states under earth surface conditions (Table 1).

Table 1

Chemical and physical properties of REEs (after Henderson, 1984).

	Symbol	Atomic number	Atomic weight g mol ⁻¹	Valence	Electronic structure		Ionic radii ^{a)} nm	Electronegativity (Pauling scale)
					Z=0	Z=+3		
Lanthanum	La	57	138.90547	3	[Xe].5d ¹ .6s ²	[Xe].4f ⁰	0.1172	1.10
Cerium	Ce	58	140.116	3,4	[Xe].4f ¹ .5d ¹ .6s ²	[Xe].4f ¹	0.1150	1.12
Praseodymium	Pr	59	140.90765	3	[Xe].4f ³ .6s ²	[Xe].4f ²	0.1130	1.13
Neodymium	Nd	60	144.242	3	[Xe].4f ⁴ .6s ²	[Xe].4f ³	0.1123	1.14
Samarium	Sm	62	150.36	3	[Xe].4f ⁶ .6s ²	[Xe].4f ⁵	0.1098	1.17
Europium	Eu	63	151.964	3,2	[Xe].4f ⁷ .6s ²	[Xe].4f ⁶	0.1087	n.a. ^{b)}
Gadolinium	Gd	64	157.25	3	[Xe].4f ⁷ .5d ¹ .6s ²	[Xe].4f ⁷	0.1078	1.22
Terbium	Tb	65	158.92535	3	[Xe].4f ⁹ .6s ²	[Xe].4f ⁸	0.1063	n.a. ^{b)}
Dysprosium	Dy	66	162.500	3	[Xe].4f ¹⁰ .6s ²	[Xe].4f ⁹	0.1052	1.22
Holmium	Ho	67	164.93032	3	[Xe].4f ¹¹ .6s ²	[Xe].4f ¹⁰	0.1041	1.23
Erbium	Er	68	167.259	3	[Xe].4f ¹² .6s ²	[Xe].4f ¹¹	0.1030	1.24
Thulium	Tm	69	168.9342	3	[Xe].4f ¹³ .6s ²	[Xe].4f ¹²	0.1020	1.25
Ytterbium	Yb	70	173.04	3	[Xe].4f ¹⁴ .6s ²	[Xe].4f ¹³	0.1008	n.a. ^{b)}
Lutetium	Lu	71	174.967	3	[Xe].4f ¹⁴ .5d ¹ .6s ²	[Xe].4f ¹⁴	0.1001	1.27

^{a)}Ionic radii for a coordination VI octahedral in the 3+ oxidation state; ^{b)}n.a. non available data.

REEs occur in more than 200 minerals distributed in a wide variety of mineral classes (Henderson, 1984; Kanazawa and Kamitani, 2006). REEs are thus present in most primary and secondary minerals in soils. As a consequence, through the dissolution of primary minerals, REEs are released into the soil solution. Once in soil solution, REEs preferentially migrate through the weathering profile according to their relative solubility and mobility. Then they are either lost from the weathering profile or incorporated into newly formed soil minerals, mainly clay minerals, carbonates, and Fe- and Mn-oxides. The whole process induces REE fractionations. At last, REEs are probably translocated in soils by biological and physical processes, such as lessivage of clay minerals, complexation with organic matters or plant recycling.

All these processes must fractionate REEs in different ways. Thus, REEs can probably be used as tracers of the pedogenetic processes.

Table 2

The coordination numbers and abundances of LREEs and HREEs in the structural sites of REE-bearing minerals; (○) and (●) are LREEs and HREEs, respectively. The size of circles shows rough abundance of REEs for each mineral class. After Kanazawa and Kamitani (2006).

Mineral class	Coordination number					
	11	10	9	8	7	6
	-----○LREE-----			-----●HREE-----		
Carbonates	○	○	○	○		
Silicates		○	○	○	○	○
Phosphates			○	○		
Titanates				○		
Fluorides			○			

We discuss in this paper how the pedogenetic processes fractionate REEs, and consequently how REE signatures can be used to trace them, from their release into solution by primary mineral dissolution to their fixation onto secondary minerals and their subsequent redistribution by leaching and redox processes. Their content and origin in soils, as well as the way they are classically presented in earth science studies, are first discussed.

2. Contents and origins of REEs in soils

The knowledge of the possible inputs of REEs into soils by different sources is of prime importance to assess the interpretation of REE distributions and thus their use as tracers.

The total REE contents of soils vary greatly (Table 3), highly depending on the type of soil and of the parent material from which they are issued (Liu, 1988; Hu *et al.*, 2006a). Other REE sources in soils are atmospheric depositions (atmospheric particles, rainwater and snow) and anthropogenic spreadings (waste samples, irrigation and sewage waters, and especially fertilizers) (Aubert *et al.*, 2002).

Table 3

Minimum, maximum and average concentrations (mg kg⁻¹) of REEs in different matrices.

Matrices	Range	Average	References
Soil	16-700 mg kg ⁻¹	165 mg kg ⁻¹	Tyler, 2004b; Liang <i>et al.</i> , 2005; Hu <i>et al.</i> , 2006b
Soil parent materials :	basic and acid igneous rocks, sandstones and shales	174-219 mg kg ⁻¹	Hu <i>et al.</i> , 2006b and references therein
	loess and calcareous rocks	137-174 mg kg ⁻¹	
Atmospheric particles	0.22-0.33 ng m ⁻³		Hu <i>et al.</i> , 2006b and references therein
Rainwater:	Beijing, China	690 ng L ⁻¹	Hu <i>et al.</i> , 2006b and references therein
	Strasbourg, France	260 ng L ⁻¹	
	Vosges Mountains, France	9.8 ng L ⁻¹	
Snow	Alps, France	47.4-66.4 ng L ⁻¹	Aubert <i>et al.</i> , 2002
Throughfall	Vosges Mountains, France	90.3 ng L ⁻¹	Aubert <i>et al.</i> , 2002
River	13.8-476 ng L ⁻¹	78.3 ng L ⁻¹	Goldstein and Jacobsen, 1988; Elderfield <i>et al.</i> , 1990; Han and Liu, 2006
Seawater	11.5-365 ng L ⁻¹	14.4 ng L ⁻¹	Henderson, 1984; Tachikawa <i>et al.</i> , 1999
Groundwater	1.1-1196 ng L ⁻¹	57.2 ng L ⁻¹	Smedley, 1991; Johannesson <i>et al.</i> , 1997; Gruau <i>et al.</i> , 2004
Sewage waters	1.1-34.4 µg L ⁻¹	10.2 µg L ⁻¹	Wang <i>et al.</i> , 2003
Fertilizers:	Phosphogypsum and phosphate fertilizers	27-45 mg kg ⁻¹ for La 39-61 mg kg ⁻¹ for Ce	Hu <i>et al.</i> , 2006b and references therein
	superphosphates	2.6 g kg ⁻¹ maximum	

Parent material content in REEs is a function of its mineralogical composition (Bonnot-Courtois, 1981; Benes, 1989; Yamasaki *et al.*, 2001). Hu *et al.* (2006b) identified two major types of parent materials according to their REE contents and the REE contents in

the soils issued from their weathering: basic or acid igneous rocks, sandstones and shales on the one hand, and loess and calcareous rocks on the other hand (Table 3).

Atmospheric deposition occurs as dry or wet deposition (Aubert *et al.*, 2002). Dry deposition, as particles, display low REE contents (Table 3). Wet depositions, such as rain, snow and throughfall, are of larger importance (Table 3; Zhang *et al.*, 1999). REE concentrations in rainwater and snow vary with their particle load contents and notably with the proximity of city areas (Table 3). Throughfall results from the leaching by rain of atmospheric particles deposited on foliage and from leaf excretion, and is thus richer in REEs than rain or snow (Zhang *et al.*, 1999; Aubert *et al.*, 2002; Hu *et al.*, 2006b). However, atmospheric depositions are a minor source of REEs into soils (Wang *et al.*, 2004).

Human activities, such as irrigation with river or groundwater, P-fertilisation and waste spreading on soils, are also responsible for REE inputs to soils (Aubert *et al.*, 2002). Inputs through irrigation are of minor importance as REE concentrations of river or groundwaters are of the same order of magnitude to one order lower than those of rainwater or snow (Table 3; Wang *et al.*, 2004). On the opposite, P-fertilizers display high REE contents (Table 3). P-fertilizers are generally produced from natural phosphates that are rich in REEs (Hu *et al.*, 1998; Martin and McCulloch, 1999), as REEs have a high affinity for P-compounds (Tyler, 2004b). They are thus a relevant anthropogenic source of REEs in soils (Volokh *et al.*, 1990). Calculations show that REE inputs range from 30 to 170 g ha⁻¹ year⁻¹ with a P-fertilization of 300 kg ha⁻¹ year⁻¹ (Hu *et al.*, 2006b) and that REE content in the soil may double in 159 years with continuous intensive application of natural phosphates as P-fertilizers (Wang *et al.*, 2004).

At last, wastes exhibit a broad range of REE concentrations according to their nature: incinerator bottom ashes, slurries, sewage sludges, food industry sludges and chemical industry sludges. However, they are not responsible for significant REE accumulations into soils, except for Eu and Sm where sewage sludges or incinerator bottom ashes are spread continuously (Kawasaki *et al.*, 1998; Zhang *et al.*, 2001). Sewage waters display REE concentrations of three orders of magnitude higher than those of rain and river (Table 3), so that their continuous discharge onto fields can contaminate soils with REEs along time.

Nevertheless, human inputs of REEs in soils are usually rather limited in non-polluted areas and reasonably amended agricultural soils (Wang *et al.*, 2004). Liu (1988) concluded that REEs in soils mainly originate from parent materials. This renders them of high interest for pedogenetic studies.

3. Normalization and anomalies

As mentioned before, REEs generally occur as a group in geogenic materials and display close properties with some particularities according to their mass or to their ability to have different oxidation states under surface conditions. As a consequence, when used as tracers in earth sciences, they are generally analysed all together and interpreted both as a group with some elements displaying what is considered as anomalies. To do so, REEs are generally represented on graphs ranking them by increasing atomic numbers (REE patterns).

However, REEs display very contrasted concentrations, with an overall decrease from La to Lu, even if REEs with even atomic numbers have generally higher concentrations than their neighbours with odd atomic numbers (Henderson, 1984). To get rid of these two phenomena and be able to compare REE contents, their concentrations are commonly

normalized to a reference (Henderson, 1984). This reference is chosen according to the system under investigation.

Several classical references are available (Table 4). Usually, in soil science, the reference chosen is either internal (like the parent material or the geological substratum) or external (like the Upper Continental Crust) to the soil system under investigation. The use of an internal reference allows evidencing REE fractionations and anomalies during pedogenesis (Bonnot-Courtois, 1981). Furthermore, Laveuf *et al.* (2008, cf. Chapitre 4.2.1.) demonstrated that a careful choice of the reference, which may change with the soil horizon under consideration, allows better analysis of a single pedogenetic process.

Table 4

REE concentrations in some classical references used for normalization.

	Crustal abundance mg kg ⁻¹	U.C.C. ^{a)} mg kg ⁻¹	Deep Sea Carbonates ^{b)} mg kg ⁻¹	Carbonates ^{b)} mg kg ⁻¹	NASC ^{c)} mg kg ⁻¹	Chondrites ^{c)} mg kg ⁻¹
La	30	30.00	10.00	n.a. ^{d)}	32	0.330
Ce	60	64.00	35.00	11.50	73	0.88
Pr	7	7.1	3.30	1.10	7.9	0.112
Nd	25	26.00	14.00	4.70	33	0.60
Sm	5	4.50	3.80	1.30	5.7	0.181
Eu	1	0.88	0.60	0.20	1.24	0.069
Gd	4	3.80	3.80	1.30	5.2	0.249
Tb	0.7	0.64	0.60	0.20	0.85	0.047
Dy	3.5	3.50	2.70	0.90	n.a. ^{d)}	n.a. ^{d)}
Ho	0.8	0.80	0.80	0.30	1.04	0.070
Er	2.3	2.30	1.50	0.50	3.4	0.200
Tm	0.32	0.33	0.10	0.04	0.50	0.030
Yb	2.2	2.20	1.50	0.50	3.1	0.200
Lu	0.4	0.32	0.50	0.20	0.48	0.034

^{a)}References: UCC (Upper Continental Crust) cited from Taylor and McLennan (1985); ^{b)}Deep Sea Carbonates and Carbonates cited from Reeder and America (1983); ^{c)}NASC North American Shale Composite and Chondrites cited from Haskin *et al.* (1968); ^{d)}n.a. non available data.

REE patterns allow identifying contrasted concentrations in light versus heavy REEs, or relative concentration or depletion in Ce or Eu, for instance. These differences are respectively called fractionation and anomalies and are further quantified by the use of ratios. The fractionation between LREEs and HREEs is generally evidenced through the use of two distinct ratios, La/Lu and La/Yb – depending on the Lu contents, sometimes too small to be accurately quantified – or by the sum of the LREEs divided by the sum of the HREEs. In all cases, the concentrations used into the calculation of the fractionation ratios are the normalised concentrations. The anomalies are quantified by the ratio of the normalized concentration of the considered REE by the half of the sum of the normalized concentrations of its neighbours. Different calculations are proposed in the literature for these anomalies (see *e.g.* Bonnot-Courtois, 1981).

We see here that the choice of the reference is crucial for the subsequent interpretation of the fractionations and anomalies.

4. Impact of weathering on REE mobilization

Weathering consists in the dissolution of primary minerals and the hydrolysis of the elements released (Price, 1995).

The behaviour of REEs during weathering has been extensively studied (see e.g. Nesbitt, 1979; Duddy, 1980; Topp *et al.*, 1984; Braun *et al.*, 1990; Walter, 1991; Braun *et al.*, 1993; Boulangé and Colin, 1994; Marker and de Oliveira, 1994; Condie *et al.*, 1995; Öhlander *et al.*, 1996; Braun *et al.*, 1998; Taunton *et al.*, 2000; and references therein). The mobility of REEs varies between that of Ti to that of Fe through weathering (Bonnot-Courtois, 1981).

When REEs are released into solution, they are either lost from the weathering profile via the soil solution or incorporated, partially or totally, into secondary minerals that may be subsequently weathered (Öhlander *et al.*, 1996; Panahi *et al.*, 2000; Taunton *et al.*, 2000; Gnandi and Tobschall, 2003). The REE redistribution during weathering is related to:

- the solid primary phase, *i.e.* its mineralogical composition and relative mineral stability (Nesbitt, 1979; Braun *et al.*, 1990; Walter, 1991; Marker and de Oliveira, 1994; Condie *et al.*, 1995; Öhlander *et al.*, 1996; Braun *et al.*, 1998; Panahi *et al.*, 2000; Tyler, 2004b);
- the properties of the different REEs in solution (Nesbitt, 1979; Braun *et al.*, 1990; Walter, 1991; Marker and de Oliveira, 1994; Condie *et al.*, 1995; Braun *et al.*, 1998; Panahi *et al.*, 2000; Tyler, 2004b); as well as
- the degree of weathering (Walter, 1991; Huang and Gong, 2001).

4.1 REEs in primary minerals

As mentioned in introduction, REEs are hosted by more than 200 different types of minerals. However, some of these minerals display higher REE contents than others, or are present in higher amounts in the parent material than others. In both cases, they may greatly impact the REE signature of the parent material, and their weathering will have important consequences on the REE signature of the soil.

4.1.1. Minerals with high REE concentrations

They are mainly of two types: heavy minerals and phosphates.

Heavy minerals are known to host REEs, especially Zr- and Ti-bearing phases, such as anatase, ilmenite, sphene, rutile and zircon, which contain HREEs as "impurities" (Braun *et al.*, 1990; Walter, 1991; Braun *et al.*, 1998; Aubert *et al.*, 2001; Aide and Pavich, 2002; Takahashi *et al.*, 2003; Kanazawa and Kamitani, 2006). Since most of the heavy minerals are rather stable through weathering (Nickel, 1973), REEs and especially HREEs bound to them are not expected to be highly mobilized during pedogenesis.

Phosphates typically contain thousands of mg kg⁻¹ of REEs (Henderson, 1984; Hughes *et al.*, 1991; Iqdari, 1992; Frietsch and Perdahl, 1995; Taunton *et al.*, 2000; Aide and Pavich, 2002; Tyler, 2004b). Concentrations vary according to their origin and genesis (Iqdari, 1992; Picard *et al.*, 2002). Phosphates exhibit an LREE-enrichment compared to HREEs (Table 2; Henderson, 1984; Hughes *et al.*, 1991; Walter, 1991; Iqdari, 1992; Condie *et al.*, 1995;

Frietsch and Perdahl, 1995; Taunton *et al.*, 2000; Aide and Pavich, 2002), as well sometimes as a MREE-enriched patterns (Watson and Green, 1981; Henderson, 1984; Hughes *et al.*, 1991; Walter, 1991; Grandjeanlécuyer *et al.*, 1993; Byrne *et al.*, 1996; Compton *et al.*, 2003). In most cases, a negative Ce-anomaly is observed (Bernat, 1975; Bonnot-Courtois, 1981; Henderson, 1984; Iqdari, 1992; Grandjeanlécuyer *et al.*, 1993; Gnandi and Tobschall, 2003).

Therefore, phosphate weathering would be expected to release important REE quantities and, even at small amounts, phosphates may greatly influence the REE signature and budget of soils (Bonnot-Courtois, 1981; Papoulis *et al.*, 2004; Galán *et al.*, 2007). In addition, some authors argued that the solubility of Ce in soil was controlled by CePO₄ (Diatloff *et al.*, 1996; Tyler, 2004a). Phosphates are thus a peculiarly phase to be considered for soil studies.

When primary phosphates (allanite, monazite, apatite) weather, the released REEs precipitate as immobile secondary REE-phosphates (florencite, rhabdophane, xenotime) (Jonasson *et al.*, 1988; Banfield and Eggleton, 1989; Braun *et al.*, 1993; Braun and Pagel, 1994), without formation of a Ce-anomaly (Braun *et al.*, 1990; Taunton *et al.*, 2000). Laboratory-based studies showed that REEs can be relatively quickly trapped into the apatite structure (Watson and Green, 1981; Iqdari, 1992), thus that apatite may also partially control the fractionation of REEs from soil solutions. However, in highly weathered material, secondary phosphates disappear (Taunton *et al.*, 2000). Thus, the control of REE content in soils by phosphate will be mainly important for the first stage of the weathering for parent material containing high content of phosphates, that is mainly in sedimentary rocks (Zapata and Roy, 2004).

4.1.2. REE-bearing minerals abundant in soils and parent materials

Two main types fall into this group: silicate primary minerals and parent carbonates.

Silicate primary minerals are non-negligible REE-bearing minerals (Kanazawa and Kamitani, 2006). However, their REE content varies a lot according to the primary silicate considered. In the following, we present the association REE-silicate in crescent order of REE concentration.

Quartz does not contain REEs (Compton *et al.*, 2003). Feldspars contain negligible amounts of REEs, except Eu (Condie *et al.*, 1995). Feldspars are the only primary silicate minerals to always display a positive Eu-anomaly (Chase *et al.*, 1963; Towell *et al.*, 1969; Henderson, 1984; Aubert *et al.*, 2001; Compton *et al.*, 2003; Galán *et al.*, 2007), due to the replacement of Ca²⁺, Sr²⁺, and Na⁺ by Eu²⁺ (Nagasawa, 1971; Gromet and Silver, 1983; Panahi *et al.*, 2000), hence its specific compartment compared to the other MREEs (Walter, 1991).

Other silicates crystallizing concomitantly with feldspars, such as hornblende, augite, biotite, or clinopyroxene, display negative Eu-anomalies as a result of the preferential incorporation of Eu in feldspars during crystallization of the rocks (Chase *et al.*, 1963; Philpotts, 1970).

Mica can display either a positive Eu-anomaly (Philpotts, 1970), or a negative one (Chase *et al.*, 1963).

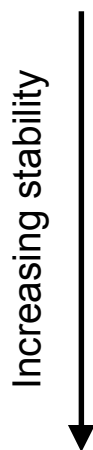
As a consequence, the weathering of plagioclases, micas or feldspars may involve Eu redistribution (Panahi *et al.*, 2000), and parent materials rich in such minerals may be

characterized by a preferential leaching of Eu over other REEs (Öhlander *et al.*, 1996; Ling and Liu, 2002).

Garnet are preferentially enriched in HREEs (Walter, 1991), sphene displays a small negative Eu-anomaly (Gromet and Silver, 1983; Condie *et al.*, 1995) and allanites (epidot group) may contain more than 20% of REEs (Braun *et al.*, 1993; Ercit, 2002), notably LREEs (Pan *et al.*, 1994; Tyler, 2004b).

As well-known, primary silicates weather at different rates, in inverse order to their precipitation according to the Goldich sequence (Goldich, 1938; Fig. 1). The relative concentration in REEs within the different silicates, combined with the relative weatherability of these last, will partially govern their fate through pedogenesis. As an example, quartz and feldspars that are REE-poor but relatively resistant to weathering will act as diluent in soils as already observed for trace elements (Hardy and Cornu, 2006).

Least stable: first to weather



Most stable: last to weather

Olivine	Calcic plagioclase
Augite	Calc-alkalic plagioclase
Hornblende	Alkali-calcic plagioclase
Biotite	Alkalic plagioclase
Potash feldspar	
Muscovite	
Quartz	
Zircon	

Fig. 1 Weathering sequence of primary minerals (after Goldich, 1938).

Parent carbonates generally display low REE concentrations (Table 4; Bonnot-Courtois, 1981; Reeder and America, 1983; Henderson, 1984) and act as a diluent (Bernat, 1975), except those formed from hydrothermal solutions or from carbonatite magma (Christie *et al.*, 1998; Stipp *et al.*, 2006). However, the important quantities of carbonates dissolved during soil formation result in large REE losses in the weathering profile as demonstrated by mass balance calculations (Laveuf *et al.*, 2008, cf. Chapitre 4.2.1.). Carbonates are thus a relevant phase to consider for soil studies.

Because of coordination numbers and ionic radii considerations (Tables 1 and 2), parent carbonates show a particularly homogeneous distribution (Haskin and Gehl, 1962; Reeder and America, 1983; Henderson, 1984), with an LREE-enrichment compared to HREEs, a negative Ce-anomaly and no Eu-anomaly (Christie *et al.*, 1998; Kanazawa and Kamitani, 2006). Parent carbonates may be MREE-enriched relative to LREEs and HREEs when diagenesis affects the materials (Lécuyer *et al.*, 1998; Picard *et al.*, 2002).

As a conclusion, the solid phase will play on the differential mobilization of some REEs over others during weathering. Differential REE release into soil solution is explained by the weathering of common silicates such as hornblende, epidote, feldspar, mica and plagioclase, of phosphates such as apatite, or of rare but REE-rich minerals such as allanite and monazite (Öhlander *et al.*, 1996). Besides, some phases are not dissolved, such heavy minerals or cerianite, what may lead to the passive generation of positive anomalies by the progressive loss of other REEs during weathering, as seen for Ce (Braun *et al.*, 1990; Boulangé and Colin, 1994; Koppi *et al.*, 1996; Taunton *et al.*, 2000).

4.2. Impact of the properties of the different REEs in solution on their distribution within weathering profiles

The composition of the liquid phase governs the differential transport of some REEs over others during weathering (Ling and Liu, 2002). As the energy of desolvation is a function of the atomic number, HREEs release the water molecules from their hydration sphere more easily than LREEs (Coppin, 2002). As a consequence, HREEs are more easily complexed than LREEs, *i.e.* LREEs are more susceptible to occur as free species than HREEs (Table 5; Cantrell and Byrne, 1987; Walter, 1991). Hence the preferential leaching of HREEs during weathering (Ma *et al.*, 2002). However, at pH < 6 approximately, REEs should be present mainly as free ions (Turner *et al.*, 1981; Wood, 1990; Smedley, 1991), so that complexation ability is less predominant. This evidences the importance of pH conditions during weathering (Nesbitt, 1979). The solubility product of REE-hydroxides at 25°C decreases regularly from La ($K_s=1.0 \cdot 10^{-19}$ mol L⁻¹) to Lu ($K_s=2.5 \cdot 10^{-24}$ mol L⁻¹) (Latimer, 1938), so LREEs are more soluble than HREEs (Table 5). Finally, adsorption/desorption can also act on REE redistribution. According to the lanthanide contraction, HREEs are more adsorbed than LREEs in the same trivalent state (Goldschmidt, 1958).

Table 5

Compartments of REEs in solution.

	LREEs	HREEs	References
Behaviour close to ... (according to Goldschmidt potential Z/r)	Ca	Al	Goldschmidt, 1937; Bernat, 1975
Complexation ability	+	++	Henderson, 1984; Cantrell and Byrne, 1987; Walter, 1991
Solubility	++	+	Goldschmidt, 1937; Latimer, 1938; Courtois, 1974; Bernat, 1975; Bonnot-Courtois, 1981; Henderson, 1984
Mobility	+/-	+/-	Courtois, 1974; Henderson, 1984; Sholkovitz, 1992; Panahi <i>et al.</i> , 2000; Ling and Liu, 2002

4.3. Impact of the degree of weathering on the REE distribution into weathering profiles

The REE stock generally decreases with an increasing weathering degree (Bonnot-Courtois, 1981; Boulangé and Colin, 1994; Öhlander *et al.*, 1996; Taunton *et al.*, 2000). REEs are generally depleted in the upper part compared to the bottom part of weathering profiles, where possible reprecipitation may even induce an enrichment (Braun *et al.*, 1993; Nesbitt and Markovics, 1997; Ma *et al.*, 2002).

In most cases, weathering results in a relative enrichment of LREEs over HREEs in the residual profile (Nesbitt, 1979; Duddy, 1980; Topp *et al.*, 1984; Braun *et al.*, 1990; Xing and Dudas, 1993; Boulangé and Colin, 1994; Ma *et al.*, 2002; Compton *et al.*, 2003). However, LREEs that have accumulated in alkaline phases of weathering can then be leached during more acidic phases (Ronov *et al.*, 1967; Bonnot-Courtois, 1981; Huang and Gong, 2001).

As a conclusion, REE concentrations in soils are determined to a significant extent by processes occurring during chemical weathering (Taunton *et al.*, 2000; Aide and Smith, 2001). It is thus important to well characterize the initial REE distribution into the different primary minerals to understand the redistribution of REEs following their release from primary mineral dissolution, and their fixation onto secondary minerals. Moreover, studies do not always take into account the volumetric modification of the parent materials during weathering, and consider only REE concentrations, hence the controversies on REE mobility and LREE/HREE enrichments, besides the degree of weathering (Walter, 1991). The interpretation of results based on stocks or mass balance calculations, as proposed by Brimhall and Dietrich (1987), could however solve this uncertainty (Braun *et al.*, 1993; Laveuf *et al.*, 2008, cf. Chapitre 4.2.1.). Since weathering induces REE fractionations and since the secondary minerals may display different affinities for an individual REE or group of REEs as discussed below, REE behaviour could be used as a tracer of weathering processes (Gnandi and Tobschall, 2003).

5. Secondary mineral formation and REE immobilisation

5.1. Clay mineral formation

Weathering of primary silicates leads to the formation of secondary clay minerals (Duchaufour, 1972; Sposito, 1989). Clay minerals are known to contain REEs (Roaldset, 1975; Henderson, 1984; Li *et al.*, 2006). These clay minerals are generally the new carriers of REEs in soil and weathering profiles (Condie *et al.*, 1995; Öhlander *et al.*, 1996; Gnandi and Tobschall, 2003; Papoulis *et al.*, 2004; Galán *et al.*, 2007), and control the REE stocks in soils (Bonnot-Courtois, 1981; Walter, 1991; Xing and Dudas, 1993; Ran and Liu, 1999).

The relatively important ionic radii of the REEs, except for Ce(IV), hinder their substitutions in octahedral – and a fortiori in tetrahedral – sites of the lattice of clay minerals, at least in significant amounts (Nesbitt, 1979; Duddy, 1980; Bonnot-Courtois, 1981; Braun *et al.*, 1993). However, they easily substitute for alkali metals and alkaline earths (Mosser, 1980), adsorbed onto the surface (Wan and Liu, 2005) and in the interlayer sites (*e.g.* Coppin *et al.*, 2002) of clay minerals. The adsorption of REEs onto clays is stronger than that of alkali metals and alkaline earths because of their trivalent state (Roaldset, 1975), and its kinetic is fast (Beall *et al.*, 1979; Aja, 1998; Coppin, 2002). The REE adsorption is controlled by the nature of the clay minerals, and the pH and ionic strength of the solution (Laufer *et al.*, 1984; Aja, 1998; Coppin *et al.*, 2002; Wan and Liu, 2005). The structure of the clay mineral plays on the ability of REEs to displace alkali-metals and alkaline earths (Bonnot-Courtois, 1981). The pH and the ionic strength play on the nature of the adsorption and on the amount of REEs adsorbed onto clay minerals. At acidic pH and low ionic strength, REEs adsorb as outer-sphere complexes onto basal surfaces (weak physiosorption, related to the permanent structural charge), whereas at alkaline pH they adsorb as inner-sphere complexes onto

amphoteric sites at the edges of the particles (strong chemisorption, variable pH-dependent charge). At last, REE adsorption generally increases with increasing pH (Aja, 1998; Coppin, 2002). Desorption of REEs from clay minerals is also pH dependent (Ran and Liu, 1992; Wen *et al.*, 2002), but limited and slow (Bonnot-Courtois, 1981; Laufer *et al.*, 1984).

Because of these properties, the different types of clay minerals do not exhibit the same REE composition (Cullers *et al.*, 1975; Coppin *et al.*, 2002; Compton *et al.*, 2003; Wan and Liu, 2005). Table 6 recaps and compares the REE signature of the different types of clay minerals. Chlorite is the REE-richest clay mineral. Smectite and montmorillonite are depleted in MREEs compared to LREEs and HREEs, while chlorite is enriched. Smectite and chlorite are enriched in HREEs compared to LREEs, while illite and vermiculites are enriched in LREEs. Chlorite, illite and vermiculite present a negative Ce-anomaly while smectite presents a positive one. The immobilization and fractionation of REEs by clay minerals will thus depend on the clay mineral composition of the soils. This explains the apparent contradictory behaviours described in the literature for unspecified mix of clay minerals that are either enriched in HREEs (see *e.g.* Bonnot-Courtois, 1981; Coppin *et al.*, 2002) or in LREEs (see *e.g.* Ran and Liu, 1992; Li *et al.*, 2006; Galán *et al.*, 2007) according to the different studies.

Table 6

Comparison of the REE contents and some properties of different types of clay minerals.

	Kaolinite	Chlorite	Illite	Vermiculite	Smectite	Montmorillonite	References
CEC	Low	Low	Moderate	High	High	High	Sposito, 1989
PZC	<4.5	<5	<5	<3	<8	<8	Lorenz, 1969; Goldberg <i>et al.</i> , 1996; Appel <i>et al.</i> , 2003
REE content ^{a)}	++/--	+	+/-	-	+/-	++/--	Cullers <i>et al.</i> , 1975; Nesbitt, 1979; Duddy, 1980; Braun <i>et al.</i> , 1993; Coppin <i>et al.</i> , 2002
LREE/HREE	<1<	<1	>1	>1	<1	<1<	Cullers <i>et al.</i> , 1975; Coppin <i>et al.</i> , 2002; Wan and Liu, 2005
MREE-enrichment	Yes/no	Yes	Yes/No	Yes/No	No	No	Cullers <i>et al.</i> , 1975; Coppin <i>et al.</i> , 2002
Eu/Eu*	<1<	<1	<1	>1	<1	<1	Cullers <i>et al.</i> , 1975; Condie <i>et al.</i> , 1995; Coppin <i>et al.</i> , 2002
Ce/Ce*	<1<	<1	<1	<1	>1	<1<	Cullers <i>et al.</i> , 1975; Bonnot-Courtois, 1981; Dubiel <i>et al.</i> , 1997; Coppin <i>et al.</i> , 2002

^{a)}The sign + and – denote respectively high and low REE content within the clay minerals. The sign +/- means that the clay mineral can have high or low REE content, but in a restricted range, while the sign ++/-- implies a broader range of concentration.

5.2. Fe-Mn-oxide formation

Weathering of primary minerals release Fe²⁺ and Mn²⁺ into soil solution that, for a part of them, reprecipitate within Fe- and Mn-oxides (Sposito, 1989). We discuss here the consequences of the formation of these different oxides on the REE redistribution.

Oxides of Fe and Mn are known to contain REEs (Rankin and Childs, 1976; Walter, 1991; Palumbo *et al.*, 2001), in varying amounts according to the soil type (Li *et al.*, 1998; Wang *et al.*, 2001; Zhang and Shan, 2001) and to depth (Land *et al.*, 1999; Yan *et al.*, 1999), without correlation with Fe and Mn contents (Steinmann and Stille, 1997; Land *et al.*, 1999;

Yan *et al.*, 1999). Scavenging of REEs by Fe-Mn-oxides can proceed through one or a combination of the following mechanisms: coprecipitation; adsorption; surface complex formation; ion exchange; and penetration of the lattice (Courtois, 1974; Chao and Theobald, 1976; Cao *et al.*, 2001). However, ionic radii differences between REEs and Fe and Mn imply that:

- (i) REEs can hardly substitute for Fe and Mn in the lattice of Fe-Mn-oxides (Braun *et al.*, 1993);
- (ii) REEs, as other trace elements, hinder the crystallization of Fe-Mn-oxides (Cornell and Giovanoli, 1987);
- (iii) Fe-oxides tend to expulse REEs during ageing and crystallization process (Courtois, 1974);
- (iv) as a consequence REE contents are generally higher in amorphous Fe- and Mn-oxides, than in crystalline ones (Courtois, 1974; Land *et al.*, 1999; Yan *et al.*, 1999; Compton *et al.*, 2003).

As incorporation of REE in Fe-Mn-oxide structure is limited, sorption is one of the main mechanisms of REE scavenging onto Fe-Mn-oxides, that is why their PZC should be considered since it will greatly influence this scavenging. The PZC of Fe-Mn-oxides rank as follow: Mn-oxides (*e.g.* birnessite or vernadite, around 2) > Fe-oxides (*e.g.* goethite, lepidocrocite, hematite, around 5.3-6.5) > amorphous Fe-oxides (*e.g.* ferrihydrite, around 5.3-8.8) (Parks, 1965; Schwertmann and Fechter, 1982; Goldberg *et al.*, 1996; Appel *et al.*, 2003). As a consequence, under soil pH conditions, Mn-oxides are more susceptible to have a significant negative residual charge. This results in a higher REE sorption capacity of Mn-oxides than Fe ones (Piper, 1974; Elderfield and Greaves, 1981; Walter, 1991), and a faster kinetic of REE sorption onto Mn-oxides (Koeppenkastrup and De Carlo, 1992).

The fractionation of LREEs, MREEs and HREEs in Fe- and Mn-oxides is subjected to debates (Land *et al.*, 1999). Some are enriched in HREEs (Elderfield and Greaves, 1981; Marker and de Oliveira, 1994; Huang and Wang, 2004), as expected by coordination numbers and electronegativity (Tables 1 and 2; Henderson, 1984), while others are enriched in LREEs (Courtois, 1974; Bernat, 1975; Koeppenkastrup and Decarlo, 1993). A MREE-enrichment is observed in some cases.

In Fe- and Mn-oxides, the Eu-anomaly is weak, sometimes positive, sometimes negative (Bernat, 1975; Addy, 1979), without significant relationship with Fe contents (Philpotts, 1970).

All soil, amorphous or crystalline, Fe-Mn-oxides, nodules, or concretions display a positive Ce-anomaly (Rankin and Childs, 1976; Xing and Dudas, 1993; Steinmann and Stille, 1997; Land *et al.*, 1999; Yan *et al.*, 1999; Coelho and Vidal-Torrado, 2000; Marques, 2000; Palumbo *et al.*, 2001; Ma *et al.*, 2002; Compton *et al.*, 2003; Huang and Wang, 2004). Fe-Mn-oxides thus particularly trap Ce. As a proof, in the oxidized zone of a lateritic profile, Ma *et al.* (2002) measured that up to 70% of total Ce was bound to Fe-Mn-oxides.

As for clay minerals, these differences are probably related to the proportions of the different Fe-Mn-oxides in presence. Indeed, amorphous Fe-Mn-oxides do not display a significant LREE/HREE fractionation, but rather a MREE-enrichment (Steinmann and Stille, 1997; Land *et al.*, 1999; Yan *et al.*, 1999), while LREEs sorbs preferentially and more rapidly on Mn-oxides than HREEs (de Baar *et al.*, 1988), particularly with increasing pH in solution (Fendorf and Fendorf, 1996; Ohta and Kawabe, 2001).

These differences may also be linked to their way of formation and to the solution composition. The MREE-enrichment appear more often in Fe-Mn-oxides formed at pH>5 in low-salinity solutions with a low organic acid content (Bau, 1999; Ohta and Kawabe, 2001; Davranche *et al.*, 2004; Pourret *et al.*, 2007b).

5.3 Formation of pedogenetic carbonates

Pedogenetic carbonates can be formed in soils in two main contexts: either in soils undergoing decalcification and subsequent precipitation at depth of carbonates, or in arid soils by ascension of calcium through the soil due to evaporation (Bockheim and Gennadiyev, 2000). In arid to semi-arid soils, the evaporation of the soil solution (Bellanca and Neri, 1993; Salomon and Pomel, 1997) or the biological influence (Phillips *et al.*, 1987) induce the precipitation of pedogenetic carbonates at or near the soil surface, which may cause their accumulation in a cemented horizon, known as calcrete. In carbonated soil, carbonates are dissolved at the soil surface and Ca is leached through the soil profile (Bellanca and Neri, 1993). Secondary carbonates then precipitate at depth where pH and pCO₂ increase (Bellanca and Neri, 1993; Arakaki and Mucci, 1995). The carbonate saturation is reached. The secondary carbonates generally overgrow primary ones and precipitate as coating or as concretions or may form cemented petrocalcic or petrogypsic horizons (West *et al.*, 1988; Reheis *et al.*, 1992; Shankar and Achyuthan, 2007).

In soil solution, REE complex with carbonate ions, and migrate into soil profile, as dissolved carbonates enhance the mobility of REEs (Walter, 1991; Land *et al.*, 1999). This complexation increases with increasing pH of soil solution and is the highest at pH 10 (Pourret *et al.*, 2007b). REEs are mainly transported as bicarbonates (REEHCO₃)²⁺, then as carbonates (REECO₃)⁺, polycarbonates – REE(CO₃)₃³⁻ and (REE(CO₃)₄)⁵⁻ (Pang, 1999) – and free species REE³⁺. Carbonate complexes do not fractionate REEs, while bicarbonate complex more HREEs than LREEs (Cantrell and Byrne, 1987; Lee and Byrne, 1993; Pourret *et al.*, 2007b). Besides, HREE (bi)carbonate complexes have a higher solubility than the LREE ones (McLennan and Taylor, 1979; Michard *et al.*, 1987), due to the increasing stability constant for (bi)carbonate complexes from La to Lu (Lee and Byrne, 1993). Therefore, soil solution will preferentially carry HREEs released by carbonate dissolution (Koppi *et al.*, 1996) and only few Ce compared to the other LREEs.

Soil solution migrates and REE carbonate complexes precipitate when reaching adequate soil pH conditions (Bellanca and Neri, 1993; Arakaki and Mucci, 1995) or because of oversaturation during evaporation (Bockheim and Gennadiyev, 2000). REEs are then mainly incorporated into carbonate minerals through isomorphic exchange for Ca²⁺ in the CaCO₃ lattice, because of the similarity of REE³⁺ and Ca²⁺ ionic radius (Table 1; Reeder and America, 1983).

The pedogenetic carbonates formed are expected to be HREE-enriched compared to LREEs (Land *et al.*, 1999; Yan *et al.*, 1999; Compton *et al.*, 2003), with a negative Ce-anomaly and without Eu-anomaly (Steinmann and Stille, 1997; Yan *et al.*, 1999; Huang and Wang, 2004). They also sometimes display MREE-enrichments (Steinmann and Stille, 1997; Land *et al.*, 1999).

Thus, the identification of pedogenetic carbonates from parent carbonates, that may be uneasy (West *et al.*, 1988; Kraimer *et al.*, 2005), is likely possible on the basis of HREE- and LREE-fractionations. MREEs, Eu and Ce are not of interest.

6. Impact of biological recycling and organic matter on REE mobilization

6.1 Biological recycling of REEs and REE mobilisation

Impact of plant recycling on element budget in soils is well known, leading to an enrichment in the topsoil, especially in forest context (Toutain, 1974). This recycling has strong consequence in terms of soil evolution, as demonstrated by Lucas *et al.* (1993) for the stability of kaolinites in Amazonian latosols. As other elements, REEs are recycled by plants (Tyler, 2004b; Hu *et al.*, 2006b).

Plant uptake depends on several soil parameters, notably pH, Eh, CEC, contents of clay minerals and of Fe-Mn-oxides (Wahid *et al.*, 2003; Tyler, 2004b; Hu *et al.*, 2006b; Miao *et al.*, 2007). It increases with decreasing soil pH, as well as with decreasing Eh, with increasing clay mineral and organic matter (OM) contents. Besides, the uptake varies greatly according to the plant under consideration (Tyler, 2004b; Hu *et al.*, 2006b), but transfer from soils to plants remains usually limited (Tyler, 2004b; Hu *et al.*, 2006b). Except some hyperaccumulators, such as ferns, REE contents in plants are usually low, but may vary of several orders of magnitude, ranging between few ng g⁻¹ to few mg g⁻¹ dry weights. The different parts of plants do not accumulate similarly REEs (Wahid *et al.*, 2003; Tyler, 2004b; Wang *et al.*, 2005; Hu *et al.*, 2006b), and are generally ranked as:

roots > leaves/needles > stems/branches > flowers/fruits/seeds

Plant uptake does not exhibit a pronounced preference for a REE group (Tyler, 2004b). Only slight and not systematic fractionations of either LREEs, or MREEs or HREEs are recorded by different studies (Wang *et al.*, 2005; Ding *et al.*, 2006; Miao *et al.*, 2007). Nevertheless, individual REE may sometimes be fractionated during uptake: positive anomalies for Eu (Wang *et al.*, 2005; Ding *et al.*, 2006), Sm (Wahid *et al.*, 2003), Tb and Nd (Wang *et al.*, 2005) were recorded.

As a conclusion, plant uptake only slightly fractionates REEs from the soil. However, this uptake may induce, as for other elements (Toutain, 1974), a biological accumulation of REEs in the upper soil horizons. In addition, REE recycling by plants modifies their speciation: they are preferentially uptaken by plants in the weakly bound REE pool, and returned to the soil as bound to OM. The Nd-, Sm-, Eu- or Tb-anomalies may be useful to evaluate the amount of REEs transferred to plants, which highly depend on plant and soil types.

6.2. Complexation by organic matter and REE mobilisation

Organic matter has many negatively charged groups per unit dry weight, and thereby, a high capacity to complex, adsorb or chelate positively charged REEs (Tyler, 2004b, 2004a; Pourret *et al.*, 2007a). The REE content bound to OM varies strongly according to the type, composition and content of OM, to the pH of the soil, and to the redox conditions (Wang *et al.*, 2001; Grybos *et al.*, 2007). The complexes formed by OM with HREEs are more stable than with LREEs (Table 5; Henderson, 1984; Byrne and Li, 1995; Sonke, 2006). As a consequence, OM is enriched in HREEs and MREEs compared to LREEs (Land *et al.*, 1999; Aubert *et al.*, 2001; Aubert *et al.*, 2004). Ma *et al.* (2002) observed a strong positive Ce-anomaly in REE patterns of OM, probably because humic acids have a larger complexation capacities and higher formation constants with respect to Ce than to the other LREEs (Geng *et*

al., 1998), but also because it can precipitate as cerianite CeO₂ at the surface of colloids (Sholkovitz, 1992).

Soil OM, because of its mobility, plays a key role in the development of some soil types as in podzolization (Duchaufour, 1957; Buurman and Jongmans, 2005; Sauer *et al.*, 2007). In podzols, the percentage of total REEs bound to OM increases with soil depth (Land *et al.*, 1999; Aubert *et al.*, 2004). This is either due to a migration of REEs as organic complexes or to their readsorption onto OM as pH increase at depth (Pourret *et al.*, 2007a). This phenomenon is especially marked for HREEs and MREEs compare to LREEs (Land *et al.*, 1999; Aubert *et al.*, 2004). As HREE complexes are more stable than LREE ones (Table 5), the preferential scavenging of HREEs suggest that accumulation of REEs at depth is more linked to a migration of these elements as organic complexes. These fractionation can be use to detect early stages of podzolisation in soils.

7. Remobilisation of secondary mineral by pedogenetic processes and REE mobilisation

7.1. Lessivage

Lessivage or argilluviation (eluviation and illuviation) is the result of a physical transfer of fine particles in soils from a so-called eluviated horizon to a so-called illuviated horizon (Duchaufour, 1972; Jamagne and Pédro, 1981). As a result, the eluviated horizon is depleted in fine particles while the illuviated horizon is enriched. This process was described in a large range of soils (Bockheim and Gennadiyev, 2000). The translocated particles consist mainly in clay minerals (Duchaufour, 1972; Jamagne and Pédro, 1981). As clay minerals contain REEs, as discussed previously, lessivage certainly leads to redistribution of REEs within the soil profile.

On a theoretical point of view, as lessivage is purely physical, this REE redistribution should not induce any REE fractionation and simple mass balance calculation on the REEs should allow estimating the quantity of clay eluviated and illuviated. In practice, Laveuf *et al.* (2008, cf. Chapitre 4.2.1.) demonstrated that the situation is more complex.

Indeed, lessivage preferentially transfer the smallest clay minerals than the biggest ones (Nguyen Kha and Paquet, 1975; De Coninck *et al.*, 1976; Jamagne and Pédro, 1981). Since all clay minerals do not exhibit the same REE compositions (Cullers *et al.*, 1975; Coppin *et al.*, 2002; Compton *et al.*, 2003; Wan and Liu, 2005), as previously detailed (Table 6), fractionations likely occur during lessivage.

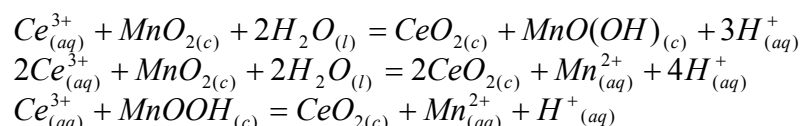
From the comparison of the REE signature of the clay minerals (Table 6), the following conclusions can be given. Since the Eu-anomaly is always negative, except for vermiculite, Eu may be used as a tracer of lessivage: the Eu-anomaly of the eluviated horizon is expected to increase, while that of the illuviated horizon is expected to decrease. The MREE signature may be used as a tracer, depending on lessivage intensity. For a restricted lessivage, mobilizing mainly the smallest clay minerals, depleted in MREEs, the MREE content of the eluviated horizon will increase relatively with respect to LREEs and HREEs, while, in the illuviated horizon, MREEs will be relatively depleted with respect to LREEs and HREEs. For a more intense lessivage, mobilizing all sizes of clay minerals, no REE fractionation will be observed as clay fractionation will be less pronounced. In addition to these potential tracers, Nd can also be used as a tracer, since it shows a great association with illuviated clay minerals according to Aide and Smith-Aide (2003), notably with illite (Hu *et al.*, 2006b).

7.2 Hydromorphy and soil degradation

Redox processes are very common in soils (Bockheim and Gennadiyev, 2000). They are responsible for bleaching as well as the segregation of Fe and Mn as oxide coatings, as concretions or as pedotubules (Chao, 1972). They are either due to an excess of water into the soil or to a large amount of OM as it is the case in podzolisation (Lindsay, 1991; Schwertmann, 1991). In podzolisation Fe-oxides are reduced by OM and Fe is translocated downwards as organic complex, then reprecipitates (Buurman and Jongmans, 2005; Sauer *et al.*, 2007), notably as ferrihydrate (Schwertmann and Fischer, 1973). Because of the preferential translocation of HREEs as organic complexes, the Fe-oxides that precipitate in the podzolic horizon are rather HREE-enriched compared to LREEs (Land *et al.*, 1999; Aubert *et al.*, 2004). The amorphous Fe-oxides are MREE-enriched (Land *et al.*, 1999; Aubert *et al.*, 2004).

REEs are strongly linked to Fe-Mn-oxides as described before. Among REEs, Ce and Eu display two redox states under earth surface conditions (Henderson, 1984) and are thus of peculiar interest to trace redox conditions. Indeed REE fractionations have been shown to be related to drainage conditions (Marker and de Oliveira, 1994). However, the reduction of Eu require strong reducing conditions (Ronov *et al.*, 1967; Courtois, 1974; Bonnot-Courtois, 1981; Henderson, 1984; Panahi *et al.*, 2000) rarely encountered in soils. As a consequence, the Eu-anomaly cannot be used to trace redox processes in soils. Since the oxidation of Ce(III) to Ce(IV) occur at Eh frequently encountered in soils, around 0.3 V (Ronov *et al.*, 1967; Courtois, 1974), our attention will be focussed on Ce.

Observations and experiments suggest that the occurrence of a positive Ce-anomaly is linked to oxidation of Ce(III) to Ce(IV) (Takahashi *et al.*, 2000) leading to the precipitation of cerianite CeO_2 , coupled with the reduction of Mn(IV) to Mn(III) at the surface of Mn-oxides (Ran and Liu, 1992; Marker and de Oliveira, 1994; Bau, 1999; Ohta and Kawabe, 2001), following:



This is consistent with standard free energy changes of both half reactions (Elderfield and Greaves, 1981), and with the similar oxidation-precipitation and reduction-dissolution cycling of MnO_2 and CeO_2 (Brookins, 1988; de Baar *et al.*, 1988). The coupling of both reactions is also relevant, considering the higher Ce enrichment of Mn-oxides than Fe ones, even within nodules or concretions (Piper, 1974; Rankin and Childs, 1976; Elderfield and Greaves, 1981; Braun *et al.*, 1990; Koppi *et al.*, 1996). For instance, Coelho and Vidal-Torrado (2000) found Ce accumulations only into petroplinthic nodules with Mn coatings, probably deposited during the definitive lowering of a water table.

Under oxidative conditions, Fe and Mn will precipitate as oxides incorporating preferentially Ce, as cerianite, over the other REEs, which leads to the apparition of a positive Ce-anomaly. On the contrary, under reducing conditions, these Fe-Mn-oxides are dissolved, releasing all REEs (Cao *et al.*, 2001), but Ce as cerianite, whose dissolution is more related to pH than to Eh or pO_2 (see equations above), will thus not dissolve significantly under reducing conditions. The positive Ce-anomaly will remain while Fe- and Mn-oxides disappear. That is why Koppi *et al.* (1996) found positive Ce-anomaly in bleached clayey domains during flooding and drainage. The use of Ce to trace reducing conditions is thus

linked to the pH of the soil. Therefore, redox processes, could be traced using the Ce-anomaly, resulting from the occurrence of cerianite.

8. Conclusions

We discussed here the fate of REEs through pedogenetic processes in order to evaluate their ability to trace these processes, *i.e.* to better quantify the respective contribution of the different processes on pedogenesis.

During weathering a significant part of REEs from the parent material are lost, even where similar or higher REE concentrations are recorded in soils compare to the parent material. This was demonstrated by mass balance calculations. Weathering also fractionates REEs on the basis (i) of the nature and relative abundance of the primary minerals hosting them; (ii) of the weathering conditions (intensity, pH, complexes in soil solution...) and (iii) of the nature and relative abundance of the secondary minerals formed.

The recycling of REEs by plants induces a weak mobilization of REEs and their accumulation in the topsoil, with a modification of their speciation from the more soluble fractions to the one bound to organic matter.

Lessivage preferentially mobilises the smallest clay minerals over the biggest ones. These minerals having different REE signatures, complex fractionations can result from this process depending of its intensity and of the clay mineral composition of the soil. The use of the MREE-enrichment and of the Eu-anomaly as tracers of lessivage seems notably promising.

The use of the positive Ce-anomaly to trace redox processes is well evidenced and relevant according to our literature review, since Ce concentrates, as cerianite, in Fe-Mn-oxides and notably in Mn ones. Besides, Mn-oxides are expected to be LREE-enriched and amorphous Fe-oxides MREE-enriched during their formation, allowing using them to trace their oxidation/precipitation and reduction/dissolution. However, as Fe- and Mn-oxides commonly occurred as mixed phases, it is necessary to well characterize each oxide type in Fe-Mn-oxides.

We evidenced that REEs could interestingly trace some widespread pedogenetic processes. These elements are certainly more powerful tracers than trace elements, as they are more evenly distributed into minerals; they mainly originate from parent materials with very limited anthropogenic sources; and they evolve as a group through weathering and pedogenesis, with appearance of internal fractionations and/or anomalies.

However, due to the complexity of pedogenetic process on REE fate, no valuable information will be obtain without high characterization of the REE-bearing minerals, a careful choice of the reference used to normalise them and a mass balance calculation.

9. Acknowledgments

The authors are grateful to the INRA department “Environnement et Agronomie”, through the “Projet Innovant Terres Rares” and to the Région Centre, France, for their financial support.

4.2. Mise en point méthodologique d'utilisation des terres rares comme traceurs des processus pédogénétiques et validation de cette méthode sur un autre site

Ce sous-chapitre est subdivisé en deux sous-parties : la première partie consiste en un article en anglais publié dans CR Geoscience sur la mise au point méthodologique d'utilisation des terres rares comme traceurs des processus sur le site de l'Auxois ; la seconde partie est une validation de cette méthodologie sur le site de la Terre-Plaine et propose des améliorations au vu des conclusions de la première partie.

4.2.1. Mise en point méthodologique d'utilisation des terres rares comme traceurs des processus pédogénétiques

CR Geoscience 2008, 340: 523-532 (doi:10.1016/j.crte.2008.07.001)

Rare Earth Elements as Tracers of Pedogenetic Processes

Cédric Laveuf^{a,*}, Sophie Cornu^a, Farid Juillot^b

^a INRA, UR0272 Science du Sol, Centre de recherche d'Orléans, BP 20619, 45166 Olivet cedex, France.

^b IMPMC, UMR CNRS 7590, Universités Paris 6 et 7 – IPGC, 75252 Paris cedex 05, France.

Abstract

To discern and quantify, the impact of the successive processes on pedogenesis, an approach using REE as tracers of processes was developed. Considering that a given horizon results from the evolution of the underlying horizon under a given pedogenetic process, we proposed to normalize the REE contents of that horizon by the REE contents of the underlying horizon. Pedological features representative of the considered pedogenetic process can also be used. We applied it to a well-characterized solum developed from limestones that underwent two different phases of redox conditions. Results evidenced that the two stages of redox conditions acted differently on REE mobilization. The first stage induced the enrichment of Ce in Fe-Mn concretions, while the second stage induced an impoverishment in MREE following the dissolution of the Fe/Mn-(hydr)oxides cementing the finest soil fractions. This approach of normalization emphasizes the potential of REE as tracers of pedogenetic processes, even if some difficulties remain.

* Corresponding author.

E-mail: laveuf@orleans.inra.fr (C.Laveuf)

Résumé

Les terres rares comme traceurs des processus pédogénétiques. Pour discerner et quantifier l'impact des processus successifs sur la pédogenèse, une approche utilisant les Terres Rares (TR) comme traceurs de ces processus a été développée. Considérant qu'un horizon résulte du processus pédogénétique qui affecte l'horizon sous-jacent, nous proposons de normaliser les concentrations en TR de cet horizon, ou du trait pédologique représentatif du processus pédogénétique considéré, par les concentrations en TR de l'horizon sous-jacent. Cette approche a été appliquée à un solum bien caractérisé issu de calcaires qui a subi deux cycles de conditions rédox. Ces deux cycles rédox ont agi différemment sur la mobilisation des TR, le premier induisant un enrichissement en Ce des concrétions Fe-Mn, et le second induisant un appauvrissement en TR moyennes suite à la dissolution des (hydr)oxydes Fe/Mn cimentant les particules fines du sol. Cette approche de normalisation illustre le potentiel des TR comme traceurs des processus pédogénétiques, même si certaines difficultés restent à résoudre.

Keywords: Lanthanides, soil, limestone, redox conditions, decarbonation

Mots clés : Lanthanides, sol, roches calcaires, conditions redox, décarbonation

1. Introduction

To understand pedogenesis, studies classically rely on the interpretation of the distribution of the major and minor elements and of the mineralogical phases that constitute the different soil horizons. Since these elements are localized in a wide variety of mineral phases, their mobilization is not specific of a given pedogenetic process, hence the difficulties encountered to infer and quantify the role of these different processes on pedogenesis. In addition, minor elements can originate from both natural and anthropogenic sources, which render their use as tracers of pedogenetic processes less straightforward. Rare earth elements (REE), *i.e.* the 14 natural elements of the lanthanide series (La to Lu), have a close but however distinct geochemical behavior in natural systems, according to the individual REE or the group of REE under consideration (Henderson, 1984). Due to their properties, REE have already been extensively used as tracers of genesis and of origin, or of various geochemical processes in several disciplines, like hydrology (Leleyter *et al.*, 1999; Pinto-Coelho *et al.*, 1999), geochemistry (Iqdari *et al.*, 2003) or geology (Moukadiri and Pin, 1998; Bentahila *et al.*, 2002). The results of such studies let us suppose that the physical and chemical behaviors of these elements could be rather specific of a given pedogenetic process, and that REE could be efficiently combined with the classical study of major elements and mineral phases to trace pedogenetic processes. However, whereas REE in soils mainly arise from parent materials by opposition to anthropogenic sources (Hu *et al.*, 2006), up to now, the potential of REE as tracers of pedogenetic processes remains almost unexploited and the few works existing in soil science mainly deal with the geochemical fate of REE but rarely with their pedological behavior (see however, Braun *et al.*, 1993; Dequincey *et al.*, 2002; Aide and Smith-Aide, 2003; Chabaux *et al.*, 2003; Dequincey *et al.*, 2006). In addition, considering their wide ranges of concentrations and their close behavior in natural systems, REE concentrations in the studied material are normalized with respect to a chosen reference material to be compared (Henderson, 1984) and in the case of pedological studies the geological bedrock is

usually chosen as reference for the normalization of all horizons (e.g., Dequincey *et al.*, 2002; Aide and Smith-Aide, 2003; Chabaux *et al.*, 2003; Dequincey *et al.*, 2006). Since soil horizons result from the action of several pedogenetic processes, this way of normalization does not allow to differentiate the impact of the successive processes on REE mobilization.

This study presents an innovative methodology to use REE normalizations, which aims at separating the signal of a pedogenetic process from the others in order to discern their respective impact on REE mobilization and fractionation. Since pedological evolution results from successive transformation fronts of different pedogenetic processes (Boulet *et al.*, 1982; Fritsch *et al.*, 1986; Lucas *et al.*, 1988), the differentiation of pedological features are mainly expressed behind the transformation front of the process creating them and before the following front, *i.e.* more or less in a given horizon. Thus, normalizing the REE concentrations of the pedological feature to the REE concentrations of the material from which it developed should allow to differentiate the impact of the pedogenetic process involved. This approach is only possible if we have previously determined:

- which pedological feature is the most representative of the action of each pedogenetic process;
- which horizon is the most representative of each pedogenetic process;
- what is the material from which the pedological feature developed.

In the present study, this methodology has been applied to a solum that displays (Baize and Chrétien, 1994):

- a pedogenesis sufficiently expressed, so that REE fractionations are strongly pronounced, hence an old solum;
- high REE concentrations to facilitate the analyses;
- a well-known succession of pedogenetic processes.

2. Material and methods

2.1. Pedological context

The chosen solum, at the northeastern margin of Morvan Mountain (Bourgogne, France), consists in the non-truncated end-member of a soil catena. It developed in the clay material resulting from the autochthonous decarbonation of Sinemurian- and Lotharingian-aged limestones that consist in hard and compact crystalline calcite. These limestones display high REE contents following mineralization events during the Lias epoch (Baize and Chrétien, 1994). The solum then underwent successive pedogenetic processes, namely succession of oxidative and reductive conditions and eluviation (Baize and Chrétien, 1994). It is composed of six horizons A, E, Bgd, BP, Bc and C (Fig. 1), each one being considered as more representative of a given pedogenetic process (Table 1; Laveuf *et al.*, 2009, cf. Chapitre 3.1.).

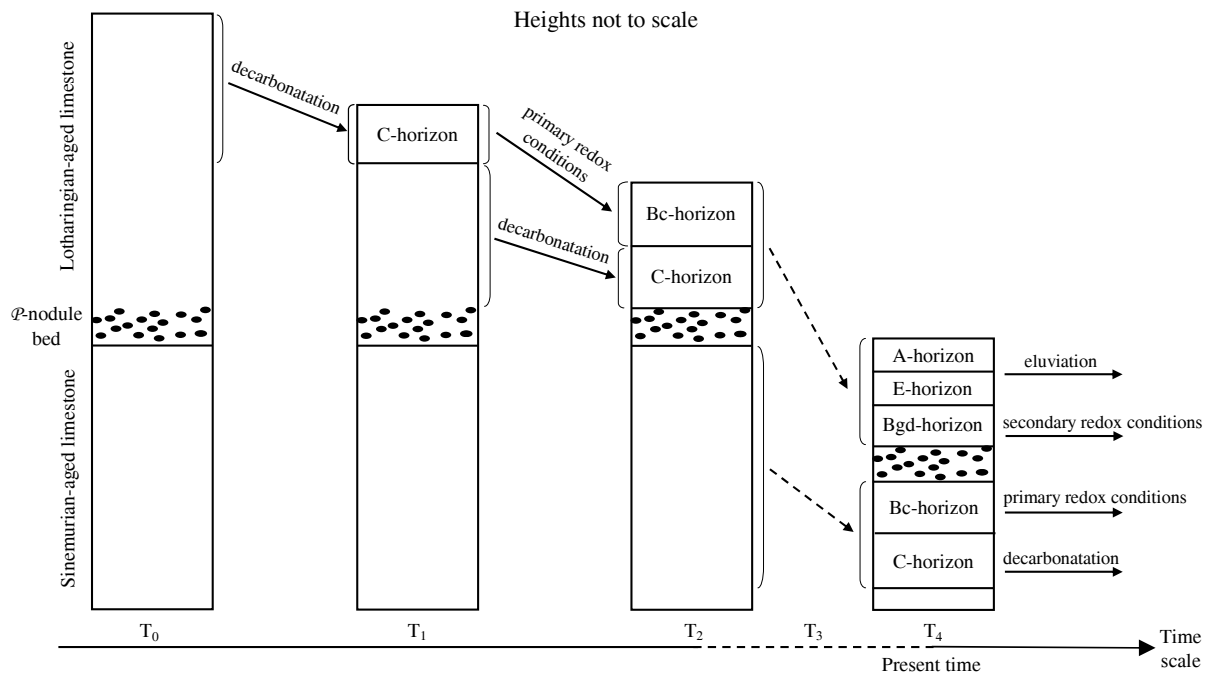


Fig. 1. Pedogenesis of the studied solum based on the vertical transformation fronts of the successive pedogenetic processes. Processes identified by Baize and Chrétien (1994) and Laveuf *et al.* (2009, cf. Chapitre 3.1.).

Pédogenèse du solum étudié basée sur les fronts de transformation verticaux des processus pédogénétiques successifs. Les processus ont été identifiés lors d'études antérieures (Baize et Chrétien, 1994 ; Laveuf et al., 2009, cf. Chapitre 3.1.).

Table 1

Pedogenetic processes, with their location in the solum horizons, and the derived pedological features. Normalization proposed to differentiate their respective impact on REE mobilization.

Processus pédogénétiques, avec leur localisation dans le solum, et les traits pédologiques dérivés. Normalisation proposée pour différencier leur impact respectif sur la mobilisation des Terres Rares.

Pedogenetic process	Horizon of the considered transformation front	Pedological feature derived	Normalization proposed (fraction studied / material from which it developed)
decarbonation	C	residue of decarbonation	residue of decarbonation / parent limestone
primary redox	Bc	Fe-Mn concretions	Fe-Mn concretions / bulk fraction of the C-horizon
secondary redox	Bgd	fraction <2 µm without Fe/Mn-(hydr)oxides	residue of extraction / fraction <2 µm
eluviation	A and E	fraction <2 µm	fraction <2 µm / fraction <2 µm of the Bgd-horizon

2.2. Pedogenetic processes and pedological features

For complete description of the soil profile and pedological processes, refer to [Laveuf et al. \(2009, cf. Chapitre 3.1.\)](#). We summarize here the main features.

In the C-horizon, not completely decarbonated, the dominant process is decarbonation. To study this process, we experimentally decarbonated parent limestones (see below). The residues of decarbonation were used as pedological features of this process instead of the C-horizon, as we could not find a horizon equivalent to the C one for the Lotharingian-aged limestone.

In the Bc-horizon, the dominant process is the occurrence of seasonal variations of redox conditions in the zone of water-table fluctuations, leading to the concentration and individualization of Fe/Mn-(hydr)oxides as Fe-Mn concretions ([Baize and Chrétien, 1994; Laveuf et al., 2009, cf. Chapitre 3.1.](#)). This process is called hereafter primary redox conditions.

The occurrence of the BP-horizon (horizon rich in phosphate nodules) results from the inheritance of a bed of pluricentimetric phosphate nodules at the bottom of the Lotharingian-aged limestone ([Mouterde, 1952; Baize and Chrétien, 1994](#)). Indeed, a precedent investigation on Zn behavior indicated that pedogenesis does not greatly influence the mineralogical composition of the limestone-phosphate nodules ([Laveuf et al., 2009, cf. Chapitre 3.1.](#)). In this study, the inheritance of the REE composition will be checked by comparing the REE patterns of the BP-horizon and of the limestone-phosphate nodules. The horizons underlying the BP-horizon are considered as deriving from the autochthonous weathering of the Sinemurian-aged limestone, while the others are considered as deriving from the autochthonous weathering of the Lotharingian-aged limestone ([Baize and Chrétien, 1994](#)).

In the Bgd-horizon, the dominant process is the occurrence of unfavorable redox conditions for the stability of dispersed Fe/Mn-(hydr)oxides, leading to the dissolution of these cements of finest particle-size fractions ([Laveuf et al., 2009, cf. Chapitre 3.1.](#)). This process is called hereafter secondary redox conditions.

In the A- and E-horizons, the dominant process is eluviation ([Laveuf et al., 2009, cf. Chapitre 3.1.](#)). This process leads to the translocation of fines particles (mainly phyllosilicates in this solum) after a more or less complete dissolution of the cementing Fe/Mn-(hydr)oxides and a sufficient desaturation of the adsorbing complex ([Bottner, 1972](#)).

2.3. Samplings and experiments

All horizons and both parent limestones were sampled.

Blocks of unweathered limestone samples without phosphate nodules and limestone-phosphate nodules were isolated from the bulk samples. Their carbonates were dissolved as follow. About 10 g of roughly grounded rock were put in closed batches with 30 mL of MilliQ[®] water and placed onto a magnetic agitator at room temperature. The pH was monitored along the experiment. A solution of HCl 1M was introduced drop by drop, regulating the flow so as the pH remained greater than 5 to avoid partial or total dissolution of Fe/Mn-(hydr)oxides or phyllosilicates.

The Fe-Mn concretions of the Bc-horizons larger than a 1 mm were handpicked and cleaned. For each horizon, the less than 2 μm particle-size fraction was separated from the bulk soil by sedimentation in deionized water according to the Stokes law, after a first wet-

sieve at 50 μm in deionized water. An eight-step extraction procedure, adapted from Hall *et al.* (1996) and Cornu *et al.* (2006), was performed on 1 g of the bulk sample ground to 50 μm for the A-, E-, Bgd- and C-horizons and of the less than 50 μm fraction for the Bc-horizon, as described by Laveuf *et al.* (2009, cf. Chapitre 3.1.). Chemical and mineralogical controls were performed during sequential extractions to verify the correct dissolution of the minerals and the recovery rates. All controls were found to be acceptable and are available in Laveuf *et al.* (2009, cf. Chapitre 3.1.).

All different limestone and soil fractions were analyzed for REE by ICP-MS after LiBO_2 fusion at the “Service d’analyse des roches et des minéraux of the centre de recherche pétrologique et géochimique” of the CNRS, Vandoeuvre-lès-Nancy, France (SARM-CRPG).

3. REE pattern of the parent limestones, the limestone-phosphate nodules and the bulk soil fraction of the different horizons

The REE patterns of the Lotharingian- and Sinemurian-aged limestones are similar (Fig. 2). Both limestones are slightly depleted in light REE (LREE, La to Pr) and heavy REE (HREE, Ho to Lu), and slightly enriched in medium REE (MREE, Nd to Dy) compared to the upper continental crust (UCC; Taylor and McLennan, 1985). This enrichment is characteristic of the Lias epoch (Lécuyer *et al.*, 1998; Picard *et al.*, 2002).

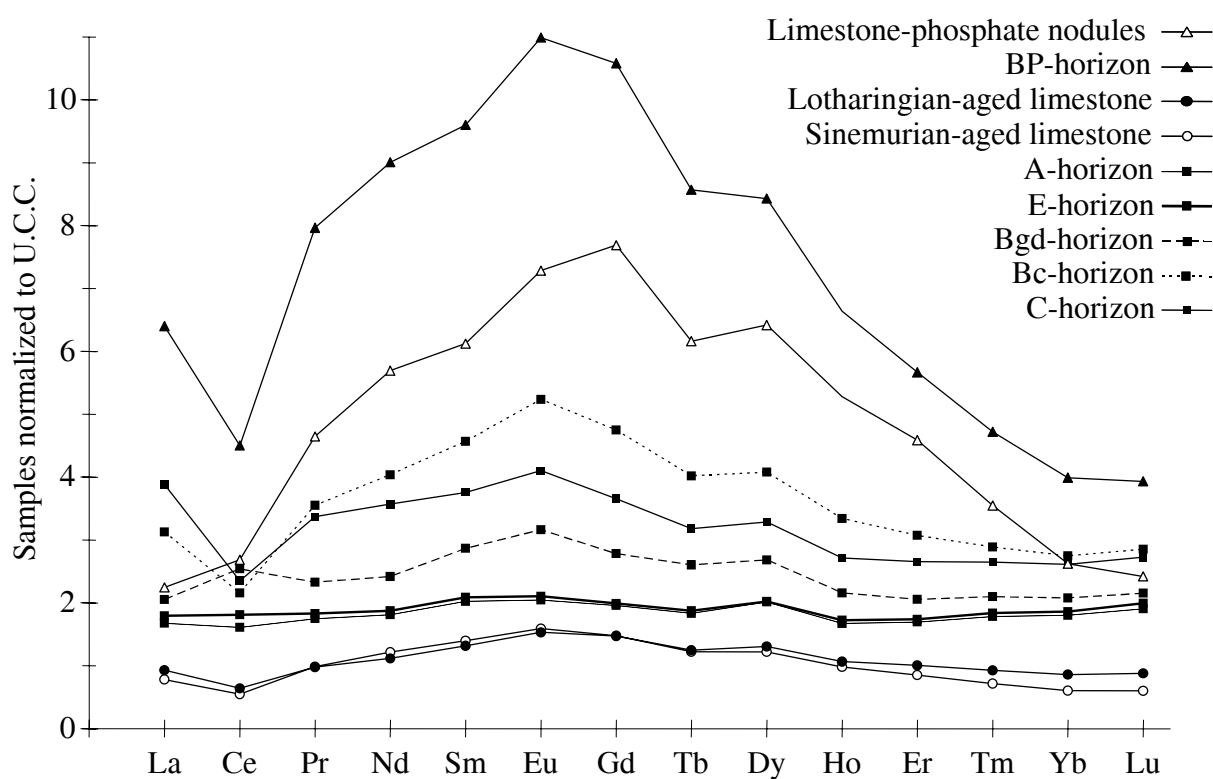


Fig. 2. REE patterns of parent materials (limestone-phosphate nodules and Lotharingian- and Sinemurian-aged limestones) and of the soil horizons normalized to the Upper Continental Crust (U.C.C.).

Spectres de terres rares des matériaux parentaux (nodules phosphatés du calcaire et calcaires d’âge Lotharingien et Sinémurien) et des horizons du solum normalisés à la Croûte Continentale Supérieure (U.C.C.).

The limestone phosphate nodules are enriched in all REE, notably in MREE, compared to the UCC (Fig. 2). This enrichment of the phosphate nodules, mainly composed of fluorapatite (Laveuf *et al.*, 2009, cf. Chapitre 3.1.), is related to the strong affinity of REE for phosphated compounds (Henderson, 1984). Experimental decarbonation of the limestone-phosphate nodules influenced slightly their composition, since their REE pattern remained flat and no REE losses could be recorded (Fig. 3). As the REE stocks released into solution during experimental decarbonation are assumed representative of those released into soil solution during pedogenetic decarbonation, these results indicate that pedogenetic decarbonation does not affect the REE composition of the limestone-phosphate nodules. The other pedogenetic processes do not influence their REE composition greatly, since the REE pattern of the BP-horizon, mainly composed of phosphate nodules, is close to that of the limestone-phosphate nodules (Fig. 2). These results confirm the inheritance of the phosphate nodules (Laveuf *et al.*, 2009, cf. Chapitre 3.1.) and justify that the BP-horizon, mainly inherited, is not taken into account in the rest of this paper.

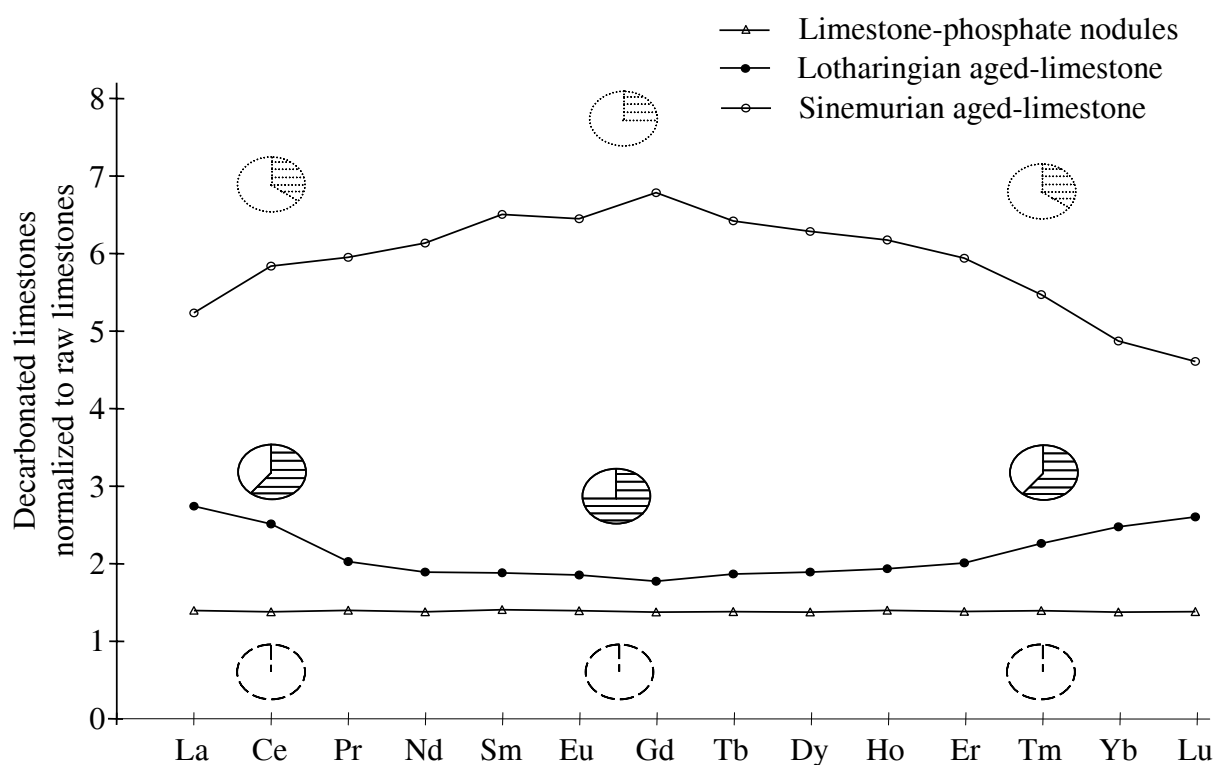


Fig. 3. REE patterns of the decarbonated geological parent materials (limestone-phosphate nodules and Lotharingian- and Sinemurian-aged limestones) normalized to their corresponding carbonated parent materials. The pie charts depict the stocks of LREE (La to Pr), MREE (Nd to Dy) and HREE (Ho to Lu) of the different geological materials and the striped zones represent the average percentage of REE released into solution during the experiment of decarbonation.

Spectres de Terres Rares dans les matériaux parentaux décarbonatés normalisés aux matériaux parentaux correspondants. Les graphiques à secteurs représentent les stocks de TR légères (La à Pr), moyennes (Nd à Dy) et lourdes (Ho à Lu) des différents matériaux parentaux et les zones hachurées indiquent le pourcentage moyen de TR libéré en solution au cours de l'expérience de décarbonation.

The soil horizons are enriched in REE compared to the UCC (Fig. 2) and to the corresponding parent limestones (Fig. 4). The REE patterns of the soil horizons normalized to the UCC discriminate three groups of soil horizons with contrasted REE signatures, A and E, Bgd and Bc and C (Fig. 2). Thus, the contrasted REE signatures of the different horizons normalized to their corresponding parent limestones result from pedogenesis and not from the change of reference between surface and deep horizons (Fig. 4). If all soil horizons are REE enriched compared to the parent limestone, this enrichment decreases when going from the deepest C-horizon toward the surface (A- and E-horizons). This evolution is likely due to pedogenesis, since this process, more marked in the surface horizons than in the deepest ones, is known to induce a depletion in all REE (see e.g., Koppi *et al.*, 1996; Land *et al.*, 1999; Aubert *et al.*, 2001) and consists in the first difference in REE signature between the different horizons. The second difference in REE signature among them is related to a preferential retention of Ce in the A- to Bc-horizons, which exhibit a large positive Ce anomaly. Considering the well-known redox sensibility of Ce, this difference between the different horizons likely reflects some pedogenetic processes connected to variations in redox conditions. These results indicate that several pedogenetic processes can modify the REE distribution, which emphasizes the need for a new approach, allowing a distinction between the respective impact of these successive pedogenetic processes on REE mobilization. This approach is described in the following sections.

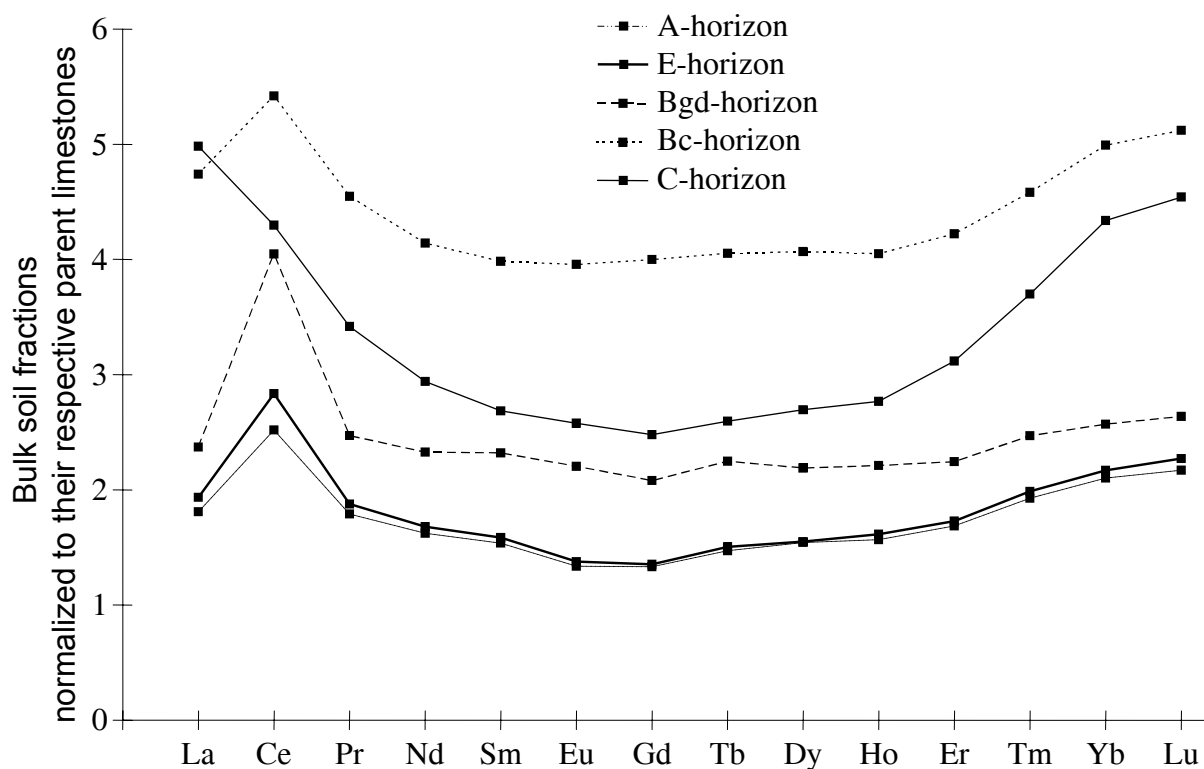


Fig. 4. REE patterns of the bulk soil fraction of each horizon normalized to the corresponding parent limestones. The A- to BP-horizons are issued from the weathering of the Lotharingian-aged limestone, while the Bc- and C-horizons are issued from the weathering of the Sinemurian-aged limestone.

Spectres de concentration des Terres Rares dans la fraction totale de chaque horizon normalisés au calcaire parental correspondant. Les horizons A à BP sont issus de l'altération du calcaire d'âge Lotharingien, tandis que les horizons Bc et C sont issus de l'altération du calcaire d'âge Sinémurien.

4. Impact of the successive pedogenetic processes on REE mobilization and fractionation

To differentiate the impact of the successive pedogenetic processes on REE mobilization and fractionation (Fig. 1), the main pedological features representing the main pedogenetic processes were normalized as proposed in Table 1.

4.1. Decarbonation

For both limestones, decarbonation induces REE enrichments in the residues (Fig. 3). The Lotharingian- and the Sinemurian-aged limestones are mainly composed of calcite (87.2 and 88.0%, respectively). During decarbonation, REE are enriched by the preferential dissolution of calcium carbonate that leads to a leaching of Ca and a residual enrichment of less mobile elements (Table 2). However, the two limestones displayed contrasted behaviors during the decarbonation experiment, with a loss of REE ranging from 25 to 75% of the REE stocks, depending on the limestone and group of REE under consideration (Fig. 3). Indeed, the REE loss was higher for the Lotharingian-aged limestone than for the Sinemurian-aged limestone and the Lotharingian-aged limestone preferentially lost MREE, while the Sinemurian-aged limestone preferentially lost LREE and HREE.

Table 2

Concentrations of major elements (in g/kg) in the bulk and the residues of the Lotharingian- and Sinemurian-aged limestones, with corresponding initial stock losses (in percentage) during experimental decarbonation.

Concentrations en éléments majeurs (en g/kg) des échantillons bruts et des résidus des calcaires d'âge Lotharingien et Sinémurien, avec les pertes correspondantes du stock initial (en pourcentage) durant la décarbonation expérimentale.

		Al	Ca	Fe	K	Mg	Mn	P	Si	Ti
		g/kg								
Lotharingian-aged limestone	Bulk	9.3	333.4	23.7	4.1	2.8	1.9	4.0	26.8	0.7
	Residue	65.9	14.4	164.0	28.4	7.3	0.9	14.4	182.6	5.1
	% lost	9	99	11	12	67	94	53	13	13
Sinemurian-aged limestone	Bulk	8.3	352.5	10.3	3.1	4.3	2.3	5.6	21.9	0.5
	Residue	59.3	91.7	81.4	21.3	6.2	0.4	44.6	162.8	3.9
	% lost	17	97	8	20	83	98	8	13	10

These differences in the geochemical behavior of REE between the two limestones may arise from differences in the REE-bearing minerals, as evidenced by their composition in major elements (Table 2). By comparing the stock losses of major elements during decarbonation, it appears that Al, K, Mg and P are not lost similarly in both limestones, while Ca, Fe, Mn, Si, Ti are about (Table 2). Indeed, the Lotharingian-aged limestone lost more P and less Al, K and Mg than the Sinemurian-aged limestone. The preferential loss of MREE in the Lotharingian-aged limestone may thus be related to a lower proportion of MREE in the residual minerals (Cao *et al.*, 2000) or to the occurrence of P-bearing minerals (Henderson, 1984). However, it is not due to a potential dissolution of some phosphate nodules, which are noteworthy MREE bearers (Tyler, 2004), since the decarbonation experiment of phosphate nodules does not induce REE losses or fractionations (Fig. 3). The preferential loss of HREE from the Sinemurian-aged limestone is in agreement with the

literature, since, in carbonated environments, the HREE are preferentially complexed by carbonate ions and carried away (Compton *et al.*, 2003). The preferential loss of LREE and HREE in the Sinemurian-aged limestone may also be due to the occurrence of sulfide compounds, as evidenced by Laveuf *et al.* (2009, cf. Chapitre 3.1.) or of Al-Mg-K-bearing minerals. However, these minerals could not be identified at the moment and further analyses are in progress to reach this goal.

Note that to study the fate of REE, we must not consider only the values of the normalized concentrations, which show an enrichment of the decarbonation residues compared to the parent limestones, but also the evolution of REE stocks (see pie charts in Fig. 3), which show important REE losses during decarbonation. This statement is crucial when the pedogenetic process induces a high variation of volume as demonstrated for other elements (Egli and Fitze, 2000).

4.2. Redox conditions

4.2.1. Primary redox conditions

As evidenced by Laveuf *et al.* (2009, cf. Chapitre 3.1.), parent limestones are free of ferruginous Fe oolites, which indicates that Fe-Mn concretions are of pedogenetic origin (Baize and Chrétien, 1994). Seasonal variations of redox conditions in the zone of water table fluctuations lead to the formation of Fe-Mn concretions that are particularly abundant and well individualized in this concretion-rich Bc-horizon (Baize and Chrétien, 1994; Laveuf *et al.*, 2009, cf. Chapitre 3.1.). In the Fe-Mn concretions of the Bc-horizon, all REE are one to two times enriched compared to the bulk fraction of the C-horizon, except Ce, which is up to 3.5 times enriched (Fig. 5). This strong positive Ce anomaly in the pedogenetic Fe-Mn concretions is likely related to the occurrence of Fe/Mn-(hydr)oxides in these concretions. During primary redox conditions, the fraction of Ce^{3+} released upon the dissolution of primary Ce-bearing minerals can be oxidized to Ce^{4+} by secondary Fe/Mn-(hydr)oxides. Once oxidized, Ce is much less mobile because of the stronger sorption of Ce^{4+} onto Fe/Mn-(hydr)oxides (Koppi *et al.*, 1996; Coelho and Vidal-Torrado, 2000; Neaman *et al.*, 2004) or its possible precipitation as cerianite (CeO_2) (Braun *et al.*, 1998; Bau, 1999; Dia *et al.*, 2000). This very low mobility of Ce^{4+} in soil profiles – when Fe/Mn-(hydr)oxides capable of oxidizing Ce^{3+} to Ce^{4+} occur – can then lead to the appearance of a positive Ce anomaly in REE patterns (Henderson, 1984; Tyler, 2004). A strong geochemical relationship between Ce and Mn in earth-surface environments has been evidenced by several studies (Koppi *et al.*, 1996; Coelho and Vidal-Torrado, 2000; Takahashi *et al.*, 2000; Neaman *et al.*, 2004), notably cerianite with Mn oxides (Braun *et al.*, 1998), likely because of the close redox behaviors of Ce and Mn (Brookins, 1988). As concentrations of Ce and Mn in the Fe-Mn concretions are more much enriched than for Fe (Table 3), it may indicate an association of Ce with Mn oxides.

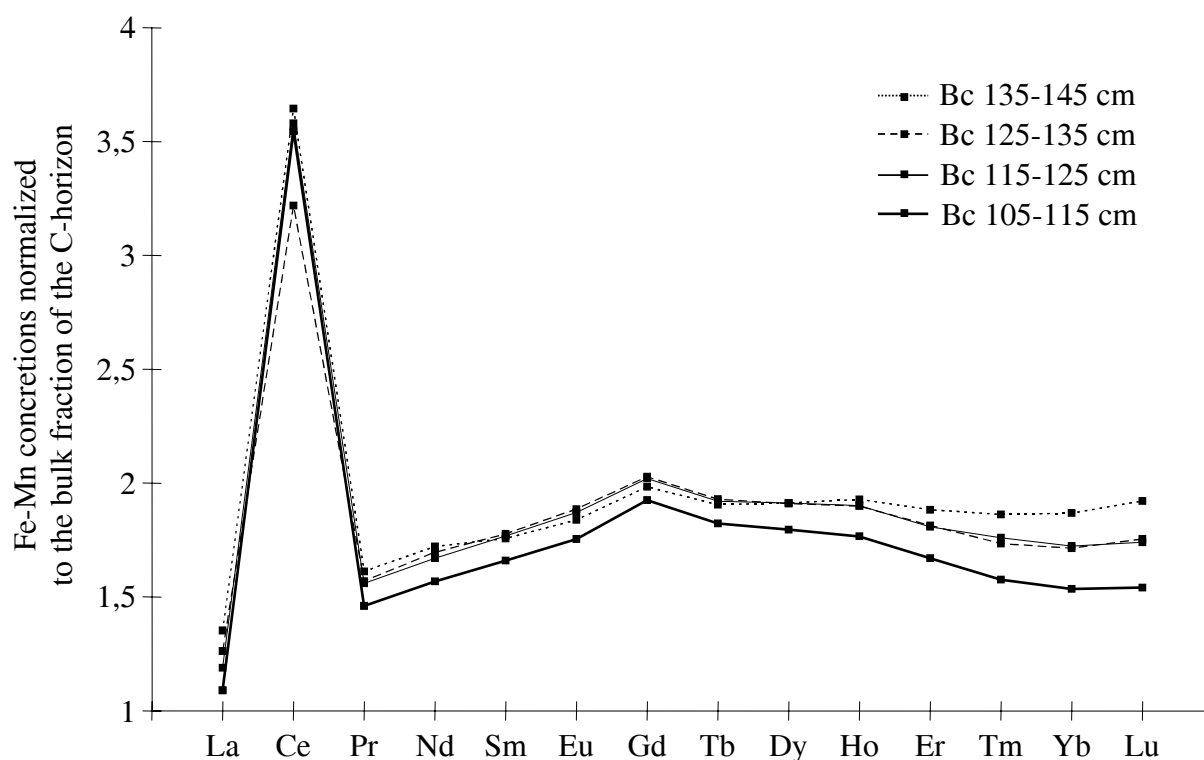


Fig. 5. REE patterns of the Fe-Mn concretions of the Bc-horizon for different depths normalized to the bulk fraction of the C-horizon.

Spectres de Terres Rares des concrétions Fe-Mn de l'horizon Bc pour différentes profondeurs normalisés à la fraction totale de l'horizon C.

Table 3

Iron, manganese and cerium concentrations of the Fe-Mn concretions, of the less than 50 μm fraction of the Bc-horizon (115-125 cm) and of the bulk fraction of the C-horizon from which the Bc-horizon was developed.

Concentrations en fer, manganèse et cérium des concrétions Fe-Mn, de la fraction inférieure à 50 μm de l'horizon Bc (115-125 cm) et de la fraction totale de l'horizon C au dépend de laquelle l'horizon Bc s'est développé.

		Fe	Mn	Ce
		g/kg	g/kg	mg/kg
Bc-horizon (115-125 cm)	Fe-Mn concretions	151	68	538.0
	<50 μm fraction	75	6.1	96.3
C-horizon		90	8.0	150.3

4.2.2. Secondary redox conditions

Seasonal variations of redox conditions in the Bgd-horizon lead to the dissolution of dispersed Fe/Mn-(hydr)oxides that cement the finest fractions (Laveuf *et al.*, 2009, cf. Chapitre 3.1.). To study the impact of such redox processes on REE fractionation, we studied the less than 2 μm fraction normalized to the residue of extraction (Laveuf *et al.*, 2009, cf. Chapitre 3.1.). Indeed, the less than 2 μm particle-size fraction consists of Fe and Mn oxyhydroxides, of phyllosilicates and of quartz. The residue of extraction consists of phyllosilicates and quartz. As REE do not bind to quartz, they are therefore bound to the

phyllosilicates and to the Fe/Mn-(hydr)oxides. Therefore, the normalization of the less than 2 μm particle-size fraction to the residue of extraction allows to depict the REE pattern of the Fe/Mn-(hydr)oxides, since these minerals are totally absent in the residue of extraction and since phyllosilicates occur in both samples. Globally, the less than 2 μm fractions are enriched in MREE compared to the residues of extraction (Fig. 6), which indicates that Fe/Mn-(hydr)oxides are enriched in MREE. Consequently, the more the horizons will be affected by secondary redox conditions, the less the MREE will be enriched in the less than 2 μm fractions compared to the residues of extraction. This assumption is supported by the known MREE enrichment of colloidal Fe particles in soil waters (de Siena *et al.*, 1998; Dia *et al.*, 2000). That is why, along the studied solum, MREE enrichment decreases toward soil surface. This global trend also confirms our pedological observations, that is, that the Bc- and C-horizons are not affected by secondary redox processes, on the opposite to the A-, E- and Bgd-horizons.

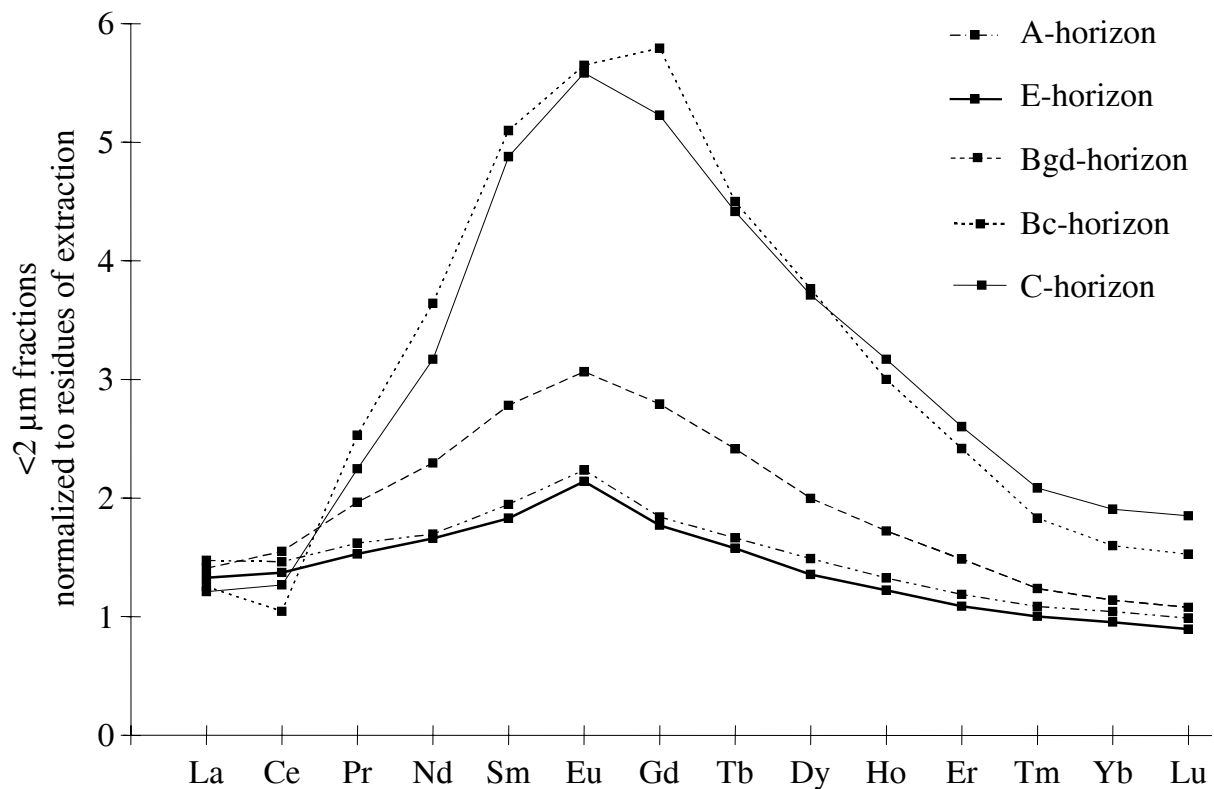


Fig. 6. REE patterns of the less than 2 μm particle-size fractions of each horizon normalized to the residue of extractions of the corresponding bulk soil fractions.

Spectres de Terres Rares des fractions granulométriques inférieures à 2 μm de chaque horizon normalisés au résidu d'extraction de la fraction totale correspondante.

4.3. Eluviation

Eluviation is a physical process, involving the translocation of fine particles, mainly phyllosilicates. Since this process is only physical, it should not fractionate REE within the less than 2 μm fraction, as the whole fraction is supposed to be removed. However, the

normalization of the less than 2 μm fraction of the A- and E-horizons to that of the Bgd-horizon, which is neither eluviated nor significantly illuviated, evidences that eluviation fractionates REE in these soil horizons (Fig. 7). All REE, and particularly MREE, are depleted in the less than 2 μm fraction of the A- and E- horizons compared to that of the Bgd-horizon, except Ce which exhibits a positive anomaly. The positive Ce anomaly is likely due to the fact that Ce is not bound to eluviated phyllosilicates and is thus not affected by this pedogenetic process. This hypothesis has to be confirmed, notably by the finding of the Ce-bearing phases. The larger loss of MREE, compared to the other REE, can be due to a preferential association of MREE with phyllosilicates. However, this hypothesis is in contradiction with *Cao et al. (2000)*, who showed with chemical extractions that MREE have lower proportions of residual form than LREE and HREE. Another explanation could be the preferential eluviation of the smallest phyllosilicates (smectite, illite, vermiculites; *Nguyen Kha et al., 1976*), since they do not exhibit the same REE compositions as the biggest ones (kaolinite and chlorite; *Coppin, 2002; Compton et al., 2003; Wan and Liu, 2005*). Finally, the integration of another pedogenetic process because of an insufficient segregation of the REE pattern of the phyllosilicates through our normalization could also explain the observed differences.

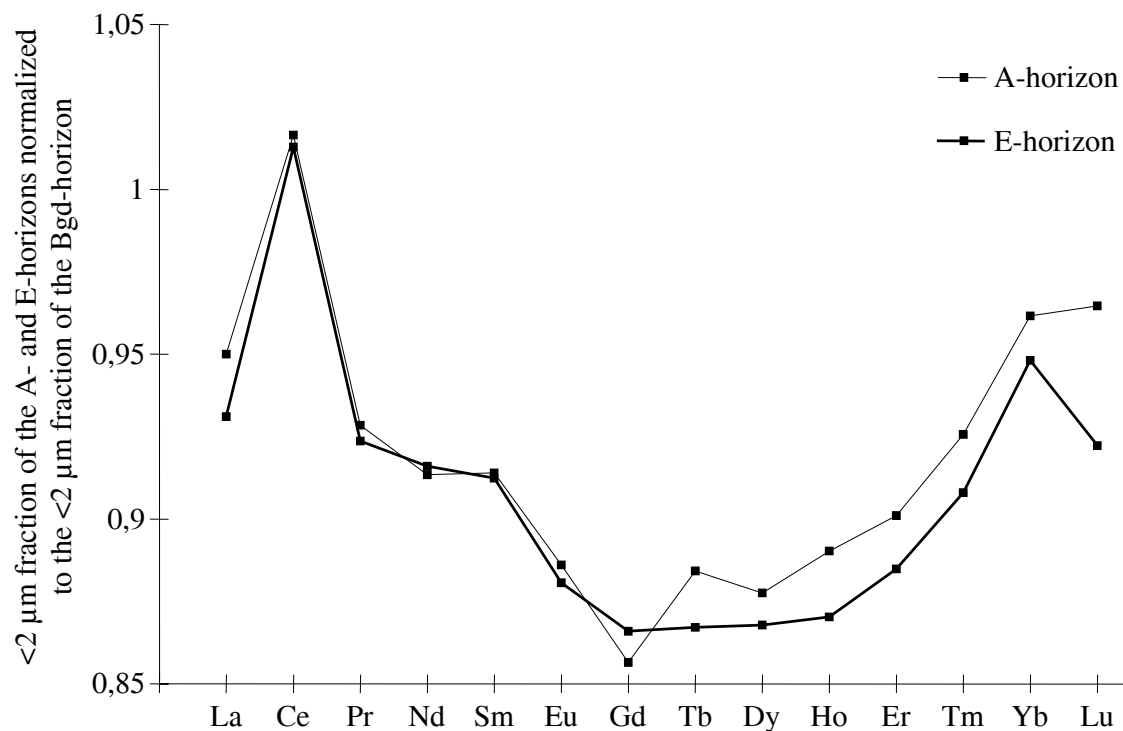


Fig. 7. REE patterns of the less than 2 μm fraction of the A- and E-horizons normalized to the less than 2 μm fraction of the Bgd-horizon.

Spectres de Terres Rares dans la fraction inférieure à 2 μm des horizons A et E normalisés à la fraction inférieure à 2 μm de l'horizon Bgd.

5. Conclusion

Despite some remaining difficulties and uncertainties, the first results obtained in this study indicate that the proposed REE normalization approach is informative and that it could be used to exploit the potential of REE as tracers of pedogenetic processes. Concerning redox conditions, results obtained on our selected solum demonstrate that the two stages of redox conditions identified acted differently on the Fe/Mn-(hydr)oxides and associated REE. Primary redox conditions lead to the formation of Fe-Mn concretions in which all REE are enriched, but which exhibit a strong positive Ce anomaly because of preferential sorption onto Fe/Mn-(hydr)oxides. Cerium may thus be used as a useful tracer of the quantitative mobilization of Fe/Mn during primary redox conditions. Secondary redox conditions induce the dissolution of the Fe/Mn-(hydr)oxides that cement the finest particle-size fractions and the concomitant release of associated MREE. MREE may thus potentially serve as tracers of the loss of Fe/Mn-(hydr)oxides during secondary redox conditions. Concerning the role of eluviation on REE fractionation, our approach is not sufficiently constrained, probably because of a preferential translocation of some phyllosilicates with different REE compositions or an insufficient enhancement of the signature of the pedological feature resulting from eluviation through our normalization.

However, since the proposed approach is based on the normalization of the REE concentrations of a pedological feature in a given horizon to the REE concentrations of the material from which it developed, it necessitates that the pedogenetic process, related to the selected pedological feature, is dominant. This condition indicates that a more accurate identification of the pedogenetic processes related to the various possible pedological features is strongly required to better differentiate the impact of these processes on REE fractionation. For instance, quantification of the preferential translocation of some phyllosilicates with different REE compositions is fundamental to better understand the role of eluviation on REE fractionation. In addition, the REE normalization approach proposed would strongly benefit from a better characterization of the material from which the studied pedological feature has developed. For instance, actual speciations of Ce and MREE in the Fe-Mn concretions are needed to emphasize the relative role of primary and secondary redox conditions on REE fractionation.

Acknowledgments

The authors would particularly like to thank O. Josière for technical support and D. Baize for scientific comments and advices. This work has been carried out thanks to the financial support of the Projet Innovant Terres Rares of the INRA Department “Environnement et Agronomie” and of the “Région Centre”. It also benefited from funding by the “GDR TRANSMET” Program of the Centre national de la recherche scientifique (CNRS) through the action “Comportement biogéochimique, minéralogique et cristallographique des éléments métalliques et des métalloïdes à proximité des gisements et des anomalies géochimiques”.

4.2.2. Validation de notre démarche méthodologique sur le site de Savigny-en-Terre-Plaine

Après avoir développé une méthode d'utilisation des terres rares comme traceurs de la pédogenèse sur le site de Pouilly-en-Auxois (bordure Nord-Est du Massif granitique du Morvan, Côte d'Or ; cf. [Laveuf et al. \(2008\)](#) au [Chapitre 4.2.1.](#) précédent), j'ai testé sa reproductibilité sur le site de Savigny-en-Terre-Plaine (bordure Nord du Massif du Morvan, Yonne).

Si j'ai conservé le principe de normalisation dans ses grandes lignes (normalisation des teneurs en terres rares des traits pédologiques aux teneurs en terres rares des matériaux aux dépens desquels ils se sont respectivement développés, *i.e.* matériaux initiaux), j'ai néanmoins fait les modifications suivantes :

- afin de quantifier la mobilisation des terres rares, j'ai normalisé dans ce qui suit non pas des concentrations mais des stocks. En effet, [Laveuf et al. \(2008, cf. Chapitre 4.2.1.\)](#) ont démontré l'importance de la prise en compte des stocks pour la mise en évidence d'éventuelles pertes en terres rares. En effet, les processus géochimiques notamment sont à l'origine de la mise en solution d'un certain nombre de phases minérales et donc vraisemblablement de pertes en terres rares associées ;
- une des conclusions de [Laveuf et al. \(2008, cf. Chapitre 4.2.1.\)](#) portait sur la nécessité d'améliorer le choix des traits pédologiques supposés résulter de l'expression des différents processus et le choix du matériau de référence considéré comme le matériau initial à partir duquel le processus ciblé a différencié le trait pédologique considéré.

Dans les paragraphes suivants je présenterais d'abord une analyse comparative des différences entre les deux normalisations employées, puis les résultats pour le site de la Terre-Plaine, processus par processus.

4.2.2.1. Les méthodes de normalisation des terres rares

Le [Tableau 1](#) résume les traits pédologiques et les matériaux de référence servant à la normalisation des terres rares pour chacun des processus considérés sur les deux sites étudiés.

Tableau 1. Comparaison des normalisations des terres rares, *i.e.* des traits pédologiques et des matériaux de référence, pour chacun des processus sur les deux sites étudiés.

Processus ciblé	Auxois (Laveuf et al., 2008)		Terre-Plaine	
	Trait pédologique	Matériau de référence	Trait pédologique	Matériau de référence
Décarbonatation	Résidu de décarbonatation	Calcaire parental non décarbonaté	Résidu de décarbonatation	Calcaire parental non décarbonaté
Redox primaire	Nodules Fe-Mn	Horizon C	Nodules Fe-Mn	Horizon C
Redox secondaire	Fraction <2µm	Résidu d'extraction de l'échantillon total	Résidu d'extraction de la fraction <50 µm	Fraction <50 µm
Eluviation secondaire	Fraction <2 µm des horizons éluviés A et E	Fraction <2 µm de Bgd	Résidu d'extraction de la fraction 0-2 µm de LE	Résidu d'extraction de la fraction 0-2 µm de C

Pour les processus de décarbonatation et de redox primaire, j'ai utilisé les mêmes traits pédologiques et matériaux de référence sur les deux sites. Néanmoins la méthode de

décarbonatation expérimentale a évolué entre les deux études. Dans l’Auxois, nous avons utilisé une solution d’acide chlorhydrique HCl diluée en veillant à ce que le pH soit maintenu supérieur à 5 (Laveuf *et al.*, 2008, cf. Chapitre 4.2.1.). Cette attaque est relativement agressive vis-à-vis des oxydes et des argiles. En conséquence, sur le site de la Terre-Plaine, la décarbonatation expérimentale a été réalisée avec une solution d’acide acétique (a.r., ChemLab) tamponnée à pH 5,5 par de l’acétate de sodium (a.r., ChemLab), réactif recommandé pour la dissolution des carbonates au cours d’extractions séquentielles (Han et Banin, 1995 ; Cornu et Clozel, 2000).

Pour ce qui est des processus de rédox secondaire et d’éluviation, une réflexion plus approfondie sur la nature des processus m’a conduit à modifier le choix des traits pédologiques ciblés ou des matériaux de référence utilisés pour la normalisation.

Les processus rédox secondaires entraînent la dissolution des oxy-hydroxydes de fer et de manganèse qui cimentent les fractions fines du sol (Pedro *et al.*, 1978). Dans Laveuf *et al.* (2008, cf. Chapitre 4.2.1.), nous avons normalisé la fraction inférieure à 2 µm au résidu d’extraction de la fraction totale, seul résidu d’extraction disponible dans cette étude. Or, des quantités significatives d’oxydes de fer sont détectées par diffraction des rayons X dans toutes les fractions granulométriques inférieures à 50 µm. Ainsi, les oxy-hydroxydes cimentent les différentes fractions granulométriques inférieures à 50 µm et non seulement la fraction inférieure à 2 µm. J’ai donc normalisé ici le stock en terres rares du résidu d’extraction de la fraction inférieure à 50 µm (obtenu selon le protocole reporté au Chapitre 6.2.), supposé représentative des zones blanchies par le processus de dégradation morphologique, au stock de terres rares de la fraction inférieure à 50 µm qui correspond alors au matériau initial.

Enfin, l’éluviation secondaire consiste en un entrainement des minéraux argileux fins – fraction inférieure à 2 µm principalement (Nguyen Kha *et al.*, 1976) – hors des horizons éluviés, après destruction préalable des ciments formés par les oxydes ferro-manganiques (Bottner et Paquet, 1972 ; Jamagne et Pédro, 1981). J’ai ainsi choisi de normaliser le résidu d’extraction de la fraction inférieure à 2 µm (obtenu selon le protocole reporté au Chapitre 6.2.), et non la fraction inférieure à 2 µm dans son ensemble comme dans Laveuf *et al.* (2008, cf. Chapitre 4.2.1.), d’un horizon éluvié à celle d’un horizon profond non éluvié. Pour ce dernier, dans Laveuf *et al.* (2008, cf. Chapitre 4.2.1.), nous avons choisi l’horizon Bgd sur le site de l’Auxois. Or, dans le profil de la Terre-Plaine, l’évolution de la teneur en fraction 0-2 µm avec la profondeur montre une diminution de cette fraction vers la surface dès l’horizon Bgd (Figure 1). En conséquence, notre choix s’est porté ici sur un autre horizon, plus approprié, l’horizon C

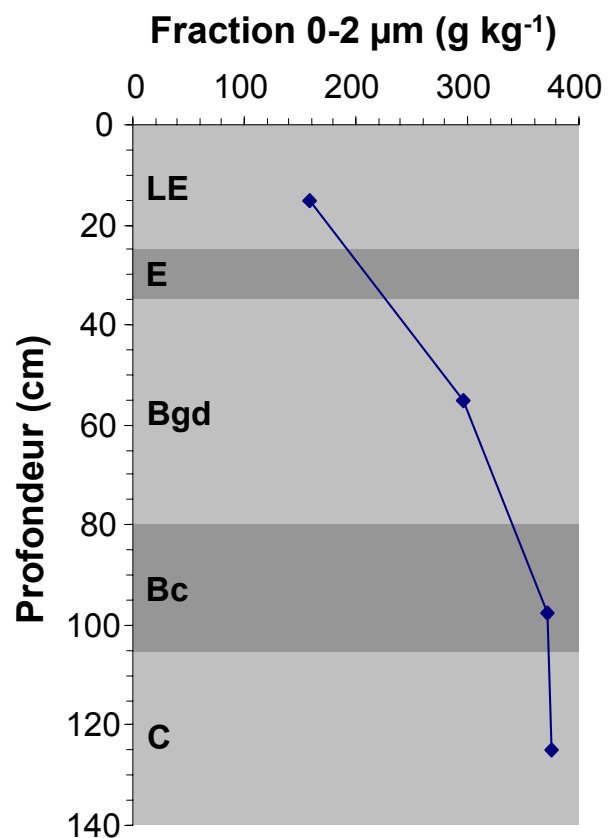


Figure 1. Teneurs en fraction inférieure à 2 µm en fonction de la profondeur.

qui présente la composition en argiles la plus représentative de celle héritée des matériaux parentaux.

4.2.2.2. Impact des différents processus d'altération et de pédogenèse sur les stocks en terres rares

4.2.2.2.1 Le processus de décarbonatation

Le stock de terres rares dans les résidus de décarbonatation représente entre 50% et 60% du stock initial en terres rares dans les calcaires parentaux d'âge sinémurien selon l'échantillon considéré (Figure 2). Le résidu de décarbonatation de C1 contient un stock en terres rares significativement plus élevé que les autres échantillons, plus proche de celui observé dans l'Auxois (Laveuf *et al.*, 2008, cf. Chapitre 4.2.1.). Les résidus de décarbonatation sont appauvris en terres rares lourdes comparés aux terres rares moyennes et légères (Figure 2). Cela signifie qu'au cours de la décarbonatation, les terres rares lourdes sont plus mises en solution que les terres rares légères ou moyennes. Ainsi les terres rares lourdes sont donc plus liées à la calcite que les autres terres rares (Laveuf *et al.*, soumis, cf. Chapitre 5.1.). Cela est cohérent avec la complexation préférentielle des terres rares lourdes avec les ions bicarbonates dans les matrices carbonatées (Cantrell et Byrne, 1987 ; Lee et Byrne, 1993 ; Koppil *et al.*, 1996 ; Pourret *et al.*, 2007). Dans l'Auxois, les terres rares lourdes étaient aussi plus perdues que les terres rares moyennes (Laveuf *et al.*, 2008, cf. Chapitre 4.2.1.).

Enfin, les spectres des résidus de décarbonatation de C1 et C2 présentent une anomalie positive en Ce (Figure 2), impliquant que cet élément est moins mis en solution que les autres terres rares légères. Cette anomalie n'avait pas été observée dans l'Auxois (Laveuf *et al.*, 2008, cf. Chapitre 4.2.1.), mais est en accord avec les conclusions de Laveuf et Cornu (soumis, cf. Chapitre 4.1.) sur la moindre complexation de Ce par les ions carbonates dans les solutions de sol au cours de la décarbonatation par rapport aux autres terres rares légères.

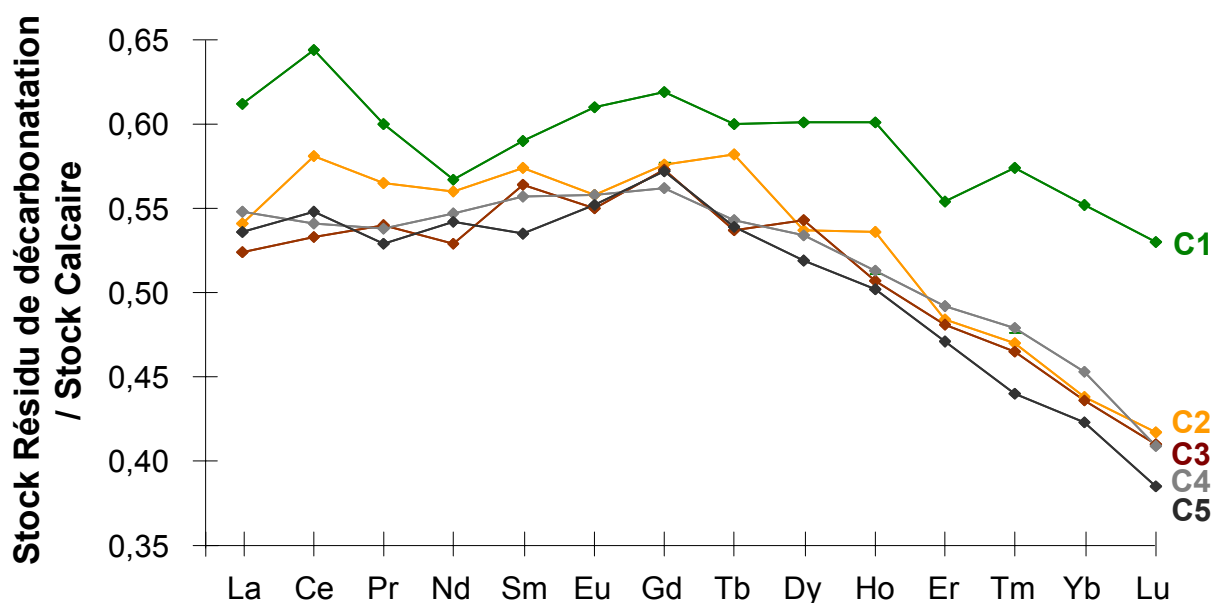


Figure 2. Stocks en terres rares des résidus expérimentaux de décarbonatation normalisés aux stocks en terres rares des calcaires parentaux pour les cinq strates calcaires d'âge sinémurien échantillonnées (C1 à C5).

Le comportement des calcaires au cours de la décarbonatation diffère donc. Trois groupes principaux de calcaires peuvent être identifiés : C1, C2 à C5 et les calcaires de l'Auxois. Ces différences sont probablement liées à des différences de composition minéralogique et chimique entre les différents calcaires. En effet, la composition du calcaire d'âge sinémurien évolue à la fois selon la strate considérée (Laveuf *et al.*, soumis, cf. Chapitre 5.1.), mais aussi selon sa localisation sur le pourtour du massif du Morvan (cf. Chapitre 2). Ainsi, par exemple, les calcaires d'âge sinémurien de la Terre-Plaine sont plus riches en carbonates que celui de l'Auxois (entre 92% et 94% dans la Terre-Plaine contre 87% dans l'Auxois) ce qui explique partiellement des pertes plus importantes en terres rares lourdes dans les échantillons de la Terre-Plaine.

4.2.2.2.2. Processus redox primaires

Tous les nodules Fe-Mn sont appauvris, en termes de stocks, en terres rares vis-à-vis de l'horizon C (Figure 3). Les nodules Fe-Mn de l'horizon Bc, horizon de formation des nodules, contiennent 37% du stock de terres rares de l'horizon C. Les nodules Fe-Mn de l'horizon C, en début de formation, contiennent 24% de ce stock, tandis que ceux en dégradation de l'horizon LE n'en contiennent que 17%. Les nodules Fe-Mn de tous les horizons présentent en outre une anomalie positive en Ce (Figure 3). Celle-ci est très marquée dans l'horizon Bc où les deux tiers du stock de Ce de l'horizon C se concentrent dans les

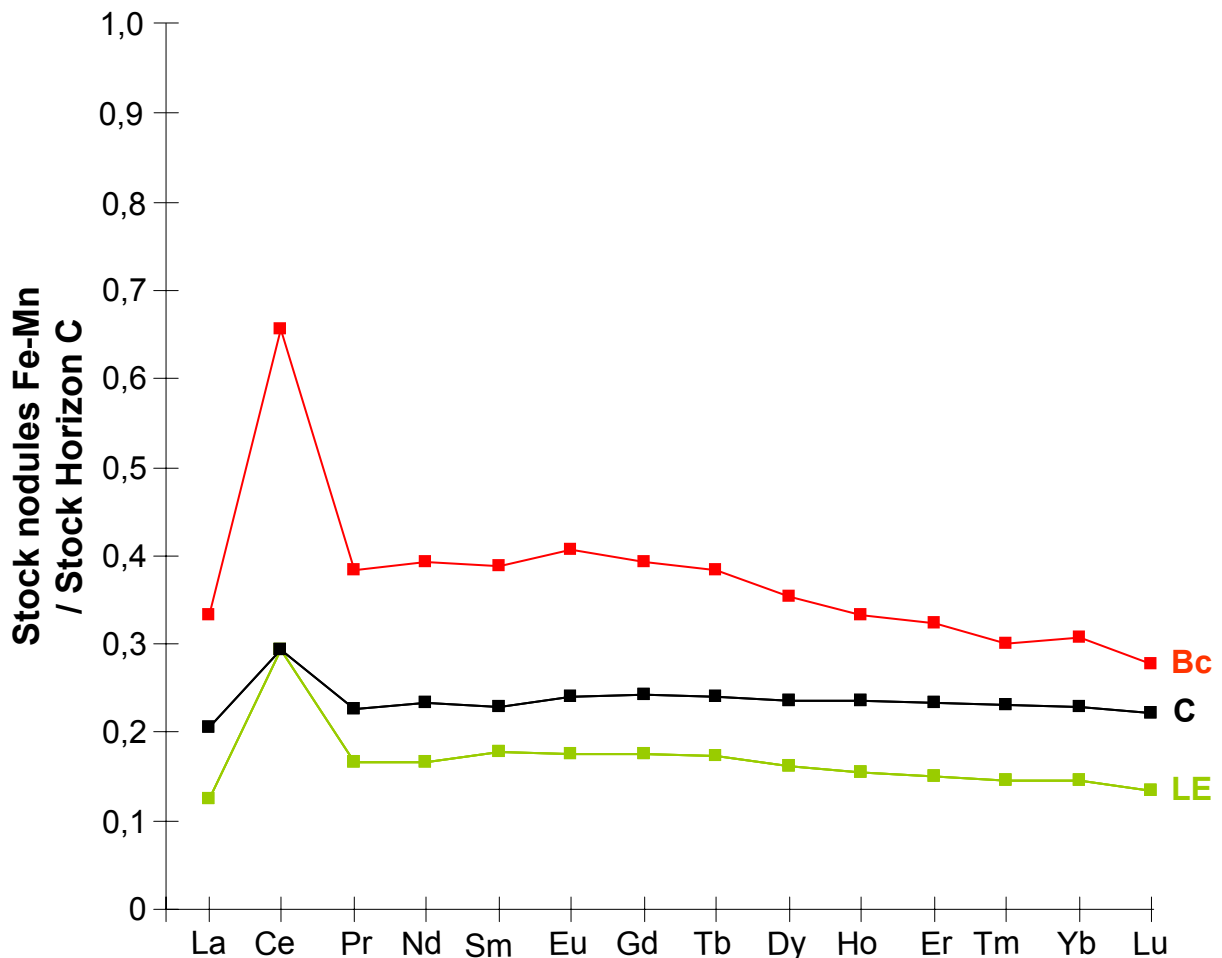


Figure 3. Stocks en terres rares des nodules Fe-Mn dans les horizons LE, Bc et C du sol complet normalisé aux stocks en terres rares de l'horizon C.

nodules Fe-Mn, tandis que ces stocks n'en représentent qu'un tiers dans les autres horizons (Figure 3). Les nodules Fe-Mn de l'horizon Bc sont aussi légèrement enrichis en terres rares légères et moyennes par rapport aux lourdes (Figure 3).

On retrouve l'enrichissement caractéristique en Ce des nodules Fe-Mn, déjà mis en évidence sur le site de l'Auxois (Laveuf *et al.*, 2008, cf. Chapitre 4.2.1.). Mais alors qu'en concentrations on observait un enrichissement relatif en terres rares vis-à-vis de l'horizon C, l'analyse des rapports des stocks de terres rares met en évidence l'existence d'une perte des terres rares lors de la dissolution des oxydes Fe-Mn dispersés dans l'horizon C et de leur condensation dans les nodules Fe-Mn.

4.2.2.2.3. Processus redox secondaires

L'ensemble des résidus des fractions inférieures à 50 µm des différents horizons du sol complet de la Terre-Plaine est appauvri en terres rares moyennes par rapport aux terres rares légères et aux lourdes (Figure 4).

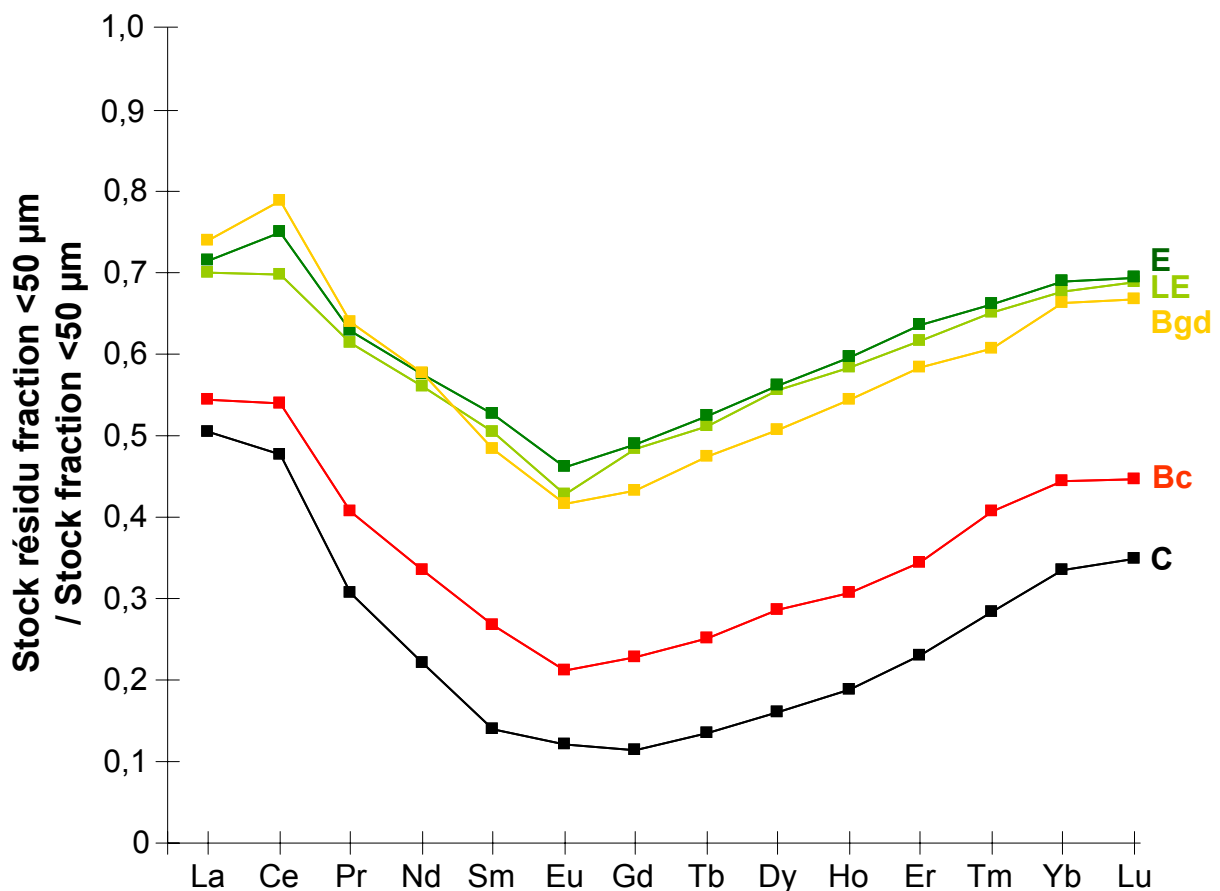


Figure 4. Stocks en terres rares du résidu d'extraction de la fraction <50 µm normalisés aux stocks en terres rares de la fraction <50 µm du même horizon, pour les horizons LE, E, Bgd, Bc et C du sol complet.

De plus, trois groupes d'horizons se distinguent par leur comportement :

- (i) le résidu de la fraction inférieure à 50 μm de l'horizon C, très appauvri en l'ensemble des terres rares, et en moyennes en particulier, par rapport à sa fraction inférieure à 50 μm ;
- (ii) les résidus des fractions inférieures à 50 μm des horizons dégradés Bgd, E et LE, légèrement appauvris en terres rares, avec un appauvrissement cependant plus marqué pour les terres rares moyennes, par rapport à leurs fractions inférieurs à 50 μm respectives ;
- (iii) le résidu de la fraction inférieure à 50 μm de l'horizon Bc, avec une situation intermédiaire, néanmoins plus proche de celle de l'horizon C que de celle des horizons dégradés.

Ainsi, du bas en haut du solum, les stocks normalisés en terres rares dans les résidus tendent vers un rapport de 1. Cela signifie que les fractions inférieures à 50 μm évoluent vers leurs résidus d'extraction respectifs, autrement dit, qu'elles évoluent vers les zones blanchies et qu'elles sont donc de plus en plus dégradées. En conséquence, l'évolution des spectres de terres rares reflète l'évolution de la dégradation depuis l'horizon C, non dégradé, aux horizons LE, E et Bgd, les plus dégradés. Cette dégradation croissante induit des pertes croissantes en toutes les terres rares (Figure 4). Les terres rares moyennes sont perdues préférentiellement, ce qui est cohérent avec l'enrichissement des terres rares moyennes dans les oxy-hydroxydes de fer et de manganèse observé dans l'Auxois (Laveuf *et al.*, 2008, cf. Chapitre 4.2.1.) et également observé dans la Terre-Plaine (Figure 5).

On met en évidence ici que les autres terres rares sont aussi affectées par le processus, dans une moindre mesure, contrairement à ce que l'on avait supposé précédemment (Laveuf *et al.*, 2008, cf. Chapitre 4.2.1.).

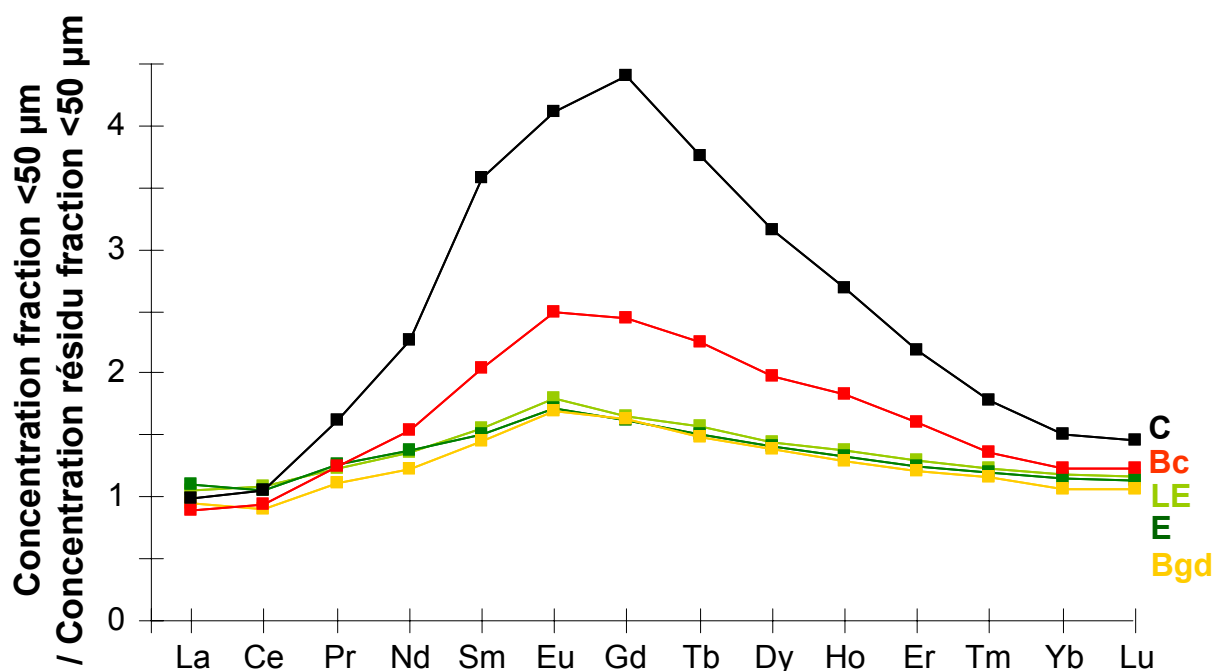


Figure 5. Concentrations en terres rares de la fraction <50 μm normalisées aux concentrations en terres rares du résidu d'extraction de la fraction <50 μm du même horizon, pour les horizons LE, E, Bgd, Bc et C du sol complet.

4.2.2.2.4. Eluviation secondaire

Les teneurs en fraction inférieure à 2 μm (sans destruction préalable des ciments ferromanganiques) tendent à décroître de l'horizon Bc vers l'horizon LE, de 375 à 160 g kg⁻¹ (Figure 1).

Les concentrations en terres rares moyennes du résidu de la fraction inférieure à 2 μm de l'horizon LE sont significativement supérieures à celles de l'horizon C (jusqu'à 1,7 fois), alors que celles en terres rares légères et lourdes ne le sont pas (Figure 6). Le résidu d'extraction est composé d'argiles et de quartz. Le quartz ne contient pas de terres rares. Ainsi l'évolution des profils de concentrations en terres rares dans la fraction inférieure à 2 μm est liée à l'évolution des argiles le long du solum.

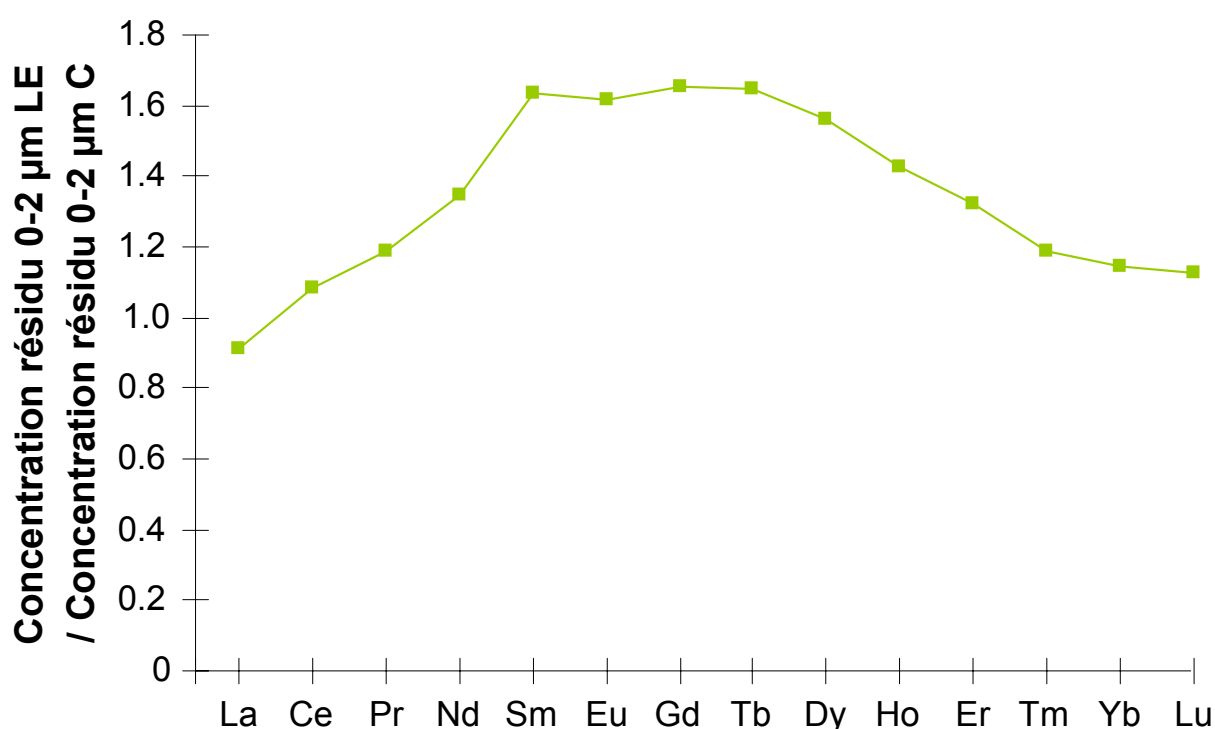


Figure 6. Concentrations en terres rares du résidu d'extraction de la fraction inférieure à 2 μm de l'horizon LE normalisées à celles de l'horizon C.

Deux processus peuvent être responsables de cette évolution : la néoformation d'argiles ou leur éluviation. Pour ce qui est de la néoformation d'argiles, la littérature montre que le rayon ionique important des terres rares limite leur substitution dans le réseau des argiles, du moins en quantités significatives (Nesbitt, 1979 ; Duddy, 1980 ; Bonnot-Courtois, 1981 ; Braun *et al.*, 1993). Ainsi, ce processus n'induit vraisemblablement pas une telle évolution des concentrations avec la profondeur. L'éluviation consiste en une perte d'argiles sous forme physique, compatible avec l'évolution de la teneur en fractions inférieures à 2 μm avec la profondeur. A cette perte doit être associée une perte en terres rares. Pour le confirmer, j'ai normalisé les stocks de terres rares. Le stock du résidu d'extraction de la fraction inférieure à 2 μm de l'horizon LE est inférieur à celui de l'horizon C, et ce de façon plus marquée pour les terres rares légères et les terres rares lourdes que pour les terres rares

moyennes (Figure 7). Ainsi, l'éluviation mobilise donc préférentiellement des argiles appauvries en terres rares moyennes.

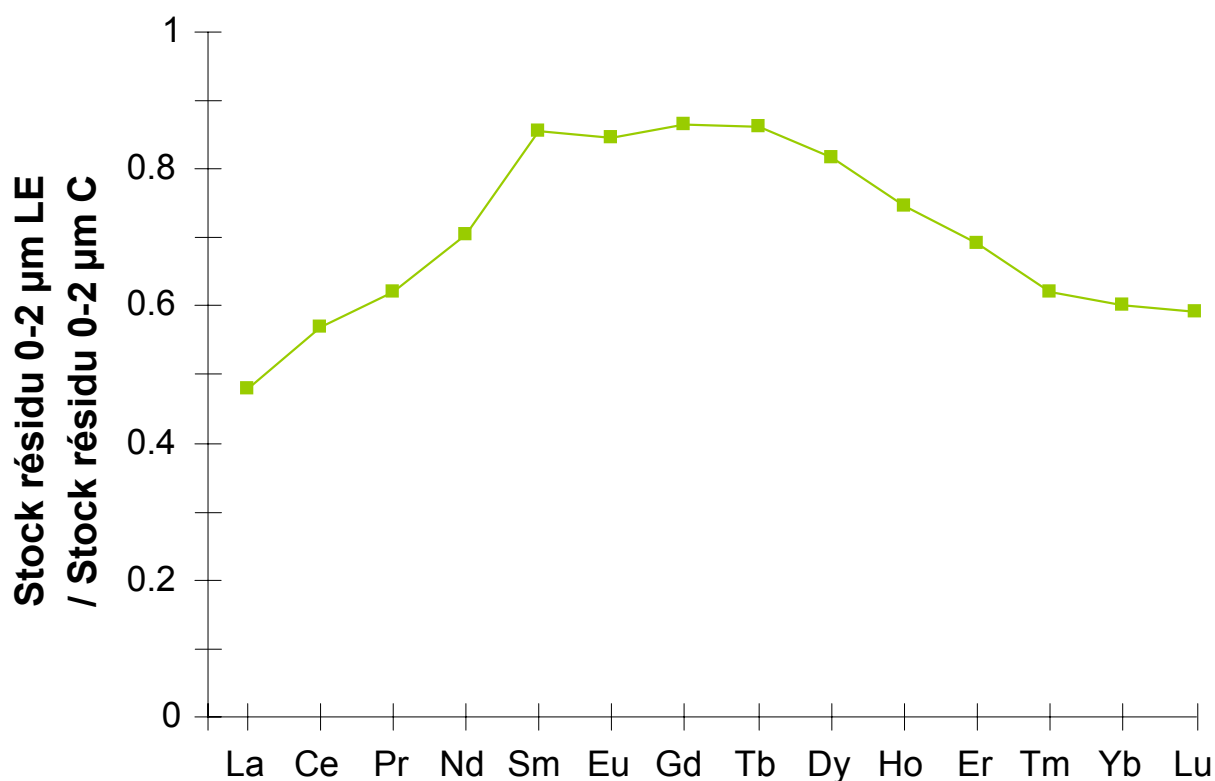


Figure 7. Spectre des stocks en terres rares du résidu d'extraction de la fraction inférieure à 2 µm de l'horizon LE normalisés aux stocks en terres rares du résidu d'extraction de la fraction inférieure à 2 µm de l'horizon C.

L'approche employée dans l'Auxois, utilisant des matériaux non déferriés ne permettait pas une déconvolution des deux processus, rédox secondaire et éluviation.

4.3. Conclusions

La synthèse bibliographique montre que les terres rares semblent prometteuses pour tracer les conditions redox et le lessivage et met en évidence l'importance du choix de la référence de normalisation dans l'analyse des fractionnements des terres rares par les différents processus.

La méthode de normalisation proposée dans la seconde partie du chapitre, malgré quelques difficultés et incertitudes résiduelles, est riche en enseignements comme le montre les premiers résultats obtenus sur les deux sites d'étude. Ainsi, les terres rares peuvent permettre de tracer certains processus pédogénétiques tels que les processus d'oxydo-réduction et le lessivage notamment.

En effet, lorsqu'on utilise la même normalisation, notre démarche conduit à des résultats similaires sur les deux sites étudiés concernant les processus redox primaires,

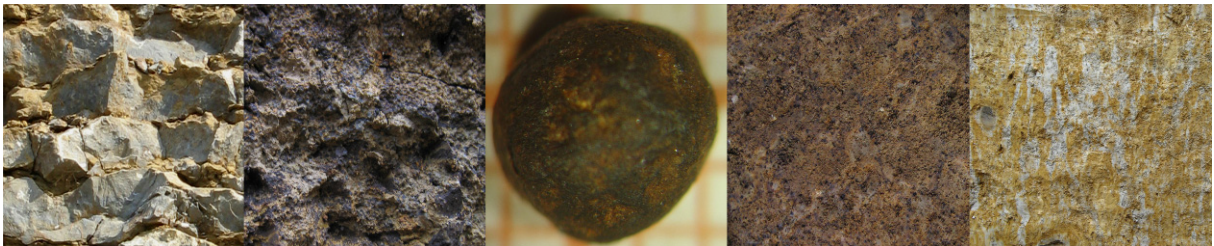
excepté pour le processus de décarbonatation due à la différence de composition minéralogique des calcaires d'âge sinémurien sur le pourtour du Massif du Morvan. Ainsi, les processus redox primaires induisent une concentration de toutes les terres rares dans les nodules Fe-Mn formés, et plus particulièrement en Ce, même si une fraction de ces terres rares est perdue au cours du processus comme l'a montré l'approche en stocks. L'enrichissement en Ce est supposé être lié à la présence des oxydes de Mn dans les nodules Fe-Mn. Une étude de la spéciation de Ce et Mn dans les nodules Fe-Mn permettrait de vérifier cette hypothèse.

Par contre, une meilleure définition des traits pédologiques issus d'un processus pédogénétique donné et du matériau sur lequel ce processus s'est appliqué (matériau initial de référence), ainsi que la prise en compte des stocks de terres rares mobilisés au cours des processus fournissent un nouvel éclairage des résultats. Les processus redox secondaires mobilisent toutes les terres rares, même si effectivement les terres rares moyennes sont les plus mobilisées.

L'éluviation secondaire mobilise plus les terres rares légères et les terres rares lourdes que les terres rares moyennes, sans fractionner Ce par rapport aux autres terres rares légères, vraisemblablement du fait de la mobilisation différentielle des différents types d'argiles. Il serait intéressant de déterminer les signatures en terres rares de ces différentes argiles.

Chapitre 5

Reconstruction des matériaux parentaux



La quantification des processus pédogénétiques nécessite le calcul des flux passés, accessibles par un bilan de masse de type *Brimhall et al. (1987)* entre autres (*Hoosbeek et Bryant, 1992* ; *Minasny et al., 2008*). De plus, l'étude bibliographique a montré l'intérêt d'un bilan de masse pour utiliser les terres rares comme traceurs des processus pédogénétiques.

Ce chapitre présente donc les résultats du bilan de masse, de type *Brimhall et al. (1987)*, des éléments majeurs et des terres rares en relation avec les processus pédogénétiques identifiés dans le solum complet de la Terre-Plaine.

Le prérequis à la quantification des flux passés est l'accès aux stocks initiaux, c'est-à-dire aux matériaux parentaux à partir desquels le solum s'est développé. Nous proposons donc dans un premier temps une méthodologie innovante pour reconstituer les matériaux parentaux, permettant l'application du bilan de masse de type *Brimhall et al. (1987)* au contexte sédimentaire hétérogène du site d'étude de la Terre-Plaine.

Ce chapitre se présente sous forme d'un article en anglais soumis à *Geoderma*.

5.1. Méthodologie de reconstitution des matériaux parentaux et bilan de masse

Reconstruction of former parent materials and pedological behavior of major elements and Rare Earth Elements with mass balance calculations in a soil developed from a heterogeneous complex sedimentary deposit

Cédric Laveuf^{a,†}, Sophie Cornu^a, and Farid Juillot^b

^a INRA, UR0272 Science du Sol, Centre de Recherche d'Orléans, CS 40001 Ardon, 45075 Orléans Cedex 2, FRANCE.

^b IMPMC, UMR CNRS 7590, Universités Paris 6 et 7 – IPGC, 75252 Paris Cedex 05, FRANCE.

Abstract

Mass balance calculation is a powerful approach to quantify pedogenesis. However, this approach necessitates a precise characterization of the parent material and its application is thus generally limited to the cases where the parent material can be considered homogeneous.

We propose here to apply this methodology to a complex parent material made of a succession of limestones layers and marl beds of sinemurian-age. This approach relies on the identification of the former parent material of each soil horizon on the basis of the concentrations of selected immobile elements in soil horizons and in remaining sinemurian formation. To do so, we first corrected from pedological impacts the concentrations of soil horizons in the selected immobile elements, Zr and Hf. We then experimentally determined the proportions of the residues from carbonate dissolution of limestone and marl samples, which best describe the corrected concentrations of the selected immobile elements in each soil horizon. After correction from weathering, we finally calculated the proportions and thicknesses of limestone and marl layers necessary to form each soil horizon. The coherence of the obtained reconstructed former parent materials was assessed by comparison with the existing geological logs of the studied area.

Once the parent materials of each soil horizon characterized, we first crosschecked mass balance calculations for Zr and Hf to confirm their immobility during pedogenesis compared to other elements usually considered as immobile (*i.e.* Ti, Th, V, Nb or Y). In a second step, mass balance calculations were computed for major elements (Si, Al, Fe and Mn) and REEs. These calculations show that major elements and REEs are highly mobilized during weathering and pedogenesis, leading to their exportation from the solum. No significant REE fractionations were evidenced, except for Ce. Such a peculiar behavior for this last REE could be related to its incorporation in Fe-Mn nodules formed during pedogenesis.

Keywords: immobile elements, lanthanides, limestone, marl, fluxes, pedogenesis

[†] Corresponding author. Tel.: +33 2 38 41 78 00. Fax: +33 2 38 41 78 69. E-mail address: laveuf@orleans.inra.fr (C. Laveuf)

1. Introduction

The quantification of soil processes has always been matter of interest for pedologists (Hoosbeek and Bryant, 1992). Since few decades, the growing interest in modelling of pedogenesis has led to a need in quantitative data on soil processes (Cornu *et al.*, 2008; Minasny *et al.*, 2008), in order to better predict soil evolution under forcing factors, such as human activities or climate change, and to use soils, which are non-renewable resources on the human time-scale, on a sustainable basis.

The quantification of element translocation during pedogenesis, and its interpretation in terms of pedogenetic processes, are usually based on the comparison of the chemistry and mineralogy of the different soil horizons to those of the parent material, and on the fluxes in elements, computed by mass balance calculations, which are responsible for the soil horizon development at the expense of the parent material (Hoosbeek and Bryant, 1992; Brantley *et al.*, 2007; Cornu *et al.*, 2008; Minasny *et al.*, 2008). These calculations are based on (i) the determination of the parent material and on (ii) the ratios of element supposed to be immobile during pedogenesis, *i.e.* not fractionated or translocated (Brimhall and Dietrich, 1987; Chadwick *et al.*, 1990; Brimhall *et al.*, 1991). Although powerful and fully informative, mass balance calculations are limited by these two crucial assumptions.

Classically, immobile elements used in mass balance calculations are Ti and Zr (Brimhall and Dietrich, 1987; Brimhall *et al.*, 1991; Freyssinet, 1994; Jersak *et al.*, 1995; Nesbitt and Markovics, 1997; Murphy *et al.*, 1998; Blaser *et al.*, 2000; Egli and Fitze, 2000; Horton *et al.*, 2001; Courchesne *et al.*, 2002; Navarre-Sitchler and Brantley, 2007; Buss *et al.*, 2008; Price *et al.*, 2008), but Al, Th, Nb, Y, V, Sc or quartz are sometimes also used (Beauvais and Colin, 1993; van der Weijden and van der Weijden, 1995; Steinmann and Shotyck, 1997; White *et al.*, 1998; Mathe *et al.*, 1999; Shotyck *et al.*, 2000; Turner *et al.*, 2003; Oh and Richter, 2005; Montagne *et al.*, 2008; Ndjigui *et al.*, submitted). Hafnium is also considered immobile since it mainly occurs as hafnon HfSiO_4 , proved to be highly stable (Milnes and Fitzpatrick, 1989; Cerny *et al.*, 2007). However, in some pedological context, these elements were shown to be mobile to a certain extent (Kaup and Carter, 1987; Cornu *et al.*, 1999; Mathe *et al.*, 1999; Chiquet *et al.*, 2000; Delattre *et al.*, 2007; Ndjigui *et al.*, 2008). In order to assess the immobility of these elements, we propose to use them simultaneously and to crosscheck the results obtained thanks to calculations performed with the different potential immobile elements. Such an approach has rarely been performed in other studies, where the authors took the immobility of the chosen elements for granted.

Soil horizons are developed from parent materials that no longer exist due to weathering and pedogenesis. The authors then hypothesize that the composition of the underlying bedrock, or the C-horizon, or the least-weathered soil horizon, is representative of the former parent material for the whole solum (Brimhall and Dietrich, 1987; Chadwick *et al.*, 1990; Brimhall *et al.*, 1991; Boulangé and Colin, 1994; Jersak *et al.*, 1995; Chiquet *et al.*, 2000; Egli and Fitze, 2000; Panahi *et al.*, 2000; Oh and Richter, 2005). However, the composition of the parent materials often varies vertically and laterally in space, and this hypothesis is thus relevant only in cases of homogeneous parent materials and only if the C- or least-weathered soil horizons have not undergone important modifications of their initial composition (White, 1995). To apply mass balance calculations to heterogeneous parent materials, it is first necessary to reconstruct the composition of the former parent material.

In the present study, we propose a methodology, based on the variation in the concentrations of several immobile elements with depth, to reconstruct the former parent materials of each soil horizon of a solum developed from a complex mixture of limestones and marls. After the parent material composition of each soil horizon has been estimated, we computed mass balance calculations for major elements and for Rare Earth Elements (REEs), according to the procedure described by [Brimhall *et al.* \(1991\)](#) and revised by [Egli and Fitze \(2000\)](#). We determined the impact of pedogenetic processes on the mobilization of major elements and on the fractionation of REEs, since it is commonly admitted that pedogenesis induces fractionations among these latter elements ([Tyler, 2004](#); [Hu *et al.*, 2006](#); [Laveuf *et al.*, 2008](#), cf. [Chapitre 4.2.1.](#)).

2. Materials and methods

2.1. Geological context of the study site

The study site is located on the northern sedimentary Liasic margin of the granitic Morvan Mountain (Burgundy, France) on a structural limestone surface dated from the sinemurian stage ([Mouterde, 1952](#); [Fig. 1a](#)).

This formation, about 5 to 10 m thick, consists in an irregular alternation of hard and compact crystalline grey-blue limestone layers and of soft grey-rust marl beds. The thicknesses of the limestone layers and of the marl beds are highly variable, both vertically and laterally, varying from 5 to 80 cm and from few mm to 15 cm, respectively ([Collenot, 1873](#); [Mouterde, 1952](#)).

During the Lias epoch, this formation underwent mineralization events due to hydrothermal fluids rising along fault lines ([Mégnyen, 1960](#); [Sizaret, 2002](#)), and responsible for their high Fe, Mn and REE contents ([Laveuf *et al.*, 2008](#), cf. [Chapitre 4.2.1.](#)).

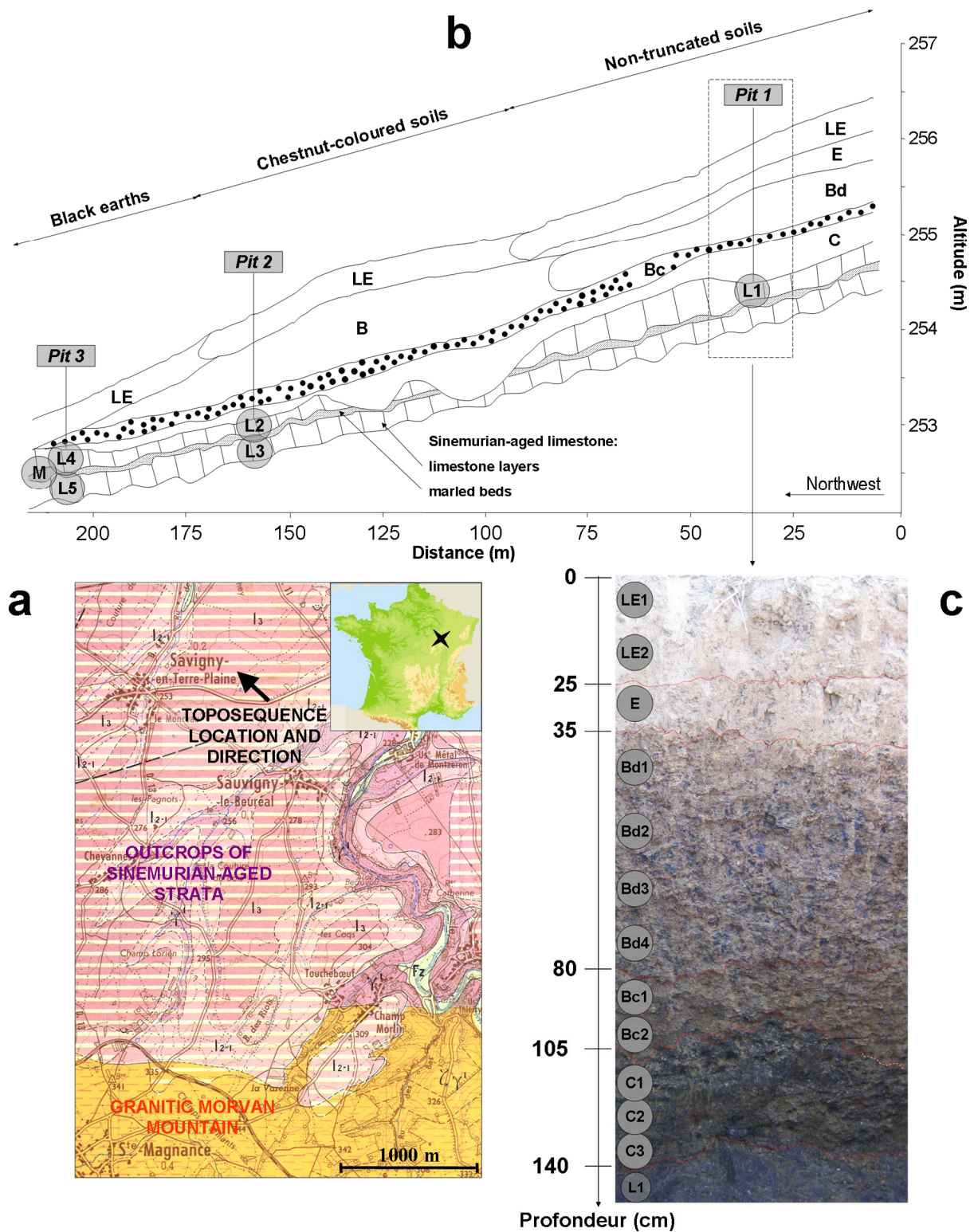


Fig. 1. (a) Location of the study site. (b) Studied toposequence and location of the remaining sinemurian formation samples (L1, L2, L3, L4, L5 and M). (c) Non-truncated profile of pit 1 and location of the soil horizons sampled (LE1, LE2, E, Bd1, Bd2, Bd3, Bd4, Bc1, Bc2, C1, C2 and C3).

Table 1. Concentrations of major elements and REEs in the different soil horizons.

Soil horizon	g kg ⁻¹										mg kg ⁻¹												
	Si	Al	Fe	Mn	Ca	La	Ce	Pr	Nd	Sm	Eu	Gd	Tb	Dy	Ho	Er	Tm	Yb	Lu	REEs	LREEs	MREEs	HREEs
LE1	307.8	55.3	54.3	4.41	4.52	55.9	111.2	13.8	53.2	10.4	2.03	8.98	1.38	8.10	1.58	4.43	0.68	4.44	0.71	273.3	180.9	84.2	11.8
LE2	311.3	56.4	49.8	4.29	4.79	54.9	112.0	13.3	51.3	10.1	1.96	8.70	1.35	7.99	1.57	4.43	0.68	4.40	0.68	290.2	180.2	81.3	11.8
E	305.1	58.7	50.9	4.60	4.99	57.7	120.3	14.2	54.5	10.5	2.09	9.09	1.42	8.26	1.62	4.50	0.71	4.72	0.73	265.4	192.1	85.8	12.3
Bd1	276.5	77.4	61.2	5.66	6.07	55.1	108.2	13.0	49.6	9.73	1.99	8.22	1.28	7.46	1.48	4.11	0.62	4.10	0.64	290.7	176.2	78.3	11.0
Bd2	278.3	78.1	65.9	7.14	6.93	57.5	122.2	13.9	54.3	10.7	2.20	9.19	1.40	7.96	1.55	4.36	0.65	4.30	0.64	279.7	193.5	85.7	11.5
Bd3	264.2	81.3	63.7	6.71	7.10	57.2	111.9	13.8	53.6	10.5	2.19	9.15	1.41	8.15	1.62	4.47	0.66	4.31	0.67	295.2	182.9	85.0	11.7
Bd4	250.0	81.6	74.0	9.38	7.47	62.2	112.1	15.1	59.0	11.5	2.41	10.1	1.53	8.82	1.74	4.77	0.70	4.49	0.70	322.6	189.4	93.3	12.4
Bc1	242.4	81.5	72.8	11.1	10.3	69.6	119.0	16.7	66.4	13.0	2.71	11.1	1.67	9.51	1.84	4.97	0.73	4.63	0.71	357.6	205.3	104.4	12.9
Bc2	236.9	81.0	87.8	18.3	13.3	72.3	144.4	17.4	70.1	13.7	2.96	11.9	1.72	9.87	1.87	5.12	0.75	4.79	0.73	335.2	234.1	110.2	13.3
C1	182.3	78.8	114.0	27.1	30.1	76.8	115.9	17.8	72.0	13.3	2.90	11.8	1.72	9.82	1.92	5.16	0.74	4.69	0.73	334.5	210.5	111.5	13.2
C2	188.5	83.3	106.2	21.4	38.2	75.6	112.8	17.8	72.7	14.1	3.06	12.5	1.82	10.3	1.98	5.46	0.77	4.84	0.72	308.3	206.2	114.5	13.8
C3	190.1	84.6	97.3	21.0	30.4	72.8	103.6	16.3	65.9	12.9	2.73	11.0	1.60	9.17	1.77	4.80	0.70	4.40	0.68	276.8	192.7	103.3	12.3

2.2. Pedological context of the study site

The soils developed from the weathering (resulting in carbonate dissolution) of the sinemurian-aged formation. They thus exhibit high Fe, Mn and REE concentrations (Table 1). They are organized in an erosion-driven sequence, ranging from non-truncated soils to the so-called “black earths” via the so-called “chestnut colored soils” (Baize and Chrétien, 1994; Fig. 1b). These soils are mainly cropped. In order to integrate the highest complexity in terms of number of limestone layers and marl beds weathered, we studied the thickest solum, which is the non-truncated solum. This solum, located at Savigny-en-Terre-Plaine (Fig. 1a), is characterized by the following succession of soil horizons from top to bottom (Fig. 1c):

- from 0- to 25-cm depth, a beige (2.5Y7/4) silty clayey cultivated eluviated and ploughed LE-horizon;
- from 25- to 35-cm depth, a beige (2.5Y7/4) silty clayey eluviated E-horizon;
- from 35- to 80-cm depth, an yellowish brown (10YR5/4) clay silty degraded Bd-horizon;
- from 80- to 105-cm depth, a brown ochre (10YR5.5/8) clayey B-horizon with abundant Fe-Mn nodules (called Bc-horizon);
- from 105- to 140-cm depth, a C-horizon composed of a mixture of black (10YR2/1) and grey-beige (2.5Y6/2) highly clayey materials;

- the limit with an unweathered sinemurian-aged layer undulates around 140 cm.

The sinemurian-aged layer is compact and not fissured, and thus hinders water percolation. Therefore, a water table develops quickly after abundant rainfalls. Our field observations showed that this water table was continuously present from November to May in the C-horizon and from February to April in the Bc-horizon. Consequently, during winter and spring, the C-horizon is submitted to prolonged reducing conditions, while the Bc-horizon is submitted to water table fluctuation along the year, leading to alternations of reducing and oxidative conditions. During winter, a second water table appears in the Bd-horizon, which is thus submitted to reducing conditions.

According to [Baize and Chrétien \(1994\)](#) and [Laveuf *et al.* \(2009\)](#), cf. [Chapitre 3.1.](#)), these types of soil underwent successive pedogenetic processes, namely primary redox conditions (water table fluctuations), secondary redox conditions (perched water table) and eluviation, whose transformation fronts are mainly located in the Bc, Bd, and LE- plus E-horizons, respectively ([Fig. 2](#)).

2.3. Sampling strategy

Five limestone samples (noted L1 to L5), coming from different limestone layers, were sampled at the bottom of three pits dug along a 200 m toposequence ([Fig. 1a](#) and [1b](#)), in order to determine the variability of the parent material composition. For technical reasons, only one marl bed (M) was sampled at the bottom of Pit 3 ([Fig. 1b](#)).

The different soil horizons were sampled on the whole width of Pit 1 ([Fig. 1c](#)). When homogeneous, only one sample was collected for each soil horizon, while up to four were collected when an evolution with depth could be evidenced ([Fig. 1c](#)).

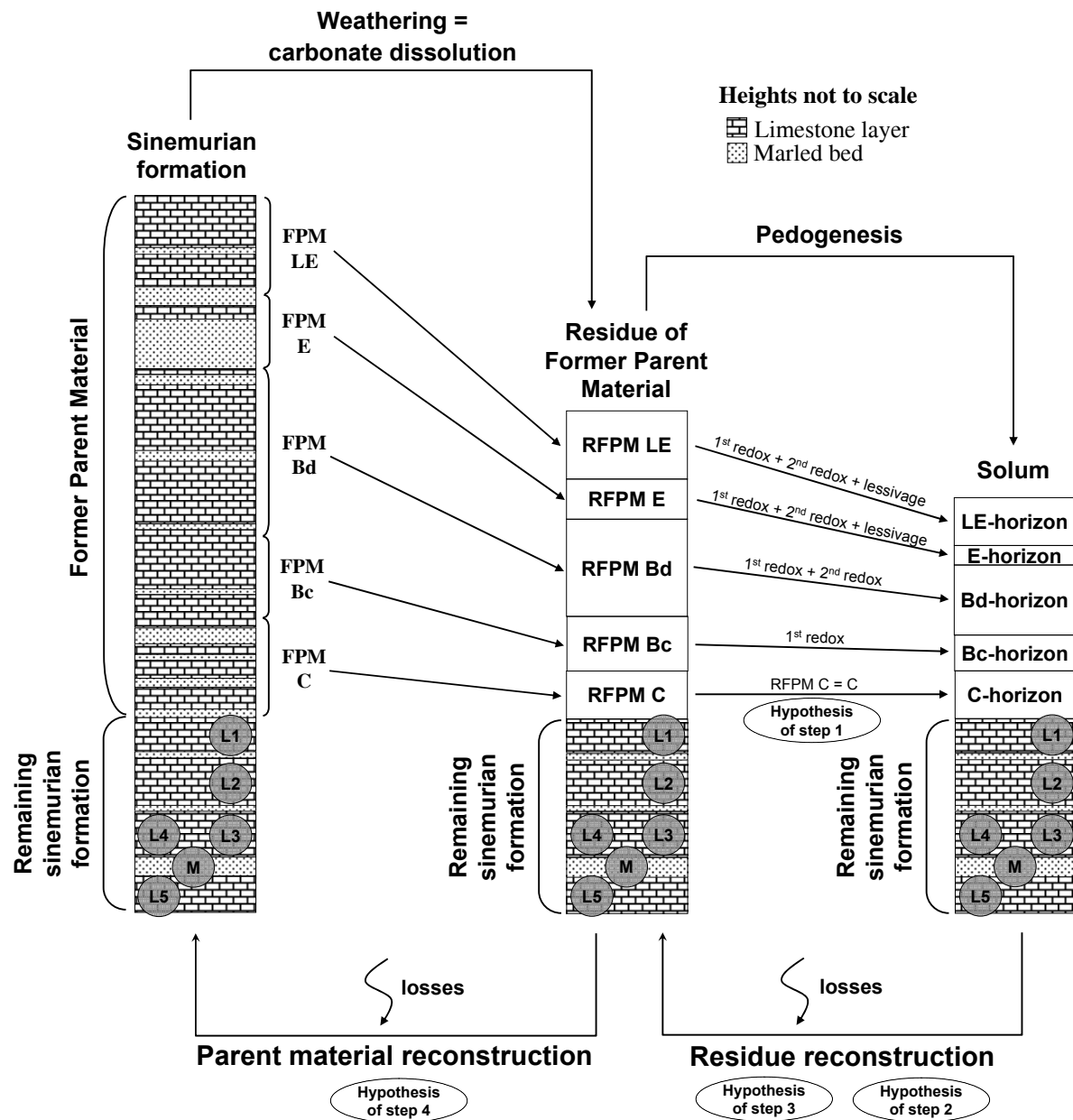
2.4. Density measurements, sampling preparation and analyses

Bulk density of each soil horizon was determined in triplicate by the cylinder method (volume of 500 mL when possible, if not 250 mL) after drying at 105°C. Three unweathered parts of each limestone were selected (sizes of about 5x5x5 cm³). Their bulk densities were determined in triplicate by volume displacement in kerosene after drying at 40°C. The bulk density of the marl bed was measured in triplicate by the membrane densitometer method after drying at 105°C.

All soil and parent material samples were ground to <50 µm, quartered and chemically analyzed at the [SARM-CRPG](#) (Vandœuvre-lès-Nancy, France). Major elements were measured by ICP-AES and trace elements (REEs and immobile elements) by ICP-MS, after LiBO₂ fusion. Carbonate contents were determined by calcimetry at the [LAS-INRA](#) (Arras, France).

Quartz was quantified by XRD in all soil and parent material ground powder samples doped with 25% of ZnO. Five replicates were performed under the following experimental conditions: 2θ ranging from 54° to 60°, a counting time of 2 s per step of 0.005°, CoKα radiation (35 kV, 40 mA).

The <2 µm fraction of horizons LE2, Bd2, Bc and C2 was separated by sedimentation in deionized water according to Stokes law following a preliminary sieving at 50 µm of the bulk samples.



o **Hypothesis of step 1:** $RFPM_C = C$

o **Hypothesis of step 2:** $RFPM_{Horizon} = \sum(x_{RRSF} RRSF)$

with RRSF the residues from experimental carbonate dissolution of the remaining sinemurian samples and x_{RRSF} their proportions in the residue from weathering of the former parent material RFPM of the considered horizon $RFPM_{Horizon}$

o **Hypothesis of step 3:** Horizon = pedogenesis of $RFPM_{Horizon}$

$$= \sum(x_{RRSF} RRSF) - \text{losses due to pedogenesis}$$

o **Hypothesis of step 4:** $\sum x_{RRSF} RRSF = \sum(x_{RSF} RSF - \text{losses due to weathering})$

with x_{SPM} the proportions of the SPM in the FPM

Fig. 2. Formation of the different soil horizons from different former parent materials (FPMs) by pedogenetic processes. Each soil horizon results from the weathering and pedogenesis of several layers of limestones and marls, which may vary in composition and thickness.

2.5. Experimental carbonate dissolution of parent materials

Unweathered limestone samples were roughly grounded (<2 mm) and carbonates were dissolved using CH₃COONa 1M (up, Chem-Lab) adjusted to pH 5.5 with CH₃COOH 99-100% (up, Chem-Lab) as recommended by Han and Banin (1995) for soil samples. Successive extractions were performed until disappearance of degassing. For the marl sample, a sequential extraction procedure, following the protocol described in Laveuf *et al.* (2009, cf. Chapitre 3.1.), was performed on one gram of bulk material ground to <50 µm.

Differential XRD (DXRD) was performed following the method of Schulze (1981) to check the total dissolution of carbonates and the absence of dissolution of some oxides. Bulk samples and residues from carbonate dissolution were analyzed on powder for 2θ ranging from 0° to 75° with a counting time of 10 s per step of 0.005°, using CoKα radiation (35 kV, 40 mA).

The residues from carbonate dissolution and from sequential extractions were analyzed for major elements, REEs, immobile elements and quartz as described above.

Table 2. Bulk densities of the remaining sinemurian formation samples and of soil horizons with their associated standard deviations.

		ρ_{PM} g cm ⁻³	S.D.
Remaining sinemurian formation	L1	2.63	0.005
	L2	2.65	0.013
	L3	2.62	0.019
	L4	2.58	0.037
	L5	2.56	0.005
	M	1.95	0.090
Soil horizons	LE1	1.29	0.01
	LE2	1.38	0.07
	E	1.60	0.11
	Bd1	1.46	0.01
	Bd2	1.45	0.01
	Bd3	1.43	0.04
	Bd4	1.44	0.06
	Bc1	1.45	0.05
	Bc2	1.46	0.04
	C1	1.32	0.04
	C2	1.19	0.05
	C3	1.29	0.09

* S.D. is the standard deviation determined in triplicate for each soil horizon, for the marl bed (M) and for the limestone parent materials (L).

3. Results and discussion

3.1. Choice of the immobile elements

Among the elements and minerals analyzed, those classically considered immobile in the literature are Ti, Zr, Th, Nb, Y, V, Hf and quartz (Brimhall and Dietrich, 1987; Brimhall

2.6. Errors and uncertainties on calculations

Errors and uncertainties on the calculations of the reconstruction of the parent materials and on mass balance were calculated by the classical mathematical methodology of the total differential equations (see *e.g.* Polyaniin and Zaitsev, 2003). For chemical concentrations, the considered errors were the analytical errors given by the [SARM-CRPG](http://helium.crpq.cnrs-nancy.fr/SARM:indexangl_ais.html) and the [LAS-INRA](http://www.arras.inra.fr/index.htm) (available on their respective websites http://helium.crpq.cnrs-nancy.fr/SARM:indexangl_ais.html and <http://www.arras.inra.fr/index.htm>), while for bulk densities, the experimental standard deviations were used (Table 2).

et al., 1991; Beauvais and Colin, 1993; Freyssinet, 1994; Jersak *et al.*, 1995; van der Weijden and van der Weijden, 1995; Nesbitt and Markovics, 1997; Steinmann and Shotyky, 1997; Murphy *et al.*, 1998; White *et al.*, 1998; Mathe *et al.*, 1999; Blaser *et al.*, 2000; Egli and Fitze, 2000; Shotyky *et al.*, 2000; Horton *et al.*, 2001; Courchesne *et al.*, 2002; Turner *et al.*, 2003; Oh and Richter, 2005; Navarre-Sitchler and Brantley, 2007; Buss *et al.*, 2008; Montagne *et al.*, 2008; Price *et al.*, 2008; Ndjigui *et al.*, submitted). This immobility has however to be checked in the studied pedological context.

As mentioned above, the solum investigated derives first from the autochthonous weathering (*i.e.* from carbonate dissolution in the present case) of the limestone and marl parent materials, and from different pedological processes. Such a hypothesis is in agreement with Baize and Chrétien (1994) who demonstrated the autochthony of these soils by petrography coupled with geochemical and mineralogical analyses. Therefore, no significant contribution of loess deposits occurred in the studied area, and thus no allochthonous immobile elements were added to the solum.

In order to check the immobility of the chosen elements during weathering, we performed experimental carbonate dissolutions on the remaining sinemurian formation (RSF) samples. DXRD analyses and differential chemical analyses (Table 3) showed that CaCO₃ in the parent limestones were totally dissolved by CH₃COOH/CH₃COONa at pH 5.5.

Table 3. Concentrations of CaCO₃ and of some elements classically considered immobile in the different remaining sinemurian formation samples (RSFs = L1, L2, L3, L4, L5 and M), in their residues from carbonate dissolution (LR1, LR2, LR3, LR4, LR5 and MR respectively) and associated percentages of the stocks of elements released from the RSFs into solution during the experiment.

		Immobile elements							
		CaCO ₃ g kg ⁻¹	Ti	Zr	Nb	Y	V	Th	Hf
Remaining sinemurian formation samples	L1	915	340	11.1	1.12	8.6	19.1	1.25	0.27
	L2	942	340	9.4	1.11	10.5	19.1	0.98	0.23
	L3	932	380	10.1	1.41	12.3	31.1	0.98	0.26
	L4	935	350	10.2	1.40	14.0	37.0	6.96	0.24
	L5	922	470	13.6	1.66	12.1	32.3	6.12	0.34
	M	573	2840	86.1	12.0	49.9	140.1	27.4	2.16
Residues from carbonate dissolution	LR1	-	4000	121.3	13.3	58.5	254.7	14.8	2.98
	LR2	-	4050	116.7	14.4	82.3	285.9	14.4	2.83
	LR3	-	3660	104.7	14.3	80.5	414.7	11.9	2.48
	LR4	-	4060	111.8	15.8	87.4	448.1	12.7	2.67
	LR5	-	4200	126.7	15.8	67.5	455.9	12.6	3.07
	MR	-	6640	201.7	28.1	117.0	328.2	64.2	5.00
Percentage of the RSF stock released into solution		%	%						
	L1	100	3	10	2	4	-10	2	8
	L2	100	26	24	21	5	9	10	24
	L3	100	30	25	27	53	4	1	31
	L4	100	13	19	16	53	7	1	17
	L5	100	28	25	23	55	4	10	28
	M*	100	5	17	7	80	44	67	21

* Determined on residues from sequential extractions.

Mass losses during the experiment (data not shown) are in agreement with CaCO₃ contents (Table 3), with less than 1% difference. Ti, Zr, Th, Nb, Y, V, Hf are enriched in the residues

from carbonate dissolution of all remaining sinemurian formation samples (LR1, LR2, LR3, LR4, LR5 and MR; [Table 3](#)). However, the stocks of the selected elements after carbonate dissolution were lower than the initial ones. Considering the experimental uncertainties, we considered that the differences lower than 20% were indicative of an absence of lost of elements. Since the differences recorded for Y, V and Th for some samples were higher than 20%, these elements were considered mobile during carbonate dissolution thus discarded ([Table 3](#)). Considering this last point, only Ti, Zr, Nb, Hf and quartz were further considered as possible immobile elements.

In order to check the immobility of these remaining elements during pedogenesis, we analyzed the evolution of their concentrations with depth. Results indicate significant cross-correlations ([Table 4](#)). However, since Ti, Zr, Nb, Hf and quartz show a contrasted geochemical behavior in soils, these elements should not be all cross-correlated if they had been mobilized. These results then indicate a similar behavior of Ti, Zr, Nb, Hf and quartz within the solum during pedogenesis, which is only possible if these elements have been immobile. We can thus assume that Ti, Zr, Nb, Hf and quartz have all been immobile during pedogenesis in the pedological context of the studied site.

Table 4. Matrix of correlations of the concentrations of Ti, Zr, Nb, Hf and quartz in the different soil horizons. All values are significant at the threshold $\alpha = 0.050$ for the bilateral test (coefficients of Pearson).

	Ti	Zr	Nb	Hf	Quartz
Ti	1.000	0.911	0.989	0.925	0.848
Zr	0.911	1.000	0.879	0.995	0.978
Nb	0.989	0.879	1.000	0.886	0.803
Hf	0.925	0.995	0.886	1.000	0.975
Quartz	0.848	0.978	0.803	0.975	1.000

3.2. Identification of the former parent materials for each soil horizon

3.2.1. Chemical variability of the remaining sinemurian formation samples

According to a Kruskal-Wallis test for independent samples, the concentrations of major elements and REEs are significantly different among the limestone samples (L), as well as among their residues from carbonate dissolution (LR; [Table 5](#)). Besides, the marl sample (M) exhibits a chemical composition significantly different from those of the limestone samples, with higher concentrations of all elements except Ca and Mn ([Table 5](#)). The CaCO_3 contents of the marl bed and of the limestone layers are 57% and more than 91% respectively ([Table 3](#)). The marl residue from carbonate dissolution (MR) also shows a chemical composition significantly different from those of the limestone residues (LR), with higher concentrations in most elements except Fe, Ca, La and Ce ([Table 5](#)). The sinemurian-aged formation is thus composed of different layers of limestones and marl varying significantly in composition both vertically and laterally. Such differences indicate that the choice of a reference material as a parent material for the soil is not straightforward and justify the procedure detailed below.

Table 5. Concentrations of major elements and of REEs in the different remaining sinemurian formation samples (L1, L2, L3, L4, L5, M) and in their residues from carbonate dissolution (LR1, LR2, LR3, LR4, LR5).

Sample	Si	Al	Fe	Mn	Ca	mg kg ⁻¹																	
	g kg ⁻¹					La	Ce	Pr	Nd	Sm	Eu	Gd	Tb	Dy	Ho	Er	Tm	Yb	Lu	REEs	LREEs	MREEs	HREEs
L1	12.7	3.97	10.6	7.75	366	12.2	17.7	2.71	11.1	1.94	0.40	1.59	0.23	1.27	0.24	0.68	0.09	0.58	0.09	50.8	32.6	16.5	1.68
L2	8.18	2.80	10.0	7.45	374	11.5	16.3	2.51	10.4	1.93	0.43	1.72	0.24	1.47	0.28	0.80	0.11	0.73	0.11	48.5	30.3	16.2	2.03
L3	8.20	2.90	11.2	8.92	370	11.7	17.0	2.55	10.8	1.95	0.44	1.79	0.28	1.59	0.33	0.94	0.14	0.99	0.16	50.7	31.3	16.9	2.56
L4	8.83	3.20	11.2	8.35	371	11.9	17.7	2.68	11.2	2.16	0.48	2.00	0.30	1.79	0.37	1.06	0.16	1.10	0.18	53.1	32.3	17.9	2.87
L5	10.9	3.85	11.9	7.84	367	10.9	15.7	2.34	9.49	1.86	0.40	1.62	0.25	1.55	0.32	0.95	0.16	1.09	0.18	46.8	28.9	15.2	2.70
M	87.7	36.9	34.9	4.02	239	41.5	65.2	9.93	42.1	9.15	2.08	8.93	1.30	7.51	1.46	3.91	0.54	3.24	0.49	197	117	71.1	9.64
LR1	162	55.7	118	2.48	56.7	90.3	139	19.7	76.6	13.9	2.96	11.9	1.68	9.25	1.75	4.56	0.64	3.85	0.56	377	249	116	11.4
LR2	135	48.8	137	2.15	53.0	102	155	23.3	94.9	18.1	3.91	16.3	2.32	12.9	2.46	6.34	0.88	5.25	0.76	444	280	148	15.7
LR3	116	44.2	131	3.88	94.1	85.1	126	19.2	79.3	15.3	3.34	14.3	2.07	12.0	2.32	6.31	0.92	5.97	0.88	373	230	126	16.4
LR4	122	47.0	131	3.61	88.1	87.8	129	19.5	82.6	16.2	3.59	15.2	2.20	12.9	2.55	7.01	1.04	6.68	1.01	387	236	133	18.3
LR5	136	51.3	128	3.40	85.1	72.0	106	15.3	63.5	12.3	2.72	11.5	1.68	9.92	1.95	5.55	0.84	5.68	0.87	310	193	102	14.9

* Not presented for MR, since obtained by sequential extractions, thus only valid for immobile elements not targeted by the different extractions.

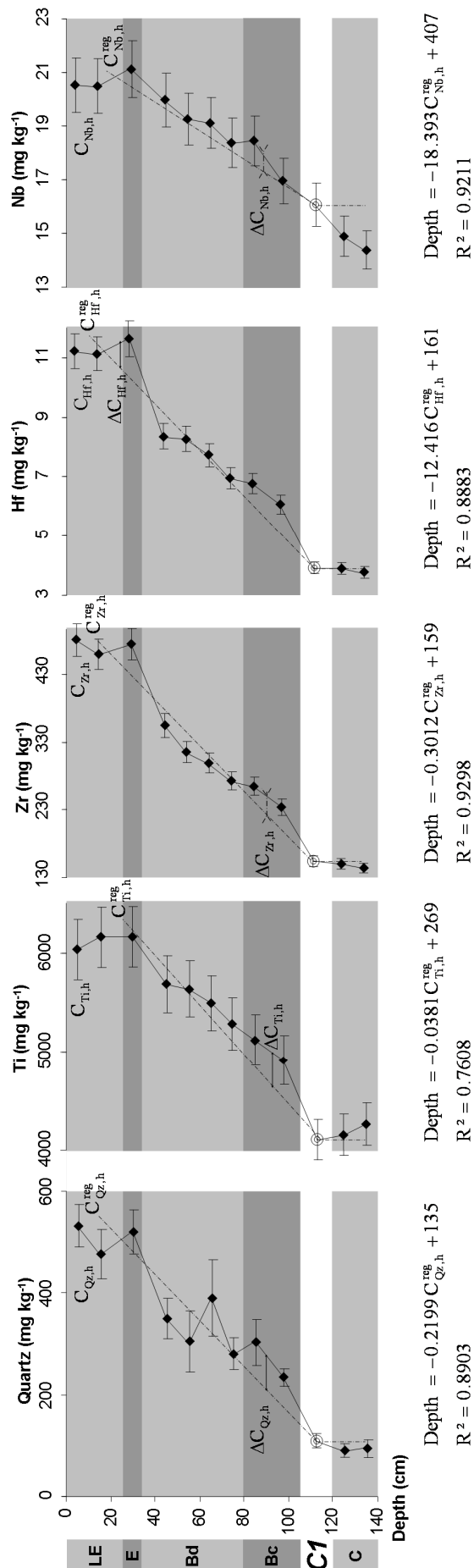


Fig. 3. Evolution with depth of the concentration of the best candidates as immobile elements $C_{i,h}$ (plain line).

This evolution can be described by a regression line starting from the upper C sample, C1, to LE1 (dotted line) and by variations along this line. The linear trend is interpreted as the result of pedogenesis and the variations around this trend are assigned to the original chemical heterogeneities of the former parent material. At each depth, $C_{i,h}^{reg}$ can be calculated thanks to the regression equations. The differences $\Delta C_{i,h}$ between $C_{i,h}$ and $C_{i,h}^{reg}$ quantify the variations in concentration of the immobile element due to the vertical heterogeneity in the composition of the parent material.

3.2.2. Reconstruction of former parent materials

Each soil horizon developed from a former parent material (FPM), which does not exist anymore (Fig. 2). This former parent material consisted of a certain total thickness of limestone layers and of a certain total thickness of marl beds, whatever their successions. As these parent materials exhibit different chemical compositions, it is necessary to reconstruct their respective thicknesses within each former parent material in order to be able to determine the impact of weathering and pedogenesis on the mobility of the elements.

The evolution of the concentrations of quartz with depth show an increase towards the soil surface, except in the C-horizon where concentrations are more or less constant with depth (Fig. 3). Such an increase is classical and interpreted as a relative enrichment due to weathering and pedogenesis in temperate climate zones (Baize, 1980), where the weathering of resistant minerals is very restricted. The general trend of this increase is linear from the C1- to the LE1-horizon. However, slight variations around this linear trend of quartz concentrations can be observed (Fig. 3). The other selected immobile elements show the same behavior than quartz, with a general linear evolution of their concentration with depth and slight variations around this

trend (Fig. 3). These variations around the linear trend can be interpreted as reflecting the variations in the composition of each former parent material from which the different soil horizons are derived.

The concentrations of the selected immobile elements in the C-horizon can be considered representative of the chemical composition of the residues of former parent materials. In this horizon, the concentrations of Ti, Zr, Nb and Hf should not evolve significantly with depth if carbonate dissolution is the only process that mobilized these elements. This hypothesis is verified for all selected elements but Nb, which was thus no further considered immobile (Fig. 3). In addition, due to higher uncertainties on quartz quantifications than on chemical analyses, this mineral species was not retained in the following calculations.

Table 6. Calcium carbonate concentrations and abundance of the <2 μm fractions in the different soil horizons.

Horizon	Sampling depth (in cm)	CaCO ₃ g kg ⁻¹	<2 μm
LE1	0-10	1.28	n.d.
LE2	10-25	1.34	158
E	25-35	<LQ	n.d.
Bd1	35-50	<LQ	n.d.
Bd2	50-60	<LQ	297
Bd3	60-70	<LQ	n.d.
Bd4	70-80	<LQ	n.d.
Bc1	80-90	<LQ	371
Bc2	90-105	<LQ	371
C1	105-120	1.47	n.d.
C2	120-130	2.04	375
C3	130-140	2.15	n.d.

<LQ: inferior to the limit of quantification

n.d.: not determined

Table 7. Concentrations $C_{i,h}$ of the immobile elements i (Ti, Zr or Hf) in each soil horizon h.

Horizon	Sampling depth (in cm)	$C_{i,h}$		
		Ti	Zr	Hf
		mg kg ⁻¹		
LE1	0-10	6036	480.8	11.2
LE2	10-25	6162	459.0	11.1
E	25-35	6162	473.9	11.7
Bd1	35-50	5682	354.3	8.3
Bd2	50-60	5628	314.7	8.3
Bd3	60-70	5485	297.5	7.7
Bd4	70-80	5281	271.3	6.9
Bc1	80-90	5107	263.5	6.7
Bc2	90-105	4915	233.7	6.1
C1	105-120	4100	154.5	3.9
C2	120-130	4148	150.4	3.9
C3	130-140	4262	144.4	3.7

Based on the interpretation of Fig. 3 and on the chemistry of the different remaining sinemurian formation samples, we propose an approach to calculate the composition of the former parent materials of each soil horizon. Since carbonate dissolution is almost complete in the C-horizon (Table 6), the chemical composition of this horizon can be considered representative of that of the residues of its former parent materials (Fig. 2 Hypothesis 1). Indeed, the concentrations of Ti, Zr and Hf in the C-horizon (Table 7) are comprised between those of the limestones residues (LR) and those of the marl residue (MR; Fig. 4).

Assuming that remaining sinemurian formation samples (RSFs) are representative of the entire sinemurian-aged formation, we can express the concentration of an immobile element in the C-horizon as a linear combination of its concentrations in the different RSFs (Fig. 2 Hypothesis 2). The relative contribution of the different residues from carbonate dissolution of the RSFs to the C-horizon can thus be calculated as:

$$C_{i,C} = \sum_{n=1}^{n=6} X_{RRSF_n} \times C_{i,RRSF_n} \quad (1)$$

where $C_{i,C}$ is the concentration of the immobile element i in the residue of the former parent material (FPM) of the C-horizon (Table 7), x_{RRSF_n} is the respective proportions of the 6 residues of the remaining sinemurian formation samples (RRSF) in the C-horizon (with $x_{RRSF_n} \geq 0$ and $\sum_{n=1}^{n=6} x_{RRSF_n} = 1$) and $C_{i,RRSF_n}$ is their respective concentrations of the immobile element i (Table 3).

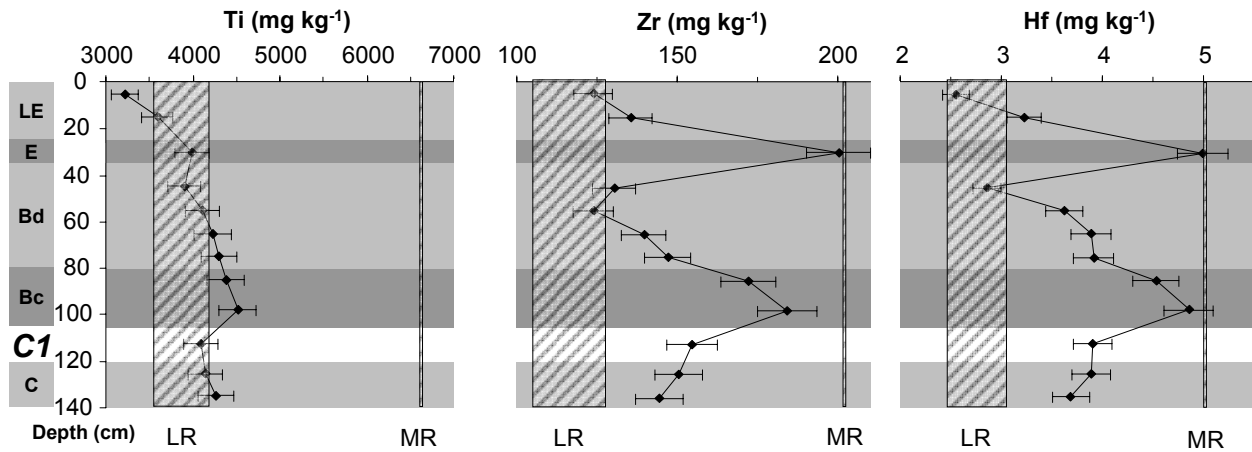


Fig. 4. Evolution with depth of the concentrations of Ti, Zr and Hf in the residues of former parent materials (calculated with equation (2) with the C1-horizon as reference). The concentrations of the residues of the remaining sinemurian formation samples – the marl (MR) and the different limestones (LR1 to LR5) – are reported on the figure as a vertical line and a vertical hatched rectangle respectively.

These calculations were performed for Zr, Hf and Ti as immobile elements. As explained previously, the concentrations of the selected immobile elements with depth show an increase towards soil surface, which is well described by a linear trend from the C1- to the LE1-horizon (Fig. 3). We choose the C1-horizon as reference among the C-horizons, because it is the most weathered C-horizon that contains no more carbonates (Table 6). The C1-horizon should thus be the most representative of a soil horizon resulting from the weathering of a mixing of remaining sinemurian formation samples in the studied solum. If such a hypothesis is valid, the concentration of the immobile elements in the residue of the former parent material should then not vary too much around those of the C1-horizon. Therefore, we estimated by a linear regression from the C1- to the LE1-horizons, the increase of the concentration of these immobile elements in each soil horizon relative to the C1-horizon due to pedogenesis (Fig. 2 Hypothesis 3 and Fig. 3). For all soil horizon h , except the C1-horizon, the differences between the measured concentrations at each depth and those estimated by the linear regression ($\Delta C_{Ti,h}$, $\Delta C_{Zr,h}$ and $\Delta C_{Hf,h}$ for Ti, Zr and Hf respectively) should quantify the variations in the concentrations of the immobile elements in the residue of each former parent material RFPM relative to that of the C1-horizon (Fig. 3). This difference can be expressed following equation (2):

$$\Delta C_{i,h} = C_{i,h} - C_{i,h}^{reg} \quad (2)$$

where $C_{i,h}$ is the measured concentration of the immobile element i in the soil horizon h (Table 7) and $C_{i,h}^{reg}$ is the concentration of the immobile element i in the soil horizon h estimated by the linear regression.

Finally, the concentration of an immobile element in the residue of the former parent material (RFPM) is thus calculated as:

$$C_{i,RFPM_h} = C_{i,C1} + \Delta C_{i,h} \quad (3)$$

where $C_{i,C1}$ is the concentration of the immobile element i in the C1-horizon.

These concentrations $C_{i,RFPM_h}$ were calculated for each soil horizons and values are comprised between those of the limestones residues (LR) and of the marl residue (MR; Fig. 4), as seen previously for the C-horizon. It is however not the case for Ti in the LE-horizon (Fig. 4), which indicates that the mixing law fails to describe its concentration in the former parent materials of the LE-horizon. Previous works already showed the mobility of Ti in some pedo-geological contexts (Kaup and Carter, 1987; Cornu *et al.*, 1999; Mathe *et al.*, 1999; Chiquet *et al.*, 2000). Such a mobility could explain the low Ti concentration calculated for the former parent material of the LE-horizon compared to the lowest concentrations of the remaining sinemurian formation samples (Fig. 4). Considering this last point, Ti was not retained as an immobile element in the rest of the calculations.

The proportions of the different remaining sinemurian formation samples in the former parent material weathered to form a given soil horizon were then determined on the basis of their residues from carbonate dissolution. These proportions were calculated for each soil horizon with Zr and Hf, expressing equation (1) with $C_{i,RFPM_h}$ instead of $C_{i,C}$ (Table 8). Results show that only two remaining sinemurian formation samples are necessary to reconstruct the former parent material of each soil horizon, the marl sample being necessary for all soil horizons. The remaining sinemurian formation samples L2, L4 and L5 were never used for the reconstruction of the former parent materials (Table 8). The errors on the estimation of $C_{i,RFPM_h}$ – difference between the value estimated with the reconstructed former parent material and the value calculated by equation (3) – were always smaller than 20 %, and even smaller than 10 %, except in three cases (LE1-horizon for Zr and Bd2- and Bd3-horizons for Hf; Table 8).

Once the proportions of the different weathered remaining sinemurian formation samples in the weathered former parent material of a given soil horizon estimated (Fig. 2 Hypothesis 2), the corresponding proportions of the remaining sinemurian formation samples were calculated considering the losses during weathering (Table 8 and Fig. 2 Hypothesis 4). These losses were estimated by the results of the experimental carbonate dissolution (Table 3).

Finally, the equivalent chemical compositions of the unweathered former parent material of each soil horizon were computed using the estimated proportions of unweathered remaining sinemurian formation samples (Table 8) and their respective chemical compositions (Table 5). Other physico-chemical characteristics of the unweathered former parent material of each soil horizon, such as bulk density, were estimated in the same way.

Table 8. Proportions X_{RSPM_n} and X_{SPM_n} of the different residues from carbonate dissolution of the remaining sinemurian formation samples (RRSFs) and of the different remaining sinemurian formation samples (RSFs=limestone L and marl M samples), respectively, in the weathered and non-weathered former parent materials (FPMs) of each soil horizon, respectively. The errors in the estimation of the concentration $C_{i,RSPM_h}$ of the immobile element i (either Zr or Hf) are calculated comparing the values estimated with the proportions X_{RSPM_n} to those derived from [equation \(3\)](#).

FPM of soil horizon...	Best immobile element	X_{RRSF_n} (in %)						X_{RSF_n} (in %)						Error of estimation on $C_{i,RRSF_h}$ (in %)	
		L1	L2	L3	L4	L5	M	L1	L2	L3	L4	L5	M	Zr	Hf
		LE1	Hf	0	0	96.3	0	0	3.7	0	0	99.2	0	0	0.8
LE2	Hf	0	0	69.6	0	0	4	0	0	91.5	0	0	8.5	0.9	
E	Zr	2.0	0	0	0	0	98.0	7.9	0	0	0	0	92.1		0.2
Bd1	Hf	0	0	83.9	0	0	16.1	0	0	96.1	0	0	3.9	7.7	
Bd2	Zr	96.7	0	0	0	0	3.3	99.2	0	0	0	0	0.8		16.7
Bd3	Zr	76.8	0	0	0	0	23.2	93.4	0	0	0	0	6.6		11.8
Bd4	Zr	68.1	0	0	0	0	31.9	90.1	0	0	0	0	9.9		7.6
Bc1	Zr	36.5	0	0	0	0	63.5	71.1	0	0	0	0	28.9		5.9
Bc2	Zr	22.0	0	0	0	0	78.0	54.6	0	0	0	0	45.4		5.9
C1	Zr	58.6	0	0	0	0	41.4	85.8	0	0	0	0	14.2		2.3
C2	Zr	63.8	0	0	0	0	36.2	88.3	0	0	0	0	11.7		4.7
C3	Zr	71.3	0	0	0	0	28.7	91.4	0	0	0	0	8.6		3.8

3.2.3. Former parent material thickness weathered for each soil horizon

We calculated the thicknesses of the former parent materials weathered to form each soil horizon and we compared them to geological descriptions of the sinemurian-aged formation in the studied area ([Mouterde, 1952](#)). Thicknesses were computed using the volumetric strain (ε) approach, *i.e.* the soil volume change through time, as defined by [Brimhall et al. \(1991\)](#):

$$\varepsilon = \frac{\rho_{FPM_h} \times C_{i,FPM_h}}{\rho_h \times C_{i,h}} - 1 \quad (4)$$

where ρ_{FPM_h} (in g cm^{-3}) and C_{i,FPM_h} (in mg kg^{-1}) are respectively the bulk density and the concentration of the immobile element i in the former parent material (FPM) of the soil horizon h , ρ_h (in g cm^{-3}) and $C_{i,h}$ (in mg kg^{-1}) are respectively the bulk density and the concentration of the immobile element i in the soil horizon h ([Table 2](#) and [Table 7](#)). The volumetric strain ε was calculated with both Zr and Hf as immobile elements i .

The volumetric strain ε of the solum is highly negative ([Fig. 5a](#)), which means that the volume was drastically reduced from the former parent materials to the derived soil horizons. This reduction of volume is due to the dissolution of the large amounts of CaCO_3 originally occurring in the former parent materials ([Table 3](#)).

Variations in the volumetric strain with depth were considered to result from variations in the initial CaCO_3 contents of the former parent materials of each soil horizon. To check this hypothesis, we normalized the volumetric strain ε of each soil horizon to the CaCO_3 content of their corresponding former parent material. Such a volumetric strain corrected for CaCO_3 is low – around 1% ([Fig. 5b](#)) – and thus considered insignificant. This

result indicates that the observed reduction of volume is mainly due to carbonate dissolution. However, results depicted on Fig. 5b show that the E-horizon has been more compressed than the other soil horizons. This higher compaction of the E-horizon is likely related to its higher bulk density (Table 2), probably due to the compaction from agricultural machinery traffic.

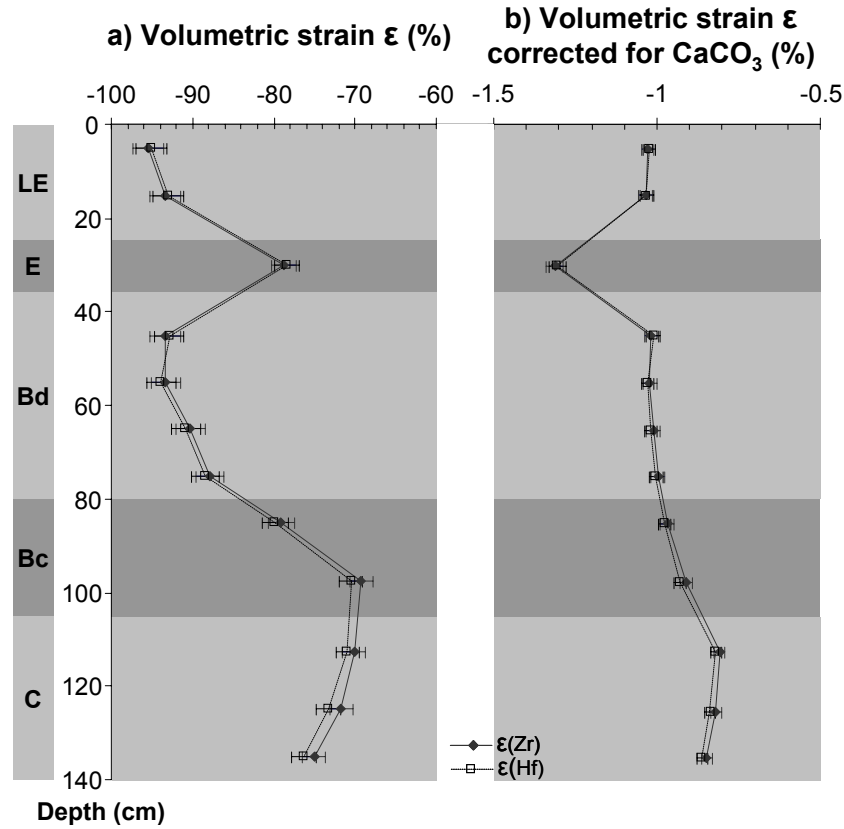


Fig. 5. (a) Calculated volumetric strain ϵ (in %) along the studied solum using Zr and Hf as immobile elements. (b) Calculated volumetric strain normalized to the CaCO_3 contents of the corresponding former parent material reconstructed for each soil horizon.

Since the volumetric strain ϵ is not significantly different between Zr and Hf (Fig. 5a), both immobile elements were used for the rest of the mass balance calculations. The results, obtained using either Zr or Hf as immobile element are similar, which validates the immobility of these two elements during pedogenesis. However, for clarity, only the results of the calculations performed with Zr as the immobile element will be shown hereafter.

The thickness H_{FPM_h} (in cm) of the former parent material FPM required to develop the soil horizon h is given by equation (5):

$$H_{\text{FPM}_h} = H_h \times \frac{1}{\epsilon + 1} \quad (5)$$

where H_h is the thickness of the soil horizon h (in cm).

The thickness H_{SPM_h} of each remaining sinemurian formation sample within the thickness of the former parent material (FPM) can be calculated for each soil horizon by

weighting the thickness H_{FPM_h} of the FPM by the respective percentages (x_{SPM_n}) of the remaining sinemurian formation (RSF) samples (Table 8), following equation (6):

$$H_{RSF_n} = x_{RSF_n} \times H_{FPM_h} \quad (6)$$

Results of these two calculations indicate that the total thickness of former parent materials required to form the whole soil profile is about 12.8 m, with almost 5 m of limestone L1, 6.5 m of limestone L3, and only 1.4 m of marl M (Table 9). This total thickness compares well with the 12 m given for the sinemurian-aged formation in this area (Mouterde, 1952).

Table 9. Thickness (in cm) of the former parent material (FPM) of each soil horizon and of the remaining sinemurian formation samples (L1, L3 and M) based on volumetric strains ε calculated with Zr.

FMP of soil horizon...	Thickness (in cm)			
	L1	L3	M	Total
LE1	0	220	2	222
LE2	0	205	19	224
E	4	0	43	47
Bd1	0	219	9	228
Bd2	148	0	1	149
Bd3	96	0	7	103
Bd4	74	0	8	82
Bc1	34	0	14	48
Bc2	27	0	22	49
C1	43	0	7	50
C2	31	0	4	35
C3	37	0	3	40
Whole profile	494	644	139	1 277

The calculated thicknesses of the parent materials weathered to form the different soil horizons vary from 31 to 220 cm for the sum of the different limestone layers and from 1 to 43 cm for the sum of the different marl beds (Table 9). This corresponds to the total thickness of limestone or of marl for a given soil horizon, without consideration of their arrangement with depth (several limestone layers and marl beds, or only one of each). These thicknesses of remaining sinemurian formation samples are in good agreement with the 5 to 80 cm and few mm to 15 cm reported in the literature for individual limestone layer and marl bed, respectively (Collenot, 1873; Mouterde, 1952).

Finally, the correspondence between the FPMs and the geological descriptions of the sinemurian-aged formation in the studied area evidences the relevance of the methodology applied, which permits to reconstruct the former parent material of each soil horizon with a fairly good precision.

3.3. Elemental fluxes during weathering and pedogenesis

Fluxes of major elements and REEs (j) during weathering and pedogenesis were estimated by mass balance calculations as proposed by Brimhall *et al.* (1991) and modified by Egli and Fitze (2000), using Zr and Hf as immobile elements.

The open-system mass-transport function $\tau_{j,h}$, *i.e.* the mass fraction of major elements and REEs gained or lost (positive or negative values respectively) from the soil horizon h during weathering and pedogenesis relative to their initial stocks in the former parent material (FPM), was calculated for each soil horizon according to equation (7):

$$\begin{aligned} \tau_{j,h} &= \left(\frac{\rho_h \times C_{j,h}}{\rho_{FPM_h} \times C_{j,FPM_h}} \right) \times (\varepsilon + 1) - 1 \\ &= \left(\frac{C_{j,h} \times C_{i,FPM_h}}{C_{j,FPM_h} \times C_{i,h}} \right) - 1 \end{aligned} \quad (7)$$

where $C_{j,h}$ (in mg kg^{-1}) and C_{j,FPM_h} (in mg kg^{-1}) are the concentrations of major elements and REEs in the soil horizon h (Table 1) and in its FPM, respectively.

Mass fluxes of major elements and REEs $m_{j,\text{flux},h}$ (in mg cm^{-2}) were then calculated for each soil horizon h according to equation (8):

$$\begin{aligned} m_{j,\text{flux},h} &= \rho_{\text{FPM}_h} \times C_{j,\text{FPM}_h} \times \tau_{j,h} \times H_h \times \left(\frac{1}{\varepsilon + 1}\right) \\ &= \rho_{\text{FPM}_h} \times C_{j,\text{FPM}_h} \times \tau_{j,h} \times H_{\text{FPM}_h} \end{aligned} \quad (8)$$

After that, current stocks of major elements and REEs were also calculated for each soil horizon by equation (9):

$$S_{j,h} = \rho_h C_{j,h} H_h \quad (9)$$

where $S_{j,h}$ is the stock of major elements and REEs (in mg cm^{-2}), ρ_h and H_h are respectively the bulk density (in g cm^{-3} ; Table 2) and the thickness (in cm ; Table 6) of the considered soil horizon h .

Finally, initial stocks of major elements and REEs in the former parent material (FPM) of each soil horizon h S_{j,FPM_h} were calculated according to equation (10):

$$S_{j,\text{FPM}_h} = \rho_{\text{FPM}_h} \times C_{j,\text{FPM}_h} \times H_{\text{FPM}_h} \quad (10)$$

3.3.1. Mobility of the selected immobile elements during pedogenesis

The mass-transport function of Hf calculated with Zr as immobile element is always lower than 9% in the different soil horizons, which indicates that Hf is immobile through pedogenesis within the errors on the calculations (Table 10), considering its losses during weathering (Table 3). Similarly, the mass-transport function of Zr, calculated with Hf as immobile element, is always lower than 10% (data not shown). These mass-transport functions are much lower than those calculated for the other elements initially considered potentially immobile and finally discarded, *i.e.* Ti, Nb, Y, V, Th (data not shown). This first result confirms that Zr and Hf elements can be considered as the most immobile elements throughout pedogenesis, and thus validate our initial hypothesis.

Table 10. Mass-transport function (in %) calculated for Hf, major elements and REEs in each soil horizon with Zr as immobile element.

Soil horizon	Major elements				REEs																	
	Hf	Si	Al	Mn	La	Ce	Pr	Nd	Sm	Eu	Gd	Tb	Dy	Ho	Er	Tm	Yb	Lu	REEs	MREEs	HREEs	
LE1	-9±3	-23±6	-61±16	-89±17	-99±22	-90±22	-86±21	-88±22	-89±22	-90±29	-89±24	-89±27	-89±26	-90±27	-90±27	-90±31	-90±27	-90±32	-89±25	-88±22	-89±26	-90±29
LE2	-5±1	-25±5	-65±17	-86±16	-98±22	-86±22	-81±20	-85±21	-86±22	-88±26	-87±23	-87±25	-86±25	-87±25	-87±25	-86±30	-87±25	-87±30	-86±24	-84±21	-87±24	-86±27
E	-2±0	-37±4	-71±15	-74±10	-82±16	-75±15	-67±13	-74±15	-77±15	-79±20	-82±16	-80±16	-80±19	-80±16	-79±16	-76±23	-74±15	-73±22	-76±17	-72±14	-80±17	-76±18
Bd1	-8±2	-10±2	-33±8	-81±15	-98±22	-79±20	-83±21	-85±21	-84±29	-85±26	-85±23	-85±25	-85±25	-85±25	-86±25	-85±30	-86±25	-86±30	-84±24	-82±21	-85±25	-86±27
Bd2	9±3	-22±6	-31±8	-77±15	-97±21	-80±24	-82±21	-80±24	-80±25	-79±21	-78±23	-78±22	-78±22	-77±23	-77±23	-75±37	-73±22	-73±36	-78±24	-80±20	-80±23	-75±28
Bd3	7±2	-19±4	-29±7	-72±14	-95±21	-78±20	-76±23	-76±23	-76±23	-77±23	-76±21	-75±21	-74±21	-73±21	-73±21	-71±32	-69±20	-68±31	-74±22	-75±19	-76±21	-71±25
Bd4	5±1	-15±3	-23±6	-61±12	-91±18	-70±17	-72±18	-70±18	-70±18	-71±21	-70±19	-69±19	-68±20	-67±19	-67±19	-65±29	-63±18	-62±28	-68±20	-69±17	-70±20	-65±22
Bc1	3±1	-12±2	-25±6	-49±9	-79±15	-66±16	-68±16	-66±16	-66±16	-62±17	-63±17	-62±16	-61±18	-61±16	-62±16	-59±23	-57±15	-56±22	-59±16	-56±14	-61±17	-59±19
Bc2	4±1	-2±0	-17±4	-22±4	-42±8	-44±11	-46±12	-49±15	-51±13	-53±14	-54±14	-54±14	-53±16	-54±14	-51±19	-48±12	-48±18	-47±13	-39±10	-51±14	-51±16	-45±11
C1	3±1	10±2	28±7	15±3	-47±9	-33±8	-35±9	-37±11	-36±10	-37±10	-37±10	-37±10	-36±10	-34±9	-36±10	-33±14	-31±8	-29±12	-34±10	-33±8	-36±10	-33±11
C2	6±2	16±3	41±11	5±1	-61±12	-36±9	-34±8	-35±9	-33±10	-32±9	-32±9	-32±9	-32±9	-32±9	-32±9	-29±13	-28±8	-29±12	-32±9	-35±9	-33±9	-30±10
C3	5±2	21±5	51±13	-6±1	-66±13	-42±11	-41±10	-42±10	-39±12	-39±12	-40±11	-40±11	-38±11	-38±11	-39±11	-35±16	-33±9	-32±15	-38±11	-41±10	-40±11	-36±12

3.3.2. Mobility of major elements and REEs during weathering and pedogenesis

The results of mass balance calculations show that major elements and REEs are mainly exported from the solum during weathering and pedogenesis, as shown by their negative mass-transport functions and mass fluxes along the solum (Table 10 and Fig. 6). These losses tend to increase from the bottom to the soil surface, reaching up to 90% of the initial stock of the former parent material in the most evolved LE-horizon, except for Si and Al that are less lost (Table 10). Along the solum, Si and Al, on the one hand, and Fe and Mn, on the other hand, display contrasted behavior. While the Si and Al losses increase especially from the Bd- to the E- and LE-horizon, those of Fe and Mn increase abruptly from the C- to the Bc-horizon, as well as also from the Bc- to the Bd-horizon (Table 10). This difference can be related to the mobilization of Si and Al by mainly eluviation and clay dissolution, whereas Fe and Mn are mainly mobilized by redox processes. Processes are best expressed, *i.e.* most active, in the C-horizon for weathering, in the Bc-horizon for primary redox conditions, in the Bd-horizon for secondary redox conditions, and in the LE- and E-horizons for eluviation (Fig. 2), which explains the different behavior of Si, Al, Fe and Mn along the studied solum.

Besides, to understand how a pedogenetic process influences major elements and REEs, we compare the mobilization of these elements in a horizon where a process is active to that in another horizon where the same process is not active. Indeed, comparing mass-transport functions of an element among different horizons is classically interpreted as a differential mobilization due to the different pedological processes because these horizons are supposed to be derived from the same homogeneous former parent material. However, when the former parent material is heterogeneous, the variation in the initial stock and speciation due to the parent material heterogeneity is also included within the mass transport functions, which must therefore be handled with caution. For this reason, only the largest variations and the clearest tendencies are discussed hereafter.

Weathering – Only Mn and REEs seem to be exported from the C-horizon during weathering (Fig. 6). The mass-transport functions of Mn and REEs show that these elements lost respectively about two and one third of their initial stock in the C-horizon during weathering, without significant fractionations among REEs (Table 10). Since weathering refers to the dissolution of carbonates contained in the former parent materials (Fig. 2), these results suggest that Mn and REEs were probably bound to carbonates in the former parent materials.

Redox processes – Concerning Fe, loss and gains are restricted in the C3- to Bc2-horizons, and increase abruptly in the overlying soil horizons (Table 10). The high Mn losses recorded in the C3- and C2-horizons decrease in the C1- and Bc2-horizons, and then increase again abruptly in the overlying soil horizons (Table 10).

During winter and spring, the water table in contact with the sinemurian-aged formation fluctuates regularly, leading to alternations of reducing and oxidative conditions in the top of the C-horizon and of the Bc-horizon, so-called primary redox conditions (Fig. 2). These alternations were shown to be responsible for the formation of Fe-Mn nodules (McKenzie, 1989; Khan and Fenton, 1994; Zhang and Karathanasis, 1997) that are abundant in these horizons of these soils and that are particularly enriched in Mn (Baize and Chrétien, 1994; Laveuf *et al.*, 2009, cf. Chapitre 3.1.).

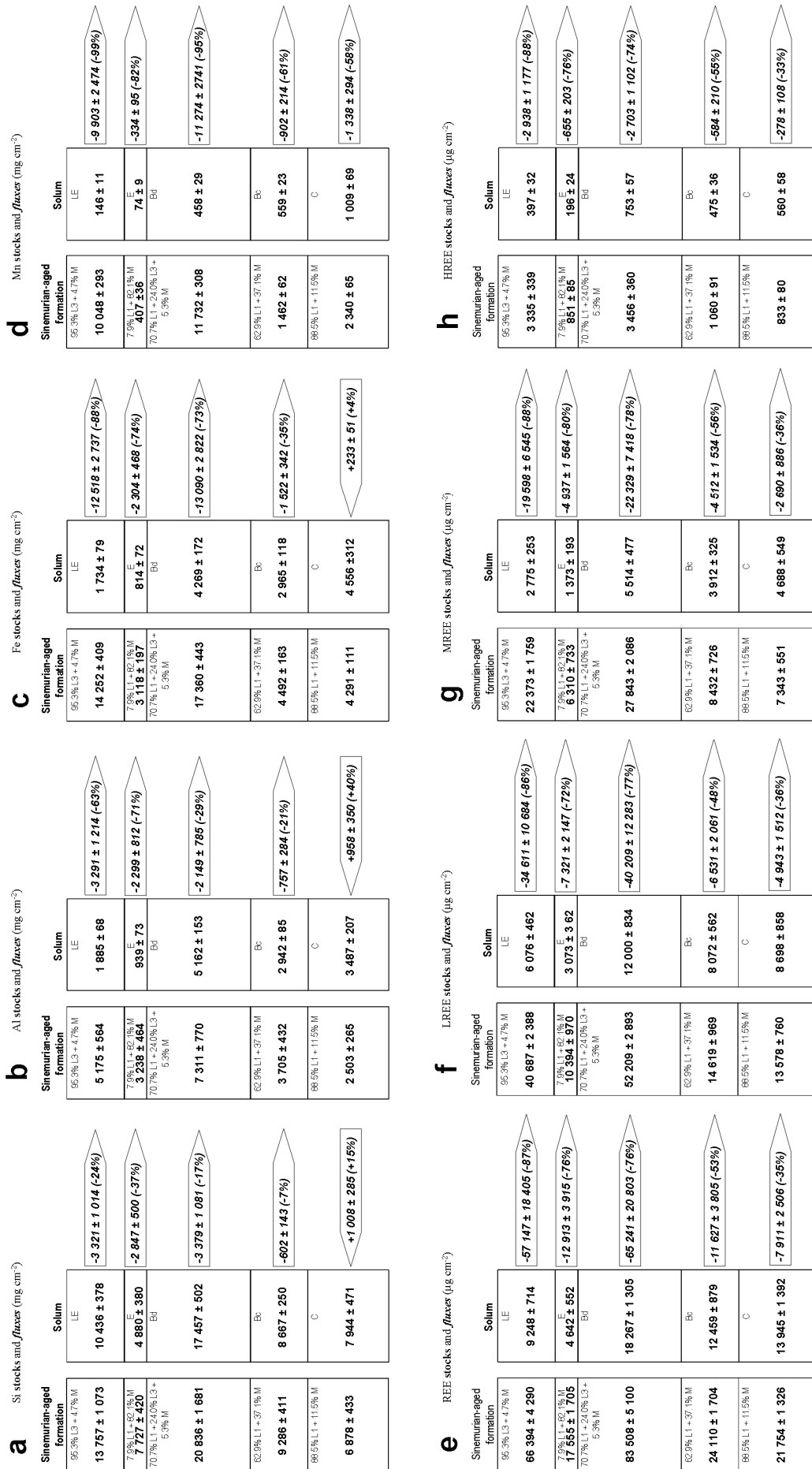


Fig. 6. Initial stocks (\pm errors) in the former parent material of each soil horizon, actual stocks (\pm errors) in the soil horizons and mass fluxes (\pm errors and percentage of initial stock mobilized) during pedogenesis within each soil horizon for **(a)** Si, **(b)** Al, **(c)** Fe, **(d)** Mn, **(e)** REEs, **(f)** LREEs, **(g)** MREEs, **(h)** HREEs.

When reducing conditions are strong enough, Fe- and Mn-oxides are dissolved. Once in solution, Fe and Mn are redistributed locally on the centimeter scale or on a larger scale during water table fluctuations, and then precipitate and concentrate in Fe-Mn nodules. The behavior of Fe differs from Mn, because of the differential redox sensitivity of these elements (Brookins, 1988). This explains the lack of correlation between Fe and Mn fluxes in the C- and Bc-horizons (Fig. 6c and 6d). The lower losses of Mn in the Bc2- and C1-horizons, where Fe-Mn nodules are in formation, than in the underlying soil horizons, suggests that Mn is transferred from the C2- to the C3-horizons during temporary water table elevation (Table 10). Local redistribution may also occur. Since no Fe losses are recorded in the C-horizon (Table 10), we assume that Fe is released into soil solution during temporary water table elevation in the Bc-horizon, and then locally redistributed and partly precipitated as Fe-Mn nodules during water table lowering. In the Bc2-horizon, Ce is significantly less lost than the other LREEs (Table 10). According to the literature, soil Fe-Mn nodules are enriched in Ce compared to other REEs (Rankin and Childs, 1976; Coelho and Vidal-Torrado, 2000; Palumbo *et al.*, 2001). This is in agreement with the results of Laveuf *et al.* (2008, cf. Chapitre 4.2.1.) for Fe-Mn nodules developed in the same soil type. This result was interpreted as resulting from a coupled Ce oxidation and Mn reduction at the surface of Mn-oxides, as already suggested by other studies (Ran and Liu, 1992; Marker and de Oliveira, 1994; Bau, 1999; Takahashi *et al.*, 2000; Ohta and Kawabe, 2001). The larger incorporation of Ce in Fe-Mn nodules thanks to its higher affinity for Mn-oxides compared to the other REEs explain its lower loss compared to the other REEs in the Bc2-horizon (Table 10). However, no correlation between Ce and Mn fluxes could be evidenced, showing a more complex behavior of these elements on the soil horizon scale during primary redox conditions. Finally, REEs, Mn and Fe are exported from the solum during primary redox conditions, as shown by their large negative fluxes (Fig. 6c to 6h). The Fe inputs in the C-horizon could finally result from the translocation, during water table lowering, of the Fe dissolved into soil solution in the Bc-horizon and/or from lateral transfer through the water table (Fig. 6).

The losses of Fe and Mn increase abruptly from the Bc- to the Bd-horizon (Fig. 6c and 6d). Indeed, Mn losses are higher larger than 90 % of the initial stock of this element, while those of Fe range from 60 to 80% (Fig. 6c and 6d and Table 10). Concomitantly, REE losses increase (Fig 6e), without significant fractionations (Table 10 and Fig. 6f to 6h). During winter, reducing conditions appear in the Bd-horizon, due to the occurrence of a perched water table (Fig. 2). These secondary redox conditions lead to the morphological degradation of the Bd-horizon (Baize and Chrétien, 1994; Laveuf *et al.*, 2009, cf. Chapitre 3.1.), as defined by Pedro *et al.* (1978), *i.e.* the dissolution of the Fe-oxides cementing the finest soil fractions under reducing conditions. Such a process is evidenced by the bleached zones in the Bd-horizons (Fig. 1). These results mean that, once secondary redox conditions appear, REEs, Fe and Mn are highly mobilized and exported from the solum since no gains of the same order are recorded in the other soil horizons (Fig. 6c to 6e). In addition, Mn fluxes and Fe fluxes within the Bd-horizon show a significant correlation (Fig. 7a). It proves their somewhat similar behavior during secondary redox conditions, whereas no correlations between the fluxes of these two elements could be evidenced during primary redox processes. REE mass fluxes are well correlated with both Fe and Mn mass fluxes in the Bd-horizon (Fig. 7b and 7c). It suggests that the losses of REEs could be due to the dissolution of both Fe- and Mn-oxides. LREE and MREE mass fluxes show a strong positive correlation with Fe and Mn

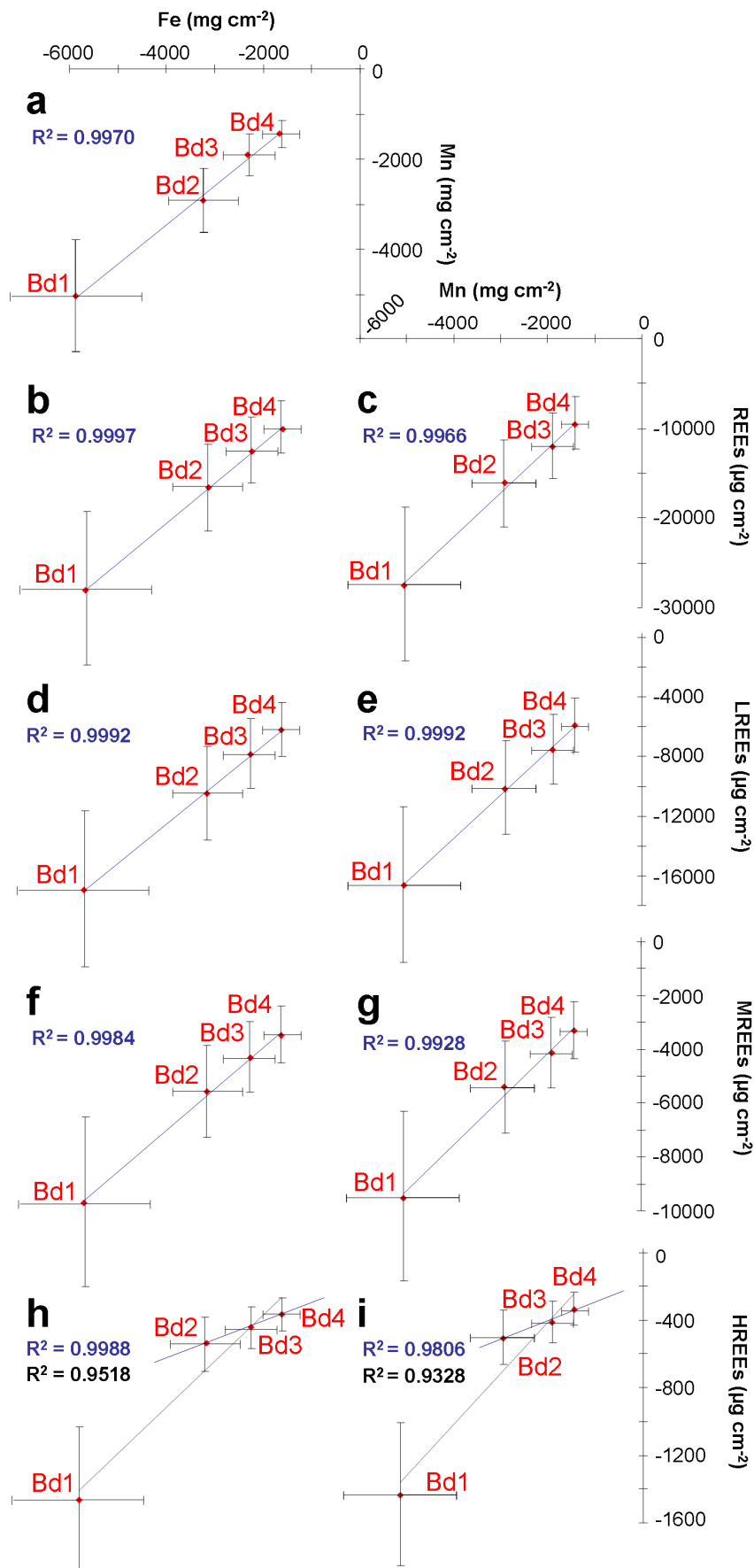


Fig. 7. Linear regression of the masse fluxes of Fe and Mn, within the Bd-horizon, with respect to each other (a), to REEs (b) and (c), to LREEs (d) and (e), to MREEs (f) and (g), and to HREEs (h) and (i).

mass fluxes (Fig. 7d and 7e), while HREE mass fluxes show a good correlation with Fe and Mn mass fluxes only in the horizons Bd4 to Bd2 (Fig. 6d to 6h). Since Mn-oxides are known to be LREE-enriched (Fendorf and Fendorf, 1996; Ohta and Kawabe, 2001) and amorphous Fe-oxides rather MREE-enriched (Steinmann and Stille, 1997; Land *et al.*, 1999; Yan *et al.*, 1999), the correlations of LREEs and MREEs losses with Fe and Mn losses suggest that these oxides are effectively dissolved during secondary redox conditions. The lack of correlation of HREE losses with Fe and Mn ones in the Bd1-horizon suggests that HREE losses are not only related to the dissolution of Fe- and Mn-oxides in this horizon.

Clay mobilization – The fluxes and mass-transport function of Si and Al evidence larger losses from the Bd- to LE-horizons than from the Bc-horizon (Fig. 6a and 6b). The fluxes exiting these horizons are much higher than those entering the C-horizon (Fig. 6a and 6b) and the proportion of the <2 μm fraction also decreases from the Bc-horizon towards the soil surface (Table 6). These fluxes have similar values for Si and Al, which suggests that these elements are mostly exported from the solum and responsible for the decrease in the proportion of the <2 μm fraction towards the soil surface. These exportations could be explained by eluviation, which has already been described in the LE- and E-horizons of similar non-truncated soils (Baize and Chrétien, 1994; Laveuf *et al.*, 2009, cf. Chapitre 3.1.). The increase of REE losses, without significant fractionations (Table 10 and Fig. 6f to 6h), as well as that of Fe, in the LE-horizon compared to the Bd-horizon (Fig. 6e), suggest that REEs and Fe are further mobilized by clay eluviation. Finally, the inputs of Si and Al in the C-horizon could result from a vertical transfer within the solum and/or from a lateral transfer through the water table occurring in the C-horizon.

4. Conclusion

We proposed an approach to identify the parent material of each soil horizon in the case of a solum developed from a complex succession of limestone layers and marl beds. This approach is based on concentrations of immobile elements in soil horizons and in parent materials. Zr and Hf are found to be the best immobile elements with quartz in that pedological context among the one classically used (Hf, Zr, Ti, Th, Nb, Y, V). However, this immobility is only verified during pedogenesis, since Hf and Zr losses can be recorded during weathering, as shown by experimental carbonate dissolutions. It would be interesting to check the immobility of these elements in term of stocks in lab-experiments simulating the different pedological processes.

We demonstrated that, under certain conditions, it is possible to apply the mass-balance approach on heterogeneous parent materials by the reconstruction of the former parent materials. However, this approach is only possible as long as the remaining parent materials still exist and are representative of the variability of the weathered parent materials. In addition, this approach is based on the hypothesis that pedogenesis is responsible for a linear increase of the concentrations of immobile elements towards the surface along the studied solum.

Mass transport functions and mass fluxes show that major elements and REEs are highly mobilized during weathering and pedogenesis. Due to the initial different content and speciation of REEs, and major elements in the different former parent materials of each soil horizon, caution should be paid when comparing results among soil horizons.

Weathering leads to important Mn and REE losses. Redox processes, which mainly act on Fe and Mn, induce large REEs, Fe and Mn losses. During primary redox conditions, Ce is preferentially retained over the other REEs in the soil horizon where Fe-Mn nodules are forming. This behavior is attributed to the higher affinity of Ce for Mn-oxides compared to the other REEs. During secondary redox conditions, Fe- and Mn-oxides in the finest fractions of the Bd-horizon are dissolved. The behaviors of Fe, Mn, LREEs and MREEs are linked during this process, as shown by the correlations between their fluxes. Finally, eluviation further mobilizes REEs and Fe, in addition to Si and Al.

Further investigations are necessary to better understand the relationship between Ce and Mn fluxes during primary redox conditions and to distinguish the impact of the dissolution of amorphous and crystalline Fe- and Mn-oxides on the mobilization of REEs during secondary redox processes.

5. Acknowledgements

The authors are grateful to the INRA department “Environnement et Agronomie” and to the Région Centre, France, for their financial support.

5.2. Conclusions

Notre approche de reconstitution des matériaux parentaux permet de s'affranchir de l'hypothèse d'homogénéité des matériaux parentaux dans l'approche bilan de masse et ainsi d'appliquer cette approche à des matériaux hétérogènes.

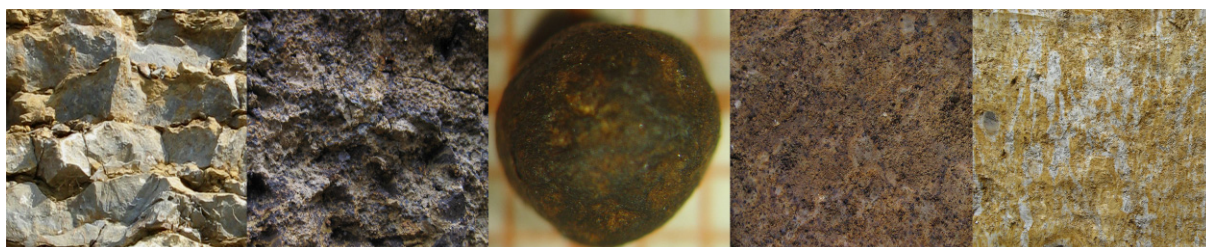
Néanmoins, il s'avère que les bilans de masse sont peu informatifs sur les fractionnements en terres rares au cours de la pédogenèse si l'on prend en compte les incertitudes élevées de ces calculs. De plus, contrairement au cas de matériaux parentaux homogènes, la comparaison des flux d'éléments au cours de la pédogenèse doit être menée avec précaution. En effet, comme le matériau parental de chaque horizon présente une composition chimique et minéralogique différente, il n'est pas possible de comparer les flux entre horizons sans prêter attention à cette variabilité en contexte hétérogène. La déconvolution quantitative du rôle des différents processus pédogénétiques sur la mobilisation des terres rares n'est donc pas immédiate.

Ainsi, la méthodologie de normalisation présentée au [Chapitre 4](#) précédent est plus informative sur les fractionnements en terres rares que l'approche intégrée du bilan de masse telle que présentée dans ce chapitre.

Pour affecter aux différents processus pédogénétiques les flux en éléments qu'ils engendrent, une approche prenant en compte les traits pédologiques est donc nécessaire. C'est ce que je réalise dans le [Chapitre 6](#) lors de l'étude de l'impact des conditions redox sur la mobilisation des terres rares. Dans ce chapitre qui suit, j'envisage tout d'abord la redistribution des terres rares au cours du processus de décarbonatation.

Chapitre 6

**Impact des processus
sur la redistribution des terres rares**



L'objectif de ce chapitre est de tenter de quantifier l'impact de deux processus pédogénétiques particulièrement importants dans les sols étudiés (*i.e.* la décarbonatation, puis les conditions rédox) sur le comportement des terres rares, afin de mieux évaluer le potentiel de ces éléments à tracer ces processus dans les sols. L'hypothèse initialement formulée pour les sols étudiés est que ces deux processus se suivent au cours de la pédogenèse. Je vais donc les envisager successivement, en commençant par celui qui concerne l'altération du substratum carbonaté des sols étudiés : la décarbonatation.

6.1. Redistribution des terres rares au cours du processus de décarbonatation

Le processus de décarbonatation conduit à la dissolution des carbonates des lits marneux et des bancs calcaires. Au cours de ce processus, les éléments potentiellement liés aux phases minéralogiques carbonatées sont ainsi mis en solution. Nous avons vu précédemment que le devenir de ces éléments dépendait de la quantité de carbonates contenue dans les calcaires et de la spéciation des différents éléments dans ces calcaires.

Pour quantifier la mise en solution des terres rares au cours du processus de décarbonatation, puis leur devenir une fois en solution, je propose d'étudier la localisation de ces éléments dans les différents calcaires et de comparer la quantité libérée au cours de la dissolution expérimentale des matériaux parentaux au flux sortant de l'horizon C affecté par ce processus (flux calculé par bilan de masse). Ceci permet de conclure sur la fixation éventuelle des éléments mis en solution lors de la décarbonatation sur des phases minérales résiduelles et/ou néoformées.

6.1.1. Matériels et méthodes

Les blocs de calcaire d'âge sinémurien *sensu largo (s.l.)* ont été prélevés sur les deux sites (cf. [Chapitre 2](#)) afin de mettre en évidence une éventuelle variabilité verticale et latérale dans la composition chimique et minéralogique du calcaire. Les zones présentant des traces d'altération ont été écartées et les zones saines ont été décarbonatées par attaque acide.

Classiquement, des solutions d'acide chlorhydrique diluées sont utilisées pour décarbonater les échantillons hautement carbonatés ([Robert et Tessier, 1974](#) ; [Mathieu et Pieltain, 1998](#)). C'est ce qui a été réalisé dans un premier temps pour les calcaires de l'Auxois. Néanmoins, ces solutions sont agressives vis-à-vis des phases minérales constituant le résidu calcaire, et notamment vis-à-vis des oxy-hydroxydes de Fe, même lorsque le pH est maintenu supérieur à 5. C'est la raison pour laquelle, pour les calcaires de Terre-Plaine, j'ai utilisé une solution de décarbonatation d'acide acétique (a.r. ChemLab) tamponnée à pH 5,5 par de l'acétate de sodium (a.r. ChemLab), réactif recommandé pour la dissolution des carbonates au cours d'extractions séquentielles ([Han et Banin, 1995](#)). Le protocole expérimental, qui consiste à répéter cette extraction jusqu'à l'absence de dégagement gazeux, est le même que celui présenté dans le [Chapitre 5](#).

Les échantillons de calcaire brut et les résidus d'extraction ont été analysés au [SARM-CRPG](#) (Vandœuvre-lès-Nancy, France) par ICP-AES pour l'analyse des éléments majeurs et par ICP-MS pour les terres rares, après fusion alcaline au LiBO₂, ainsi qu'au [LAS-INRA](#) (Arras, France) pour l'analyse des teneurs en carbonates.

La composition minéralogique des échantillons de calcaire et de leurs résidus de décarbonatation a été déterminée par diffraction des rayons X (DRX). Ces analyses DRX permettent également de vérifier que la dissolution de la calcite est complète dans les résidus de décarbonatation. Les analyses DRX ont été acquises sur poudres, dopées avec 10% de corindon, avec un angle 2 θ variant de 0° à 75° et un temps de comptage de 10 s par pas de 0,005°, en utilisant la radiation K α de Co (35 kV, 40 mA). Les évolutions minéralogiques quantitatives ont été estimées sur la base d'un rapport d'intensité des pics de diffraction normalisés au pic (001) du corindon.

Des lames minces (45 x 60 mm², 25 µm d'épaisseur) ont été préparées sur des blocs de calcaires sains par induration en surface. Ces lames minces ont été micropolies, puis recouvertes d'une couche de carbone de 20 nm d'épaisseur. La localisation des éléments dans les différents calcaires a été déterminée par microscopie optique et microscopie électronique à balayage (MEB, Cambridge Stereoscan 90B) couplée à des micro-analyses par EDS (Energy Dispersive Spectrometer), ainsi que par des analyses par microsonde (Cameca SX50 avec une tension d'accélération de 15 keV, une intensité de courant de 50 nA et des temps de comptage de 10 s pour Ca, P, Si, Al, Fe, Mn, de 40 s pour S et de 60 s pour Ce) et par micro-fluorescence X (XGT-5000 Horiba avec une tension d'accélération de 50 keV et une intensité de courant de 1 mA pour Ca, P, Si, Fe, Mn, S et Ce).

Enfin, des bilans de masse ont été calculés en utilisant la méthode de [Brimhall *et al.* \(1991\)](#) amendée par [Egli et Fitze \(2000\)](#), afin de déterminer les quantités d'éléments évacuées ou fixées dans l'horizon C suite à leur mise en solution lors de la décarbonatation des calcaires.

6.1.2. Signature en terres rares des calcaires

Les calcaires de la Terre-Plaine sont nettement moins riches en terres rares que ceux de l'Auxois. Au sein de chacun des sites, en revanche, les concentrations totales en terres rares des différents calcaires sont similaires ([Figure 1](#)).

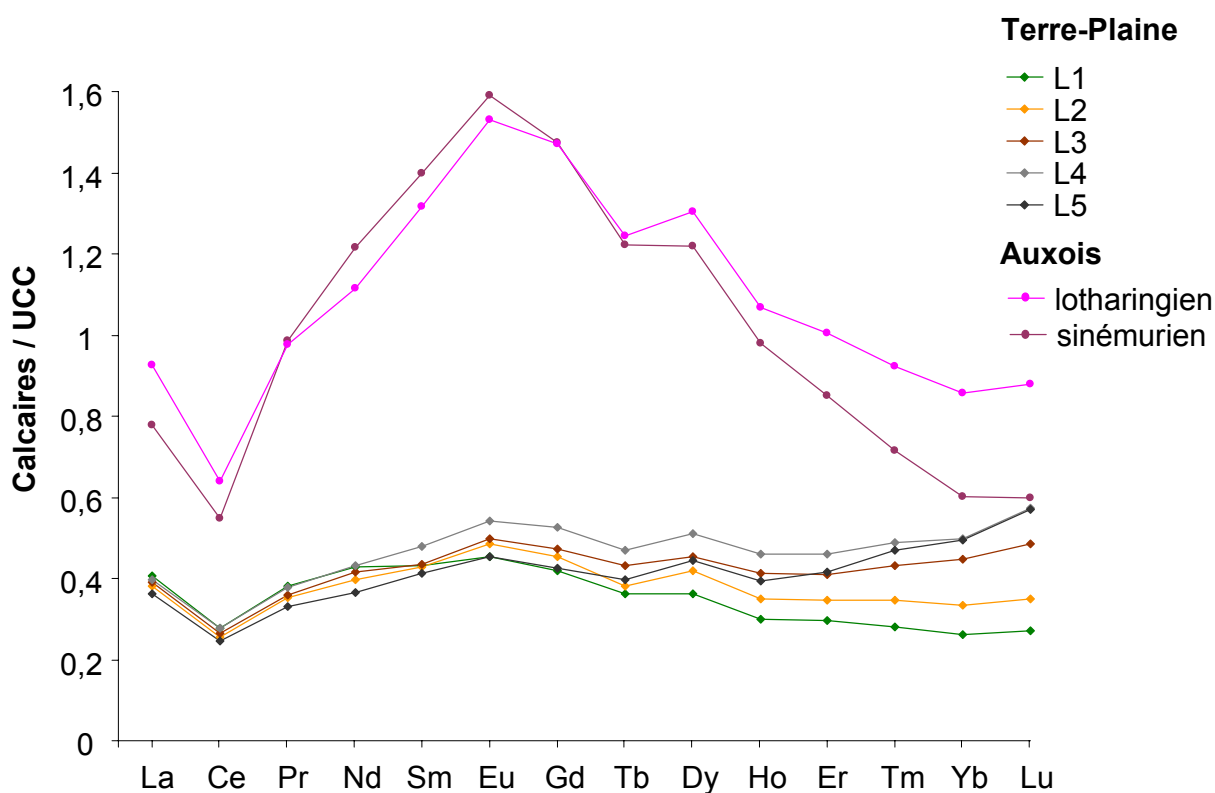


Figure 1. Spectres des concentrations en terres rares des calcaires L1 à L5 de la Terre-Plaine et des calcaires d'âge lotharingien et sinémurien de l'Auxois normalisées à la Croûte Continentale Supérieure (UCC ; Taylor et McLennan, 1985).

Les calcaires de la Terre-Plaine sont appauvris en terres rares par rapport à la Croûte Continentale Supérieure (Taylor et McLennan, 1985 ; Figure 1). Les calcaires de l’Auxois sont, quant à eux, enrichis en terres rares moyennes et appauvris en terres rares légères et lourdes par rapport à cette même Croûte Continentale (Figure 1). Les spectres de terres rares des deux sites sont caractérisés par un enrichissement en terres rares moyennes, seulement par rapport aux terres rares légères pour L3 à L5, et une anomalie négative en Ce (Figure 1). Cette anomalie négative en Ce est une constante des matériaux géologiques carbonatés (Haskin et Gehl, 1962 ; Reeder et America, 1983 ; Henderson, 1984), qui peuvent, par ailleurs, s’enrichir en terres rares moyenne au cours de la diagenèse (Picard *et al.*, 2002 ; Lécuyer *et al.*, 2004).

6.1.3. Mise en solution des terres rares au cours de la décarbonatation

Le comportement des calcaires de la Terre-Plaine au cours de la décarbonatation diffère d’un échantillon à l’autre (Figure 2). En effet, les terres rares sont significativement moins libérées lors de la décarbonatation du calcaire dans L1 par rapport aux autres échantillons de la Terre-Plaine (39% contre en moyenne 48%). Le comportement des calcaires de l’Auxois au cours de la décarbonatation est beaucoup plus contrasté (Figure 2). L’échantillon d’âge sinémurien de l’Auxois libère nettement moins de terres rares (32%) que ceux de la Terre-Plaine, tandis que celui d’âge lotharingien en libère beaucoup plus (73%).

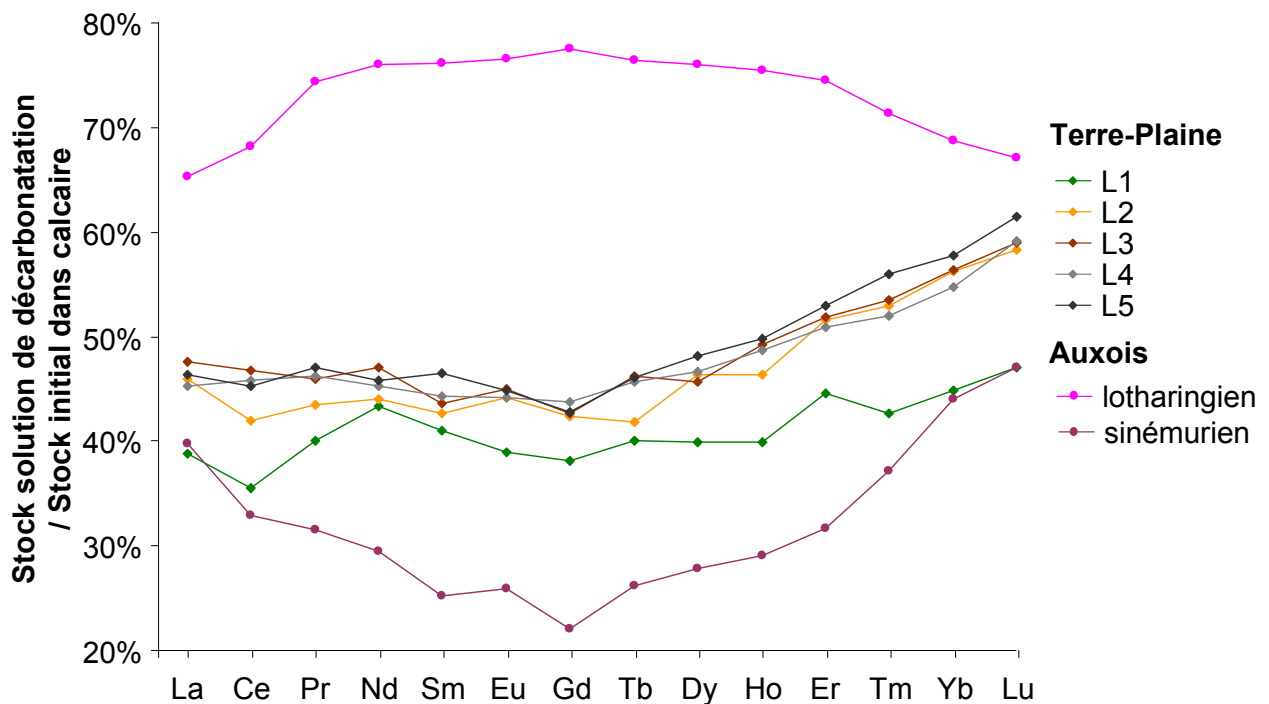


Figure 2. Spectres du pourcentage du stock initial de terres rares mises en solution au cours de la décarbonatation expérimentale des différents échantillons de calcaires de la Terre-Plaine (L1 à L5) et des calcaires d’âge sinémurien et lotharingien de l’Auxois

Par ailleurs, dans les calcaires d'âge sinémurien *sensu stricto* (s.s.), les terres rares lourdes sont préférentiellement libérées par rapport aux autres terres rares (Figure 2). Dans le calcaire d'âge sinémurien de l'Auxois, les terres rares moyennes sont moins libérées que les autres terres rares, alors que c'est le contraire dans le calcaire d'âge lotharingien. Une anomalie négative en Ce apparaît dans les solutions de décarbonatation de quatre calcaires d'âge sinémurien (L1, L2, L5 et Auxois ; Figure 2), celle-ci étant particulièrement marquée pour L1.

Ainsi, bien que les spectres de terres rares des calcaires d'âge sinémurien *s.l.* soient très semblables (Figure 1), la spéciation des terres rares en leur sein diffère comme montré par les différences entre les spectres du pourcentage de terres rares mises en solution au cours de la décarbonatation des différents échantillons (Figure 2). Sur la base de ces différences, quatre groupes peuvent être identifiés : (i) les calcaires L2 à L5, (ii) L1, (iii) le calcaire sinémurien de l'Auxois et (iv) le calcaire lotharingien. Dans une étude préliminaire, Laveuf *et al.* (2008, cf. Chapitre 4.2.1.) ont supposé que ces différences de pertes en terres rares moyennes entre les calcaires étaient liées à des différences de proportions de minéraux résiduels. C'est ce que je vais tenter de vérifier dans la suite de ce chapitre.

6.1.4. Spéciation des éléments dans les calcaires

La mise en solution de Ca au cours de la décarbonatation expérimentale est proche de 100% (Tableau 1), ce qui indique que l'expérimentation de décarbonatation a détruit la grande majorité des carbonates des échantillons (Figure 3). De plus, les pertes de masse au cours de l'expérimentation sont similaires aux teneurs en carbonates pour chacun des calcaires (Tableau 1), avec moins de 1% de différence. La fraction résiduelle est plus importante dans le calcaire L1, ce qui peut expliquer, en partie, la plus faible libération de terres rares au cours de sa décarbonatation. Néanmoins, la teneur en carbonates n'est pas la seule à contrôler la quantité de terres rares libérées, puisque le calcaire L5, dont la fraction résiduelle est significativement plus importante que L2, L3 et L4, libère une quantité de terres rares non significativement différente de ceux-ci (Figure 2). Ceci appuie encore l'hypothèse d'une spéciation variable des terres rares au sein des différents calcaires.

Lors de la dissolution des carbonates, on observe trois types de comportement selon les éléments :

- des éléments majoritairement mis en solution, à l'instar de Ca, et qui sont donc probablement majoritairement contenus dans les carbonates (principalement représentés par la calcite, seule phase carbonatée mise en évidence dans ces calcaires par les analyses DRX ; Figure 3) ;
- des éléments majoritairement contenus dans le résidu d'extraction (noté RL) ;
- des éléments présentant un comportement intermédiaire.

Tableau 1. Concentrations en CaCO₃ (équivalentes à la perte de masse), en éléments majeurs et en terres rares des différents calcaires de la Terre-Plaine, de leurs résidus de décarbonatation respectifs, et pourcentages correspondant mis en solution.

Echantillon	CaCO ₃ g kg ⁻¹	g kg ⁻¹											mg kg ⁻¹											TR légère	TR moy.	TR lourde		
		Si	Al	Fe	Mn	Mg	Ca	K	P	La	Ce	Pr	Nd	Sm	Eu	Gd	Tb	Dy	Ho	Er	Tm	Yb	Lu				TR	TR
L1	915	12.	3.9	10.	7.7	2.6	366	1.9	1.0	12.	17.	2.7	11.	1.9	0.4	1.5	0.2	1.2	0.2	0.6	0.0	0.5	0.0	50.	32.6	16.6	1.67	
L2	942	8.1	2.8	10.	7.4	2.2	374	1.4	0.8	11.	16.	2.5	10.	1.9	0.4	1.7	0.2	1.4	0.2	0.8	0.1	0.7	0.1	48.	30.3	16.1	2.04	
L3	932	8.2	2.9	11.	8.9	1.9	370	1.3	0.8	11.	17.	2.5	10.	1.9	0.4	1.7	0.2	1.5	0.3	0.9	0.1	0.9	0.1	50.	31.2	16.8	2.56	
L4	935	8.8	3.2	11.	8.3	2.0	371	1.4	1.1	11.	17.	2.6	11.	2.1	0.4	2.0	0.3	1.7	0.3	1.0	0.1	1.1	0.1	53.	32.3	17.9	2.87	
L5	922	10.	3.8	11.	7.8	2.0	367	1.9	0.8	10.	15.	2.3	9.4	1.8	0.4	1.6	0.2	1.5	0.3	0.9	0.1	1.0	0.1	46.	28.9	15.2	2.69	
RL1	0	162	55.	118	2.4	6.5	56.	21.	11.	90.	139	19.	76.	13.	2.9	11.	1.6	9.2	1.7	4.5	0.6	3.8	0.5	376	249	116	11.4	
RL2	0	135	48.	137	2.1	5.8	53.	18.	12.	102	155	23.	94.	18.	3.9	16.	2.3	12.	2.4	6.3	0.8	5.2	0.7	444	280	148	15.7	
RL3	0	116	44.	131	3.8	5.5	94.	17.	10.	85.	126	19.	79.	15.	3.3	14.	2.0	12.	2.3	6.3	0.9	5.9	0.8	373	230	126	16.4	
RL4	0	122	47.	131	3.6	5.8	88.	18.	12.	87.	129	19.	82.	16.	3.5	15.	2.2	12.	2.5	7.0	1.0	6.6	1.0	387	236	133	18.3	
RL5	0	136	51.	128	3.4	6.4	85.	19.	9.2	72.	106	15.	63.	12.	2.7	11.	1.6	9.9	1.9	5.5	0.8	5.6	0.8	310	193	102	14.9	
	%																											
Solution	100	-5	-15	8	97	79	99	9	8	39	36	40	43	41	39	38	40	40	40	45	43	45	47	39	37	42	44	
Solution	100	-1	-6	17	98	84	99	23	11	46	42	43	44	43	44	42	42	46	46	52	53	56	58	44	44	44	53	
Solution	100	-2	-10	16	97	79	98	7	11	48	47	46	47	44	45	43	46	46	49	52	54	56	59	47	47	46	54	
Solution	100	-3	-9	13	97	78	98	7	19	45	46	46	45	44	44	44	46	47	49	51	52	55	59	46	46	45	53	
Solution	100	-1	-8	13	96	74	98	18	12	46	45	47	46	47	45	43	46	48	50	53	56	58	62	46	46	46	55	

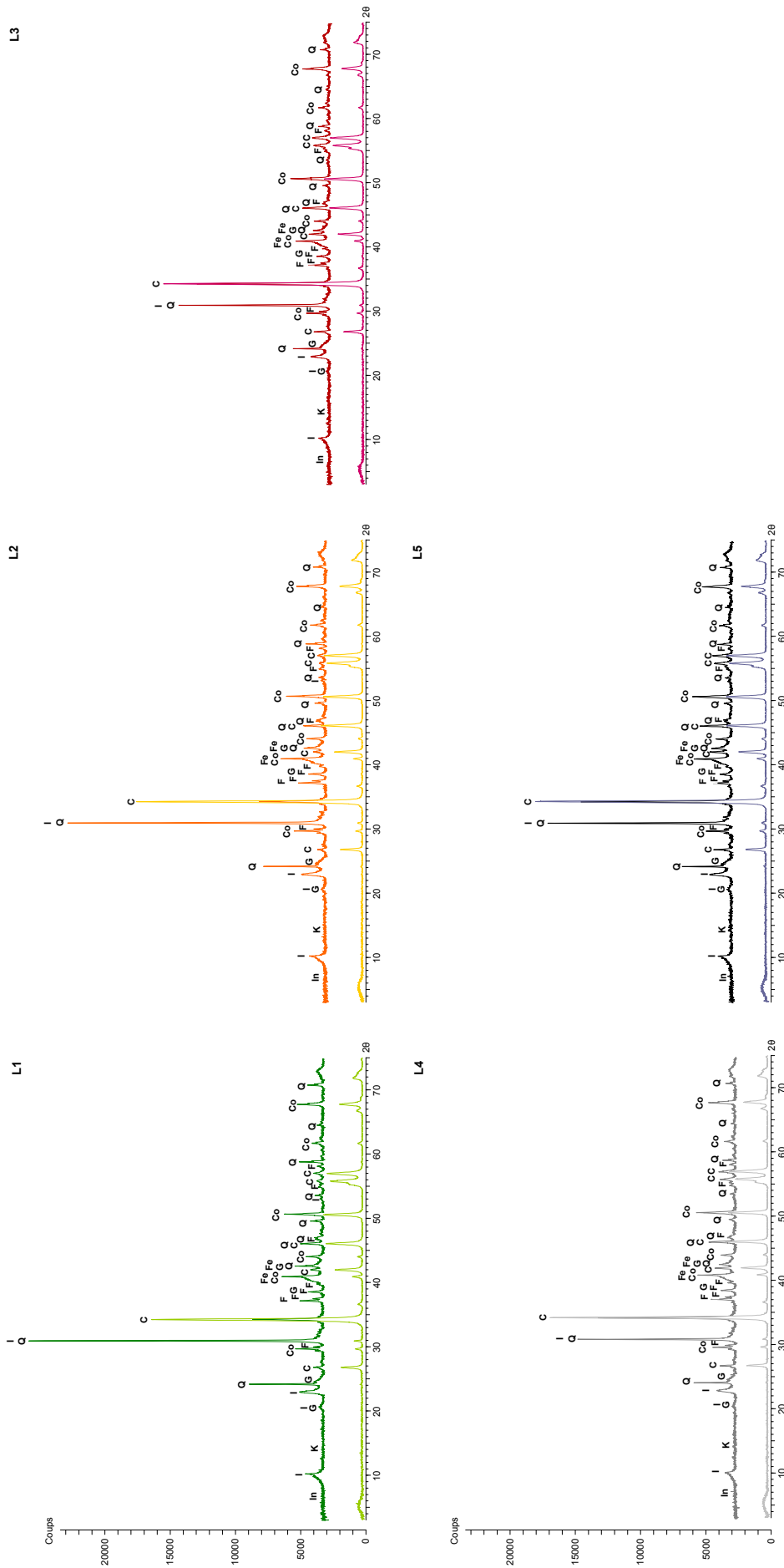


Figure 3. Diagrammes DRX des échantillons calcaires de la Terre-Plaine (en bas de chaque figure) et de leurs résidus de décarbonation (en haut de chaque figure). Les pics principaux des différents minéraux identifiés sont annotés selon la nomenclature suivante : Q = quartz, F = (fluor)apatite, G = goëthite, Fe = ferrisilicate, B = birnessite, I = illite, K = kaolinite, In = argiles interstratifiées, C = calcite et Co = corindon (ayant servi au dopage des échantillons).

6.1.4.1. Spéciation des éléments majoritairement contenus dans les résidus de décarbonatation : Si, Al, P, Fe et K

Les éléments majoritairement contenus dans le résidu de décarbonatation sont Si, Al, P, Fe et K. En effet, la décarbonatation n'induit pas de mise en solution significative de P, compte tenu des incertitudes liées à ces expérimentations, sauf peut-être pour L4 (Tableau 1). Laveuf *et al.* (2008, cf. Chapitre 4.2.1.) avaient déjà vérifié que, dans les conditions expérimentales alors choisies, l'attaque acide des matériaux parentaux ne permet pas de dissoudre les phosphates. Ces derniers, présents en quantités importantes dans les calcaires d'âge sinémurien *s.l.*, se trouvent sous forme de (fluor)apatite (Figure 3 ; Forest-Bize, 2000). Dans les conditions expérimentales choisies ici, cette absence de dissolution de la (fluor)apatite est à relier au pH trop élevé de la solution de décarbonatation employée et à la faiblesse de l'acide utilisé (Welch *et al.*, 2002). En effet, ce minéral est toujours présent après l'attaque, comme le mettent en évidence les analyses par DRX (Figure 3). Les concentrations de P plus faibles dans les résidus de décarbonatation RL3 et RL5 que dans les autres sont en adéquation avec la plus faible intensité des pics de diffraction de la (fluor)apatite dans ces échantillons (Figure 3). Dans le cas de l'échantillon L4, une fraction significative de P est mise en solution lors de la décarbonatation, ce qui indique qu'une part importante de P était probablement co-précipitée avec CO_3^{2-} dans la calcite (Ishikawa et Ichikuni, 1981).

Les pourcentages de Si et Al mis en solution au cours de la décarbonatation expérimentale ne sont pas significatifs, compte tenu des incertitudes liées à ces expérimentations (Tableau 1). Nous pouvons donc en conclure que la décarbonatation du calcaire n'entraîne pas de pertes de Si et Al. Ces éléments sont vraisemblablement contenus dans le quartz et les argiles identifiées dans les résidus de décarbonatation par les analyses DRX (Figure 3). Les teneurs plus élevées en Si dans l'échantillon L1 par rapport aux autres calcaires (Tableau 1) correspondent sans doute à une plus forte teneur en quartz, d'après les analyses DRX (Figure 3). Cette hypothèse est cohérente avec un taux de résidu supérieur dans cet échantillon par rapport aux autres calcaires (Tableau 1).

Les pourcentages de K mis en solution au cours de la décarbonatation ne sont pas significatifs, compte tenu des incertitudes liées à ces expérimentations, excepté pour les échantillons L2 et L5 (Tableau 1). Cet élément est vraisemblablement principalement associé aux illites qui sont identifiées par DRX dans la phase silicatée du résidu de décarbonatation (Figure 3). Dans les échantillons L2 et L5, les proportions non négligeables mises en solution, suggèrent que K puisse également se trouver sous forme de kalicinite (KHCO_3) ou sous une autre forme carbonatée, et être libéré lors de la dissolution des carbonates.

La combinaison de teneurs plus faibles en Si, Al, Mg et K dans les résidus de décarbonatation RL3 et RL4 par rapport aux autres résidus (Tableau 1), alors que leur rapport Si/Al est similaire à celui de RL2 et RL5 (2.66 ± 0.07), est sans doute liée à des teneurs en argiles plus faibles dans les échantillons L3 et L4. Effectivement, les pics de diffraction de l'illite présentent une intensité plus faible dans ces échantillons (Figure 3). L'intensité des pics de diffraction des autres argiles est trop faible pour pouvoir comparer leurs proportions entre les échantillons, voire les identifier.

Enfin, la décarbonatation des calcaires met en solution moins de 15% du stock initial de Fe (Tableau 1), l'échantillon L1 se différenciant des autres échantillons analysés par une mise en solution non significative de cet élément. Les diagrammes DRX des résidus de décarbonatation montrent la présence de goéthite et suggèrent celle de ferrihydrite (bombement de la base entre 20 39 et 45° indiquant du matériel ferrique amorphe) en

quantités importantes, ainsi que d'argiles contenant du Fe (Laveuf *et al.*, 2009, cf. Chapitre 3.1. ; Figure 3). Ces phases minérales ne sont pas mises en solution lors des dissolutions expérimentales des calcaires, ce qui explique que 80% à 90% du Fe soient contenus dans les résidus de décarbonatation (Tableau 1).

6.1.4.2. Spéciation des éléments majoritairement contenus dans les carbonates : Mn et Mg

Les éléments majoritairement libérés lors de la décarbonatation expérimentale des calcaires sont Mn et Mg. En effet, la quasi-totalité du stock initial de Mn est mise en solution, quel que soit le calcaire considéré (Tableau 1). La littérature indique que Mn peut se trouver sous forme de solution solide calcite (CaCO_3) / rhodochrosite (MnCO_3) (Lee *et al.*, 2002). La dissolution de ces phases minérales lors de la décarbonatation expérimentale expliquerait alors la forte libération du Mn.

La décarbonatation libère également près de 80% du stock initial de Mg des calcaires (Tableau 1). La présence majoritaire de Mg sous forme de carbonates (dolomite $\text{CaMg}(\text{CO}_3)_2$, ankérite $\text{Ca}(\text{Fe},\text{Mg},\text{Mn})(\text{CO}_3)_2$ ou magnésite MgCO_3 ou de calcite magnésienne $(\text{Ca},\text{Mg})\text{CO}_3$) dans les calcaires est classique (Lamouroux, 1972). La fraction résiduelle de Mg représente une vingtaine de pour cent de son stock initial dans les calcaires (Tableau 1). Cette fraction est probablement incluse dans les argiles, seuls minéraux du résidu de décarbonatation susceptibles de contenir du Mg (Figure 3).

6.1.4.3. Spéciation des éléments contenus à la fois dans le résidu de décarbonatation et les carbonates : les terres rares

Comme mentionné précédemment, entre le tiers et la moitié du stock de terres rares est mis en solution au cours de la décarbonatation des échantillons calcaires (Tableau 1). Les carbonates, essentiellement sous forme de calcite, étant les principaux minéraux dissous au cours de cette expérience (Figure 3), la signature en terres rares des solutions de décarbonatation correspond donc à celle des carbonates des différents calcaires. La mise en solution préférentielle des terres rares lourdes lors de la décarbonatation des calcaires d'âge sinémurien s'explique par leur présence spécifique dans les carbonates. Ceci est en accord avec la complexation préférentielle des terres rares lourdes avec les polycarbonates (Cantrell et Byrne, 1987 ; Lee et Byrne, 1993 ; Pourret *et al.*, 2007).

Comparativement aux terres rares lourdes, les terres rares légères sont moins mises en solution au cours de la décarbonatation (Tableau 1). Elles sont donc préférentiellement associées aux phases minérales non attaquées par la décarbonatation et identifiées dans les résidus de décarbonatation. Ceci est particulièrement vrai pour Ce dans certains calcaires, d'où l'anomalie négative en Ce dans la calcite (Figure 2).

Pour préciser la répartition préférentielle des terres rares dans les résidus de décarbonatation de la Terre-Plaine et la comparer à celle des résidus de l'Auxois, deux Analyse en Composantes Principales (ACP) ont été réalisées avec les concentrations en éléments majeurs comme variables principales et celles en terres rares comme variables supplémentaires. La première ACP a été réalisée sur l'ensemble des résidus des calcaires des deux sites (Figure 4) et la deuxième sur les seuls résidus des calcaires de la Terre-Plaine (Figure 5). Les calcaires des deux sites présentant des compositions assez différentes, cette deuxième ACP devrait permettre de mettre en évidence des différences d'association plus subtiles entre éléments majeurs et terres rares.

Dans la première ACP, le plan formé par les deux premiers facteurs explique 93 % de la variabilité géochimique des résidus des calcaires d'âge sinémurien *s.l.*, dont 65 % est expliqué par le premier facteur. Ce premier facteur oppose un pôle défini par Si, Al, K, Mg, c'est-à-dire les silicates, et Ti, à un pôle formé par Ca et Mn, soit les oxydes de Mn et les carbonates résiduels. Deux terres rares, Lu et Yb, sont clairement associées à Ca (Figure 4). Cette association est cohérente avec l'enrichissement en terres rares lourdes des carbonates des calcaires (Figure 2). L'espace des individus montre que ce premier axe différencie deux populations de résidus de calcaires, celui d'âge lotharingien riche en silicates et oxydes de Fe et ceux de Terre-Plaine – à l'exception de l'échantillon L1 – riches en oxydes de Mn (Tableau 1).

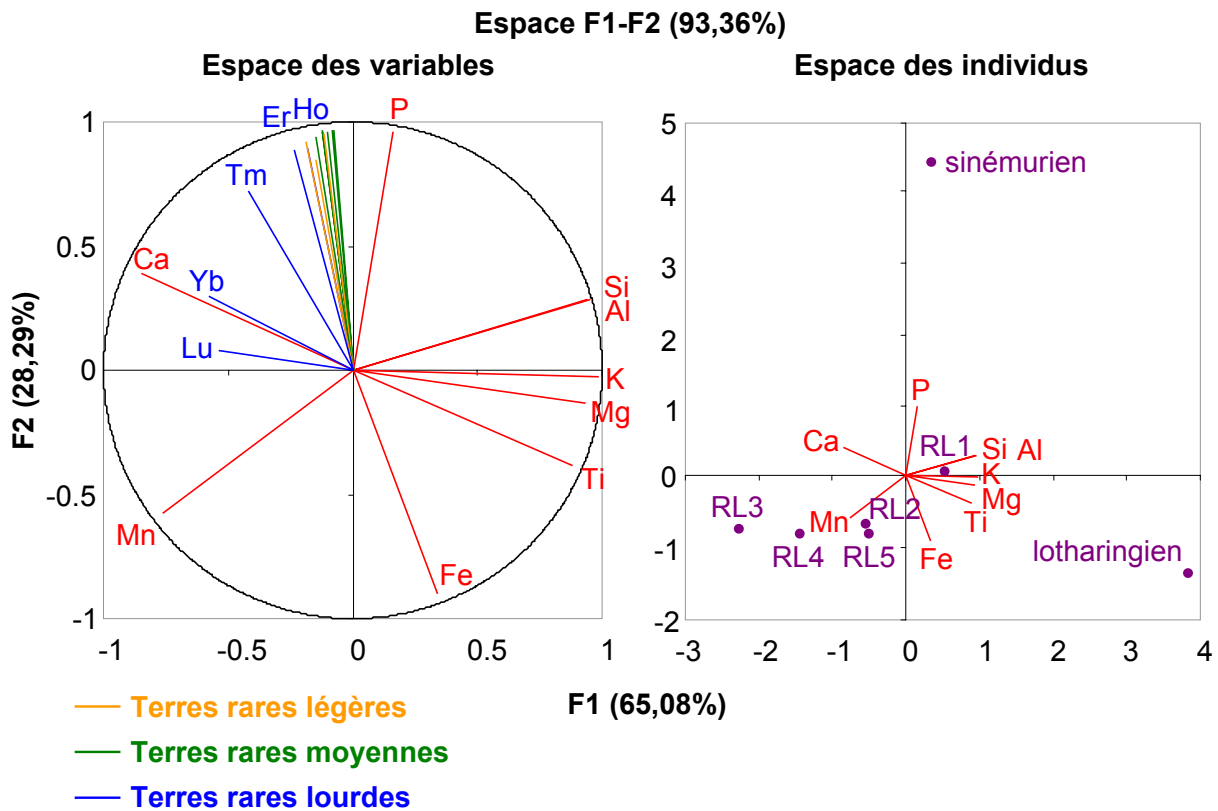


Figure 4. Espace F1-F2 des variables et des individus de l'Analyse en Composante Principale réalisée sur les concentrations des résidus de décarbonatation des calcaires de la Terre-Plaine et de l'Auxois avec les éléments majeurs (plus Ti) en variables principales et les terres rares en variables supplémentaires.

Le second facteur de l'ACP explique 28% de la variabilité des résidus des calcaires. Il oppose P, associé à l'ensemble des terres rares à l'exception des deux terres rares lourdes précitées, et interprété comme la présence de (fluor)apatite dans le résidu (Figure 3), à Fe et Mn interprétés comme un pôle "oxydes de Fe et de Mn" (Figure 4). Cet axe est essentiellement défini par le résidu de décarbonatation du calcaire d'âge sinémurien de l'Auxois qui présente des concentrations en P plus de 4 fois plus élevées ($44,6 \text{ g kg}^{-1}$) que les autres calcaires (Tableau 1). Les phosphates sont par ailleurs connus pour leur enrichissement en terres rares (Henderson, 1984 ; Tyler, 2004). Laveuf *et al.* (2008, cf. Chapitre 4.2.1.) ont analysé sélectivement les spectres de terre rares de nodules de phosphates issus des sols

développés dans l'Auxois. Ces analyses mettaient en évidence un fort enrichissement de ces nodules en terres rares, notamment en terres rares moyennes. La présence d'une plus grande proportion de (fluor)apatite dans le calcaire d'âge sinémurien de l'Auxois explique donc pourquoi les terres rares moyennes y sont moins mises en solution par rapport aux autres calcaires (Figure 2).

La seconde ACP explique 85 % de la variabilité des résidus des calcaires de la Terre-Plaine par le plan formé de ses deux premiers facteurs (Figure 5).

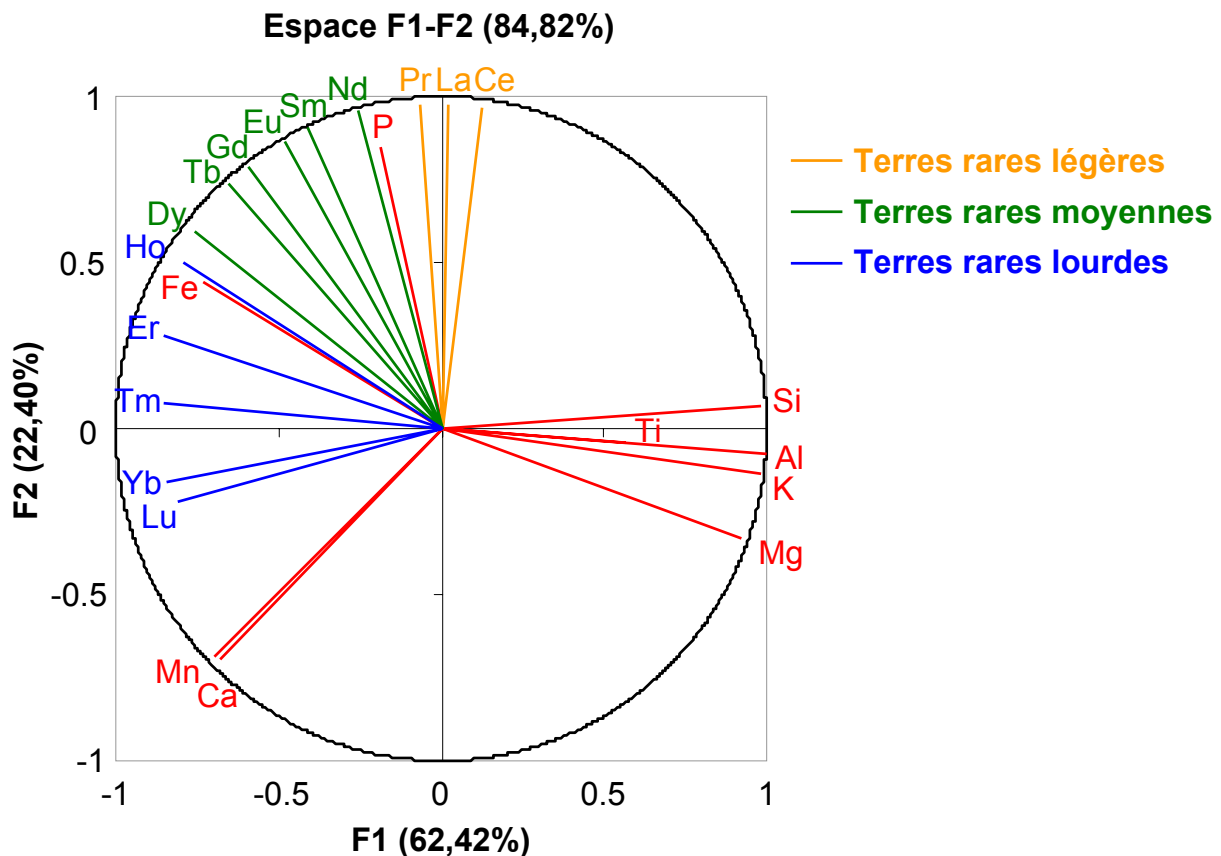


Figure 5. Espace F1-F2 des variables de l'Analyse en Composante Principale réalisée sur les concentrations des résidus de décarbonatation RL1 à RL5 de la Terre-Plaine avec les éléments majeurs (plus Ti) en variables principales et les terres rares en variables supplémentaires.

Le premier facteur représente 62 % de cette variabilité et oppose, comme précédemment, un pôle Si, Al, K, Mg, Ti à un pôle Ca, Mn. Ce dernier pôle inclut également Fe et s'associe aux terres rares lourdes et, dans une moindre mesure, aux terres rares moyennes. Ce premier facteur montre que les terres rares ne sont pas préférentiellement associées aux silicates dans le résidu, mais plutôt aux phases de type "oxydes" ainsi qu'aux carbonates résiduels, comme discuté précédemment. En effet, le quartz ne contient des terres rares qu'en quantités très restreintes (Monecke *et al.*, 2002) et il agit ainsi comme un diluant sur les teneurs en terres rares dans les résidus des calcaires. Par ailleurs, la signature en terres rares des argiles est variable suivant les milieux de formation (Laveuf et Cornu, soumis, cf.

Chapitre 4.1.). Les terres rares lourdes sont plutôt associées au pôle Fe, interprété comme un pôle "oxydes de Fe" (Figure 3), avec, comme précédemment (Figure 4), une tendance vers le pôle Mn et Ca – interprétés comme des pôles "oxydes de Mn" et "carbonates résiduels" (Figure 3) – pour les terres rares les plus lourdes (Figure 5).

Le second facteur de l'ACP explique 22 % de la variabilité des résidus des calcaires de la Terre-Plaine. Comme dans le cas de l'ensemble des résidus des calcaires des deux sites, il est défini par P, qui s'oppose à Mn et Ca (Figure 5). Les terres rares légères sont associées au pôle défini par P, ce qui est interprété, comme précédemment, par leur association à la (fluor)apatite (Figure 3). Les terres rares moyennes sont intercalées entre les pôles P et Fe. Cette intercalation des terres rares moyennes s'explique d'une part par leur affinité pour les oxydes de Fe amorphes (Steinmann and Stille, 1997 ; Land *et al.*, 1999 ; Yan *et al.*, 1999), cohérent avec la présence de ferrihydrite (Figure 3), et d'autre part par leur enrichissement particulièrement marqué dans les nodules de phosphates l'Auxois (Laveuf *et al.*, 2008, cf. Chapitre 4.2.1.).

Si l'ACP ne distingue pas Ce des autres terres rares légères, sa mise en solution plus limitée au cours de la décarbonatation de quatre des calcaires d'âge sinémurien (L1, L2, L5 et Auxois ; Figure 2) signifie que cet élément est moins lié aux carbonates que les autres terres rares légères. Les études invoquent généralement la précipitation de cérianite CeO_2 dans la zone oxygénée des océans (de Baar *et al.*, 1988) pour expliquer l'appauvrissement en Ce par rapport aux autres terres rares légères dans la calcite des calcaires (Henderson, 1984) et par conséquent son enrichissement dans la fraction résiduelle.

Pour vérifier cela, des analyses ponctuelles et cartographiques de Ce par microsonde et par micro-fluorescence X sur des lames minces des calcaires de la Terre-Plaine ont été réalisées (Figure 6). Celles-ci montrent que les zones de fortes concentrations en Ce ne sont pas corrélées à un enrichissement particulier en un des éléments majeurs analysés dans les différents calcaires étudiés (Si, Al, Fe, Mn, Ca, P, S ; Figure 6). Ces observations sont compatibles avec la présence de Ce sous forme individualisée (et donc de cérianite CeO_2) au sein des calcaires. L'intensité de l'anomalie en Ce n'est pas proportionnelle aux teneurs totales en Ce dans les résidus ou dans les calcaires (Tableau 1). Ainsi, l'anomalie négative en Ce dans les carbonates des calcaires L1, L2, L5 et sinémurien de l'Auxois et son absence dans L3 et L4 seraient liées aux teneurs respectives en cérianite des différents calcaires, sans que celles-ci soient liées à la teneur totale en Ce dans les résidus ou dans les calcaires (Tableau 1).

Finalement, l'ensemble de ces résultats indique que la variabilité de composition des calcaires explique les fractionnements en terres rares observés au cours de la décarbonatation. Ils montrent également des variations de la spéciation des terres rares dans les différents calcaires, que ne laissent pas présager la similitude de leurs spectres de terres rares.

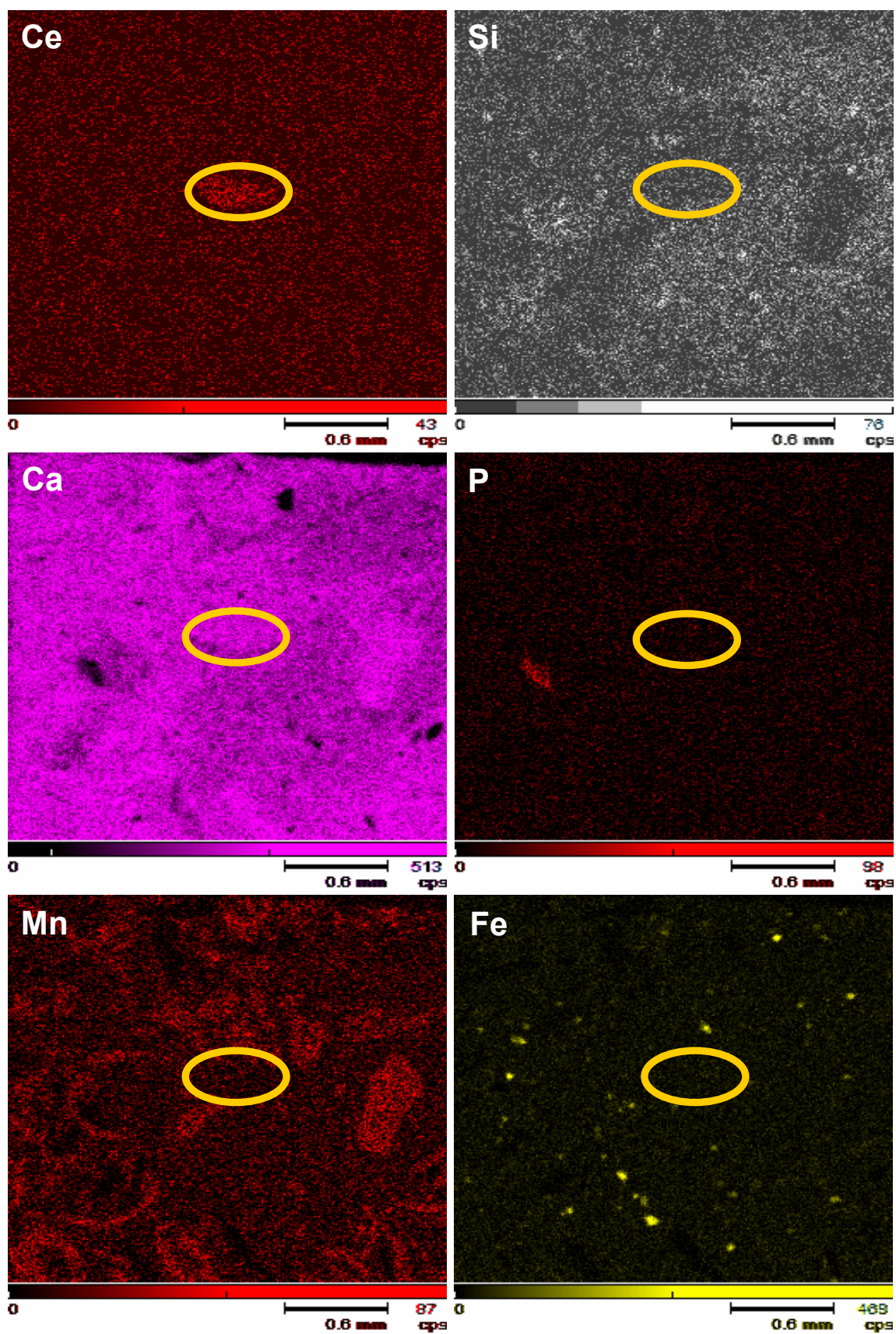


Figure 6. Cartographie par micro-fluorescence X de Ce, Si, Ca, P, Mn et Fe d'une zone sur une lame mince de l'échantillon calcaire L1 de la Terre-Plaine représentative des différents échantillons de calcaires analysés. La zone d'enrichissement en Ce (entourée en jaune) ne correspond à aucun enrichissement en un des autres éléments analysés.

6.1.5. Devenir des éléments lors de la décarbonatation des calcaires

L'horizon C3 provient principalement (à 91%) de la décarbonatation du banc calcaire L1 avec lequel il est en contact (Laveuf *et al.*, soumis, cf. Chapitre 5.1.). Pour quantifier le devenir des terres rares et des éléments majeurs au cours du processus de décarbonatation, j'ai comparé leurs flux calculés pour l'horizon C3 (Laveuf *et al.*, soumis, cf. Chapitre 5.1. ; Tableau 2) aux quantités mises en solution au cours de la décarbonatation expérimentale du banc calcaire L1 (Tableau 1). Cette approche me permet d'obtenir les quantités de terres rares et d'éléments majeurs mises en solution mais non évacuées de l'horizon C3, car repiégées par les minéraux du résidu de décarbonatation ou par des minéraux néoformés (Tableau 2).

La fonction de transport de Ca est proche de -100% dans l'horizon C3 (Tableau 2), ce qui indique que la totalité du Ca mise en solution cours du processus de décarbonatation est exportée hors de cet horizon (Tableau 2).

Les fonctions de transport de Si et Al mettent en évidence des gains dans l'horizon C3 (Tableau 2). Ces gains peuvent résulter de flux latéraux et/ou verticaux sous formes particulaire et/ou dissoute. D'une part, la présence d'une nappe dans cet horizon la majeure partie de l'année (cf. Chapitre 2) supporte l'idée des apports latéraux. D'autre part, les horizons sus-jacents à l'horizon C subissent des pertes en Si et Al (Laveuf *et al.*, soumis, cf. Chapitre 5.1.), dont le transfert vertical pourrait expliquer les gains dans l'horizon C3. Ainsi, il n'est pas possible de trancher quant à l'origine de ces gains en Si et en Al dans cet horizon, ni quant à leur nature dissoute ou particulaire.

La fonction de transport de Fe suggère que cet élément n'est pas exporté hors de l'horizon C3 après sa mise en solution lors de la décarbonatation (Tableau 2). La proportion de ferrihydrite par rapport à celle de goethite est plus importante dans l'horizon C3 que dans le résidu de décarbonatation du calcaire L1 (Figure 7). Ainsi, le Fe issu de l'altération du calcaire pourrait préférentiellement précipiter sous forme de ferrihydrite.

La fonction de transport de Mn montre qu'environ les deux tiers du stock initial de cet élément sont exportés hors de l'horizon C3 suite à la décarbonatation (Tableau 2). Le tiers restant, mis en solution et non exporté, précipite probablement sous forme d'oxydes de Mn – comme le suggère la couleur noire de cet horizon C dit "à bouillie noire" (cf. Chapitre 2 et Annexe 1) – notamment sous forme de birnessite (Figure 7 ; Manceau *et al.*, 1997).

La fonction de transport de Mg indique qu'environ les deux tiers du stock initial de cet élément sont exportés hors de l'horizon C3 (Tableau 2). Finalement, comme les deux tiers du stock initial de Mg sont mis en solution lors de la décarbonatation, cela signifie que la quasi-totalité du Mg mis en solution est exportée hors de l'horizon C3 (Tableau 2).

La fonction de transport de K indique que les quantités mises en solution au cours de la décarbonatation sont totalement exportées hors de l'horizon C3 (Tableau 2).

Les fonctions de transport des terres rares indiquent que les quantités mises en solution au cours de la décarbonatation sont, dans leur ensemble, totalement exportées hors de l'horizon, à l'exception d'Yb et Lu (Tableau 2). Nous avons vu précédemment que ces deux terres rares lourdes étaient préférentiellement associées aux carbonates (Figure 5). Les quantités résiduelles de carbonates (principalement sous forme de calcite) dans l'horizon C3 (2,15 g kg⁻¹) pourraient donc expliquer la moindre exportation de Yb et Lu. Par ailleurs, pour des raisons stériques et électroniques, les terres rares lourdes sont plus facilement adsorbées que les terres rares légères sur les minéraux argileux ou sur les oxydes (Laveuf et Cornu, soumis, cf. Chapitre 4.1.). Ce dernier point suggère que la rétention de Yb et Lu, alors que les

Tableau 2. Concentrations dans l'horizon C3 (en g kg⁻¹ pour les éléments majeurs et en mg kg⁻¹ pour les terres rares TR) et fonctions de transport de masse τ (en % du stock initial dans le matériau parental reconstitué) pour ce même horizon (Laveuf *et al.*, soumis, cf. Chapitre 5.1.). Les quantités repiégées correspondant au pourcentage du stock initial mis en solution et non évacué de l'horizon C3 sont calculées par différence entre les fonctions de transport de masse et les quantités mises en solution (Tableau 1).

	Si	Al	Fe	Mn	Mg	Ca	K	P	La	Ce	Pr	Nd	Sm	Eu	Gd	Tb	Dy	Ho	Er	Tm	Yb	Lu	TR légères	TR moyennes	TR lourdes	
Concentration dans l'horizon C3	190	84,6	97,3	21,0	7,5	30,3	22,2	10,1	72,8	104	16,3	65,9	12,9	2,73	11,0	1,59	9,17	1,77	4,80	0,70	4,40	0,67	308	193	103	12,3
Fonction de transport de masse τ	21	51	6	-66	-67	-99	-8	-12	-40	-42	-41	-42	-39	-39	-40	-40	-38	-38	-39	-35	-33	-32	-38	-41	-40	-36
Quantité repiégée	16	36	14	31	12	0	1	-4	-1	-6	-1	1	2	0	-2	0	2	2	6	8	12	15	0	-4	2	8

autres terres rares sont totalement évacuées, pourrait également s'expliquer par l'adsorption d'une fraction du Yb et du Lu libérée en solution dans l'horizon C3 lors de la dissolution du calcaire (Tableau 2).

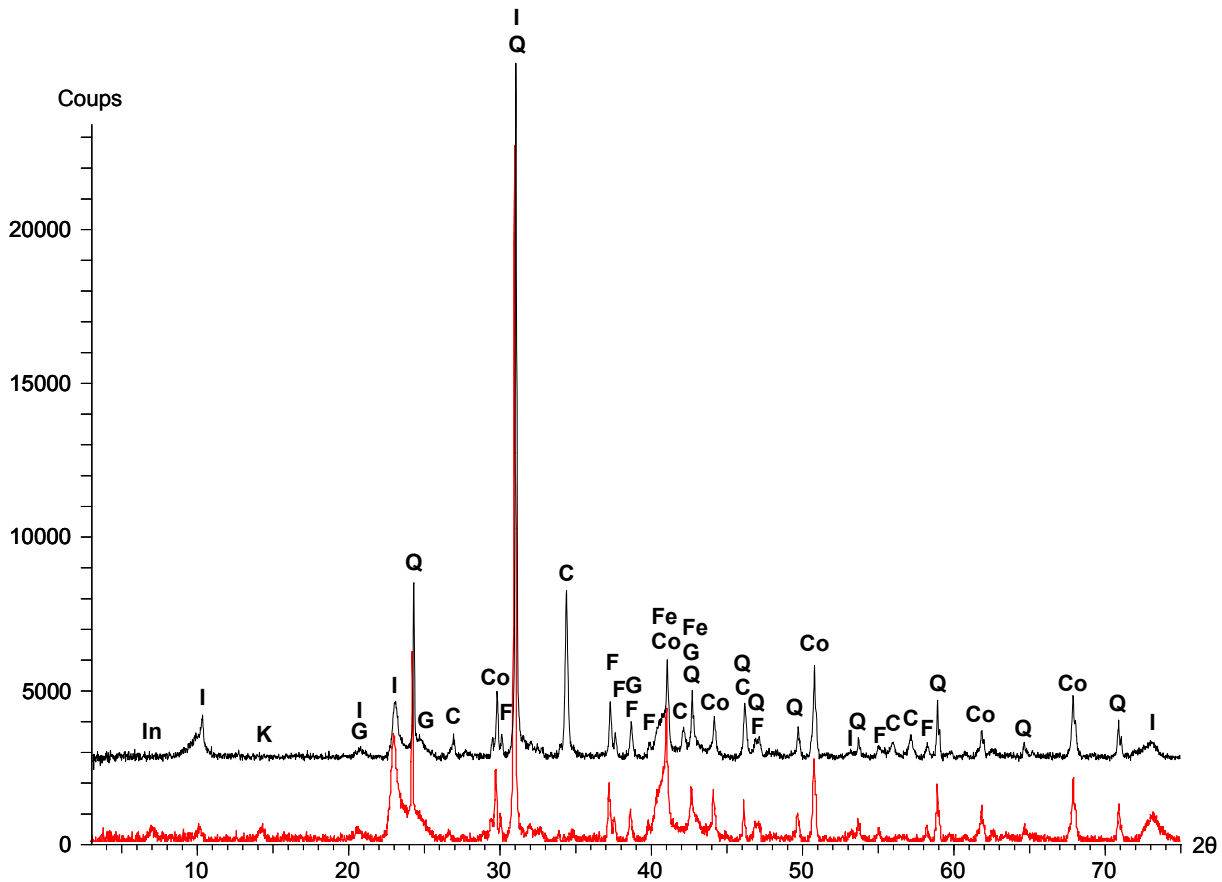


Figure 7. Diagrammes DRX de l'horizon C3 (en rouge) et du résidu de décarbonatation de l'échantillon calcaire L1 de la Terre-Plaine (en noir) au contact de l'horizon C3. Les pics principaux des différents minéraux identifiés sont annotés selon la nomenclature suivante : Q = quartz, F = (fluor)apatite, G = goéthite, Fe = ferrihydrite, B = birnessite, I = illite, K = kaolinite, In = argiles interstratifiées, C = calcite et Co = corindon (ayant servi au dopage des échantillons).

6.1.6. Conclusions sur le processus de décarbonatation

Je montre ici que la comparaison des flux d'éléments calculés par bilan de masse aux quantités mises en solution expérimentalement semble la meilleure approche pour conclure sur les mécanismes gouvernant le devenir des différents éléments et des terres rares lors de la formation d'un horizon. En effet, une approche basée uniquement sur l'un ou l'autre des paramètres peut conduire à des interprétations erronées en surestimant les quantités exportées ou en sous-estimant les quantités mises en solution. Les cas les plus caractéristiques, dans cette étude, sont ceux du Mn, du Yb et du Lu.

La spéciation des éléments majeurs et des terres rares varie suivant l'échantillon de calcaire considéré. La variabilité de spéciation est importante, à la fois entre les deux sites

d'étude de la Terre-Plaine et de l'Auxois, mais également au sein d'un même site. En effet, les calcaires d'âge sinémurien *s.s.* se différencient du calcaire d'âge lotharingien, mais également entre eux, notamment le calcaire L1 et le calcaire d'âge sinémurien de l'Auxois par rapport aux calcaires L2 à L5. Cette variabilité de spéciation explique les différences de mise en solution et les fractionnements des terres rares entre les différents échantillons de calcaires. Cette différence de mise en solution des terres rares ne peut donc pas être évaluée sur la seule base des concentrations totales en terres rares qui sont pourtant similaires au sein d'un même site.

Ainsi, selon l'échantillon de calcaire de la Terre-Plaine considéré, entre un tiers et la moitié du stock de terres rares est mis en solution lors de la dissolution des carbonates (principalement la calcite). Bien que peu marqués, des fractionnements entre les terres rares se produisent toutefois au cours de ce processus. Les terres rares lourdes sont préférentiellement mises en solution par rapport aux terres rares légères et moyennes. Parmi les terres rares légères, le Ce est moins mis en solution que les autres terres rares légères, lors de la dissolution de certains calcaires. Ce comportement particulier du Ce est probablement dû à la présence de cet élément sous forme de cérianite CeO_2 , minéral non dissous lors de l'expérimentation et donc lié à la fraction résiduelle de décarbonatation des calcaires. Finalement, alors que la totalité des terres rares légères et moyennes en solution sont exportées hors de l'horizon C, une fraction des terres rares lourdes ne l'est pas. Cette dernière est probablement fixée par certains minéraux résiduels ou néoformés.

Parmi les éléments majeurs, les seuls mis en solution et piégés dans l'horizon C sont Fe et Mn, qui précipitent probablement sous forme de birnessite et de ferrihydrite. Parmi les autres éléments majeurs, Ca et Mg sont majoritairement exportés, alors que Si et Al sont marqués par des apports latéraux et/ou verticaux. Ce dernier résultat suggère que d'autres processus pédogénétiques – tels que l'illuviation ou le transfert sous forme dissoute d'éléments – mobilisent les éléments majeurs dans l'horizon C, complexifiant alors la compréhension du processus de décarbonatation si l'on ne prend pas en compte les flux d'éléments entre les stocks initiaux et les stocks finals ainsi que les quantités mises en solution expérimentalement.

Parmi ces processus pédogénétiques, celui qui intervient après la décarbonatation est l'évolution des conditions redox le long des sols. La suite de ce chapitre s'intéresse à l'impact de ce processus sur le comportement des terres rares de manière à évaluer le potentiel de ces éléments à tracer ce processus.

6.2. Potentiel des terres rares comme traceurs des processus redox

Les terres rares sont fractionnées par les processus d'oxydo-réduction dans les sols comme je l'ai discuté auparavant (cf. [Chapitres 4 et 5](#)) et peuvent de ce fait être des traceurs intéressants de ces processus. Néanmoins, l'impact des processus rédox sur la distribution des terres rares dans les sols reste complexe et dépend vraisemblablement des phases minérales mises en jeu par ces processus (oxydes de Fe ou de Mn notamment, cf. [Chapitres 4 et 5](#)).

Nous cherchons donc ici à déterminer si les fractionnements et les redistributions en terres rares sont en relation avec la mobilisation des différents types d'oxyde ferromanganiques, l'objectif étant toujours leur utilisation comme traceurs de processus redox ou des cycles de formation/dissolution de certains oxydes.

Ce chapitre se présente sous forme d'un article en anglais en préparation qui sera soumis à Geoderma.

Impact of redox conditions on the mobilization of Rare Earth Elements in a soil sequence developed from limestone

LAVEUF Cédric¹, CORNU Sophie^{1‡}, GUILHERME Luiz Roberto G.^{1,2,3}, GUERIN Annie⁴
and JUILLOT Farid⁵

¹ INRA, UR0272 Science du Sol, Centre de Recherche d'Orléans, CS 40001 Ardon, 45075 Orléans Cedex 2.

² le STUDIUM Institute for Advanced Studies, 3D avenue de la Recherche scientifique, 45071 Orléans CEDEX 2, France.

³ Federal University of Lavras, Soil Science Dept., CP 3037, 37200-000 Lavras (MG), Brazil; CNPq (Brazilian Ministry of Science and Technology) Scholar.

⁴ INRA, US Laboratoire d'Analyses des Sols, 62000 Arras, France.

⁵ IMPMC, UMR CNRS 7590, Universités Paris 6 et 7 – IPGC, 75252 Paris cedex 05, France.

Abstract

Redox processes are widespread in soils. The classical methodology used to study these redox processes generally comes up against the difficulty to precisely quantify the different forms of poorly crystalline Fe- and Mn-oxides. We propose to use the signature of REEs to quantify them. Therefore, the present work aims at determining the oxide phases responsible for the evolution of the REE signature in the different pedological features resulting from the impact of successive redox processes.

[‡] Corresponding author: scornu@aix.inra.fr

Our results allow determining the main REE-bearing minerals involved in the mobilization of REEs during two stages of redox conditions (i) the formation and subsequent dissolution of Fe-Mn nodules and (ii) the bleaching of soil horizons. Although Mn-oxides, ferrihydrite, goethite and (fluor)apatite are all submitted to redox conditions, their impact on the mobilization of REEs varies according to their proportions initially present in the different pedological features, to their relative mobilization during redox processes and to their different REE signatures.

Indeed, Mn-oxides account for the main stock of REEs in the Fe-Mn nodules and display a positive Ce anomaly, while no conclusions could be drawn on the impact of this mineral on the stocks of REEs in the matrix where they represent a lower stock. The positive Ce anomaly is supposed to result from the occurrence of cerianite, whose proportion was thought to be linked with the nature of the Mn-oxides and with the development of the redox conditions during the formation of the Fe-Mn nodules. Ferrihydrite is enriched in MREEs in both pedological features, but displays a negative Ce anomaly only in the matrix. (Fluor)apatite is also enriched in MREEs but shows a negative Ce anomaly. The impact of these last two minerals is more important during bleaching than during the formation of the Fe-Mn nodules. As a consequence, the impact of bleaching of soil horizons is more pronounced on MREEs. The REE signature of goethite differs according to the pedological feature considered, but represents only a small proportion of the stock of REEs within the pedological features, so that this mineral has a negligible impact on the mobilization of REEs during redox conditions.

Keywords: Fe; Mn; lanthanides; oxidation-reduction; pedogenesis

1. Introduction

Redox processes extend over a large variety of soil types (Bockheim and Gennadiyev, 2000) and are among the most common pedological processes in soils (Soil Survey Staff *et al.*, 1975; Jamagne, 1978; AFES, 1995; FAO, 1998). Redox conditions were identified as one of the main factor controlling the mobilization/immobilization of elements during pedogenesis (Fiedler *et al.*, 2002; Aide, 2005), notably that of Fe and Mn (Trolard *et al.*, 1993; Schüring *et al.*, 1999; Fiedler and Sommer, 2004).

It is particularly the case in soils submitted to hydromorphic conditions. Following sufficiently prolonged reducing periods, primary and secondary Fe- and Mn-oxides are dissolved (Blume, 1988). This leads to the bleaching of soil horizons (Pedro *et al.*, 1978; Bouma, 1983) and to the formation of gley horizons (Blume, 1988). Once in soil solution, the fate of Fe and Mn within the pedosphere depends mainly on the oxidizing conditions and water fluxes. Indeed, Fe and Mn are transferred, from the decimeter to the landscape scale, either by diffusion along a concentration gradient or by mass flow transfer due to gravity in the large porosity (Van Breemen, 1988). They can thus be leached out from the soil mantle or reach a sufficiently oxidizing zone where they oxidize. In this last case, Fe- and Mn-oxides precipitate as coatings of soil ped surfaces, fillings in cracks and veins, mottles, pedotubules or nodules (Bouma, 1983; Blume, 1988; Van Breemen, 1988; Allen and Hajek, 1989; McKenzie, 1989).

To better understand the evolution of soils under hydromorphic conditions, studies should aim at relating soil water regimes with the development and intensity of the resulting redox processes, and with the pedological features formed by these processes (Vizier, 1971).

Past redox conditions are generally assessed by the comparative quantification of the dissolution/precipitation cycles of Fe- and Mn-oxides in the studied soil horizons and in a soil horizon that is supposed to be not affected by the redox processes (see *e.g.* Faulkner and Patrick, 1992; Fiedler and Sommer, 2004). This quantification classically relies on the study of the quantitative redistribution of Fe and Mn and of the mineralogical phases that constitute the Fe-Mn-oxides and their surrounding soil matrix (Lévêque, 1970; Vizier, 1971). However, as these oxides are generally poorly crystalline in soils, their mineralogy is difficult to assess, especially when quantitative estimations are required.

Another approach using Rare Earth Elements (REEs) was proposed by Laveuf *et al.* (2008, cf. Chapitre 4.2.1.) and Laveuf and Cornu (submitted, cf. Chapitre 4.1.). Through an innovative normalization approach, Laveuf *et al.* (2008, cf. Chapitre 4.2.1.) evidenced specific fractionations of REEs during bleaching and precipitation of Fe-Mn-oxides as Fe-Mn nodules in the non-truncated end-member of a soil catena at the northeastern margin of Morvan Mountain (France). In this solum, all REEs, and particularly Ce, concentrate in Fe-Mn nodules, while MREEs are relatively less concentrated in the bleached soil horizons (Laveuf *et al.*, 2008, cf. Chapitre 4.2.1.). The preferential accumulation of Ce was supposed to be related to the condensation of Mn-oxides into the Fe-Mn nodules, while the loss of MREEs during bleaching was assumed to be linked to the dissolution of amorphous Fe-oxides dispersed in the soil matrix. However, actual identification of the REE-bearing minerals is missing.

The present work aims at determining the oxide phases responsible for the evolution of the REE signature in soils submitted to redox processes. Our approach consists in quantifying amorphous and crystalline Fe- and Mn-oxides, as well as the associated REE signatures, in the different redoximorphic features along a soil sequence, thanks to the combination of chemical and physical fractionations and subsequent chemical and mineralogical characterizations.

2. Materials and methods

2.1. Geological and pedological context of the studied site

The study site is located on the northern sedimentary margin of Morvan Mountain (Burgundy, France) on a structural limestone surface dated from the sinemurian stage (Mouterde, 1952; Figure 1). The sinemurian formation is composed of a succession of thin marl beds, irregularly inserted between much thicker limestone layers. This carbonated formation (up to 90% and 55% of CaCO₃ for the limestone layers and marl beds respectively) underwent mineralization events during the Lias epoch due to hydrothermal fluids rising along fault lines (Sizaret, 2002), responsible for their high Fe, Mn and REE contents (Laveuf *et al.*, 2008, cf. Chapitre 4.2.1.).

The soils developed from the weathering of the sinemurian-aged formation (Laveuf *et al.*, submitted, cf. Chapitre 5.1.). They are organized in an erosion-driven soil sequence (Figure 2), which ranges from the non-truncated soils (NTS) at the top of the slope to the so-called “black earths” at the bottom of the slope, via the so-called “chestnut colored soils” (CCS) at an intermediate position (Baize and Chrétien, 1994).

A representative soil sequence was sampled in a cultivated plot at Savigny-en-Terre-Plaine (Burgundy, Yonne, France; Figure 1). The NTS are characterized by the complete

succession of soil horizons LE, E, Bd, Bc and C from top to bottom (Figure 2). This solum is equivalent to that studied by Laveuf *et al.* (2008, cf. Chapitre 4.2.1.). The CCS are characterized by the erosion of the silty clayey eluviated horizons, surfacing the B-horizon that is not degraded (Figure 2). Besides, the Bc-horizon is visibly richer in Fe-Mn nodules in the CCS than in the NTS. A LE-horizon also developed in the CCS.

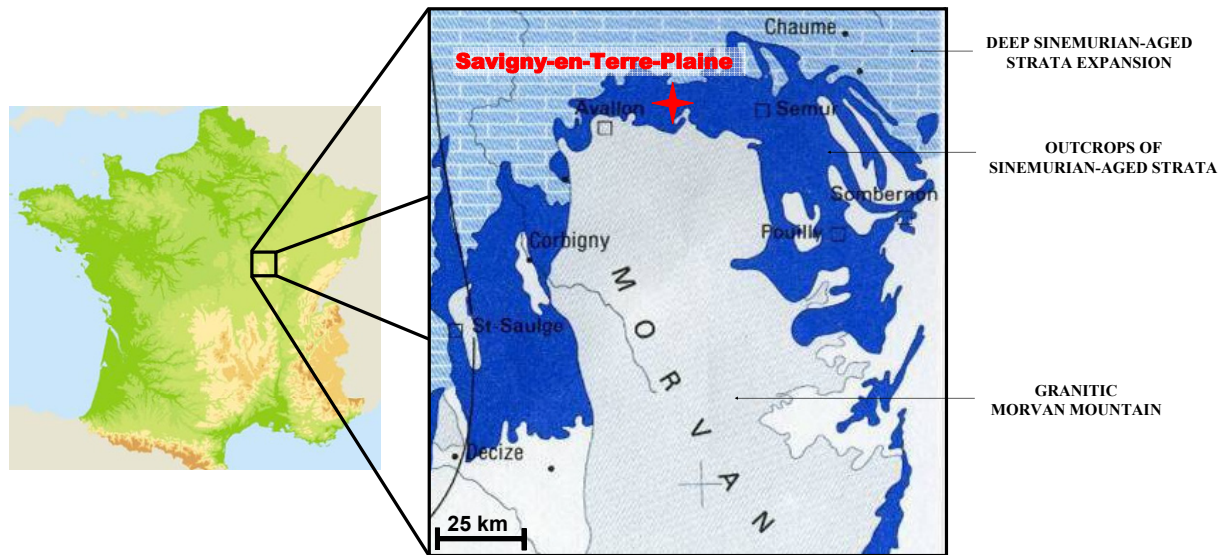


Figure 1. Localization of the studied toposequence of Savigny-en-Terre-Plaine (Yonne, France) within the geographic expansion of the Sinemurian-aged strata around the Morvan Mountain.

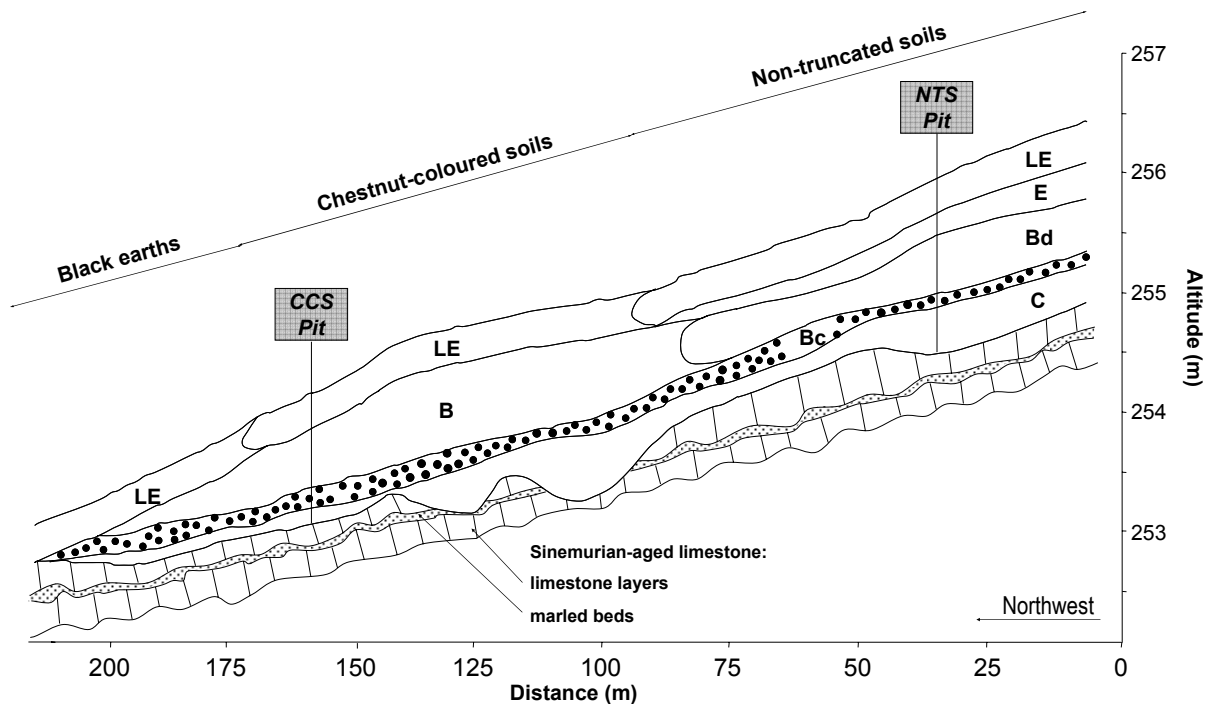


Figure 2. Toposequence of Savigny-en-Terre-Plaine (Yonne, France) developed from the sinemurian-aged formation. Sampled pits of the non-truncated solum (NTS) and of the chestnut colored solum (CCS) are indicated.

2.2. Sampling strategy and sample preparation

Soil pits were dug at the NTS and CCS locations (Figure 2). Detailed pedological descriptions were made and one bulk sample per horizon was collected on the whole width of each pit, except in the C-horizon of NTS where the top (C1) and the bottom (C2) were sampled.

Subsamples were wet-sieved at 50 μm in deionized water, without preliminary treatments. Magnetic separation was performed on the $>50 \mu\text{m}$ particle-size fractions of the Bc-horizons and of the LE- and C-horizons of NTS to separate magnetic Fe-Mn nodules from the non-magnetic fraction. The $<2 \mu\text{m}$ fraction in the LE- and C1-horizon of NTS was obtained by sedimentation in deionized water according to Stokes law.

All Fe-Mn nodules, non-magnetic $>50 \mu\text{m}$, $<50 \mu\text{m}$ and $<2 \mu\text{m}$ fractions were chemically analyzed at the [SARM-CRPG](#) (Vandœuvre-lès-Nancy, France) for major elements by ICP-AES and for REEs by ICP-MS, after LiBO_2 fusion, and at the [LAS-INRA](#) (Arras, France) for organic matter (derived from organic carbon) and CaCO_3 .

2.3. Sequential extractions of the different soil fractions

Fe- and Mn-oxides were quantified by sequential extractions performed on the Fe-Mn nodules, the $<50 \mu\text{m}$ and the $<2 \mu\text{m}$ fractions.

A 5-step extraction scheme, summarized in Table 1, was performed on 1.0 g of the $<50 \mu\text{m}$ and $<2 \mu\text{m}$ fractions. For the $<50 \mu\text{m}$ fractions, extractions were performed in triplicate. For the $<2 \mu\text{m}$ fractions, 10 replicates were started and 2 residues were stopped after each step. For the Fe-Mn nodules, a 3-step extraction scheme focused onto the extraction amorphous and crystalline Fe- and Mn-oxides (steps B, D and E) was performed on 1.2 g of sample ground to $<50 \mu\text{m}$ (Table 1). For the LE- and C1-horizons of NTS, extractions were performed in triplicates. For the Bc-horizons, 6 replicates were started and 2 residues were stopped after each step.

Table 1. Sequential extraction scheme for the $<50 \mu\text{m}$ fractions, $<2 \mu\text{m}$ fractions and Fe-Mn nodules including the extractants nature, the sample/extractant ratio (m/V ratio), the number of extractions performed per extractant and their duration.

Step	Extractants	m/V ratio	Extracted fractions		
			$<50 \mu\text{m}$ fractions	$<2 \mu\text{m}$ fractions	Fe-Mn nodules
A	CH_3COONa 1M (up, Chem-Lab) adjusted to pH 5.5 with CH_3COOH 99-100% (up, Chem-Lab)	1/20	1 x 360 min	1 x 360 min	-
B	$\text{NH}_2\text{OH.HCl}$ 0.1M (ar, Chem-Lab)/ HCl 0.1M (up, Prolabo Normatom) at pH 2.0	1/20	2 x 30 min	2 x 30 min	4 x 30 min
C	$\text{Na}_4\text{P}_2\text{O}_7$ 0.1M (ar, Prolabo Merck) at pH 10	1/10	1 x 90 min	1 x 90 min	-
D	$\text{NH}_2\text{OH.HCl}$ 0.25M (ar, Chem-Lab)/ HCl 0.25M (up, Prolabo Normatom) at pH 1.5 and 60°C	1/20	2 x 120 min	2 x 120 min	4 x 120 min
E	$\text{NH}_2\text{OH.HCl}$ 1M (ar, Chem-Lab)/ CH_3COOH 99-100% at 25% (up, Chem-Lab) at pH 1.0 and 90°C	1/30	1 x 180 min 1 X 90 min	1 x 180 min 1 X 90 min	3 x 180 min

After each step, a rinse with ultrapure water was carried out for 1h with a 1:20 m/V ratio. Extractions and rinses were performed under permanent shaking. All extraction and rinse solutions were centrifuged at 10800 g and filtered through a 0.2 μm cellulose acetate membrane. Blanks were realized in triplicate following the same extraction scheme. When needed, filtrates were acidified to 1% with HNO_3 65% (up, Chem-Lab) and individually stored at 4°C before analyses of Fe and Mn by spectroscopic flame atomic absorption. The concentrations of Fe and Mn in the blanks were below the detection limits. All residues were chemically analyzed for major elements and REEs at the [SARM-CRPG](#) as described above.

Obtained recovery rates and coefficients of variations were considered acceptable for this kind of sequential extractions (Tessier *et al.*, 1979; Quevauviller, 1998; Davidson *et al.*, 1999). For the <50 μm fractions, these rates ranged from 80% to 96% \pm 4% maximum for Fe and from 86% to 103% \pm 7% for Mn. For the <2 μm fractions, they ranged from 81% to 86% \pm 3% maximum for Fe, from 88% to 96% \pm 6% for Mn and were near 93% \pm 5% for REEs. For the Fe-Mn nodules, recovery rates ranged from 112 to 124% \pm 6% maximum for Fe, from 100 to 105% \pm 5% for Mn and were near 100% \pm 7% for REEs.

Following the discussion of Laveuf *et al.* (2009, cf. Chapitre 3.1.) for the same extraction scheme, in the same pedological context, we considered that step B extracted Mn-oxides and (fluor)apatite according to Land *et al.* (1999), steps C and D removed amorphous Fe-oxides – Fe colloids and ferrihydrite respectively – step E released elements associated with goethite, while final residues mainly consisted in silicates.

3. Results and discussion

3.1. Redox processes, associated pedological features and impact on the REE mobilization

The studied sola experienced different stages of redox processes leading to the formation of different pedological features: Fe-Mn nodules and bleaching zones. To evidence the impact of the oxide dissolution and nodule formation on the REE mobilization, we normalized the REE content of the pedological features resulting from the pedogenetic process under consideration to the REE content of the material from which it developed, as proposed by Laveuf *et al.* (2008, cf. Chapitre 4.2.1.).

The Fe-Mn nodules are formed by the fluctuation of a water table at the base of the sola. Indeed, as the compact and non-fissured sinemurian formation hinders water percolation, the C-horizon resulting from the dissolution of the limestone formation is saturated almost continuously for at least 8 months a year. During winter, the water table fluctuates in the top of the C-horizon and in the Bc-horizon. These fluctuations, which favor the migration of Fe and Mn on decimeter scales and the segregation of Fe-Mn-oxides as nodules (McKenzie, 1989; Khan and Fenton, 1994; Zhang and Karathanasis, 1997; Liu *et al.*, 2002), are responsible for the formation of the numerous black, hard and round shaped pedological Fe-Mn nodules observed in the Bc-horizons of these soils (Baize and Chrétien, 1994; Laveuf *et al.*, 2008, cf. Chapitre 4.2.1.; Laveuf *et al.*, 2009, cf. Chapitre 3.1.), as well as in the top of the C-horizon of NTS. As nodules are formed by redox processes at the expense of the C-horizon – *i.e.* of the residue of carbonate dissolution of a mixture of marl and limestone layers (Laveuf *et al.*, submitted, cf. Chapitre 5.1.) – we normalized the REE contents of Fe-Mn nodules to those of the residue from carbonate dissolution of the former parent material of the

corresponding soil horizon as computed by Laveuf *et al.* (submitted, cf. Chapitre 5.1.). Three soil horizons were considered: C1 where nodule formation begins, Bc where the nodules are the best expressed and LE where they are partially dissolved. The Fe-Mn nodules traps from 10 to 90% of the REEs initially present in the residues of their former parent materials, with affinity decreasing significantly from LREEs to HREEs in the Bc-horizons (Figure 3). The Fe-Mn nodules in formation in the C1-horizon, and especially those partially dissolved in the LE-horizon, contain a lower stock of REEs compared to the typical Fe-Mn nodules of the Bc-horizons. A positive Ce anomaly is observed in the Fe-Mn nodules. This anomaly increases during the formation of the Fe-Mn nodules and is higher in the NTS than in the CCS (Figure 3). Therefore, Ce is preferentially trapped over the other LREEs in the Fe-Mn nodules during their formation. Both the Ce anomaly and the La/Lu fractionations in Fe-Mn nodules are in agreement with results of related studies (Rankin and Childs, 1976; Laveuf and Cornu, submitted, cf. Chapitre 4.1.).

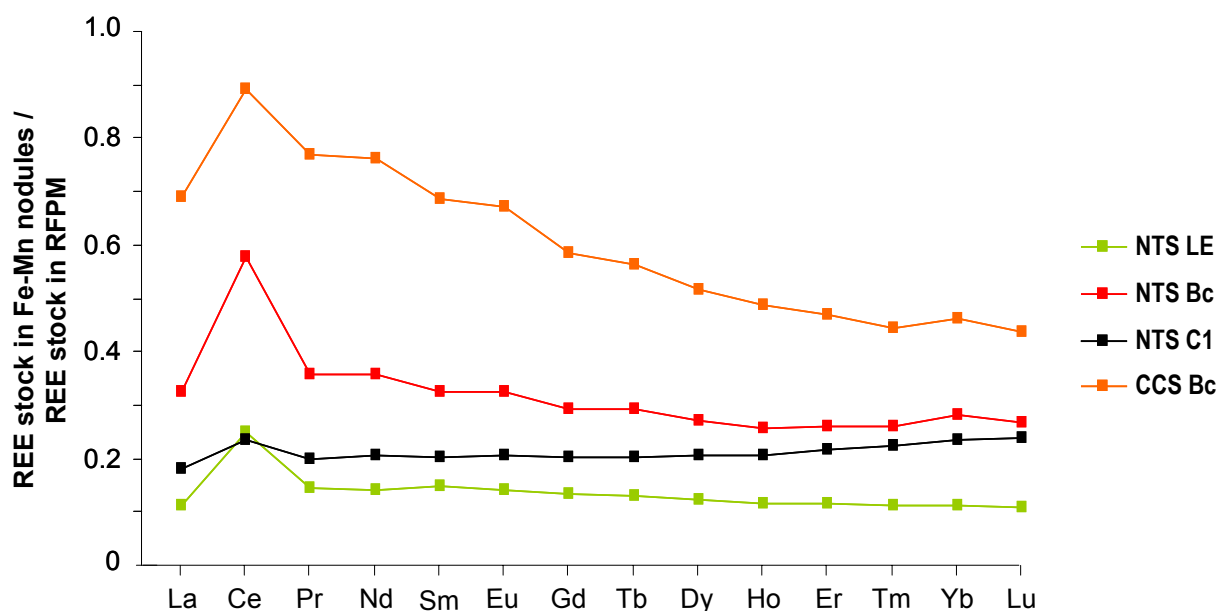


Figure 3. Patterns of stocks of REEs in the Fe-Mn nodules normalized to the residue from carbonate dissolution of their respective residues of former parent materials (RFPMs), as calculated by Laveuf *et al.* (submitted, cf. Chapitre 5.1.).

Oxide dissolution occurs at two different depths in the studied sola. First, in the C- and Bc-horizons, where parts of the released Fe and Mn are condensed into nodules, as described above. Second, in the Bd- and E-horizons, where bleached zones are formed due to of the occurrence of a perched water-table in winter and where Fe and Mn are mainly lost (Laveuf *et al.*, submitted, cf. Chapitre 5.1.). Indeed, such transient water-tables are known to yield reductive conditions that promote bleaching (Pedro *et al.*, 1978), due to the dissolution of the Fe-Mn nodules and of the cementing Fe-Mn-oxide coatings in the soil horizon matrix. We considered that the residue from the sequential extraction performed on the <50 μm fraction was representative of the bleached zones and we then normalized the residues of this extraction to the raw <50 μm fractions (*i.e.* to the materials from which they developed). In the obtained REE patterns, the difference to 1 gives the composition of the extracted phases, *i.e.* the sum of Mn-oxides, (fluor)apatite and Fe-oxides. In both sola, three groups of soil

horizons can be distinguished from the REE patterns of the residues of their < 50 fractions: (i) the C-horizons, (ii) the B(c)-horizons, and (ii) the Bd-, E- and LE-horizons (Figures 4a and 4b).

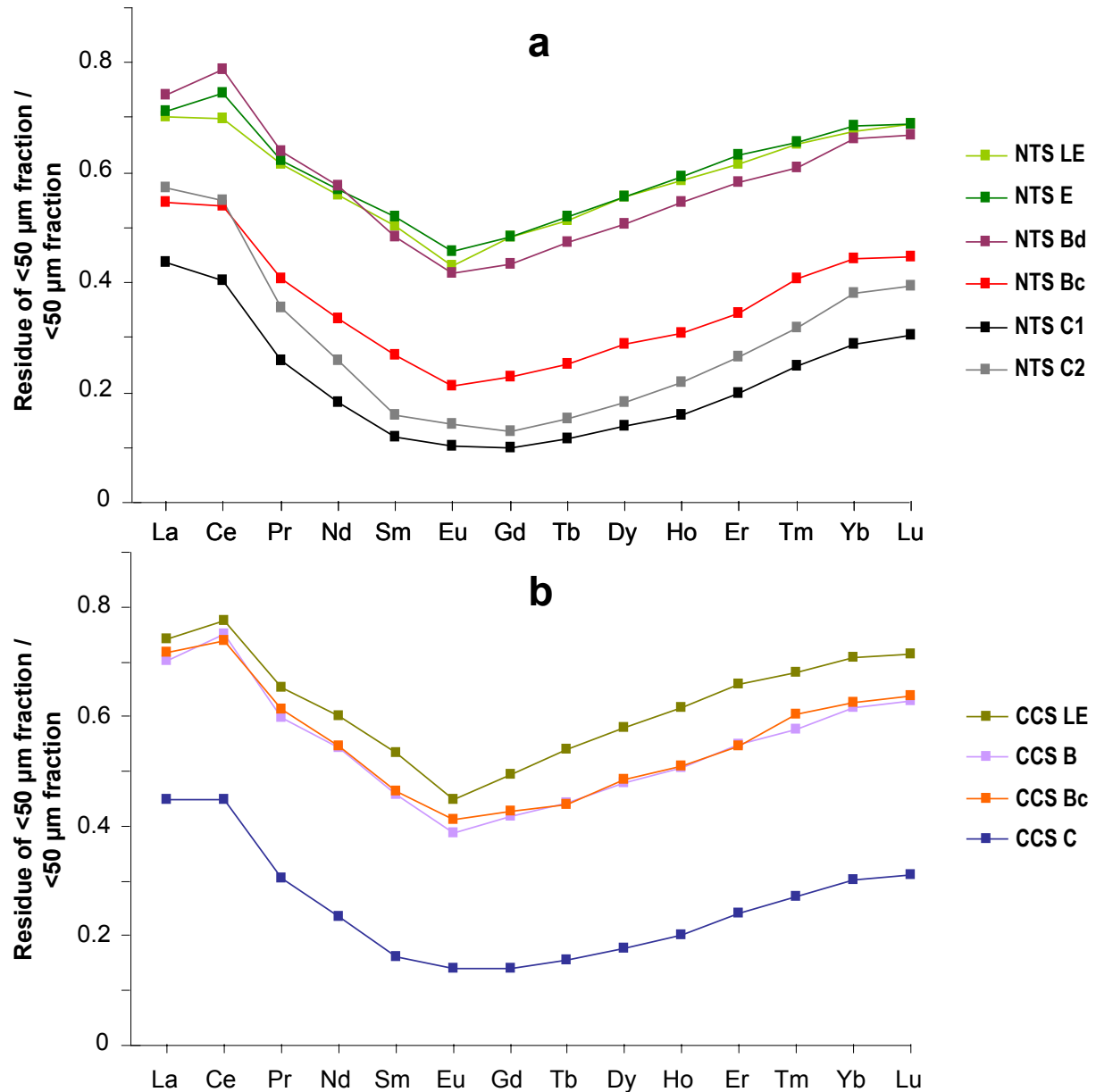


Figure 4. Patterns of stocks of REEs in the residues from extraction of the <50 μm fractions normalized to the raw <50 μm fractions for NTS (a) and CCS (b).

The REE patterns of the C- and LE-horizons are respectively similar in the two sola. In NTS, the REE pattern of the Bc-horizon is closer from that of the C-horizon than from that of the degraded horizons, while in CSS, it is closer from that of the LE- and B-horizons. All REE patterns show that the extracted phases are enriched in MREEs compared to LREEs and HREEs and display a slight negative Ce anomaly (Figures 4a and 4b). The enrichment in MREEs decreases while oxides are dissolved, *i.e.* from the C- to the LE-horizons in both sola.

Fe and Mn dissolved from the C- to the Bc-horizons are partially condensed into Fe-Mn nodules, whereas in the degraded NTS horizons they are lost. According to the REE patterns, the dissolution of the Fe-Mn oxides dispersed in the soil matrix seems to be more pronounced in the Bc-horizon of CCS than in that of NTS (Figures 4a and 4b). This is in agreement with the larger amount of Fe-Mn nodules in the Bc-horizon of CCS (Table 2).

Table 2. Main soil characteristics of the NTS and of the CCS: soil horizons names and sampling depths, particle-size distribution, contents in CaCO₃, organic matter (OM), Fe and Mn of the different fractions.

	Solum	Soil horizon	Depth sampled cm	Mass percentage in the soil horizon	CaCO ₃	OM g kg ⁻¹	Fe	Mn
<50 µm fraction	NTS	LE	10-20	86	<L.D.	21.6	32.9	1.45
		E	25-35	86	<L.D.	19.2	32.5	0.85
		Bd	50-60	87	<L.D.	10.7	45.0	1.23
		Bc	90-105	81	1	9.5	66.3	7.06
		C1	120-130	79	2.4	8.6	80.4	17.7
		C2	130-140	77	1.7	8.8	74.1	8.88
	CCS	LE	10-25	84	<L.D.	36.3	33.9	1.07
		B	40-50	83	<L.D.	12.9	41.0	1.05
		Bc	65-75	59	<L.D.	12.7	45.0	1.60
		C	85-100	79	2.1	9.7	73.9	11.8
<2 µm fraction	NTS	LE	10-20	16	<L.D.	34.3	69.1	2.76
		C1	120-130	38	2.0	10.0	74.7	5.96
Fe-Mn nodule	NTS	LE	10-20	10	<L.D.	<L.D.	204	32.5
		Bc	90-105	16	<L.D.	<L.D.	188	81.5
		C1	120-130	17	<L.D.	<L.D.	186	63.1
	CCS	Bc	65-75	38	<L.D.	<L.D.	229	93.6

<L.D.: below the limit of detection

All these results indicate that the condensation of Fe- and Mn-oxides as nodules induces a relative enrichment in REEs and the appearance of a positive Ce anomaly, while the dissolution of oxides induces a loss of MREEs and the appearance of a slight negative Ce anomaly. These evolutions of the REE signatures are probably due to the varying proportion of the different oxides known to be enriched in REEs (Rankin and Childs, 1976; Walter, 1991; Palumbo *et al.*, 2001) and to their relative affinities for LREEs, MREEs and HREEs.

3.2. REE signatures in the different mineral phases of the Fe-Mn nodules, of the <50 µm and <2 µm fractions

To evidence the affinity of REEs for the different mineral phases in the Fe-Mn nodules and in the soil matrix, we normalized their concentrations to the residues of former parent material of each considered soil horizon. The REE patterns of the different residues of former parent materials (RFPMs) are rather similar (Figure 5), allowing comparison of REE signatures between soil fractions of the different soil horizons.

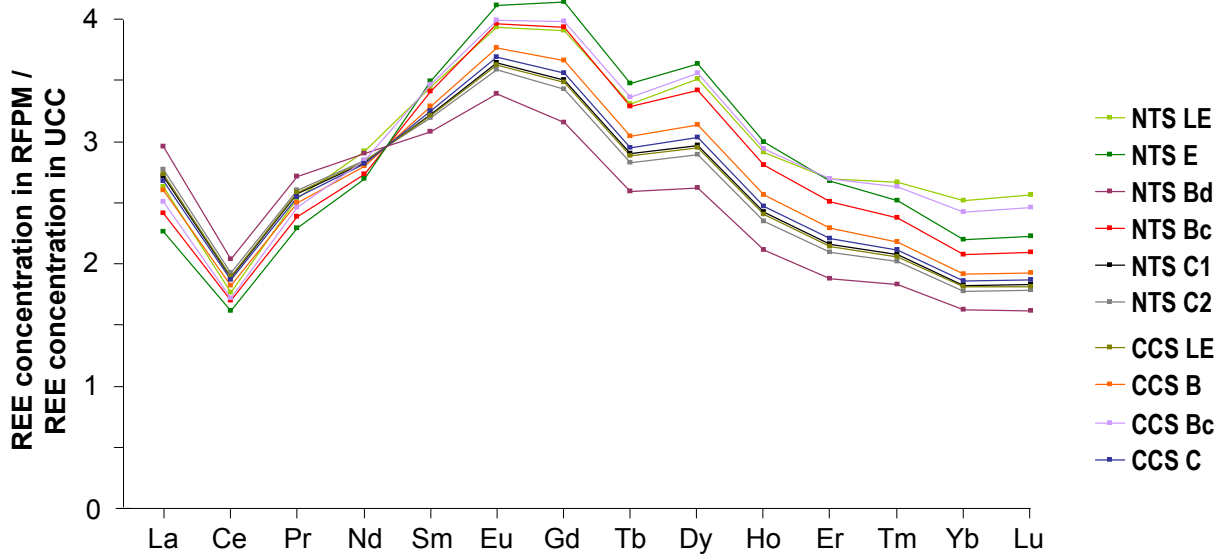


Figure 5. Patterns of REE concentrations normalized to Upper Continental Crust (UCC; Taylor and McLennan, 1985) in the residues of the former parent materials (RFPMs) for each of the sampled NTS and CCS horizons.

3.2.1. REE signature of (fluor)apatite

Non-magnetic >50 µm fractions are mainly composed of (fluor)apatite, quartz, carbonates and feldspars, with variable amounts of these minerals in the different soil horizons. The quantities of (fluor)apatite in the different non-magnetic >50 µm fractions were estimated on the basis of their contents in P and Ca, considering that P was only related to (fluor)apatite. Then, REE concentrations of the non-magnetic >50 µm fractions were plotted as a function of their (fluor)apatite quantities, evidencing a strong positive correlation (Figure 6).

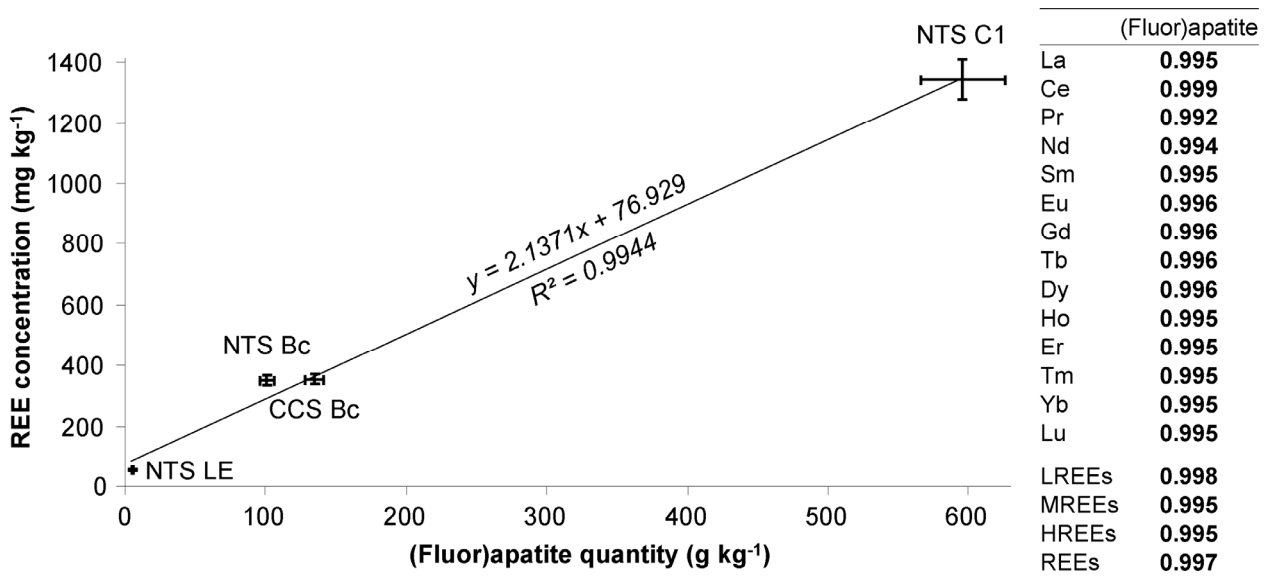


Figure 6. Concentrations of REEs in the non-magnetic >50 µm fractions as a function of their (fluor)apatite contents and Pearson's correlation coefficients of individual and groups of REEs with (fluor)apatite. Significant correlation coefficients at the threshold of $\alpha=0.05$ are reported in bold.

The Y-axis intercept represents the REE concentration of the other minerals in the non-magnetic $>50\ \mu\text{m}$ fractions, *i.e.* quartz, carbonates and feldspars, which contains only small REE contents, in accordance with literature (Henderson, 1984; Condie *et al.*, 1995; Monecke *et al.*, 2002). On the basis of these regressions, the REE content of (fluor)apatite was calculated for each REE and normalized to that in the residues of the former parent materials (RFPMs). This normalized REE pattern of (fluor)apatite is characterized by a strong enrichment in all REEs (4 to 8), especially in MREEs and a slight negative Ce anomaly (Figure 7a). These characteristics are commonly encountered in the literature for REE patterns of (fluor)apatite (Henderson, 1984; Tyler, 2004), and were notably described for phosphate nodules in similar soils (Laveuf *et al.*, 2008, cf. Chapitre 4.2.1.).

3.2.2. REE signatures of Mn-oxides

Step B of the extraction scheme dissolves both the Mn-oxides and the (fluor)apatite according to Hall *et al.* (1996) and Land *et al.* (1999). The quantities of (fluor)apatite were calculated using the quantities of Ca and P extracted. As already mentioned, the amounts of REE associated to (fluor)apatite were estimated on the basis of the REE concentrations of the (fluor)apatite in the non-magnetic $>50\ \mu\text{m}$ fractions (Figure 7a). These amounts were then subtracted from those released during step B of the extractions scheme (Figures 7b and 7c) to estimate the fraction of REEs associated to the Mn-oxides (Figures 7d and 7e).

Mn-oxides are highly enriched in REEs compared to their RFPMs, with normalized concentrations ranging from 2 to 14, with the exception of the Mn-oxides dispersed in the matrix of the C1-horizon (Figures 7d and 7e). For this sample, the negative REE pattern obtained suggests that the mass balance calculation is not acceptable. This sample contains 8 folds more (fluor)apatite (about 8 %) than Mn-oxides (about 1 %). The discrepancy on the mass balance calculation is then interpreted as resulting from the high stock of REEs bound to (fluor)apatite. Indeed, in these conditions, small uncertainties on the determination of the REE pattern of (fluor)apatite can result in large errors on that of the Mn-oxides.

Mn-oxides in the Fe-Mn nodules display a positive LREE/HREE fractionation and a positive Ce anomaly (Figure 7d), while they display a negative LREE/HREE fractionation in the $<2\ \mu\text{m}$ fraction (Figure 7e). However, due to the relatively large amount of (fluor)apatite compared to Mn-oxides in the matrix, these differences must be considered with caution and no definitive conclusions between the two kinds of Mn-oxides (in Fe-Mn nodules and in the matrix) can be drawn from these results. Further analyses are required to confirm differences between the REE signatures of the Mn-oxides in the nodules and in the matrix. In addition, the mineralogy of these different Mn-oxides remains to be characterized, since birnessite was identified in the Fe-Mn nodules (Manceau *et al.*, 1997) and in the NTS C-horizons by XRD analyses, whereas no specific Mn-species could be identified in the other soil horizons of both sola.

If real, these differences in the REE signature between samples could be related to (i) different formation conditions for Mn-oxides in the Fe-Mn nodules and in the matrix, (ii) contrasted availabilities of REEs at the time of the formation of Mn-oxides, or (iii) the actual nature of the Mn-oxides formed. Indeed, if the preferential trapping of LREEs, and especially of Ce, over HREEs in Mn-oxides is commonly reported (Rankin and Childs, 1976; Xing and Dudas, 1993; Steinmann and Stille, 1997; Land *et al.*, 1999; Yan *et al.*, 1999; Coelho and

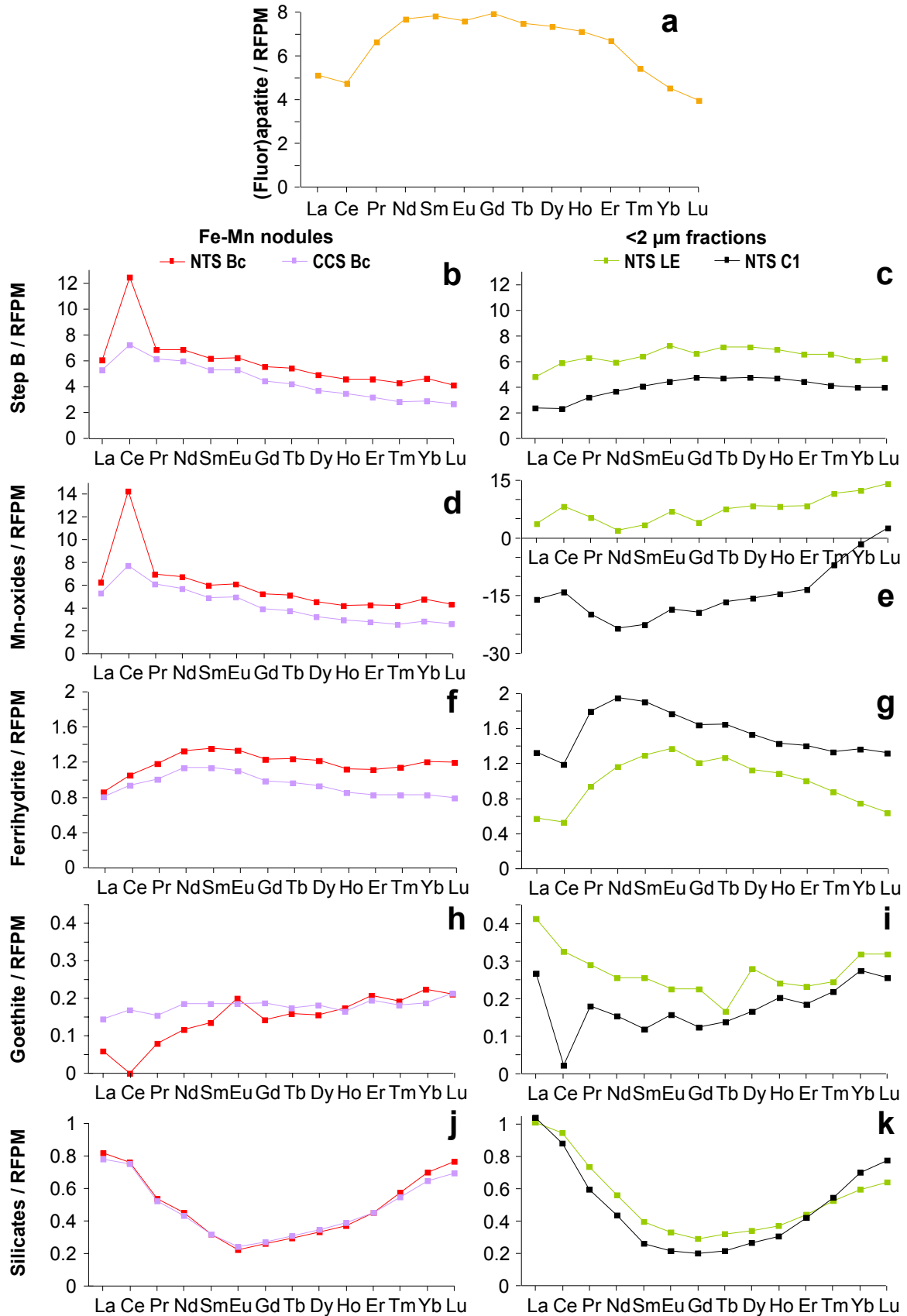


Figure 7. REE concentrations in reconstructed (fluor)apatite, Mn-oxides, ferrihydrate, goethite, and silicates of the Fe-Mn nodules and of the <2 μm fractions normalized to the REE concentrations in the residues of former parent materials (RFPMs) of their respective soil horizons, as calculated by *Laveuf et al.* (submitted, cf. Chapitre 5.1.).

Vidal-Torrado, 2000; Marques, 2000; Palumbo *et al.*, 2001; Ma *et al.*, 2002; Huang and Wang, 2004), these REE fractionations are considered to be related to the pH of the solution during REE sorption (Ohta and Kawabe, 2001).

3.2.3. REE signatures of ferrihydrite

Steps C and D of the extraction scheme target ferrihydrite. These extractions can thus be used to depict the REE concentrations of ferrihydrite. They were normalized to those of the respective RFPMs. Results indicate that the normalized REE patterns obtained range from 0.8 to 1.9, depending on the REE and on the sample considered (Figures 7f and 7g). This indicates that ferrihydrite poorly concentrates REEs from the RFPM compared to Mn-oxides. The normalized REE concentrations of ferrihydrite in the Fe-Mn nodules are in between those of the <2 μm fractions. Among all the studied fractions, the <2 μm fraction of the LE-horizon shows the lowest normalized REE concentrations.

Ferrihydrite shows an enrichment in MREEs both in the Fe-Mn nodules and in the matrix, this enrichment being more pronounced in the latter (Figures 7f and 7g). Such an enrichment of MREEs in amorphous Fe-oxides was already reported (Steinmann and Stille, 1997; Land *et al.*, 1999; Yan *et al.*, 1999; Yamasaki *et al.*, 2001). It appears more often in Fe-Mn-oxides formed at pH>5, in low-salinity solutions with a low organic acid content (Bau, 1999; Ohta and Kawabe, 2001; Davranche *et al.*, 2004; Pourret *et al.*, 2007).

Finally, a negative Ce anomaly is observed on the normalized REE pattern of ferrihydrite dispersed in the matrix (Figure 7g), whereas it is not visible on that of the Fe-Mn nodules (Figure 7f).

3.2.4. REE signatures of goethite

Step E of the extraction scheme dissolves goethite. This extraction can thus be used to obtain the REE concentrations of goethite. We normalized them to those of the respective RFPMs. The low values of these normalized REE concentrations in goethite indicate that this mineral is strongly depleted in all REEs, whatever the soil fraction considered (Figures 7h and 7i). The lower REE concentrations in goethite compared to ferrihydrite and Mn-oxides are in agreement with the lower REE concentrations in crystalline Fe-Mn-oxides than in amorphous ones (Courtois, 1974; Land *et al.*, 1999; Yan *et al.*, 1999; Compton *et al.*, 2003).

In the Fe-Mn nodules of the Bc-horizons, goethite displays rather flat normalized REE patterns. However, normalized LREE concentrations are smaller in the NTS than in the CCS, especially for Ce, which displays a slight negative anomaly (Figure 7h).

In the <2 μm fractions, goethite is MREE-depleted and the LREE content of goethite is lower in the C1- than in the LE-horizon, especially for Ce (Figure 7i). This latter element shows a strong negative anomaly in the <2 μm fraction of the C1-horizon, which is not visible in that of the LE-horizon. On the opposite to ferrihydrite, goethite in the <2 μm fraction of the LE-horizon displays the highest normalized REE concentrations of all soil fractions.

3.2.5. REE signatures of silicates

The residual fraction of the extraction scheme is indicative of silicates. The REE concentrations in silicates can thus be extrapolated from the results of this extraction and were

then normalized to those of the respective RFPMs. Results show that silicates are depleted in MREEs compared to the RFPM, in both soil fractions (Figures 7j and 7k). This observation is in agreement with the lower proportion of MREEs in the residues from extraction compared to LREEs and HREEs already shown in other studies (see e.g. Cao *et al.*, 2000).

All these results indicate that two mineral phases highly concentrates REEs from the RFPM: Mn-oxides that display variable Ce anomaly and LREE/HREE fractionation, and (fluor)apatite that show an enrichment in MREEs and a slight negative Ce anomaly. Ferrihydrite slightly concentrates MREEs, while goethite and silicates are strongly depleted in all REEs and in MREEs, respectively.

3.3 Evolution of the different mineral phases with the redox processes along the sola

3.3.1. Condensation in Fe-Mn nodules and subsequent dissolution

The Fe-Mn nodules consist of silicates, ferrihydrite, Mn-oxides, goethite and (fluor)apatite, in order of decreasing proportions. The relative proportions of these minerals vary according to the soil horizon considered, as shown by the results derived from sequential extractions (Figure 8a).

The Fe-Mn nodules in formation, as shown in the NTS C1-horizon, contain mainly ferrihydrite (18%), equal proportions of goethite and Mn-oxides (13%), and finally, smaller amounts of (fluor)apatite (4%). Once formed in the NTS Bc-horizon, their ferrihydrite and goethite proportions remain rather stable (20% and 11%, respectively), while their (fluor)apatite and especially Mn-oxide proportions increase (7% and 17% respectively). The proportions of ferrihydrite and Mn-oxides are higher in the Fe-Mn nodules of the CCS Bc-horizon (20% and 28% respectively), whereas silicate proportion is lower (37% against 50%).

Then, the subsequent dissolution of the Fe-Mn nodules induces a decrease of their amounts in the LE-horizon (Figure 8a). In this soil horizon, the proportions of (fluor)apatite and Mn-oxides decrease (to 1% and 6%, respectively), while those of ferrihydrite and goethite do not change significantly. These trends lead to an increase of the silicate proportion due to residual enrichment (61%). Therefore, considering the decrease of the amounts of Fe-Mn nodules in the LE-horizon, the dissolution of these nodules leads to a decrease of the total amounts of all Fe-Mn-oxides, with a larger influence on Mn-oxides than on Fe-oxides.

3.3.2. Dissolution of the oxide phases dispersed in the matrix

In the C-horizons of NTS and CCS, the <50 μm fractions consist in silicates (78% to 88%), goethite (about 4.5%), ferrihydrite (4% to 5.5%), (fluor)apatite (2% in the CCS and 4.5% to 7% in the NTS) and, to a lesser extend, Mn-oxides (1.5% to 3.5%) (Figure 8b).

When primary redox conditions appear in the Bc-horizons of both sola, and especially in CCS, the proportions and the absolute quantities of all Fe-Mn-oxides and of (fluor)apatite decrease in the <50 μm fractions, whereas those of silicates increase (Figure 8b). In CCS, the proportion of ferrihydrite in the Fe-Mn nodules increases from the C- to the Bc-horizon. It can thus be assumed that the oxides lost from the Bc-horizon matrix condensed into the Fe-Mn nodules, inducing larger losses from the matrix in soil horizons having more nodules. To test

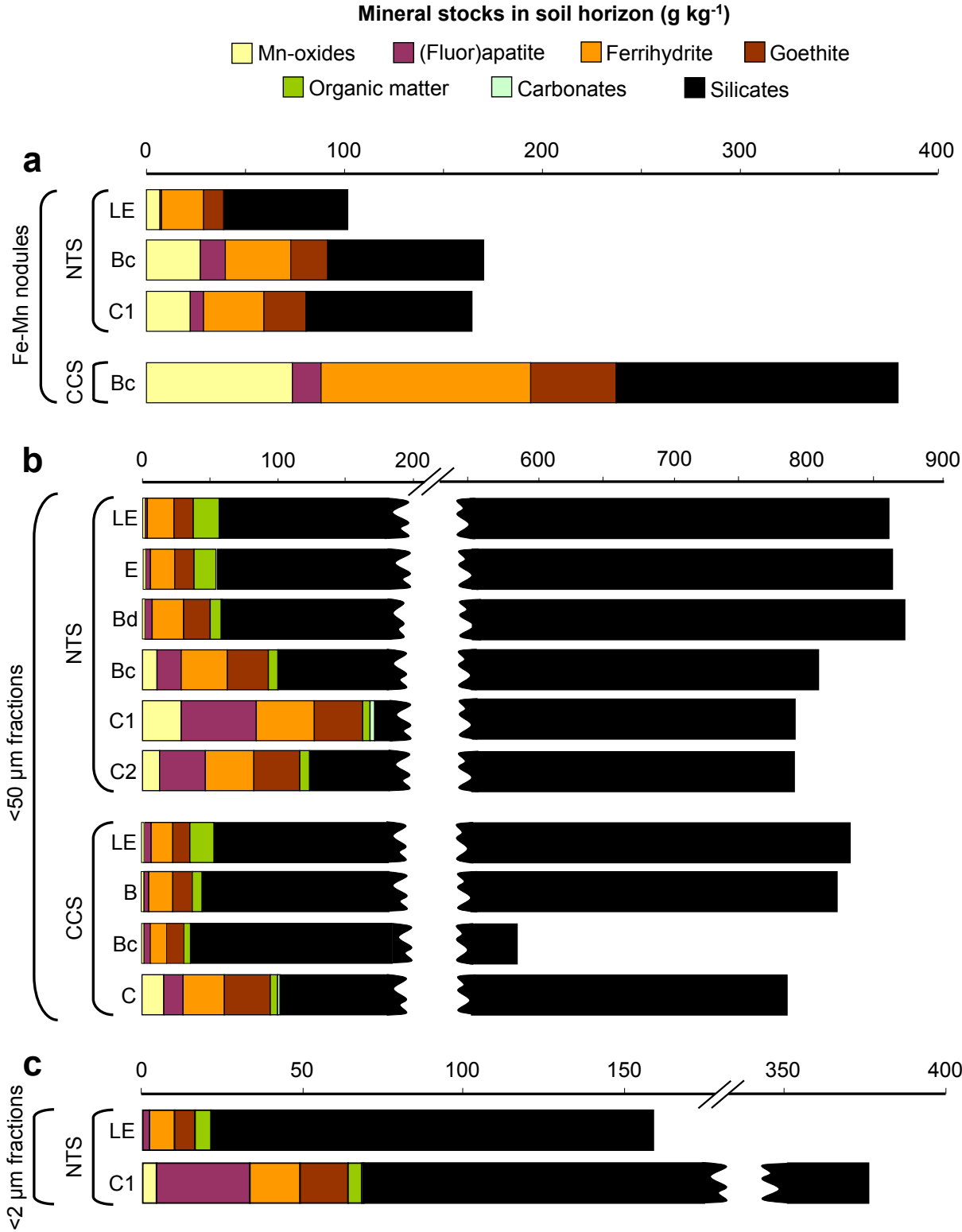


Figure 8. Mineral stocks (g kg⁻¹) in the Fe-Mn nodules (a), in the <50 μm fractions (b) and in the <2 μm fractions (c) within the different soil horizons, derived from sequential extraction results (for Mn-oxides, ferrihydrite, goethite, (fluor)apatite and silicates).

this hypothesis, mass balance calculations were performed on Fe-Mn-oxides for the C- and Bc-horizons (Figure 9). Indeed, Fe-Mn nodules and <50 μm fractions represent nearly 100 % of the C1- and Bc-horizons of NTS (Table 2). One third of the Mn-oxides dissolved in the matrix are trapped again in the Fe-Mn nodules during their formation (Figure 9). Similarly, about 20% of the Fe arising from the dissolution of ferrihydrite in the <50 μm fraction and of goethite in the <50 μm fraction and Fe-Mn nodules are trapped back into ferrihydrite during the formation of the Fe-Mn nodules. Finally, the major part of the Fe and Mn released into soil solution is exported from the Bc-horizon, in agreement with mass balance calculations computed by Laveuf *et al.* (submitted, cf. Chapitre 5.1.). Results of this mass balance thus confirms that the Fe-Mn-oxides dispersed into the matrix in the Bc-horizon are dissolved and partially recondensed into Fe-Mn nodules, this process being more expressed in CCS than in NTS.

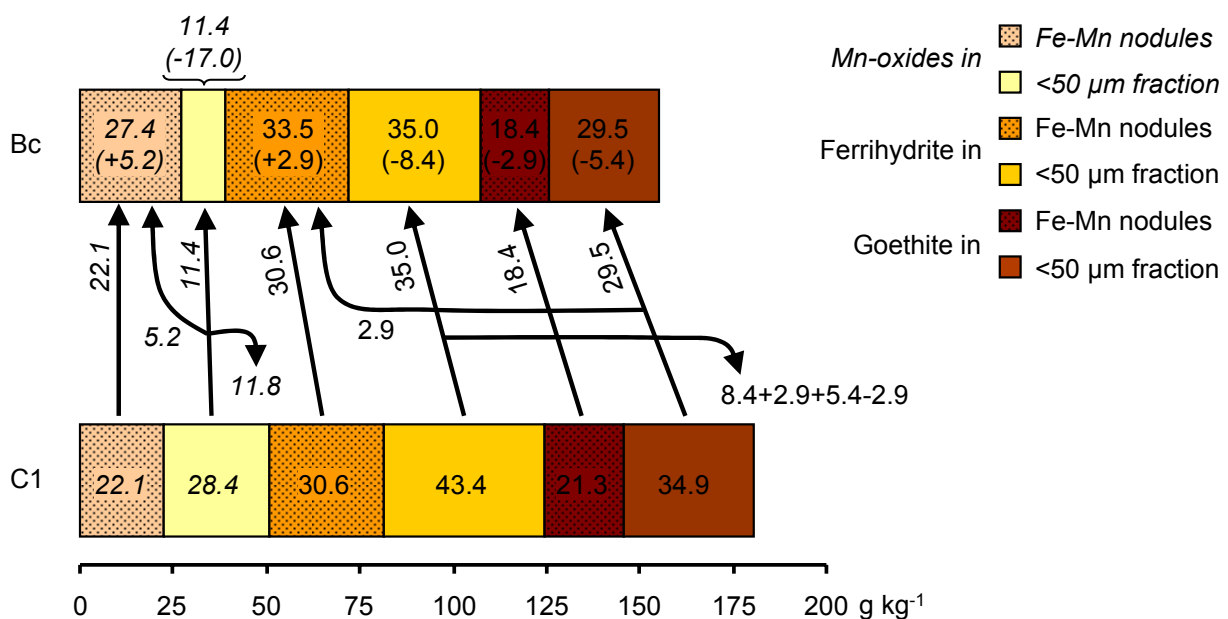


Figure 9. Mass fluxes (in g kg^{-1}) of Mn-oxides, ferrihydrite and goethite between the C1- and the Bc-horizon of NTS considering variations in the mineral stocks in the Fe-Mn nodules and concomitant dissolution of the Fe-Mn nodules and in the <50 μm fractions.

Secondary redox conditions, which occur in the Bd- to LE-horizons of NTS, as described previously, also lead to the dissolution of all Fe-Mn-oxides of the <50 μm fraction, as well as of (fluor)apatite (Figure 8b). As a result, silicate proportions increase. The conclusions are similar when considering the evolution of the mineral phases in the <2 μm fraction from the C1- to the LE-horizon (Figure 8c). Since no secondary redox condition occurs in CCS, as observed during our field observations, the quantities of Fe-Mn-oxides and of (fluor)apatite do not evolve significantly from the Bc- to the LE-horizons (Figure 8b).

3.4. Impact of the different minerals on the signature in REEs of the pedological features: implication in terms of analysis of the processes

We here aim at understanding the quantitative impact of the REE-bearing minerals on the evolution of the REE patterns during formation and subsequent dissolution of the Fe-Mn nodules (Figure 3) and during the bleaching of the soil horizons affecting the <50 μm fractions (Figure 4).

3.4.1. In the Fe-Mn nodules

Although Mn-oxides represent a limited proportion of the mineral phases in the Fe-Mn nodules (Figure 8a), they account for the main proportion of the REE stocks in the Fe-Mn nodules (Figure 10), due to their high REE concentrations (Figure 7d). This result is in agreement with the lower point of zero charge of Mn-oxides compared to Fe-oxides, leading to a higher sorption affinity of these species over Fe-oxides for REEs (Laveuf and Cornu, submitted, cf. Chapitre 4.1.). The proportion of REEs bound to Mn-oxides decreases progressively from La to Lu (Figure 10). Besides, Ce behaves differently from the other LREEs, since its proportion in Mn-oxides is significantly higher, especially in the NTS (Figure 10). These fractionations are in agreement with the literature (Rankin and Childs, 1976; Laveuf and Cornu, submitted, cf. Chapitre 4.1.).

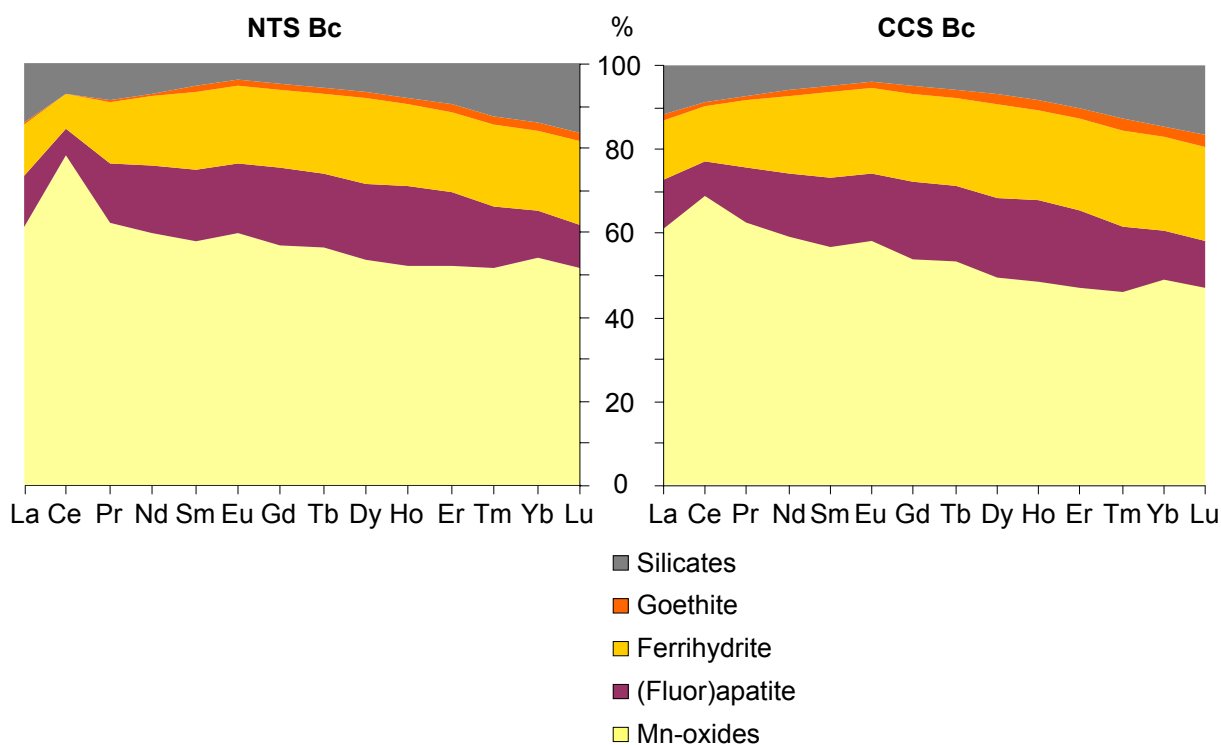


Figure 10. Repartition of the stock of REEs between Mn-oxides, ferrihydrite, goethite, (fluor)apatite and silicates within the Fe-Mn nodules of the Bc-horizons of NTS and of CCS.

Table 3. Pearson's correlation matrix of the stocks of REEs in the Fe-Mn nodules normalized to their respective RFPMs (Figure 3) with the quantities of minerals in Fe-Mn nodules (Figure 8a). Significant correlation coefficients at the threshold of $\alpha=0.05$ are reported in bold.

	Mn-oxides	Ferrihydrite	Goethite	(Fluor)apatite	Silicates
La	0.987	0.972	0.949	0.862	0.960
Ce	0.924	0.900	0.852	0.887	0.869
Pr	0.985	0.976	0.947	0.844	0.959
Nd	0.987	0.976	0.950	0.852	0.962
Sm	0.989	0.979	0.954	0.845	0.965
Eu	0.991	0.978	0.957	0.852	0.967
Gd	0.993	0.977	0.962	0.861	0.971
Tb	0.993	0.974	0.962	0.869	0.970
Dy	0.996	0.973	0.970	0.876	0.975
Ho	0.997	0.971	0.976	0.977	0.979
Er	0.993	0.959	0.973	0.894	0.975
Tm	0.988	0.947	0.972	0.903	0.971
Yb	0.978	0.929	0.958	0.925	0.956
Lu	0.974	0.924	0.962	0.917	0.958
LREEs	0.970	0.953	0.919	0.971	0.933
MREEs	0.991	0.977	0.957	0.856	0.967
HREEs	0.988	0.949	0.970	0.904	0.970
REEs	0.990	0.969	0.956	0.879	0.964

However, on the opposite of all other REEs, the stock of Ce normalized to the RFPM is not correlated with the amounts of Mn-oxides in the Fe-Mn nodules (Table 3). This difference suggests that the mechanism responsible for the incorporation of Ce into the Fe-Mn nodules is different from that responsible for the incorporation of the other LREEs. This difference leads to the positive Ce anomaly that develops during Fe-Mn nodule formation and that persists during dissolution (Figure 3). The preferential retention of Ce over the other LREEs in soil profiles and the formation of positive Ce anomalies are generally assigned to the precipitation of cerianite CeO_2 (see *e.g.* Braun *et al.*, 1990). Such a precipitation is supposed to be favored by the occurrence of Mn-oxides, since the oxidation of Ce(III) to Ce(IV) can be coupled with the reduction of Mn(IV) to Mn(III) (Ran and Liu, 1992; Marker and de Oliveira, 1994; Ohta and Kawabe, 2001). The stock of Ce trapped from the RFPM in the Fe-Mn nodules of the C1-horizon is lower than that in Fe-Mn nodules of the Bc-horizon (Figure 3). However, the Fe-Mn nodules of the C1-horizon contain as much Mn-oxides as those of the Bc-horizon (Figure 8a). The higher number of redox cycles required to form Fe-

Mn nodules in the Bc-horizons than in the C1-horizon could be responsible for the occurrence of the positive Ce anomaly in relation with cerianite precipitation. Indeed, Mn-oxides could be partially dissolved during the reduction phases of these redox cycles, while cerianite is not. Then, Mn-oxides could precipitate again onto Fe-Mn nodules during oxidation phases, incorporating Ce without fractionation compared to the other LREEs, as shown in the C1-horizon. Such a behavior would lead to an accumulation of cerianite in the Fe-Mn nodules. This hypothesis is in agreement with the positive Ce anomaly observed for the LE-horizons (Figure 3). Indeed, when Mn-oxides included in Fe-Mn nodules dissolve in the LE-horizon, all REEs, except Ce, are lost proportionally to the fraction of Mn-oxides dissolved (Table 3). Because of its occurrence as cerianite, Ce has a peculiar behavior and it is less lost (Figure 3). Therefore, the intensity of the positive Ce anomaly, in relation to the occurrence of cerianite, could trace the variations of the redox conditions at the origin of the precipitation and dissolution of Mn-oxides. Actual speciation of Ce, and especially possible occurrence of cerianite in Fe-Mn nodules, should be characterized in order to confirm this hypothesis.

The fraction of REEs bound to ferrihydrite account for about 20% of the total stock of REEs in Fe-Mn nodules (Figure 10). The patterns of the stock of REEs in ferrihydrite show a slight but significant enrichment in HREEs over LREEs in both sola, as well as a negative Ce anomaly more pronounced in the NTS Bc-horizon than in the CCS one (Figure 10). However, while the evolution of the stock of REEs is significantly correlated with that of ferrihydrite, those of HREEs and Ce are not (Table 3). Thus, ferrihydrite affects mainly the evolution of the LREE and MREE patterns of the Fe-Mn nodules along NTS, and to a lesser extent, those of Ce and HREEs (Figure 3).

Even if (fluor)apatite accounts for a non-negligible fraction of the stock of REEs in the Fe-Mn nodules (Figure 10), and especially of MREEs as for its normalized concentrations (Figure 7a), the evolution of its quantities is not significantly correlated with that of the REEs (Table 3).

The fraction of REEs bound to goethite represent less than 2% of the total stock of REEs in the Fe-Mn nodules (Figure 10). Therefore, the impact of goethite on the evolution of REE patterns of Fe-Mn nodules is non-significant, although they are significantly correlated, except for LREEs (Table 3). The lack of significant correlations between the stocks of LREEs trapped from the RFPM in the Fe-Mn nodules and goethite quantities may arise from the differences of LREE concentrations in the goethite between CCS and NTS (Figure 7h).

The stock of REEs bound to silicates is non-negligible (Figure 10), due to their large proportion in the Fe-Mn nodules (Figure 8a) and despite their low REE concentrations (Figure 7j). As for concentrations, their stock of REEs is depleted in MREE. However, the relative small evolution of the silicate fraction along NTS (Figure 8a) cannot explain the evolution of the REE patterns in Fe-Mn nodules (Figure 3), although they are significantly correlated (Table 3).

Finally, considering the repartition of the stock of REEs within the Fe-Mn nodules (Figure 10), the evolution of the REE patterns along NTS (Figure 3) is strongly related to Mn-oxides, as confirmed by Pearson's correlations (Table 3). It is also related to ferrihydrite - at the exception of HREEs (Table 3). Although the proportions of goethite and silicates are somewhat similar in all NTS Fe-Mn nodules (Figure 8a), these minerals poorly affect the evolution of the REE patterns along NTS (Figure 3), because their REE concentrations are too low (Figures 7h and 7j).

3.4.2. In the matrix

The (fluor)apatite and Mn-oxides dispersed in the matrix account for most of the extractable stock of REEs contained in the $<2\mu\text{m}$ fraction of the LE- and C1-horizons of NTS (Figure 11). These mineral species are enriched in MREEs and slightly depleted in LREEs. In the LE-horizon, Mn-oxides account for about one third of the stock of REEs bound to (fluor)apatite and Mn-oxides, this ratio being higher for HREEs than for LREEs. The proportion of Ce in Mn-oxides is not significantly larger than that of the other LREEs. The stock of REEs bound to (fluor)apatite and Mn-oxides is larger in the C1-horizon than in the LE-horizon (Figure 11), because the quantities of both minerals are larger in the C1-horizon (Figure 8c).

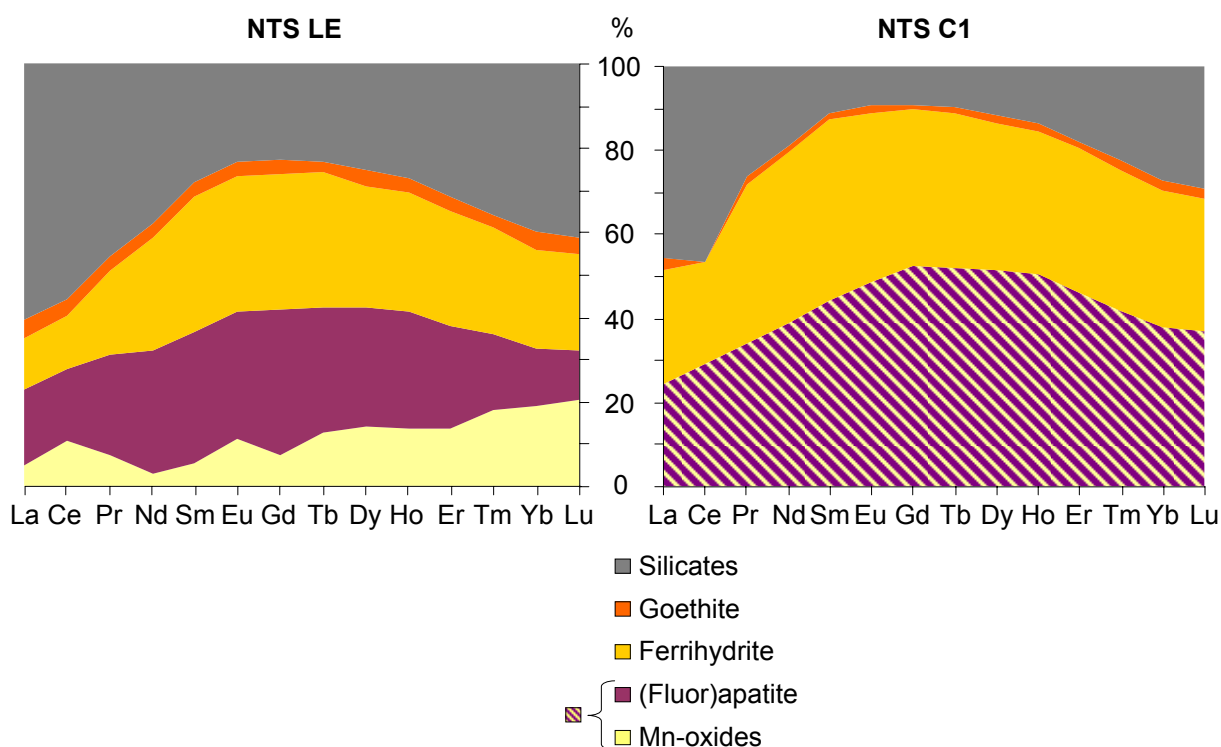


Figure 11. Repartition of the stock of REEs between Mn-oxides, ferrihydrite, goethite, (fluor)apatite and silicates within the $<2\mu\text{m}$ fraction of the LE- and C1-horizons of the NTS.

Ferrihydrite in the matrix is the second phase in terms of importance for the extractable stock of REEs in the $<2\mu\text{m}$ fractions (Figure 11). In the LE-horizon, this mineral accounts for about the same stock of REEs than (fluor)apatite. The stock of REEs in ferrihydrite is enriched in MREEs and depleted in LREEs, with a negative Ce anomaly. This reflects the REE patterns of concentrations (Figure 7g). The Ce anomaly is however more pronounced in the C1- than in the LE-horizon of NTS (Figure 11).

Goethite in the matrix only accounts for a slight proportion of the stock of REEs in the $<2\mu\text{m}$ fractions, with a negative Ce anomaly in the C1-horizon of NTS (Figure 11). This result is in agreement with the small REE concentrations in goethite (Figure 7i) and to their respective quantities in both soil horizons (Figure 8c).

Silicates account for a significant proportion of the stock of REEs in the $<2 \mu\text{m}$ fractions and are even the most important REE-bearing mineral specie in the LE-horizon (Figure 11). So, despite low REE concentrations (Figure 7k), the high proportions of silicates in the $<2 \mu\text{m}$ fraction ($>82\%$; Figure 8c) are responsible for the impact of this mineral on the stock of REEs.

Finally, the repartition of the stock of REEs among Fe- and Mn-oxides dispersed in the matrix evolves along the solum. Indeed, the proportions of the stock of REEs bound to (fluor)apatite and Mn-oxides, on the one hand, and to ferrihydrite, on the other hand, decrease from the C1- to the LE-horizon of NTS, whereas that bound to silicates increase due to residual enrichment (Figure 11). The decrease of the proportion of the stock of REEs bound to (fluor)apatite and Mn-oxides toward soil surface affects more MREEs than HREEs. LREEs are not affected. This result is in agreement with the higher REE, and especially MREE, concentrations in (fluor)apatite (Figure 7a) and with the larger decrease in (fluor)apatite quantities than in Mn-oxides in the LE-horizon (Figure 8c). The decrease of the proportion of the stock of REEs bound to ferrihydrite affects more the LREEs than other REEs. Among LREEs, Ce is less affected.

The normalization of the stock of REEs in the residues of extraction for the $<50 \mu\text{m}$ fractions to the raw $<50 \mu\text{m}$ fractions shows that extracted phases are enriched in MREEs compared to LREEs and HREEs, with a negative Ce anomaly (Figures 4a and 4b). This result is in agreement with the enrichment in MREEs of the stock of REEs bound to extracted phases in the $<2 \mu\text{m}$ fractions (Figure 11) and with the signatures of the main REE-bearing minerals (fluor)apatite and ferrihydrite which are enriched in MREEs (Figures 7a and 7g). As said previously, formation of Fe-Mn nodules induces a first decrease of the stock of REEs in the $<50 \mu\text{m}$ fractions (from the C- to the Bc-horizons; Figures 4a and 4b). Stock of REEs then keeps on decreasing (from NTS Bc- to LE-horizons) due to bleaching. Since no secondary redox condition occurs in CCS, the REE patterns of the B- and LE-horizons of CCS do not evolve significantly compared to the Bc-horizon (Figure 4b). During secondary redox conditions, all mineral phases are lost, with the exception of silicates whose proportions increase toward soil surface due to residual enrichment (Figure 8b). This enrichment leads to a larger proportion of the stock of REEs bound to silicates in the LE-horizon compared to the C1-horizon, as shown in the $<2 \mu\text{m}$ fractions (Figure 11). According to the repartition of the stock of REEs in the $<2 \mu\text{m}$ fractions (Figure 11), the evolution of the quantities of the main REE-bearing minerals, *i.e.* Mn-oxides, (fluor)apatite and ferrihydrite, is the main parameter susceptible to influence the evolution of the REE pattern from the Bc- to the overlying soil horizons of NTS (Figure 4a). This assumption is supported by the significant negative correlations between the total quantities of each mineral, except silicates, and the REE patterns of the extracted phases in the $<50 \mu\text{m}$ fractions (Table 4).

Therefore, although Mn-oxides display higher REE concentrations than ferrihydrite (Figures 7c and 7g), their much lower quantity in these soil horizons – 10 times less than ferrihydrite (Figure 8b) – results in a greater impact of ferrihydrite on the stock of REEs (Figure 11). Comparatively, although goethite quantities are close to those of ferrihydrite (Figure 8b), the much lower REE concentration in goethite compared to ferrihydrite (Figures 7i and 7g) results in a poor impact of goethite on the evolution of the stock of REEs (Figure 11).

Table 4. Pearson's correlation matrix of the stocks of REEs in the residues from extraction of the <50 μm fractions normalized to the raw <50 μm fractions (Figures 4a and 4b) with the quantities of minerals in the <50 μm fractions (Figure 8b). Significant correlation coefficients at the threshold of $\alpha=0.05$ are reported in bold.

	Mn-oxides	Ferrihydrite	Goethite	(Fluor)apatite	Silicates
La	-0.942	-0.875	-0.933	-0.773	0.515
Ce	-0.949	-0.886	-0.936	-0.803	0.544
Pr	-0.945	-0.906	-0.972	-0.835	0.562
Nd	-0.938	-0.906	-0.977	-0.843	0.582
Sm	-0.919	-0.900	-0.983	-0.838	0.600
Eu	-0.920	-0.912	-0.985	-0.833	0.574
Gd	-0.912	-0.903	-0.984	-0.836	0.598
Tb	-0.909	-0.889	-0.977	-0.828	0.625
Dy	-0.913	-0.893	-0.980	-0.829	0.612
Ho	-0.915	-0.890	-0.976	-0.826	0.621
Er	-0.918	-0.891	-0.976	-0.823	0.622
Tm	-0.922	-0.893	-0.978	-0.819	0.585
Yb	-0.928	-0.878	-0.969	-0.807	0.599
Lu	-0.924	-0.881	-0.972	-0.801	0.593
LREEs	-0.950	-0.895	-0.953	-0.810	0.545
MREEs	-0.924	-0.903	-0.982	-0.836	0.596
HREEs	-0.922	-0.888	-0.976	-0.817	0.605
REEs	-0.930	-0.899	-0.978	-0.827	0.594

4. Conclusion

This study aimed at understanding the mobilization of REEs during redox conditions and at determining possible relationships between the mobilizations of REEs and of Fe- and Mn-oxides.

Results of this study indicate that primary redox conditions induce the formation of Fe-Mn nodules, made of goethite, ferrihydrite, Mn-oxides, (fluor)apatite and silicates. Parts of the Mn and Fe in Mn-oxides and ferrihydrite in Fe-Mn nodules arise from the dissolution of these minerals and of goethite in the <50 μm fractions. During their formation, Fe-Mn nodules include a large part of the initial stock of REEs in the RFPM. The main mineral species responsible for the trapping of REEs are Mn-oxides, due to their high REE concentrations, and ferrihydrite, due to its high amounts. Of particular interest is the behavior of Ce during primary redox conditions. Our results suggest that the occurrence of a positive Ce anomaly in Mn-oxides may be related to the occurrence of cerianite. The intensity of the

Ce anomaly is supposed to result from the development and intensity of the redox conditions during water table fluctuations. Further analyses are however required to confirm this hypothesis. Indeed, despite birnessite was evidenced as Mn-oxides in Fe-Mn nodules of the same soil type, others Mn-oxides could occur. The nature of the Mn-oxides encountered in the soil could also be responsible for the development of the positive Ce anomaly. Since Mn-oxides exists in numerous crystalline and, most of the time, pseudo-crystalline forms in soils, hence the difficulties to identify them, the use of the Ce anomaly to trace the occurrence of one form or at least of the proportion of the different forms is highly interesting. Once Mn-oxides identified, we will need to asses (i) if the positive Ce anomaly effectively results from the dissolution of Mn-oxides together with REEs but not of cerianite, and (ii) if the relationship between the positive Ce anomaly and cerianite could allow tracing past intensity of redox conditions.

Secondary redox conditions induce an important dissolution of the Mn-oxides, (fluor)apatite, ferrihydrite, and goethite of the <50 μm fractions, mobilizing concomitantly mainly MREEs. The preferential mobilization of MREEs is related to the enrichment of MREEs in ferrihydrite, Mn-oxides and (fluor)apatite, which are the main REE-bearing mineral species mobilized during secondary redox conditions. However, our results do not allow quantifying precisely the respective impact of the different REE-bearing mineral species on the evolution of the REE signature along the sola, since difficulties in the mass-balance calculation were encountered. The dissolution of Fe-Mn nodules in the topsoil leads to a net decrease of all Fe-Mn-oxides, more pronounced for Mn-oxide contents. As a consequence, the REE content in the Fe-Mn nodules decreases concomitantly, although the positive Ce anomaly remains, probably due to the occurrence of cerianite.

Finally, the REE signature of the mineral species is related to the fraction of the soil considered that includes them. Indeed, ferrihydrite is always enriched in MREEs and displays a negative Ce anomaly in the matrix but not in the Fe-Mn nodules. Goethite shows a rather flat REE pattern in Fe-Mn nodules, whereas it is depleted in MREEs in the matrix.

5. Acknowledgments

The authors would particularly like to thank O. Josière, B. Renaux, P. Berche and C. Le Lay for technical support. This study was funded by the project “Terres Rares” of the INRA department “Environment and Agronomy” and benefited from a STUDIUM fellowship.

6.3. Conclusions sur l'impact des processus sur la redistribution des terres rares et leur utilisation comme traceurs

La redistribution des terres rares au cours du processus de décarbonatation est principalement dépendante de la spéciation des terres rares dans les matériaux parentaux. C'est ainsi que les terres rares lourdes sont préférentiellement mises en solution. Par ailleurs, le cérium est moins mis en solution que les autres terres rares légères au cours du processus, probablement à cause de la présence de cérianite dans les matériaux parentaux. Une fois en solution, les terres rares sont exportées hors de l'horizon C formé par le processus de décarbonatation, à l'exception d'une fraction des terres rares lourdes.

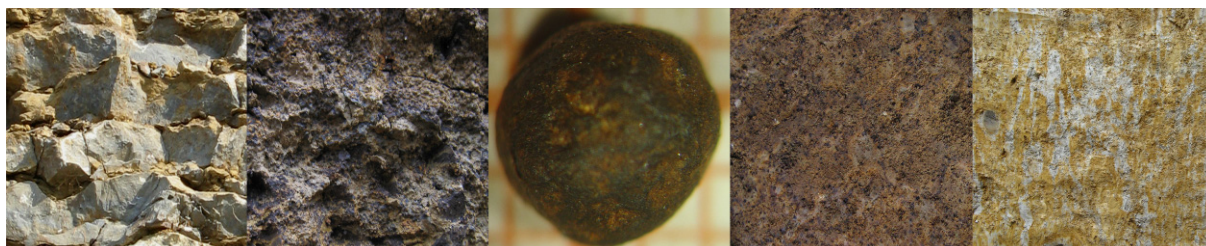
Lors des conditions redox primaires, les terres rares liées aux oxydes de fer et de manganèse, ainsi qu'à la (fluor)apatite, sont libérées en solution. Alors qu'une fraction est exportée hors de l'horizon (cf. [Chapitre 5](#)), une autre est captée par les oxydes de fer et de manganèse qui s'individualisent en concrétions ferri-manganiques qui se forment par l'alternance des conditions redox lors des battements de nappe. Les cycles de dissolution et de précipitation des oxydes de manganèse au cours du phénomène sont les principaux responsables de la mobilisation des terres rares. La succession de ces cycles semble notamment induire l'apparition d'une anomalie positive en cérium par un enrichissement relatif en cérianite formée au cours du processus dans les concrétions ferro-manganiques. A l'échelle de l'horizon, la présence de la cérianite héritée et de la cérianite néoformée entraînent une moindre exportation du cérium (cf. [Chapitre 5](#)). En conséquence, le cérium est un excellent traceur quantitatif des cycles de précipitation/dissolution des oxydes de manganèse, dont la nature et son rôle sur cette anomalie restent à déterminer. Etant donné la difficulté à quantifier les oxydes de manganèse dans les échantillons de sols de par leur faible cristallinité, et donc d'autant plus à quantifier l'impact des conditions redox sur leur mobilisation, l'utilisation de l'intensité de l'anomalie en cérium s'avère fort prometteuse.

Les conditions redox secondaires induisent ensuite une dissolution de l'ensemble des oxydes de fer et de manganèse, ainsi que de la (fluor)apatite, des fractions fines, et en particulier des oxydes de manganèse en accord avec les domaines de stabilité de ces oxydes. Bien que ce processus mobilise plus particulièrement les terres rares moyennes en relation avec la signature en terres rares des minéraux principalement mobilisés, *i.e.* ferrihydrite, (fluor)apatite, nos données ne m'ont pas permis de définir les phases minérales responsables des autres fractionnements (Ce et terres rares lourdes), en partie à cause de leur faible intensité et de la difficulté à déterminer la signature de certaines phases minérales. L'utilisation de notre méthodologie de normalisation pour mettre en évidence l'impact des processus redox secondaire est néanmoins informative, car à l'échelle de l'horizon, ces fractionnements n'apparaissent pas (cf. [Chapitre 5](#)).

En conclusion, l'utilisation des terres rares pour tracer la précipitation/dissolution des oxydes de fer dans les fractions fines et dans les concrétions ferro-manganiques a pu être démontrée au cours de ce chapitre, mais nécessite des investigations complémentaires pour quantifier les flux dus aux différents oxydes.

Chapitre 7

Conclusions générales et Perspectives



7.1. Etudier le passé pour prévoir l'avenir : le choix de la démarche pédologique

Le sol est un capital non-renouvelable à l'échelle temporelle humaine et il convient donc de le protéger des pressions anthropiques croissantes et de l'utiliser à bon escient. Pour cela, il est nécessaire d'être en mesure de séparer l'évolution naturelle des sols de l'évolution anthropique. Une approche permettant d'atteindre cet objectif consiste à identifier les différents processus pédogénétiques mis en jeu au cours de la pédogenèse et à quantifier leur importance relative sur l'évolution des sols.

La démarche pédologique semble parfaitement adaptée à cette approche. En effet, cette démarche consiste – dans la mesure où l'organisation des sols s'explique par une succession de processus, au cours des temps pédologiques, qui ont été à l'origine de flux de matière et d'énergie (Runge, 1973 ; Huggett, 1975 ; Rasmussen et Tabor, 2007) – à détecter la signature des processus passés et à reconstituer leur chronologie, *i.e.* l'histoire de la formation des sols grâce à l'analyse de ces derniers. C'est donc par une analyse du passé que l'on peut comprendre le fonctionnement des sols pour être en mesure de prédire leur évolution sous forçage anthropique. Ce cadre général réactualise les problématiques de pédogenèse, et justifie notre étude qui se veut donc un appui aux études envisageant les impacts anthropiques qui sortent du cadre de ce travail.

7.2. Face à un certain nombre de points de blocage, une approche couplant une démarche pédologique classique avec des approches innovantes

Le choix fait à l'origine de mon travail de thèse a été de considérer la démarche pédologique selon deux approches pédologiques classiques :

1. la démarche structurale qui considère que l'évolution pédologique résulte de la succession des fronts de transformation des différents processus pédogénétiques (Boulet *et al.*, 1982 ; Fritsch *et al.*, 1986 ; Lucas *et al.*, 1988) ;
2. le calcul d'un bilan de masse de type Brimhall qui permettent de quantifier les flux passés dans les sols (Brimhall *et al.*, 1991).

Ces deux approches m'ont semblé les mieux adaptées à la reconstitution de la succession des processus pédogénétiques passés. La première a inspiré la démarche appliquée au Chapitre 4 et reprise au Chapitre 6, alors que la seconde a inspiré la démarche des Chapitres 3 et 5.

Cependant, ces approches se heurtent aux points de blocage suivants :

1. une difficulté à quantifier des flux de matière engendrés par les processus pédogénétiques successifs. En effet cette quantification s'appuie généralement sur l'étude des éléments chimiques majeurs constituant les différentes phases minéralogiques. Ces éléments sont présents dans de nombreux minéraux et ne sont pas spécifiquement mobilisés par un processus unique, ce qui complique l'interprétation du rôle des différents processus sur la pédogenèse ;
2. une complexité importante des matériaux parentaux, dont l'influence sur les sols est encore forte en contexte tempéré (Cornu, 2005). De fait, l'établissement des bilans de

masse reposent sur une connaissance fine du matériau parental, si bien que son application est généralement limitée aux contextes où les matériaux parentaux sont homogènes.

Pour pallier ces limitations, l'originalité de mon travail de thèse a été de tester leur couplage avec l'utilisation de traceurs géochimiques peu utilisés jusqu'à présent en pédologie, bien que très prisés en géologie, les terres rares.

De plus, le sol est un milieu hétérogène et complexe qui présente une organisation emboîtée, dont les principaux niveaux pris en compte dans ce travail sont les constituants, les traits pédologiques et l'horizon. Ainsi, l'étude aux différentes échelles est une composante intrinsèque de l'analyse pédologique (Boulaïne, 1982). À ces échelles d'organisation correspondent des échelles de transferts et des processus différents. Mon travail de thèse a bien montré la nécessité de prendre en compte ces différentes échelles pour des processus comme l'oxydo-réduction qui sont, dans un même solum, à l'origine de mouvement d'éléments à la fois à l'échelle décimétrique dans le cas de la formation des nodules ferromanganiques, mais aussi à l'échelle du solum, voire du versant, dans le cas de la dégradation morphologique.

L'analyse des systèmes complexes a montré que le système n'est pas la somme des sous-systèmes, si bien que leur prise en compte dans leur ensemble nécessite une démarche qui allie différents « points de vue » et qui combine expérience et modèle (Legay, 1997). C'est donc une approche de ce type, alliant observations de terrain et expérimentations de laboratoire, chimie, minéralogie et modélisation de type bilan de masse, qui a été mise en œuvre durant mon travail de thèse. Cette approche multi-méthodes, multi-échelles et multi-éléments m'a permis de discriminer et quantifier l'impact de différents processus sur l'évolution des sols étudiés.

7.3. Des résultats marquants

7.3.1. La reconstitution de matériaux parentaux hétérogènes

Les sols se développent à partir de matériaux parentaux dont les caractéristiques sont généralement variables dans l'espace (verticalement et latéralement). Ces matériaux ont aujourd'hui disparu. Leur reconstitution est cependant un pré-requis au calcul des flux d'éléments engendrés par la pédogenèse.

Le premier résultat de mon travail de thèse a été de montrer qu'il est tout à fait possible de reconstituer les matériaux parentaux d'un sol à l'aide d'un ensemble d'éléments géochimiquement invariants, moyennant un certain nombre d'hypothèses. A ce titre, Hf et Zr se sont révélés être les éléments les plus immobiles dans le contexte pédologique étudié, contrairement à Ti dont la mobilité avait déjà été démontrée par certains auteurs dans d'autres contextes pédologiques (Kaup and Carter, 1987 ; Cornu *et al.*, 1999 ; Mathe *et al.*, 1999 ; Chiquet *et al.*, 2000).

Cette reconstitution des matériaux parentaux a été réalisée pour des sols développés à partir d'une succession complexe de bancs calcaires entre lesquels s'intercalent des joints marneux. Une telle démarche est applicable dans d'autres contextes géologiques à condition que des " témoins " des formations géologiques parentales subsistent.

7.3.2. Le couplage de l'expérimentation au laboratoire et des bilans de masse pour quantifier l'action des différents processus pédogénétiques

Cet aspect a été appliqué au cas particulier de la décarbonatation des matériaux parentaux, mais pourrait dans son principe être appliqué à d'autres processus pédogénétiques. Mes résultats mettent clairement en évidence que la signature en terres rares des matériaux parentaux ne présage en rien de celle de leurs résidus de décarbonatation et par conséquent de celle des horizons C formés. Une étude de la spéciation des éléments est donc requise pour comprendre les fractionnements au cours du processus de décarbonatation.

J'ai ensuite montré lors de l'étude du processus de décarbonatation que la comparaison des flux d'éléments calculés par bilan de masse aux quantités mises en solution expérimentalement est nécessaire pour parvenir à comprendre les mécanismes gouvernant le devenir des différents éléments, et notamment des terres rares, lors de la formation d'un sol. Sans cette approche couplée, l'interprétation des résultats surestime les quantités exportées ou sous-estime les quantités mises en solution, comme démontré pour Mn, Yb et Lu.

7.3.3. Le zinc un traceur mitigé des processus de la pédogenèse

L'étude de la mobilité du zinc au cours de la pédogenèse montre que la fraction libérée dans la solution du sol après dissolution des minéraux primaires est majoritairement reprise dans les oxydes de fer et de manganèse qui se forment au cours des processus rédox. Par ailleurs, le zinc est également présent en proportion significative dans les phyllosilicates, qui sont principalement hérités des matériaux parentaux. La pédogenèse n'induit pas de modification sensible des teneurs en zinc dans ces minéraux, mais le processus de lessivage peut les redistribuer de manière significative le long du solum. Ainsi, le zinc se trouvant à la fois dans les oxydes ferro-manganiques (associés aux processus rédox) et les phyllosilicates (associés au processus de lessivage), il semble peu judicieux d'utiliser cet élément pour tenter de déconvoluer l'impact de ces processus au cours de la pédogenèse. Cette conclusion concernant l'utilisation du zinc comme traceur des processus de la pédogenèse est d'autant plus vraie que, dans certains horizons du solum étudié, les oxydes ferro-manganiques et les phyllosilicates sont affectés en même temps par la pédogenèse.

Ce rejet du zinc comme traceur des processus de la pédogenèse n'est cependant pas définitif. En effet, en l'absence de processus rédox, le choix de cet élément pourrait s'avérer particulièrement judicieux pour tracer les processus de lessivage. A l'inverse, en l'absence de lessivage (ou dans les solums affectés par un très faible lessivage), le même élément pourrait parfaitement tracer certains processus d'oxydo-réduction. Des études complémentaires sur des sols mieux adaptés sont nécessaires pour confirmer ou infirmer définitivement les potentialités du zinc comme traceurs de ces deux processus de la pédogenèse que sont le rédox et le lessivage.

7.3.4. Les terres rares, des traceurs prometteurs de la pédogenèse

7.3.4.1. Une nouvelle approche de normalisation des teneurs en terres rares pour tracer les processus pédogénétiques

Les résultats des analyses de terres rares, du fait de leur abondance très contrastée dans les matériaux géologiques, sont exploités après normalisation de leurs teneurs à celles d'un matériau de référence.

Afin de mettre en évidence l'impact d'un processus donné sur la signature en terres rares de l'horizon affecté par ce processus, une méthode de normalisation originale des teneurs en terres rares inspirée de la notion de front de transformation a été testée durant mon travail de thèse. Celle-ci consiste à normaliser les stocks en terres rares des traits pédologiques identifiés aux matériaux aux dépens desquels ils se sont développés.

L'application de cette méthode de normalisation aux processus redox successifs et à l'éluviation s'est avérée fort prometteuse par rapport à d'autres approches plus classiquement utilisées en science du sol, telle que la normalisation par rapport au matériau parental. En effet, cette normalisation au matériau parental ne permet pas de mettre en évidence l'impact des processus successifs sur la signature en terres rares du sol, contrairement à l'approche développée durant mon travail de thèse.

J'ai ainsi pu déterminer les terres rares plus spécifiquement mobilisées au cours des processus pédogénétiques, *i.e.* le cérium lors des conditions redox primaires induisant la formation de nodules ferro-manganiques, les terres rares moyennes lors des conditions redox secondaires responsables de la dissolution des oxydes ferro-manganiques des fractions fines du sol, et les terres rares légères et les terres rares lourdes au cours de l'éluviation. Les hypothèses émises quant à l'origine de ces fractionnements m'ont alors permis d'orienter la suite de mes travaux, en définissant les investigations nécessaires pour confirmer l'utilisation des terres rares comme traceurs potentiels des processus pédogénétiques.

7.3.4.2. L'application au traçage des processus redox

L'application de cette nouvelle démarche méthodologique à l'étude détaillée des processus redox le long d'une catena a démontré le potentiel des terres rares comme traceurs quantitatifs des processus pédologiques. Ceci s'est avéré particulièrement vrai pour le cérium.

En effet, mes résultats suggèrent que l'intensité de l'anomalie positive en cérium dans les nodules ferro-manganiques est liée à la précipitation de cérianite à la surface des oxydes de manganèse. La succession des cycles de dissolution/précipitation des oxydes de manganèse engendrerait ainsi un enrichissement relatif de la cérianite dans les nodules ferro-manganiques. Par conséquent, l'intensité de l'anomalie en cérium permettrait de tracer la dynamique des conditions redox au cours de la pédogenèse.

De plus, cette anomalie en cérium pourrait être liée à la nature des oxydes de manganèse et à leurs proportions respectives. Comme les oxydes de manganèse existent sous de nombreuses formes, généralement peu cristallisées, d'où une identification peu aisée, l'anomalie en cérium s'avère donc fort intéressante.

7.4. Perspectives

L'utilisation de l'anomalie en cérium comme traceur des cycles redox semble prometteuse mais nécessite des investigations plus poussées. Tout d'abord, une vérification de l'hypothèse de la présence de cérianite en lien avec les oxydes de manganèse est nécessaire, ainsi que l'identification de la nature minéralogique des oxydes de manganèse concernés. Par la suite, il faudra envisager si l'anomalie positive en cérium résulte bien d'une dissolution des oxydes de manganèse sans mise en solution de la cérianite, ou si elle est plutôt liée à une variation de la nature minéralogique des oxydes formés. Enfin, des travaux devront être menés pour conclure quant au lien quantitatif entre l'intensité de l'anomalie en cérium et soit le développement des conditions redox passées, soit la nature des oxydes de manganèse formés.

Si le potentiel de l'utilisation des terres rares pour tracer les processus redox a pu être démontré au cours de mon travail de thèse, un autre processus, le lessivage, n'a été que partiellement évoqué. L'approche méthodologique devrait cependant permettre de tracer ce processus au travers de l'identification et du suivi de la signature en terres rares des diverses argiles du sol soumises au lessivage. Ce travail a été entrepris dans le cadre de ma thèse, mais le traitement des données étant toujours en cours, j'ai préféré ne pas faire figurer cette partie dans le présent manuscrit.

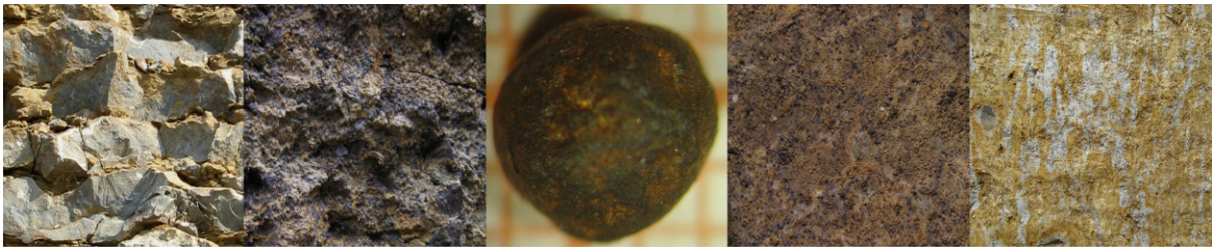
De plus, il conviendra de s'assurer de la robustesse de cette nouvelle approche méthodologique utilisant les terres rares pour retracer les différents processus pédogénétiques de la pédogenèse en la transposant à d'autres systèmes pédologiques pour lesquels ces processus sont, ou ont été, actifs.

Par ailleurs, l'approche de reconstitution des matériaux parentaux développée durant mon travail de thèse repose sur deux hypothèses fortes : (i) l'immobilité au cours de la pédogenèse des éléments considérés comme invariants et (ii) la variation linéaire de leurs concentrations vers la surface au cours de la pédogenèse. Bien que dans mon cas d'étude, la fonction d'évolution des concentrations des éléments invariants soit linéaire, la démarche de reconstitution des matériaux parentaux est applicable dans toutes les situations pédologiques où cette fonction est évaluable. Ces deux hypothèses doivent donc être vérifiées dans d'autres contextes pédologiques.

Si certains transferts latéraux ont été évoqués lors de l'analyse des bilans (cf. [Chapitres 3 et 5](#)), notre approche est restée résolument verticaliste. Pour bien contraindre ces transferts latéraux, une approche bi-, voire tridimensionnelle, serait souhaitable.

Enfin, si la quantification des processus pédogénétiques est un pré-requis à la compréhension de la pédogenèse, elle n'est pas suffisante, car les flux auxquels elle donne accès sont intégrés dans le temps. Or, comme déjà mentionné dans l'introduction du présent manuscrit, la pédogenèse fonctionne selon un régime par seuils ou par événements exceptionnels face aux modifications de l'environnement des sols par rapport à leur pouvoir tampon ([Chadwick et Chorover, 2001](#)). Il apparaît ainsi nécessaire de déterminer la cinétique des processus impliqués dans la pédogenèse, ce qui requiert une datation des différents traits pédologiques. Les avancées récentes dans le domaine de la datation isotopique longue durée – $^{40}\text{Ar}/^{39}\text{Ar}$ pour les oxydes de manganèse ([Vasconcelos, 1999](#)), et (U-Th)/He et U séries pour la goethite ([Pidgeon et al., 2004](#) ; [Bernal et al., 2005](#) ; [Bernal et al., 2006](#) ; [Heim et al., 2006](#)) – laissent envisager leur utilisation potentielle pour la datation des minéraux des sols, domaine jusqu'à présent particulièrement peu développé.

Bibliographie



- Addy, S.K. 1979. Rare earth element patterns in manganese nodules and micronodules from Northwest Atlantic. *Geochimica et Cosmochimica Acta*. **43**(7): 1105-1115.
- Adriano, D.C. 2001. Trace elements in the terrestrial environment: biochemistry, bioavailability, and risks of metals. Springer, New York. 866 pp.
- AFES (Editeur), 1995. Référentiel pédologique. INRA Editions, Paris. 332 pp.
- Aide, M. et Pavich, Z. 2002. Rare earth element mobilization and migration in a Wisconsin Spodosol. *Soil Science*. **167**(10): 680-691.
- Aide, M. et Smith-Aide, C. 2003. Assessing soil genesis by Rare-Earth elemental analysis. *Soil Science Society of America Journal*. **67**(5): 1470-1476.
- Aide, M. 2005. Elemental composition of soil nodules from two Alfisols on an alluvial terrace in Missouri. *Soil Science*. **170**(12): 1022-1033.
- Aide, M.T. et Smith, C.C. 2001. Soil genesis on peralkaline felsics in Big Bend National Park, Texas. *Soil Science*. **166**(3): 209-221.
- Aja, S.U. 1998. The sorption of the rare earth element, Nd, onto kaolinite at 25°C. *Clays and Clay Minerals*. **46**(1): 103-109.
- Allen, B.L. et Hajek, B.F. 1989. Mineral occurrence in soil environments. Dans: J.B. Dixon et S.B. Weed (Editeurs) Minerals in Soil Environments, SSSA Book Series, no. 1, Madison, WI 53711. Soil Science Society of America Inc. (SSSA) USA. pp. 199-278.
- Alloway, B.J. 1990. Heavy metals in soils, New York. 339 pp.
- Angelone, M. et Bini, C. 1992. Trace elements concentrations in soils and plants of Western Europe. Dans: D.C. Adriano (Editeur) Biochemistry of trace elements. Lewis Publisher, Boca Raton, London. pp. 19-60.
- Appel, C., Ma, L.Q., Dean Rhue, R. et Kennelley, E. 2003. Point of zero charge determination in soils and minerals via traditional methods and detection of electroacoustic mobility. *Geoderma*. **113**(1-2): 77-93.
- Arakaki, T. et Mucci, A. 1995. A continuous and mechanistic representation of calcite reaction-controlled kinetics in dilute solutions at 25°C and 1 atm total pressure. *Aquatic Geochemistry*. **1**(1): 105-130.
- Aubert, D., Stille, P. et Probst, A. 2001. REE fractionation during granite weathering and removal by waters and suspended loads: Sr and Nd isotopic evidence. *Geochimica et Cosmochimica Acta*. **65**(3): 387-406.
- Aubert, D., Stille, P., Probst, A., Gauthier-Lafaye, F., Pourcelot, L. et Del Nero, M. 2002. Characterization and migration of atmospheric REE in soils and surface waters. *Geochimica et Cosmochimica Acta*. **66**(19): 3339-3350.
- Aubert, D., Probst, A. et Stille, P. 2004. Distribution and origin of major and trace elements (particularly REE, U and Th) into labile and residual phases in an acid soil profile (Vosges Moutains, France). *Applied Geochemistry*. **19**: 899-916.
- Baize, D. 1980. Essai de bilan isoquartz sur un planosol du Bassin de Paris. Méthode et résultats. *Annales Agronomiques*. **31**(4): 337-362.

- Baize, D. 1993. Carte à 1/200 000 des Petites Régions Naturelles et "paysages pédologiques" de l'Yonne. Notice explicative. Service d'étude de sols et de la carte pédologique de France. INRA. Centre d'Orléans, Orléans. 191 pp.
- Baize, D. et Chrétien, J. 1994. Les couvertures pédologiques de la plateforme sinémurienne en Bourgogne. *Etude et Gestion des Sols*. **2**: 7-27.
- Banfield, J.F. et Eggleton, R.A. 1989. Apatite replacement and Rare-Earth mobilization, fractionation, and fixation during weathering. *Clays And Clay Minerals*. **37**(2): 113-127.
- Bau, M. 1999. Scavenging of dissolved yttrium and rare earths by precipitating iron oxyhydroxide: experimental evidence for Ce oxidation, Y-Ho fractionation, and lanthanide tetrad effect. *Geochimica et Cosmochimica Acta*. **63**(1): 67-77.
- Beall, G.W., Kettle, B.H., Haire, R.G. et Okelley, G.D. 1979. Sorption behavior of trivalent actinides and Rare-Earths on clay-minerals. *Acs Symposium Series* (100): 201-213.
- Beauvais, A. et Colin, F. 1993. Formation and transformation processes of iron duricrust systems in tropical humid environment. *Chemical Geology*. **106**(1-2): 77-101.
- Bellanca, A. et Neri, R. 1993. Dissolution and precipitation of gypsum and carbonate minerals in soils on evaporite deposits, Central Sicily - Isotope geochemistry and microfabric analysis. *Geoderma*. **59**(1-4): 263-277.
- Benes, S. 1989. Presence of rare earths in soils of the Czech Socialist Republic. *Sbornik Vysoke Skoly Zemedelske v Praze, Fakulta Agronomicka, A (Rostlinna Vyroba)*. **No. 50**: 127-142.
- Benitez, L.N. et Dubois, J.P. 1999. Evaluation of the selectivity of sequential extraction procedures applied to the speciation of cadmium in some soils of the Swiss Jura. *International Journal of Environmental Analytical Chemistry*. **74**: 289-303.
- Bentahila, Y., Ben Othman, D. et Luck, J.-M. 2002. Origine du matériel altéré et hétérogénéité du matériel originel de la météorite Foun Tatahouine (Tunisie): éléments traces et isotopes du Sr. *Comptes rendus Geosciences IIa*. **334**(4): 267-272.
- Bernal, J.P., Eggins, S.M. et McCulloch, M.T. 2005. Accurate in situ U-238-U-234-Th-232-Th-230 analysis of silicate glasses and iron oxides by laser-ablation MC-ICP-MS. *Journal of Analytical Atomic Spectrometry*. **20**(11): 1240-1249.
- Bernal, J.P., Eggins, S.M., McCulloch, M.T., Grün, R. et Eggleton, R.A. 2006. Dating of chemical weathering processes by in situ measurement of U-series disequilibria in supergene Fe-oxy/hydroxides using LA-MC-ICPMS. *Chemical Geology*. **235**(1-2): 76.
- Bernat, M. 1975. Les isotopes de l'uranium et du thorium et les terres rares dans l'environnement marin. *Cahier ORSTOM, série Géologie*. **VII**(1): 65-83.
- Bidwell, O.W. et Hole, F.D. 1965. Man as a factor of soil formation. *Soil Science*. **99**(1): 65-72.
- Blaser, P., Zimmermann, S., Luster, J. et Shotyk, W. 2000. Critical examination of trace element enrichments and depletions in soils: As, Cr, Cu, Ni, Pb, and Zn in Swiss forest soils. *The Science of the Total Environment*. **249**(1-3): 257-280.

- Blume, H.P. 1988. The fate of iron during soil formation in humid-temperate environments. *Dans: J.W. Stucki, B.A. Goodman et U. Schwertmann (Editeurs) Iron in soils and clay minerals. NATO ASI Series, C (Mathematical and Physical Sciences) Vol. 217. D. Reidel Publishing Co., Dordrecht Netherlands. pp. 749-777.*
- Bockheim, J.G. et Gennadiyev, A.N. 2000. The role of soil-forming processes in the definition of taxa in Soil Taxonomy and the World Soil Reference Base. *Geoderma. 95(1-2): 53-72.*
- Bonnot-Courtois, C. 1981. Géochimie des terres rares dans les principaux milieux de formation et de sédimentation des argiles. Thèse de l'Université de Paris Sud Orsay, Orsay. 217 pp.
- Bottner, P. 1972. Evolution des sols en milieu carbonaté - La pédogenèse sur roches calcaires dans une séquence bioclimatique méditerranéo-alpine du sud de la France. Thèse de l'Université Louis Pasteur de Strasbourg-Institut de Géologie. 156 pp.
- Bottner, P. et Paquet, H. 1972. La pédogenèse sur roches-mères calcaires tendres dans les étages bioclimatiques montagnard, subalpin et alpin des Préalpes françaises du Sud. *Science du Sol. 1: 63-78.*
- Boulaine, J. 1978. Les sols Calfersiques. *Cahier ORSTOM, série Pédologie. XVI(3): 265-291.*
- Boulaine, J. 1980. Pédologie appliquée. Collection Sciences Agronomiques. Masson, Paris. 220 pp.
- Boulaine, J. 1982. Remarques sur quelques notions élémentaires de la pédologie. 1. Pédon, Profil et Sol. 2. Les Horizons. 3. La variabilité latérale des sols. *Cahier ORSTOM, série Pédologie. XIX(1): 29-41.*
- Boulangé, B. et Colin, F. 1994. Rare earth element mobility during conversion of nepheline syenite into lateritic bauxite at Passa Quatro, Minas Gerais, Brazil. *Applied Geochemistry. 9(6): 701-711.*
- Boulet, R., Humbel, F.-X. et Lucas, Y. 1982. Analyse structurale et cartographie en pédologie. II - Une méthode d'analyse prenant en compte l'organisation tridimensionnelle des couvertures pédologiques. *Cahier ORSTOM, série Pédologie. XIX(4): 323-339.*
- Bouma, J. 1983. Hydrology and soil genesis of soils with aquic moisture regimes. *Dans: L.P. Wilding, Smeck, N.E., et Halls, G.F. (Editeurs) Pedogenesis and Soil Taxonomy: I. Concepts and Interactions. Elsevier, Amsterdam. pp. 253-281.*
- Brady, N.C. et Weil, R.R. 2001. The nature and properties of soils, 13th Edition. Prentice Hall. 960 pp.
- Brantley, S.L., Goldhaber, M.B. et Ragnarsdottir, K.V. 2007. Crossing disciplines and scales to understand the Critical Zone. *ELEMENTS. 3(5): 307-314.*
- Braun, J.-J., Pagel, M., Muller, J.-P., Bilong, P., Michard, A. et Guillet, B. 1990. Cerium anomalies in lateritic profiles. *Geochimica et Cosmochimica Acta. 54(3): 781-795.*

- Braun, J.-J., Pagel, M., Herbillon, A. et Rosin, C. 1993. Mobilization and redistribution of REEs and Thorium in a Syenitic lateritic profile - A mass-balance study. *Geochimica et Cosmochimica Acta*. **57**(18): 4419-4434.
- Braun, J.-J. et Pagel, M. 1994. Geochemical and mineralogical behavior of REE, Th and U in the Akongo lateritic profile (SW Cameroon). *CATENA*. **21**(2-3): 173-177.
- Braun, J.-J., Viers, J., Dupré, B., Polve, M., Ndam, J. et Muller, J.-P. 1998. Solid/liquid REE fractionation in the lateritic system of Goyoum, East Cameroon: The implication for the present dynamics of the soil covers of the Humid Tropical Regions. *Geochimica et Cosmochimica Acta*. **62**(2): 273-299.
- Breton, R. Note présentée par M.P. Rouveroux. 1972. Thirteen years of intensive use of grassland in the Auxois and Morvan areas. *Comptes Rendus des Séances de l'Académie d'Agriculture de France*. **58**(13): 1069-1076.
- BRGM. 1967. Carte Géologique de France, Feuille 498, Pouilly-en-Auxois. BRGM Editions, Orléans.
- BRGM. 1968. Carte Géologique de France, Feuille 467, Quarré-les-Tombes. BRGM Editions, Orléans.
- Bridges, E.M. 1972. World soils. Cambridge University Press, Cambridge. 128 pp.
- Brimhall, G.H. et Dietrich, W.E. 1987. Constitutive mass balance relations between chemical composition, volume, density, porosity, and strain in metasomatic hydrochemical systems: Results on weathering and pedogenesis. *Geochimica et Cosmochimica Acta*. **51**(3): 567-587.
- Brimhall, G.H., Christopher J. Lewis, Ford, C., Bratt, J., Taylor, G. et Warin, O. 1991. Quantitative geochemical approach to pedogenesis: importance of parent material reduction, volumetric expansion, and eolian influx in lateritization. *Geoderma*. **51**(1-4): 51-91.
- Brookins, D.G. 1988. Eh-pH diagrams for geochemistry. Springer-Verlag, Berlin Heidelberg. 176 pp.
- Bruand, A., Cousin, I., Nicoullaud, B., Duval, O. et Begon, J.C. 1996. Backscattered electron scanning images of soil porosity for analyzing soil compaction around roots. *Soil Science Society of America Journal*. **60**(3): 895-901.
- Buatier, M.D., Sobanska, S. et Elsass, F. 2001. TEM-EDX investigation on Zn- and Pb-contaminated soils. *Applied Geochemistry*. **16**(9-10): 1165-1177.
- Buol, S.W., Holfe, F.D. et McCracken, R.J. 1973. Soil genesis and classification. Iowa State University Press, Ames Iowa, USA. 360 pp.
- Burt, R., Wilson, M.A., Keck, T.J., Dougherty, B.D., Strom, D.E. et Lindahl, J.A. 2003. Trace element speciation in selected smelter-contaminated soils in Anaconda and Deer Lodge Valley, Montana, USA. *Advances in Environmental Research*. **8**(1): 51-67.
- Buss, H.L., Sak, P.B., Webb, S.M. et Brantley, S.L. 2008. Weathering of the Rio Blanco quartz diorite, Luquillo Mountains, Puerto Rico: Coupling oxidation, dissolution, and fracturing. *Geochimica et Cosmochimica Acta*. **72**(18): 4488-4507.

- Buurman, P. et Jongmans, A.G. 2005. Podzolisation and soil organic matter dynamics. *Geoderma*. **125**(1-2): 71-83.
- Byrne, R.H. et Li, B. 1995. Comparative complexation behavior of the rare earths. *Geochimica et Cosmochimica Acta*. **59**(22): 4575-4589.
- Byrne, R.H., Liu, X. et Schuf, J. 1996. The influence of phosphate coprecipitation on rare earth distributions in natural waters. *Geochimica et Cosmochimica Acta*. **60**(17): 3341-3346.
- Cambier, P. et Charlatchaka, R. 1999. Influence of reducing conditions on the mobility of divalent trace metals in soils. *Dans: H.M. Selim et I.K. Iskandar (Editeurs) Fate and transport of heavy metals in the vadose zone*. Lewis Publishers, Boca Raton. pp. 159-175.
- Cantrell, K.J. et Byrne, R.H. 1987. Rare earth element complexation by carbonate and oxalate ions. *Geochimica et Cosmochimica Acta*. **51**(3): 597-605.
- Cao, X., Chen, Y., Wang, X. et Deng, X. 2001. Effects of redox potential and pH value on the release of rare earth elements from soil. *Chemosphere*. **44**(4): 655-661.
- Cao, X.D., Chen, Y., Gu, Z.M. et Wang, X.R. 2000a. Determination of trace rare earth elements in plant and soil samples by inductively coupled plasma-mass spectrometry. *International Journal of Environmental Analytical Chemistry*. **76**(4): 295-309.
- Cao, X.D., Wang, X.R. et Zhao, G.W. 2000b. Assessment of the bioavailability of rare earth elements in soils by chemical fractionation and multiple regression analysis. *Chemosphere*. **40**(1): 23-28.
- Caravaca, F., Masciandaro, G. et Ceccanti, B. 2002. Land use in relation to soil chemical and biochemical properties in a semiarid Mediterranean environment. *Soil and Tillage Research*. **68**(1): 23-30.
- Catlett, K.M., Heil, D.M., Lindsay, W.L. et Ebinger, M.H. 2002. Soil chemical properties controlling Zinc²⁺ activity in 18 Colorado soils. *Soil Science Society of America Journal*. **66**(4): 1182-1189.
- Cattle, S.R., Koppi, A.J. et Mc Bratney, A.B. 1994. The effect of cultivation on the properties of a Rhodoxeralf from the wheat/sheep belt of New South Wales. *Geoderma*. **63**(3-4): 215-225.
- Cayeux, L. 1939. Etudes des Gites Minéraux de la France. Les phosphates de chaux sédimentaires de France (France métropolitaine et d'Outre-mer). Ministère des Travaux Publics. Services de la carte géologique de la France et des topographies souterraines, Paris. 970 pp.
- Cerny, P., Ercit, T.S., Smeds, S.A., Groat, L.A. et Chapman, R. 2007. Zirconium and hafnium in minerals of the columbite and wodginite groups from granitic pegmatites. *Canadian Mineralogist*. **45**: 185-202.
- Chabaux, F., Dequincey, O., Leveque, J.-J., Leprun, J.-C., Clauer, N., Riotte, J. et Paquet, H. 2003. Tracing and dating recent chemical transfers in weathering profiles by trace-element geochemistry and ²³⁸U---²³⁴U---²³⁰Th disequilibria: the example of the Kaya

- lateritic toposequence (Burkina-Faso). *Comptes Rendus Geosciences*. **335**(16): 1219-1231.
- Chadwick, O.A., Brimhall, G.H. et Hendricksc, D.M. 1990. From a black to a gray box — a mass balance interpretation of pedogenesis. *Geomorphology*. **3**(3-4): 369-390.
- Chadwick, O.A. et Chorover, J. 2001. The chemistry of pedogenic thresholds. *Geoderma*. **100**(3-4): 321-353.
- Chantigny, M.H. 2003. Dissolved and water-extractable organic matter in soils: a review on the influence of land use and management practices. *Geoderma*. **113**(3-4): 357-380.
- Chao, T.T. 1972. Selective dissolution of manganese oxides from soils and sediments with acidified hydroxylamine hydrochloride. *Soil Science Society of American Proceeding*. **36**: 764-768.
- Chao, T.T. et Theobald, P.K. 1976. The significance of secondary iron and manganese oxides in geochemical exploration. *Economic Geology*. **71**(8): 1560-1569.
- Chao, T.T. et Sanzalone, R.F. 1977. Chemical dissolution of sulfide minerals. *Journal of Research of the U.S. Geological Survey*. **5**: 409-412.
- Chase, J.W., Winchester, J.W. et Coryell, C.D. 1963. Lanthanum, Europium, and Dysprosium distributions in igneous rocks and minerals. *Journal of Geophysical Research (U.S.)*. **68**: 567-575.
- Chen, T., Xu, X., Lu, A., Yue, S., Wang, J. et Peng, S. 2003. Geochemical study of Rare Earth Elements on four Attapulgitic clay deposits in Jiangsu and Anhui Provinces, China. *Journal of Rare Earths*. **21**(4): 478-483.
- Chesworth, W. 1973. The residua system of chemical weathering: a model for the chemical breakdown of silicate rocks at the surface of the earth. *Journal of Soil Science*. **24**(1): 69-81.
- Childs, C.W. et Leslie, D.M. 1977. Interelement relationships in iron-manganese concretions from a catenary sequence of yellow-grey earth soils in loess. *Soil Science*. **123**(6): 369-376.
- Chiquet, A., Colin, F., Hamelin, B., Michard, A. et Nahon, D. 2000. Chemical mass balance of calcrete genesis on the Toledo granite (Spain). *Chemical Geology*. **170**(1-4): 19-35.
- Chowdhury, A.K., McLaren, R.G., Cameron, K.C. et Swift, R.S. 1997. Fractionation of zinc in some New Zealand soils. *Communication in Soil Science and Plant Analysis*. **28**(3-5): 301-312.
- Chrétien, J. 1995. Feuille N-12 de Beaune de la carte pédologique de France à 1/100 000. Notice explicative. INRA, Orléans. 286 pp.
- Christie, T., Brathwaite, B. et Tulloch, A. 1998. Mineral Commodity Report 17 - Rare Earths and Related Elements. *New Zealand Mining*. **24**: 7-19.
- Clair, A. 1987. Cartographie Géologique des Limons de l'Auxois au Sud de Pouilly-en-Auxois (Côte d'Or). Notice explicative. Comportement hydrique des matériaux, Dijon. 72 pp.

- Coelho, M.R. et Vidal-Torrado, P. 2000. Cerium (Ce) in some nodular ferricretes developed in soils of the Adamantina Formation. *Scientia Agricola*. **57**(2): 329-336.
- Collenot, J.J. 1873. Description géologique de l'Auxois. Imprimerie et Librairie Verdot, Semur. 660 pp.
- Collenot, M. 1876-1877. Du phosphate de chaux dans l'Auxois. *Bulletin de la Société Géologique de France*. **Troisième Série** (Tome Cinquième): 671-687.
- Collenot, M. 1878-1879. Description sommaire des terrains sédimentaires de l'Auxois. *Bulletin de la Société Géologique de France*. **Troisième Série** (Tome Septième): 781-804.
- Compton, J.S., White, R.A. et Smith, M. 2003. Rare earth element behavior in soils and salt pan sediments of a semi-arid granitic terrain in the Western Cape, South Africa. *Chemical Geology*. **201**(3-4): 239-255.
- Condie, K.C., Dengate, J. et Cullers, R.L. 1995. Behavior of rare earth elements in a paleoweathering profile on granodiorite in the Front Range, Colorado, USA. *Geochimica et Cosmochimica Acta*. **59**(2): 279-294.
- Contin, M., Mondini, C., Leita, L. et De Nobili, M. 2007. Enhanced soil toxic metal fixation in iron (hydr)oxides by redox cycles. *Geoderma*. **140**: 164-175.
- Coppin, F. 2002. Etude expérimentale de l'adsorption des lanthanides sur une kaolinite et une montmorillonite à 25°C. Thèse de l'Université Toulouse III - Paul Sabatier, Toulouse. 244 pp.
- Coppin, F., Berger, G., Bauer, A., Castet, S. et Loubet, M. 2002. Sorption of lanthanides on smectite and kaolinite. *Chemical Geology*. **182**(1): 57-68.
- Cornell, R.M. et Giovanoli, R. 1987. Effect of manganese on the transformation of ferrihydrite into goethite and jacobsonite in alkaline media. *Clays and Clay Minerals*. **35**(1): 11-20.
- Cornu, S., Lucas, Y., Desjardins, T. et Nitsche, S. 1995. Mise en évidence des vitesses d'altération des minéraux du sol en conditions ferrallitiques. Méthodes des minéraux tests. *Comptes Rendus de l'Académie des Sciences Série II Fascicule A-Sciences de la Terre et des Planètes*. **321**(4): 311-316.
- Cornu, S., Lucas, Y., Lebon, E., Ambrosi, J.P., Luizao, F., Rouiller, J., Bonnay, M. et Neal, C. 1999. Evidence of titanium mobility in soil profiles, Manaus, central Amazonia. *Geoderma*. **91**(3-4): 281-295.
- Cornu, S. et Clozel, B. 2000. Extractions séquentielles et spéciation des éléments traces métalliques dans les sols naturels. *Etude et Gestion des Sols*. **7**(3): 179-189.
- Cornu, S. 2005. Pédogenèses d'hier et d'aujourd'hui. Thèse d'Habilitation à Diriger des Recherches de l'Université d'Orléans, Orléans. 81 pp.
- Cornu, S., Deschatrettes, V., Salvador-Blanes, S., Clozel, B., Hardy, M., Branchut, S. et Le Forestier, L. 2005. Trace element accumulation in Mn-Fe-oxide nodules of a planosolic horizon. *Geoderma*. **125**(1-2): 11-24.

- Cornu, S., Salvador-Blanes, S., Hardy, M., Clozel, B., Crouzet, C., Proix, N. et Guerin, A. 2006. Location of trace elements in unpolluted soils by a combined method. *Communications in Soil Science and Plant Analysis*. **37**(7-8): 1077-1101.
- Cornu, S., Samouëlian, A. et Phillips, J. 2008. Modelling pedogenesis: Purpose and overview of the Special Issue. *Geoderma*. **145**(3-4): 399-400.
- Couchot, J.P., Lhégu, J. et Paquier, J. 1963. Aperçu sur les minéralisations des bordures sédimentaires du Morvan et du Charollais. Rapport 7.1.43, BRGM. 2 pp.
- Courchesne, F., Hallé, J.P. et Turmel, M.C. 2002. Bilans élémentaires holocènes et altération des minéraux dans trois sols forestiers du Québec méridional. *Géographie physique et Quaternaire*. **56**: 5-17.
- Courtois, C. 1974. Les terres rares dans quelques minerais de fer. Entraînement expérimental des lanthanides sur hydroxyde ferrique. Thèse de l'Université de Paris Sud Centre d'Orsay, Paris. 141 pp.
- Courtois, C. et Hoffert, M. 1977. Distribution des terres rares dans les sédiments superficiels du Pacifique sud-est. *Bulletin de la Société Géologique de France*. **7**(XIX n°6): 1245-1251.
- Crock, J.G. et Lichte, F.E. 1982. Determination of Rare-Earth Elements in geological-materials by Inductively Coupled Argon Plasma Atomic Emission-Spectrometry. *Analytical Chemistry*. **54**(8): 1329-1332.
- Cruickshank, J. 1972. Soil geography. David and Charles, Newton Abbot, England. 255 pp.
- Cullers, R.L., Chaudhuri, S., Arnold, B., Lee, M. et Wolf, C.W. 1975. Rare earth distributions in clay minerals and in the clay-sized fraction of the Lower Permian Havensville and Eskridge shales of Kansas and Oklahoma. *Geochimica et Cosmochimica Acta*. **39**(12): 1691-1703.
- D'Amore, D.V., Stewart, S.R. et Huddleston, J.H. 2004. Saturation, reduction, and the formation of iron-manganese concretions in the Jackson-Frazier Wetland, Oregon. *Soil Science Society of America Journal*. **68**(3): 1012-1022.
- Davidson, C.M., Ferreira, P.C.S. et Ure, A.M. 1999. Some sources of variability in application of the three-stage sequential extraction procedure recommended by the BCR to industrially-contaminated soil. *Fresenius Journal of Analytical Chemistry*. **363**(5-6): 446-451.
- Davranche, M., Pourret, O., Gruau, G. et Dia, A. 2004. Impact of humate complexation on the adsorption of REE onto Fe oxyhydroxide. *Journal of Colloid and Interface Science*. **277**(2): 271-279.
- Dawson, B.S.W., Fergusson, J.E., Campbell, A.S. et Cutler, E.J.B. 1985. Distribution of elements in some Fe-Mn nodules and an iron-pan in some gley soils of New Zealand. *Geoderma*. **35**(2): 127-143.
- de Baar, H.J.W., German, C.R., Elderfield, H. et van Gaans, P. 1988. Rare earth element distributions in anoxic waters of the Cariaco Trench. *Geochimica et Cosmochimica Acta*. **52**(5): 1203-1219.

- De Coninck, F., Favrot, J.-C., Tavernier, R. et Jamagne, M. 1976. Dégradation dans les sols lessivés hydromorphes sur matériaux argilo-sableux. Exemple des sols de la nappe détritico Bourbonnaise (France). *Pédologie*. **2**: 105-151.
- de Siena, C., Brimhall, G., Ugolini, F.C., Corti, G. et Ristori, G.G. 1998. Quantitative assessment of REE mobility during weathering of granite under Mediterranean climate. *Dans*: Conference Proceedings of the 16th World Congress of Soil Science. Montpellier.
- Delattre, S., Utsunomiya, S., Ewing, R.C., Boeglin, J.L., Braun, J.J., Balan, E. et Calas, G. 2007. Dissolution of radiation-damaged zircon in lateritic soils. *American Mineralogist*. **92**(11-12): 1978-1989.
- Delmas-Gadras, C. 2000. Influence des conditions physico-chimiques sur la mobilité du plomb et du zinc dans un sol et un sédiment en domaine routier. Thèse de l'Université de Pau et des Pays de l'Adour, Nantes. 191 pp.
- Dequincey, O., Chabaux, F., Clauer, N., Sigmarsson, O., Liewig, N. et Leprun, J.C. 2002. Chemical mobilizations in laterites: evidence from trace elements and ²³⁸U-²³⁴U-²³⁰Th disequilibria. *Geochimica et Cosmochimica Acta*. **66**(7): 1197-1210.
- Dequincey, O., Chabaux, F., Leprun, J.C., Paquet, H., Clauer, N. et Larque, P. 2006. Lanthanide and trace element mobilization in a lateritic toposequence: inferences from the Kaya laterite in Burkina Faso. *European Journal of Soil Science*. **57**(6): 816-830.
- Dère, C., Lamy, I., Jaulin, A. et Cornu, S. 2007. Long-term fate of exogenous metals in a sandy Luvisol subjected to intensive irrigation with raw wastewater. *Environmental Pollution*. **145**(1): 31-40.
- Détournay, J., De Miranda, L., Dérié, R. et Ghodsi, M. 1975. The region of stability of green rust II in the electrochemical E-pH equilibrium diagram of iron in sulphate medium. *Corrosion Science*. **15**: 295-306.
- Dia, A., Gruau, G., Olivié-Lauquet, G., Riou, C., Molénat, J. et Curmi, P. 2000. The distribution of rare earth elements in groundwaters: assessing the role of source-rock composition, redox changes and colloidal particles. *Geochimica et Cosmochimica Acta*. **64**(24): 4131-4151.
- Diatloff, E., Asher, C.J. et Smith, F.W. 1996. Concentrations of rare earth elements in some Australian soils. *Australian Journal of Soil Research*. **34**(5): 735-747.
- Ding, S., Liang, T., Zhang, C., Wang, L. et Sun, Q. 2006. Accumulation and fractionation of rare earth elements in a soil-wheat system. *Pedosphere*. **16**(1): 82-90.
- Ding, Z.L., Sun, J.M., Liu, T.S., Zhu, R.X., Yang, S.L. et Guo, B. 1998. Wind-blown origin of the Pliocene red clay formation in the central Loess Plateau, China. *Earth and Planetary Science Letters*. **161**(1-4): 135-143.
- Drouin, S. 2003. Nature, distribution et origine des éléments en traces présents dans les nodules phosphatés de sols développés sur le Sinémurien (région de Pouilly-en-Auxois, Bourgogne). Rapport du DEA Géosystèmes - Fonctionnements et Ressources, Université d'Orléans 39 pp.

- Dubiel, M., Brunsch, S., Schwieger, W. et Brenn, U. 1997. Valence state of cerium incorporated in aluminium-free layered silicates. *Journal de Physique Iv*. **7(C2)**: 813-814.
- Duchaufour, P. 1957. Sur le rôle de la matière organique dans les phénomènes de lessivage et de podzolisation. *Comptes Rendus Hebdomadaires des Séances de l'Académie Des Sciences*. **245(14)**: 1154-1157.
- Duchaufour, P. 1972. Processus de formation des sols. Biochimie et géochimie. Editions CRDP Nancy, Coll. Etudes et Recherches, Centre Régional de Recherche et de Documentation Pédagogiques de Nancy. 182 pp.
- Duchaufour, P. et Souchier, B. 1977. Pédologie, T.1, pédogenèse et classification, première édition. Masson, Paris. 477 pp.
- Duddy, L.R. 1980. Redistribution and fractionation of rare-earth and other elements in a weathering profile. *Chemical Geology*. **30(4)**: 363-381.
- Egli, M. et Fitze, P. 2000. Formulation of pedologic mass balance based on immobile elements: a revision. *Soil Science*. **165(5)**: 437-443.
- Elderfield, H. et Greaves, M.J. 1981. Negative cerium anomalies in the rare earth element patterns of oceanic ferromanganese nodules. *Earth and Planetary Science Letters*. **55(1)**: 163-170.
- Elderfield, H., Upstill-Goddard, R. et Sholkovitz, E.R. 1990. The rare earth elements in rivers, estuaries, and coastal seas and their significance to the composition of ocean waters. *Geochimica et Cosmochimica Acta*. **54(4)**: 971-991.
- Ercit, T.S. 2002. The mess that is "allanite". *Canadian Mineralogist*. **40**: 1411-1419.
- FAO, 1998. World reference base for soil resources. Rome. 91 pp.
- Faulkner, S.P. et Patrick, W.H., Jr. 1992. Redox Processes and Diagnostic Wetland Soil Indicators in Bottomland Hardwood Forests. *Soil Science Society of America Journal*. **56(3)**: 856-865.
- Feder, F., Trolard, F., Klingelhofer, G. et Bourrié, G. 2005. In situ Mossbauer spectroscopy: Evidence for green rust (fougerite) in a gleysol and its mineralogical transformations with time and depth. *Geochimica et Cosmochimica Acta*. **69**: 4463-4483.
- Fendorf, S. et Fendorf, M. 1996. Sorption mechanism of lanthanum on oxide minerals. *Clays and Clay Minerals*. **44(2)**: 220-227.
- Fiedler, S., Jungkunst, H.P.F., Jahn, R., Kleber, M., Sommer, M. et Stahr, K. 2002. Linking soil classification and soil dynamics - pedological and ecological perspectives. *Journal of Plant Nutrition and Soil Science-Zeitschrift für Pflanzenernahrung und Bodenkunde*. **165(4)**: 517-529.
- Fiedler, S. et Sommer, M. 2004. Water and redox conditions in wetland soils - Their influence on pedogenic oxides and morphology. *Soil Science Society of America Journal*. **68(1)**: 326-335.
- Fitzpatrick, R.W. 1988. Iron compounds as indicators of pedogenic processes: example from southern hemisphere. Chapter 13. *Dans*: J.W. Stucki, B.A. Goodman et U.

- Schwertmann (Editeurs) Iron in soils and clay minerals. NATO ASI Series, serie C, vol 217. pp. 351-396.
- Forest-Bize, N. 2000. Variation de la préservation des dépôts et signification des séries condensées. Les séries liasiques d'une marge en phase de rifting (Alpes) et d'une plate-forme épicontinentale (Bourgogne). Thèse de l'Université de Bourgogne Centre des Sciences de la Terre, Dijon. 366 pp.
- Forest, N. 1995. Sédimentologie, analyse séquentielle et stratigraphie dans les séries lotharingiennes de Bourgogne. Rapport du DEA Paléontologie, Dynamique sédimentaire, Chronologie, Université de Bourgogne - Centre des Sciences de la Terre 51 pp.
- Foth, H.D. 1991. Fundamentals of soils, 8th Edition. J. Wiley & Sons, New-York. 384 pp.
- Freyssinet, P. 1994. Gold mass balance in lateritic profiles from savanna and rain forest zones. *Catena*. **21**(2-3): 159-172.
- Frietsch, R. et Perdahl, J.-A. 1995. Rare earth elements in apatite and magnetite in Kiruna-type iron ores and some other iron ore types. *Ore Geology Reviews*. **9**(6): 489-510.
- Fritsch, E., Bocquier, G., Boulet, R., Dosso, M. et Humbel, F.X. 1986. Les systèmes transformant d'une couverture ferrallitique de Guyane française. Analyse structurale d'une formation supergène et mode de représentation. *Cahier ORSTOM, série Pédologie*. **XXII**(4): 361-395.
- Galán, E., Fernández-Caliani, J.C., Miras, A., Aparicio, P. et Márquez, M.G. 2007. Residence and fractionation of rare earth elements during kaolinization of alkaline peraluminous granites in NW Spain. *Clay Minerals*. **42**(3): 341-352.
- Garcia-Rizo, C., Martinez-Sanchez, J. et Perez-Sirvent, C. 1999. Environmental transfer of zinc in calcareous soils in zones near old mining sites with semi-aridic climate. *Chemosphere*. **39**(2): 209-227.
- Gavaud, M. 1977. Essai sur la classification génétique des sols. *Cahier ORSTOM, série Pédologie*. **15**(1): 63-87.
- Geng, A., Zhang, S. et Hoiland, H. 1998. Complex behaviour of trivalent rare earth elements by humic acids. *Journal of Environmental Sciences*. **10**(3): 302-308.
- Gladney, E.S. et Bower, N.W. 1985. Determination of elemental composition of Nbs-278 and Nbs-688 via Neutron-Activation and X-ray-fluorescence. *Geostandards Newsletter*. **9**(2): 261-262.
- Gnandi, K. et Tobschall, H.J. 2003. Distribution patterns of rare-earth elements and uranium in tertiary sedimentary phosphorites of Hahotoe-Kpogame, Togo. *Journal of African Earth Sciences*. **37**(1/2): 1-10.
- Goldberg, S., Forster, H.S. et Godfrey, C.L. 1996. Molybdenum adsorption on oxides, clay minerals, and soils. *Soil Science Society of America Journal*. **60**(2): 425-432.
- Goldich, S.S. 1938. A study in rock-weathering. *Journal of Geology*. **46**(1): 17-58.
- Goldschmidt, V.M. 1937. The principles of distribution of chemical elements in minerals and rocks. *Journal of the Chemical Society*. **49**: 655 - 673.

- Goldschmidt, V.M. 1958. *Geochemistry*. Oxford University Press, Oxford, England. 730 pp.
- Goldstein, S.J. et Jacobsen, S.B. 1988. Rare earth elements in river waters. *Earth and Planetary Science Letters*. **89**(1): 35-47.
- Grandjean, P., Cappetta, H., Michard, A. et Albare`de, F. 1987. The assessment of REE patterns and $^{143}\text{Nd}/^{144}\text{Nd}$ ratios in fish remains. *Earth and Planetary Science Letters*. **84**(2-3): 181-196.
- Grandjeanlécuyer, P., Feist, R. et Albarede, F. 1993. Rare-Earth Elements in old biogenic apatites. *Geochimica et Cosmochimica Acta*. **57**(11): 2507-2514.
- Gromet, P.L. et Silver, L.T. 1983. Rare earth element distributions among minerals in a granodiorite and their petrogenetic implications. *Geochimica et Cosmochimica Acta*. **47**(5): 925-939.
- Gruau, G., Dia, A., Olivie-Lauquet, G., Davranche, M. et Pinay, G. 2004. Controls on the distribution of rare earth elements in shallow groundwaters. *Water Research*. **38**(16): 3576-3586.
- Grybos, M., Davranche, M., Gruau, G. et Petitjean, P. 2007. Is trace metal release in wetland soils controlled by organic matter mobility or Fe-oxyhydroxides reduction? *Journal of Colloid and Interface Science*. **314**(2): 490-501.
- Guérin, S., Laugier, R. et Mouterde, R. 1961. Le Sinémurien supérieur ou le problème du Lotharingien. Etude détaillée du stratotype: le Lotharingien de Lorraine. Colloque sur le Lias français. Mémoires du Bureau de Recherches Géologiques et Minières n°4. Comptes rendus du congrès des sociétés savantes de Paris et des départements, Chambéry 1960. 307-308 pp.
- Gupta, S.K. et Aten, C. 1993. Comparison and evaluation of extraction media and their suitability in a simple model to predict the biological relevance of heavy metal concentrations in contaminated soils. *International Journal of Environmental Analytical Chemistry*. **51**: 25-46.
- Hall, G.E., Vaive, V.E., Beer, R. et Hoashi, M. 1996. Selective leaches revisited, with emphasis on the amorphous Fe oxyhydroxide phase extraction. *Journal of Geochemical Exploration*. **56**(1): 59-78.
- Han, F.X. et Banin, A. 1995. Selective sequential dissolution techniques for trace metals in arid-zone soils: the carbonate dissolution step. *Communication in Soil Science and Plant Analysis*. **26**(3 & 4): 553-576.
- Han, G. et Liu, C. 2006. Dissolved rare earth elements in river waters draining karst terrains in Guizhou Province, China. *Aquatic Geochemistry*. **13**(1): 95-107.
- Hardy, M., Jamagne, M., Elsass, F., Robert, M. et Chesneau, D. 1999. Mineralogical development of the silt fractions of a Podzolvisol on loess in the Paris Basin (France). *European Journal of Soil Science*. **50**(3): 443-456.
- Hardy, M. et Cornu, S. 2006. Location of natural trace elements in silty soils using particle-size fractionation. *Geoderma*. **133**(3-4): 295-308.
- Hartemink, A.E., Mc Bratney, A.B. et Cattle, J.A. 2001. Developments and trends in soil science: 100 volumes of *Geoderma* (1967-2001). *Geoderma*. **100**(3-4): 217-268.

- Hashimoto, K. et Misawa, T. 1973. The solubility of the γ FeOOH in perchloric acid at 15°C. *Corrosion Science*. **13**: 229-231.
- Haskin, L. et Gehl, M.A. 1962. Rare-Earth distribution in sediments. *Journal of Geophysical Research*. **67**(6): 2537-2541.
- Haskin, L., Wildeman, T. et Haskin, M. 1968. An accurate procedure for the determination of the rare earths by neutron activation. *Journal of Radioanalytical and Nuclear Chemistry*. **1**(4): 337-348.
- Heim, J.A., Vasconcelos, P.M., Shuster, D.L., Farley, K.A. et Broadbent, G. 2006. Dating paleochannel iron ore by (U-Th)/He analysis of supergene goethite, Hamersley province, Australia. *Geology*. **34**: 173-176.
- Henderson, P. (Editeur), 1984. Rare Earth Element Geochemistry. Developments in Geochemistry, 2. Elsevier, Amsterdam. 510 pp.
- Herbillon, A.J. et Nahon, D. 1988. Laterites and lateritization processes. Chapter 22. Dans: J.W. Stucki, B.A. Goodman et U. Schwertmann (Editeurs) Iron in soils and clay minerals. NATO ASI Series, serie C, vol. 217. pp. 779-796.
- Hita, R. et Torrent, J. 2005. Weathering of pyrite and sphalerite in soils contaminated with pyritic sludge. *Soil Science Society of America Journal*. **69**(4): 1314-1319.
- Hoosbeek, M.R. et Bryant, R.B. 1992. Towards the quantitative modeling of pedogenesis - a review. *Geoderma*. **55**(3-4): 183-210.
- Horton, T.W., Becker, J.A., Craw, D., Koons, P.O. et Chamberlain, C.P. 2001. Hydrothermal arsenic enrichment in an active mountain belt: Southern Alps, New Zealand. *Chemical Geology*. **177**(3-4): 323-339.
- Hu, X., Wang, X.-R. et Wang, C. 2006a. Bioaccumulation of lanthanum and its effect on growth of maize seedlings in a Red Loamy Soil. *Pedosphere*. **16**(6): 799-805.
- Hu, Y., Vanhaecke, F., Moens, L., Dams, R., del Castillo, P. et Japenga, J. 1998. Determination of the aqua regia soluble content of rare earth elements in fertilizer, animal fodder phosphate and manure samples using inductively coupled plasma mass spectrometry. *Analytica Chimica Acta*. **373**(1): 95-105.
- Hu, Z., Haneklaus, S., Sparovek, G. et Schnug, E. 2006b. Rare earth elements in soils. *Communications in Soil Science and Plant Analysis*. **37**(9/10): 1381-1420.
- Huang, C. et Gong, Z.T. 2001. Geochemical implication of Rare Earth Elements in process of soil development. *Journal of Rare Earths*. **19**(1): 57-62.
- Huang, C. et Wang, C. 2004. Geochemical characteristics and behaviors of Rare Earth Elements in process of Vertisol development. *Journal of Rare Earths*. **22**(4): 552-557.
- Huggett, R.J. 1975. Soil landscape systems: A model of soil genesis. *Geoderma*. **13**(1): 1-22.
- Hughes, J.M., Cameron, M. et Mariano, A.N. 1991. Rare-earth-element ordering and structural variations in natural rare-earth-bearing apatites. *American Mineralogist*. **76**(7/8): 1165-1173.

- IPCC. 2001. Climate Change 2001: The Scientific Basis. Contribution of Working Group I to the Third Assessment Report of the Intergovernmental Panel on Climate Change. Cambridge University Press, Cambridge. 572 pp.
- Iqdari, A. 1992. La diffusion des terres rares légères et du strontium dans les apatites. Mécanismes de l'enrichissement en terres rares des phosphates naturels. Thèse de l'Université Paris VI, Paris. 187 pp.
- Iqdari, A., Velde, B., Benalioulhaj, N., Dujon, S.-C. et El Yamine, N. 2003. Exchange of light rare earths for Ca in apatite. *Comptes rendus Geosciences Ila*. **335**(4): 381-390.
- Isaure, M.-P., Manceau, A., Geoffroy, N., Laboudigue, A., Tamura, N. et Marcus, M.A. 2005. Zinc mobility and speciation in soil covered by contaminated dredged sediment using micrometer-scale and bulk-averaging X-ray fluorescence, absorption and diffraction techniques. *Geochimica et Cosmochimica Acta*. **69**(5): 1173-1198.
- Ishikawa, M. et Ichikuni, M. 1981. Coprecipitation of phosphate with calcite. *Geochemical Journal*. **15**: 283-288.
- Iwasaki, K., Yoshikawa, G. et Sakurai, K. 1993. Fractionation of zinc in greenhouse soils. *Soil Science and Plant Nutrition*. **39**(3): 507-515.
- Jacquat, O., Voegelin, A. et Kretzschmar, R. 2004. Speciation of Zn in soils in relation to key soil properties. Rapport du Swiss Federal Institute of Technology (ETH) Zurich, Institute of Terrestrial Ecology. 2 pp.
- Jacquat, O., Voegelin, A. et kretzschmar, R. 2005. Elevated concentrations of zinc in soils developed from Jurassic limestones: Changes in zinc speciation during soil formation. *Dans*: Conference Proceedings of the 3rd Swiss Geoscience Meeting. Zürich. 2 pp.
- Jamagne, M. 1978. Les processus pédogénétiques dans une séquence évolutive progressive sur formations limoneuses loessiques en zone tempérée froide et humide. *Comptes Rendus Hebdomadaires des Séances de l'Académie des Sciences*. **286**(1): 25-27.
- Jamagne, M. et Pedro, G. 1981. Les phénomènes de migration et d'accumulation de particules au cours de la pédogenèse sur les formations limoneuses du Nord de la France. Essai de caractérisation du processus de 'lessivage'. *Comptes Rendus de l'Académie des Sciences, Paris. Série D*, **292**: 1329-1332.
- Jeanroy, E., Guillet, B. et Ortiz, R. 1984. Applications pédogénétiques de l'étude des formes du fer par les réactifs d'extraction: cas des sols brunifiés et podzolisés sur roches cristallines. *Science du Sol*. **3**: 199-211.
- Jenne, E.A. (Editeur), 1968. Controls on Mn, Fe, Co, Ni, Cu and Zn concentrations in soils and waters: the significant role of hydrous Mn and Fe oxides. Trace inorganics in water. Adv. Chem. American Chemical Society. 337-387 pp.
- Jenny, H. 1941. Factors of soil formation, New-York. 281 pp.
- Jenny, H. 1994. Factors of soil formation: A system of quantitative pedology. Dover Publications, Inc., New York. 281 pp.
- Jersak, J., Amundson, R. et Brimhall Jr., G. 1995. A mass balance analysis of podzolization: Examples from the northeastern United States. *Geoderma*. **66**(1-2): 15-42.

- Joffe, J.C. 1949. *Pedology*. Pedology Publications, New Brunswick, New Jersey, USA. 662 pp.
- Johannesson, K.H., Stetzenbach, K.J. et Hodge, V.F. 1997. Rare earth elements as geochemical tracers of regional groundwater mixing. *Geochimica et Cosmochimica Acta*. **61**(17): 3605-3618.
- Jonasson, R.G., Bancroft, G.M. et Boatner, L.A. 1988. Surface reactions of synthetic, end-member analogues of monazite, xenotime and rhabdophane, and evolution of natural waters. *Geochimica et Cosmochimica Acta*. **52**(3): 767-770.
- Juillot, F. 1998. Localisation et spéciation de l'arsenic, du plomb et du zinc dans des sites et sols contaminés. Comparaison avec un sol développé sur une anomalie géochimique naturelle en plomb. Géochimie fondamentale et appliquée Thèse de l'Université Paris 7 - Denis Diderot, Paris. 243 pp.
- Juillot, F., Morin, G., Ildefonse, P., Trainor, T.P., Benedetti, M., Galoisy, L., Calas, G. et Brown, G.E. 2003. Occurrence of Zn/Al hydrotalcite in smelter-impacted soils from northern France: Evidence from EXAFS spectroscopy and chemical extractions. *American Mineralogist*. **88**(4): 509-526.
- Juillot, F., Morin, G., Ildefonse, P., Calas, G. et Brown, G.E., Jr. 2006. EXAFS signature of structural Zn at trace levels in natural and synthetic trioctahedral 2:1 phyllosilicates. *American Mineralogist*. **91**(8-9): 1434-1441.
- Kabata-Pendias, A. et Pendias, H. 2001. Trace elements in soils and plants. C.R.C. Press. Boca Raton, FL. 331 pp.
- Kanazawa, Y. et Kamitani, M. 2006. Rare earth minerals and resources in the world. *Journal of Alloys and Compounds*. **408**: 1339-1343.
- Kaup, B.S. et Carter, B.J. 1987. Determining Ti source and distribution within a paleustalf by micromorphology, submicroscopy and elemental analysis. *Geoderma*. **40**(1/2): 141-156.
- Kaur, N., Singh, B., Gräfe, M. et Kennedy, B.J. 2006. Structural incorporation of trace metals in goethite (α-FeOOH) in di-metal systems. *Dans: Conference Proceedings of the 18th World Congress of Soil Science*. Philadelphia, Pennsylvania, USA.
- Kawasaki, A., Kimura, R. et Arai, S. 1998. Rare earth elements and other trace elements in wastewater treatment sludges. *Soil Science and Plant Nutrition*. **44**(3): 433-441.
- Khan, F.A. et Fenton, T.E. 1994. Saturated zones and soil morphology in a Mollisol catena of Central Iowa. *Soil Science Society of America Journal*. **58**: 1457-1464.
- Koeppenkastrop, D. et De Carlo, E.H. 1992. Sorption of rare-earth elements from seawater onto synthetic mineral particles: An experimental approach. *Chemical Geology*. **95**(3-4): 251-263.
- Koeppenkastrop, D. et Decarlo, E.H. 1993. Uptake of Rare-Earth Elements from solution by metal-oxides. *Environmental Science & Technology*. **27**(9): 1796-1802.
- Kölling, M. 1999. Comparison of different methods for redox potential determination in natural waters. *Dans: J. Schüring, H.D. Schulz, W.R. Fisher, J. Bötcher et W.H.M.*

- Duihnisveld (Editeurs) Redox: Fundamentals, processes and applications. Springer-Verlag, New-York. pp. 42-54.
- Koppi, A.J., Edis, R., Field, D.J., Geering, H.R., Klessa, D.A. et Cockayne, D.J.H. 1996. Rare earth element trends and cerium-uranium-manganese associations in weathered rock from Koongarra, Northern Territory, Australia. *Geochimica et Cosmochimica Acta*. **60**(10): 1695-1707.
- Kraimer, R.A., Monger, H.C. et Steiner, R.L. 2005. Mineralogical distinctions of carbonates in desert soils. *Soil Science Society of America Journal*. **69**(6): 1773-1781.
- Kretzschmar, R., Jacquat, O. et Voegelin, A. 2006. Changes in Zinc speciation during soil formation from Jurassic limestone: A synchrotron μ -XRF and μ -XAFS study. *Dans: Conference Proceedings of the 18th World Congress of Soil Science*. Philadelphia, Pennsylvania, USA.
- Kubiena, W.L. 1938. Micropedology, Ames, Iowa. 243 pp.
- Lalonde, C.R. et Dalton, J.L. 1982. The determination of the individual Rare-Earth Elements, Yttrium and Thorium by X-ray-fluorescence analysis using a double dilution technique. *Canadian Journal of Spectroscopy*. **27**(6): 163-170.
- Lamouroux, M. 1972. Etude des sols formés sur roches carbonatées. Pédogenèse fersiallitique au Liban. Thèse de la Faculté des Sciences de l'Université de Strasbourg, Paris. 266 pp.
- Land, M., Öhlander, B., Ingri, J. et Thunberg, J. 1999. Solid speciation and fractionation of rare earth elements in a Spodosol profile from northern Sweden as revealed by sequential extraction. *Chemical Geology*. **160**(1-2): 121-138.
- Langhor, R. 2001. L'anthropisation du paysage pédologique agricole de la Belgique depuis le Néolithique ancien — Apports de l'archéopédologie. *Etude et Gestion des Sols*. **8**(2): 103–118.
- Lanson, B., Drits, V.A., Gaillot, A.-C., Silvester, E., Plançon, A. et Manceau, A. 2002. Structure of heavy-metal sorbed birnessite: Part I. Results from X-ray diffraction. *American Mineralogist*. **87**(11-12): 1631-1645.
- Latimer, W.M. (Editeur), 1938. The oxidation states of the elements and their potentials in aqueous solution, New-York. 265 pp.
- Latrille, C., Elsass, F., van Oort, F. et Denaix, L. 2001. Physical speciation of trace metals in Fe-Mn concretions from a rendzic lithosol developed on Sinemurian limestones (France). *Geoderma*. **100**(1-2): 127-146.
- Laufer, F., Yariv, S. et Steinberg, M. 1984. The adsorption of quadrivalent cerium by kaolinite. *Clay Minerals*. **19**: 137-149.
- Laveuf, C., Cornu, S., Baize, D., Hardy, M., Josière, O., Drouin, S., Bruand, A. et Juillot, F. 2009. Effect of pedogenesis on zinc location in soils developed from limestones. *Pedosphere*. **19**(3): 292-304
- Laveuf, C., Cornu, S. et Juillot, F. 2008. Rare Earth Elements as tracers of pedogenetic processes. *CR Geosciences*. **340**(8): 523-532.

- Laveuf, C. et Cornu, S. Soumis. Potentiality of Rare Earth Elements as Tracers of Pedogenetic Processes: A Review. Soumis à *Geoderma*.
- Laveuf, C., Cornu, S. et Juillot, F. Soumis. Reconstruction of former parent materials and pedological behavior of major elements and Rare Earth Elements with mass balance calculations in a soil developed from a heterogeneous complex sedimentary deposit. Soumis à *Geoderma*.
- Le Calvez, Y. et Lefavrais-Raymond, A. 1961. Lias des sondages de la bordure du Morvan. Dans: E. Technid (Editeur) Colloque sur le Lias français. Mémoires du Bureau de Recherches Géologiques et Minières n°4. Comptes rendus du congrès des sociétés savantes de Paris et des départements, Chambéry 1960. pp. 503-534.
- Lécuyer, C., Reynard, B. et Grandjean, P. 2004. Rare earth element evolution of Phanerozoic seawater recorded in biogenic apatites. *Chemical Geology*. **204**(1-2): 63-102.
- Lécuyer, C., Grandjean, P., Barrat, J.-A., Nolvak, J., Emig, C., Florentin, P. et Robardet, M. 1998. $d^{18}O$ and REE contents of phosphatic brachiopods: A comparison between modern and lower Paleozoic populations. *Geochimica et Cosmochimica Acta*. **62**(14): 2429-2436.
- Lee, J.H. et Byrne, R.H. 1993. Complexation of trivalent Rare-Earth Elements (Ce, Eu, Gd, Tb, Yb) by carbonate ions. *Geochimica et Cosmochimica Acta*. **57**(2): 295-302.
- Lee, Y.J., Reeder, R.J., Wenskus, R.W. et Elzinga, E.J. 2002. Structural relaxation in the $MnCO_3$ - $CaCO_3$ solid solution: a Mn K -edge EXAFS study. *Physics and Chemistry of Minerals*. **29**(9): 585-594.
- Legay, J.-M. 1997. L'expérience et le modèle - Un discours sur la méthode. Sciences En Questions. 112 pp.
- Leleyter, L., Probst, J.-L., Depetris, P., Haida, S., Mortatti, J., Rouault, R. et Samuel, J. 1999. REE distribution pattern in river sediments: partitioning into residual and labile fractions. *Comptes Rendus de l'Académie des Sciences - Séries IIA - Earth and Planetary Science*. **329**(1): 45-52.
- Lévêque, A. 1970. L'origine des concrétions ferrugineuses dans les sols du socle granito-neissique au Togo. *Cahier ORSTOM, série Pédologie*. **VIII**(3): 321-348.
- Li, F.L., Shan, X.Q., Zhang, T.H. et Zhang, S.Z. 1998. Evaluation of plant availability of rare earth elements in soils by chemical fractionation and multiple regression analysis. *Environmental Pollution*. **102**(2-3): 269-277.
- Li, S., Li, R., Yue, S., Liu, Y., Wang, D., Meng, Q. et Jin, F. 2004. Geochemistry of Rare Earth Elements of Mesozoic-Cenozoic sandstones in North margin of Dabie Mountains and adjacent areas: Constraints to Source Rocks. *Journal of Rare Earths*. **22**(4): 558-562.
- Li, X., Han, Z., Yang, D. et Chen, Y. 2006. REE geochemistry of Xiashu Loess in Zhenjiang, Jiangsu Province. *Acta Pedologica Sinica*. **43**(1): 1-7.
- Liang, T., Zhang, S., Wang, L., Kung, H.T., Wang, Y., Hu, A. et Ding, S. 2005. Environmental biogeochemical behaviors of rare earth elements in soil-plant systems. *Environmental Geochemistry and Health*. **27**(4): 301-311.

- Lima, H.N., Schaefer, C.E.R., Mello, J.W.V., Gilkes, R.J. et Ker, J.C. 2002. Pedogenesis and pre-Colombian land use of "Terra Preta Anthrosols" ("Indian black earth") of Western Amazonia. *Geoderma*. **110**(1-2): 1-17.
- Lindsay, W.L. 1991. Iron-oxide solubilization by organic-matter and its effect on iron availability. *Plant and Soil*. **130**(1-2): 27-34.
- Ling, Q. et Liu, C. 2001. Behaviors of Rare Earths during fluid-rock interaction and its significance of geochemistry. *Journal of Rare Earths*. **19**(4): 292-298.
- Ling, Q. et Liu, C. 2002. Review of Rare Earths and fluid-rock interaction. *Journal of Rare Earths*. **20**(6): 570-578.
- Liu, F., Colombo, C., Adamo, P., He, J.Z. et Violante, A. 2002. Trace Elements in manganese-iron nodules from a Chinese Alfisol. *Soil Science Society of America Journal*. **66**(2): 661-670.
- Liu, Z. 1988. Rare earth elements in soil. *Dans*: B.S. Guo, Zhu, W.M., Xiong, B.K., Ji, Y.J., Liu, Z. et Wu, Z.M. (Editeurs) Rare Earth Elements in Agriculture. China Agricultural Science and Technology Press, Beijing. pp. 22-44.
- Lorenz, P.B. 1969. Surface conductance and electrokinetic properties of kaolinite beds. *Clays and Clay Minerals*. **17**(4): 223-231.
- Lucas, Y., Boulet, R. et Chauvel, A. 1988. Intervention simultanée des phénomènes d'enfoncement vertical et de transformation latérale dans la mise en place des systèmes de sols de la zone tropicale humide. Cas des systèmes sols ferrallitiques-podzols de l'Amazonie Brésilienne. *Comptes Rendus de l'Académie des Sciences, série II*. **306**: 1395-1400.
- Lucas, Y., Luizao, F.J., Chauvel, A., Rouiller, J. et Nahon, D. 1993. The relation between biological activity of the rain forest and mineral composition of soils. *Science*. **260**(5107): 521-523.
- Ma, Y.-J., Huo, R.-K. et Liu, C.-Q. 2002. Speciation and fractionation of rare earth elements in a lateritic profile from southern China: Identification of the carriers of Ce anomalies. *Dans*: Conference Proceedings of the 12th Goldschmidt Conference. Davos, Switzerland.
- Manceau, A., Hargé, J.C., Bartoli, C., Silvester, E., Hazemann, J.L., Mench, M. et Baize, D. 1997. Sorption mechanism of zinc and lead on birnessite: Application to their speciation in contaminated soils. *Dans*: Conference Proceedings of the 4th International Conference on the Biogeochemistry of Trace Elements. University of California, Berkeley, California.
- Manceau, A., Lanson, B., Schlegel, M.L., Harge, J.C., Musso, M., Eybert-Berard, L., Hazemann, J.L., Chateigner, D. et Lambelle, G.M. 2000. Quantitative Zn speciation in smelter-contaminated soils by EXAFS spectroscopy. *American Journal of Science*. **300**(4): 289-343.
- Manceau, A., Tamura, N., Marcus, M.A., MacDowell, A.A., Celestre, R.S., Sublett, R.E., Sposito, G. et Padmore, H.A. 2002. Deciphering Ni sequestration in soil

- ferromanganese nodules by combining X-ray fluorescence, absorption, and diffraction at micrometer scale resolution. *American Mineralogist*. **87**: 1494-1499.
- Manceau, A., Tamura, N., Celestre, R. S., MacDowell, A.A., Geoffroy, N., Sposito, G. and Padmore, H.A. 2003. Molecular-Scale Speciation of Zn and Ni in Soil Ferromanganese Nodules from Loess Soils of the Mississippi Basin. *Environmental Science & Technology*. **37**(1): 75-80.
- Manceau, A., Marcus, M.A., Tamura, N., Proux, O., Geoffroy, N. et Lanson, B. 2004. Natural speciation of Zn at the micrometer scale in a clayey soil using X-ray fluorescence, absorption, and diffraction. *Geochimica et Cosmochimica Acta*. **68**(11): 2467-2483.
- Mangin, Gauthier et Lacroix. 1961. Une méthode d'étude sédimentologique appliquée au stratotype du Sinémurien. Intérêt stratigraphique. Limites. Dans: E. Technid (Editeur) Colloque sur le Lias français. Mémoires du Bureau de Recherches Géologiques et Minières n°4. Comptes rendus du congrès des sociétés savantes de Paris et des départements, Chambéry 1960. pp. 297-306.
- Marker, A. et de Oliveira, J.J. 1994. Climatic and morphological control of rare earth element distribution in weathering mantles on alkaline rocks. *CATENA*. **21**(2-3): 179-193.
- Marques, J.J.G.d.S.e.M. 2000. Trace element distributions in Brazilian Cerrado soils at the landscape and micrometer scale. Thèse de la Purdue University. 173 pp.
- Martin, C.E. et McCulloch, M.T. 1999. Nd-Sr isotopic and trace element geochemistry of river sediments and soils in a fertilized catchment, New South Wales, Australia. *Geochimica et Cosmochimica Acta*. **63**(2): 287-305.
- Martin, J.M., Nirel, P. et Thomas, A.J. 1987. Sequential extraction techniques: Promises and problems. *Marine Chemistry*. **22**(2-4): 313-341.
- Mathe, P.-E., Rochette, P., Vandamme, D. et Colin, F. 1999. Volumetric changes in weathered profiles: iso-element mass balance method questioned by magnetic fabric. *Earth and Planetary Science Letters*. **167**(3-4): 255-267.
- Mathieu, C. et Pieltain, F. 1998. Analyse physique des sols: Méthodes choisies, 1. Lavoisier Tech & Doc. 274 pp.
- McBride, M.B. 1994. Environmental chemistry of soils, Oxford. 406 pp.
- McKenzie, R.M. 1975. An electron microprobe study of the relationships between heavy metals and manganese and iron in soils and ocean floor nodules. *Australian Journal of Soil Research*. **13**: 177-188.
- McKenzie, R.M. 1989. Chap 9. Manganese oxides and hydroxides. Dans: J.B. Dixon et S.B. Weed (Editeurs) Minerals in soil environments. SSSA Book Series: 1, Madison, Wisconsin, USA. pp. 439-465.
- McLennan, S.M. et Taylor, S.R. 1979. Rare earth element mobility associated with uranium mineralisation. *Nature*. **282**(5736): 247-250.
- Mégnién, C. 1960. Observations Hydrogéologiques sur le Sud-Est du Bassin de Paris. Les circulations aquifères dans le Jurassique et le Crétacé de l'Yonne. Thèse de la Faculté des Sciences de l'Université de Paris, Paris. 287 pp.

- Miao, L., Xu, R. et Xu, J. 2007. Geochemical characteristics of rare earth elements (REEs) in the soil-plant system in West Guangdong Province. *Acta Pedologica Sinica*. **44**(1): 54-62.
- Michard, A., Beaucaire, C. et Michard, G. 1987. Uranium and rare earth elements in CO₂-rich waters from Vals-les-Bains (France). *Geochimica et Cosmochimica Acta*. **51**(4): 901-909.
- Milnes, A.R. et Fitzpatrick, R.W. 1989. Titanium and zirconium minerals. Dans: J.B. Dixon et S.B. Weed (Editeurs) Minerals in Soil Environments, SSSA Book Series, no. 1, Madison, WI 53711. Soil Science Society of America Inc. (SSSA) USA. pp. 1131-1205.
- Minasny, B., Mc Bratney, A.B. et Salvador-Blanes, S. 2008. Quantitative models for pedogenesis - A review. *Geoderma*. **144**(1-2): 140-157.
- Monecke, T., Kempe, U. et Götze, J. 2002. Genetic significance of the trace element content in metamorphic and hydrothermal quartz: a reconnaissance study. *Earth and Planetary Science Letters*. **202**(3-4): 709-724.
- Montagne, D. 2006. Impact de la mise en culture et du drainage sur l'évolution récente des sols: cas des LUVISOLS DEGRADEES de l'Yonne. Thèse de l'Université d'Orléans. 252 pp.
- Montagne, D., Cornu, S., Bourennane, H., Baize, D., Ratie, C. et King, D. 2007. Effect of agricultural practices on trace-element distribution in soil. *Communications in Soil Science and Plant Analysis*. **38**(3-4): 473-491.
- Montagne, D., Cornu, S., Le Forestier, L., Hardy, M., Josière, O., Caner, L. et Cousin, I. 2008. Impact of drainage on soil-forming mechanisms in a French Albeluvisol: Input of mineralogical data in mass-balance modelling. *Geoderma*. **145**(3-4): 426-438.
- Mosser, C. 1980. Etude géochimique de quelques éléments traces dans les argiles des altérations et des sédiments. Sci. Géol. Mém., 63, Strasbourg. 229 pp.
- Moukadiri, A. et Pin, C. 1998. Géochimie (éléments majeurs et terres rares) des granulites méta-sédimentaires en xénolithes dans les basaltes alcalins quaternaires du Moyen Atlas (Maroc): arguments en faveur de la nature pour partie restitutive de la croûte inférieure. *Comptes rendus Geoscience IIa*. **327**(9): 589-595.
- Mouterde, R. 1946. Une coupe du Lias moyen au Nord d'Avallon. *Compte Rendu Sommaire des Séances de la Société Géologique de France*. **XVI**(5): 325-327.
- Mouterde, R. 1952. Etudes sur le Lias et le Bajocien des bordures nord et nord-est du Massif Central français, n°236. Bulletin du Service de la Carte Géologique de la France. 521 pp.
- Murphy, S.F., Brantley, S.L., Blum, A.E., White, A.F. et Dong, H. 1998. Chemical weathering in a tropical watershed, Luquillo Mountains, Puerto Rico: II. Rate and mechanism of biotite weathering. *Geochimica et Cosmochimica Acta*. **62**(2): 227-243.
- Nagasawa, H. 1971. Partitioning of Eu and Sr between coexisting plagioclase and K-feldspar. *Earth and Planetary Science Letters*. **13**(1): 139-144.

- Navarre-Sitchler, A. et Brantley, S. 2007. Basalt weathering across scales. *Earth and Planetary Science Letters*. **261**(1-2): 321-334.
- Ndjigui, P.D., Mungall, J.E., Bilong, P. et Dia, A. Soumis. Geochemistry of trace elements and REE in two Serpentine weathering profiles in the Lomié Ultrabasic Complex (South-East Cameroon, Central Africa rainforest). Soumis à *Chemical Geology*.
- Ndjigui, P.D., Bilong, P., Bitom, D. et Dia, A. 2008. Mobilization and redistribution of major and trace elements in two weathering profiles developed on serpentinites in the Lomie ultramafic complex, South-East Cameroon. *Journal of African Earth Sciences*. **50**(5): 305-328.
- Neaman, A., Mouélé, F., Trolard, F. et Bourrié, G. 2004. Improved methods for selective dissolution of Mn oxides: applications for studying trace element associations. *Applied Geochemistry*. **19**(6): 973-979.
- Neaman, A., Martínez, C.E., Trolard, F. et Bourrié, G. 2008. Trace element associations with Fe- and Mn-oxides in soil nodules: Comparison of selective dissolution with electron probe microanalysis. *Applied Geochemistry*. **23**: 778-782.
- Négre, P., Casanova, J. et Brulhet, J. 2006. REE and Nd Isotope stratigraphy of a late Jurassic carbonate platform, Eastern Paris Basin, France. *Journal of Sedimentary Research*. **76**(3): 605-617.
- Nelson, D.T., Smith, R.W., Johnson, G.S. et Cosgrove, D.M. 2004. Rare earth elements as natural tracers of groundwater flow in a fractured basalt aquifer: Eastern Snake River Plain aquifer, Idaho, U.S.A. *Dans: Conference Proceedings of the Annual Meeting of the Geological Society of America*. Denver. pp. 562.
- Nesbitt, H.W. 1979. Mobility and fractionation of Rare-Earth Elements during weathering of a granodiorite. *Nature*. **279**(5710): 206-210.
- Nesbitt, H.W. et Markovics, G. 1997. Weathering of granodioritic crust, long-term storage of elements in weathering profiles, and petrogenesis of siliciclastic sediments. *Geochimica et Cosmochimica Acta*. **61**(8): 1653-1670.
- Nguyen Kha et Paquet, H. 1975. Mécanismes d'évolution et de redistribution des minéraux argileux dans les PELOSOLS. *Sciences Géologiques Bulletin*. **28**(1): 15-28.
- Nguyen Kha, Roullier, J. et Souchier, B. 1976. Premiers résultats concernant une étude expérimentale du phénomène de l'appauvrissement dans les PELOSOLS. *Science du Sol*. **4**: 259-267.
- Nickel, E. 1973. Experimental dissolution of light and heavy-minerals in comparison with weathering and intrastratal solution. *Contributions to Sedimentology*. **1**: 1-68.
- Nicolini, P. 1990. Gîtologie et exploitation minière. Techniques et Documentation Lavoisier, Paris. 589 pp.
- Nriagu, J.O. 1991. Human influence on the global cycling of trace metals. *Dans: Conference Proceedings of the 8th International Conference on Heavy Metals in the Environment*. CEP, Edinburgh, UK.

- Oh, N.-H. et Richter, D.D. 2005. Elemental translocation and loss from three highly weathered soil-bedrock profiles in the southeastern United States. *Geoderma*. **126**(1-2): 5-25.
- Öhlander, B., Land, M., Ingri, J. et Widerlund, A. 1996. Mobility of rare earth elements during weathering of till in northern Sweden. *Applied Geochemistry*. **11**: 93-99.
- Ohta, A. et Kawabe, I. 2001. REE(III) adsorption onto Mn dioxide (δ -MnO₂) and Fe oxyhydroxide: Ce(III) oxidation by δ -MnO₂. *Geochimica et Cosmochimica Acta*. **65**(5): 695-703.
- Padmore, H.A. 2003. Molecular-scale speciation of Zn and Ni in soil ferromanganese nodules from loess soils of the Mississippi Basin. *Environmental Science & Technology*. **37**: 75-80.
- Palumbo, B., Bellanca, A., Neri, R. et Roe, M.J. 2001. Trace metal partitioning in Fe-Mn nodules from Sicilian soils, Italy. *Chemical Geology*. **173**(4): 257-269.
- Pan, Y.M., Fleet, M.E. et Barnett, R.L. 1994. Rare-Earth mineralogy and geochemistry of the Mattagami Lake volcanogenic massive sulfide deposit, Quebec. *Canadian Mineralogist*. **32**: 133-147.
- Panahi, A., Young, G.M. et Rainbird, R.H. 2000. Behavior of major and trace elements (including REE) during Paleoproterozoic pedogenesis and diagenetic alteration of an Archean granite near Ville Marie, Quebec, Canada. *Geochimica et Cosmochimica Acta*. **64**(13): 2199-2220.
- Pang, J. 1999. Geochemical behaviour of Rare Earth Elements in Jianchaling ore deposit in Shaanxi Province. *Journal of Rare Earths*. **17**(3): 25-36.
- Papoulis, D., Tsolis-Katagas, P. et Katagas, C. 2004. Monazite alteration mechanisms and depletion measurements in kaolins. *Applied Clay Science*. **24**(3-4): 271-285.
- Parc, S., Nahon, D., Tardy, Y. et Viellard, P. 1989. Estimated solubility products and fields of stability for cryptomelane, nsutite, birnessite, and lithiophorite based on natural lateritic weathering sequences. *American Mineralogist*. **74**: 466-475.
- Parks, G.A. 1965. The isoelectric points of solid oxides, solid hydroxides, and aqueous hydroxo complex systems. *Chemical Review*. **65**(2): 177-198.
- Patrick, W.H. et Jugsujinga, A. 1992. Sequential reduction and oxidation of inorganic nitrogen, manganese and iron in flooded soil. *Soil Science Society of America Journal*. **56**: 1071-1073.
- Pédro, G., Jamagne, M. et Begon, J.-C. 1978. Two routes in genesis of strongly differentiated acid soils under humid, cool-temperate conditions. *Geoderma*. **20**: 173-189.
- Pedro, G. 1987. Géochimie, minéralogie et organisation des sols. Aspects coordonnés des problèmes pédogénétiques. *Cahier ORSTOM, série Pédologie*. **XXIII**(3): 169-186.
- Pelfrène, A. 2008. Spéciation des métaux traces (Cd, Cu, Pb, Zn) dans les eaux d'un Planosol non pollué (Massif Central, France). Thèse de l'Université François Rabelais de Tours. 190 pp.

- Phillips, S.E., Milnes, A.R. et Foster, R.C. 1987. Calcified filaments - an example of biological influences in the formation of calcrete in South Australia. *Australian Journal of Soil Research*. **25**(4): 405-428.
- Philpotts, J.A. 1970. Redox estimation from a calculation of Eu^{2+} and Eu^{3+} concentrations in natural phases. *Earth and Planetary Science Letters*. **9**(3): 257-268.
- Picard, S., Lecuyer, C., Barrat, J.-A., Garcia, J.-P., Dromart, G. et Sheppard, S.M.F. 2002. Rare earth element contents of Jurassic fish and reptile teeth and their potential relation to seawater composition (Anglo-Paris Basin, France and England). *Chemical Geology*. **186**(1-2): 1-16.
- Pidgeon, R.T., Brander, T. et Lippolt, H.J. 2004. Late Miocene (U+Th)- ^4He ages of ferruginous nodules from lateritic duricrust, Darling Range, Western Australia. *Australian Journal of Earth Sciences*. **51**: 901-909.
- Pinto-Coelho, C., Botelho, N.F. et Roger, G. 1999. Mobilité des terres rares au cours des altérations hydrothermales: l'exemple du granite de Serra Branca, Brésil central. *Comptes Rendus Geosciences Ila*. **328**(10): 663-670.
- Piper, D.Z. 1974. Rare earth elements in ferromanganese nodules and other marine phases. *Geochimica et Cosmochimica Acta*. **38**(7): 1007-1022.
- Polyanin, A.D. et Zaitsev, V.F. 2003. Handbook of exact solutions for ordinary differential equations. 2nd edition. Chapman & Hall/CRC Press, Boca Raton. 816 pp.
- Pomel, S. 2008. La mémoire des sols. Lavoisier. 344 pp.
- Ponnamperuma, F.N., Tianco, E.M. et Loy, T. 1967. Redox equilibria in flooded soils: I. The iron hydroxide systems. *Soil Science*. **103**: 374-381.
- Pourret, O., Davranche, M., Gruau, G. et Dia, A. 2007a. Rare earth elements complexation with humic acid. *Chemical Geology*. **243**(1-2): 128-141.
- Pourret, O., Davranche, M., Gruau, G. et Dia, A. 2007b. Competition between humic acid and carbonates for rare earth elements complexation. *Journal of Colloid and Interface Science*. **305**(1): 25-31.
- Price, D.G. 1995. Weathering and weathering processes. *Quarterly Journal of Engineering Geology*. **28**: 243-252.
- Price, J.R., Heitmann, N., Hull, J. et Szymanski, D. 2008. Long-term average mineral weathering rates from watershed geochemical mass balance methods: Using mineral modal abundances to solve more equations in more unknowns. *Chemical Geology*. **254**(1-2): 36-51.
- Quantin, C., Becquer, T., Rouiller, J.H. et Berthelin, J. 2001. Oxide weathering and trace metal release by bacterial reduction in New Caledonia Ferralsol. *Biogeochemistry*. **53**: 323-340.
- Quantin, C., Becquer, T. et Berthelin, J. 2002. Mn-oxide: a major source of easily mobilisable Co and Ni under reducing conditions in New Caledonia Ferralsols. *C.R. Geosciences*. **334**: 273-278.

- Quevauviller, P. 1998. Operationally defined extraction procedures for soil and sediment analysis. I. Standardization. *Trends in Analytical Chemistry*. **17**(5): 289-298.
- Quideau, S.A., Bockheim, J.G., 1996. Vegetation and cropping effects on pedogenetic processes in a sandy prairie soil. *Soil Science Society of America Journal*. **60**: 536-545.
- Rabenhorst, M.C. et Castenson, K.L. 2005. Temperature effects on iron reduction in a hydric soil. **170**: 734-742.
- Ran, Y. et Liu, Z. 1992. Specific adsorption of trivalent La, Ce and Y by soils and ferromanganese oxides and its mechanism. *Pedosphere*. **2**(1): 13-22.
- Ran, Y. et Liu, Z. 1999. Contents and distribution of rare earth elements in main types of soil in China. *Journal of Rare Earths*. **17**(3): 213-217.
- Rankin, P.C. et Childs, C.W. 1976. Rare-earth elements in iron-manganese concretions from some New Zealand soils. *Chemical Geology*. **18**(1): 55-64.
- Rankin, P.C. et Childs, C.W. 1987. Rare earths and other trace elements in iron-manganese concretions from a catenary sequence of yellow-grey earth soils, New Zealand. (Note). *New Zealand Journal of Geology and Geophysics*. **30**(2): 199-202.
- Rasmussen, C. et Tabor, N.J. 2007. Applying a quantitative pedogenic energy model across a range of environmental gradients. *Soil Science Society of America Journal*. **71**(6): 1719-1729.
- Reeder, R.J. et America, M.S.o. (Editeurs). 1983. Carbonates: mineralogy and chemistry. Reviews in mineralogy, v. 11, 11. Mineralogical Society of America, Washington, D.C. 499 pp.
- Reheis, M.C., Sowers, J.M., Taylor, E.M., McFadden, L.D. et Harden, J.W. 1992. Morphology and genesis of carbonate soils on the Kyle Canyon Fan, Nevada, USA. *Geoderma*. **52**(3-4): 303-342.
- Renaud, L. 1961. Minéralisations de la bordure sédimentaire du Nord-Morvan. Rapport 4.2.1.8, BRGM. 15 pp.
- Richard, G., Cousin, I., Sillon, J.F., Bruand, A. et Guérif, J. 2001. Effect of compaction on the porosity of a silty soil: influence on unsaturated hydraulic properties. *European Journal of Soil Science*. **52**(1): 49-58.
- Richter, D.D. et Markewitz, D. 2001. Understanding soil change. Soil sustainability over millennia, centuries and decades, Cambridge, UK. 255 pp.
- Roaldset, E. 1975. Rare earth element distributions in some Precambrian rocks and their phyllosilicates, Numedal, Norway. *Geochimica et Cosmochimica Acta*. **39**(4): 455-469.
- Robert, M. et Tessier, D. 1974. Méthode de préparation des argiles des sols pour des études minéralogiques. *Annales Agronomiques*. **25**(6): 859-882.
- Rode, A.A. 1961. The soil forming process and soil evolution. (traduit du Russe). IPST: Israel Program for Scientific Translations, Jerusalem.

- Ronov, A.B., Balashov, Y.A. et Migdisov, A.A. 1967. Geochemistry of Rare Earths in sedimentary cycle. *Geochemistry International USSR*. **4**(1): 1-17.
- Ruellan, A. 1971. L'histoire des sols: quelques problèmes de définition et d'interprétation. *Cahier ORSTOM, série Pédologie*. **IX**(3): 335-343.
- Ruellan, A. 1983. Morphologie et fonctionnement des sols: quelques réflexions pour l'avenir de la Pédologie. *Cahier ORSTOM, série Pédologie*. **XX**(4): 265-270.
- Runge, E.C.A. 1973. Soil development sequences and energy models. *Soil Science*. **115**(3): 183-193.
- Salomon, J.N. et Pomel, S. 1997. Origin of carbonates in Argentina crusts. *Zeitschrift für Geomorphologie*. **41**(2): 145-166.
- Salomons, W., Förstner, U. et Mader, P. 1995. Heavy metals. Problems and solutions. Springer-Verlag, Berlin. 412 pp.
- Salvador-Blanes, S. 2002. Déterminisme de la distribution spatiale des éléments majeurs et traces dans les sols en contexte métamorphique. Thèse de l'Université de Tours, Tours. 287 pp.
- Samouelian, A. et Cornu, S. 2008. Modelling the formation and evolution of soils, towards an initial synthesis. *Geoderma*. **145**(3-4): 401-409.
- Sauer, D., Sponagel, H., Sommer, M., Giani, L., Jahn, R. et Stahr, K. 2007. Podzol: Soil of the year 2007. A review on its genesis, occurrence, and functions. *Journal of Plant Nutrition and Soil Science*. **170**(5): 581-597.
- Scheinost, A.C., Kretschmar, R. et Pfister, S. 2002. Combining selective sequential extractions, x-ray absorption spectroscopy, and principal component analysis for quantitative zinc speciation in soil. *Environmental Science & Technology*. **36**(23): 5021-5028.
- Schulze, D.G. 1981. Identification of soil iron oxide minerals by differential X-ray diffraction. *Soil Science Society of America Journal*. **45**: 437-440.
- Schüring, J., Schulz, H.D., Fisher, W.R., Böttcher, J. et Duijnsveld, W.H.M. (Editeurs). 1999. Redox: Fundamentals, processes and applications. Springer-Verlag New York, Inc., Berlin Heidelberg New York. 251 pp.
- Schwertmann, U. et Fischer, W.R. 1973. Natural amorphous ferric hydroxide. *Geoderma*. **10**(3): 237-247.
- Schwertmann, U. et Fechter, H. 1982. The point of zero charge of natural and synthetic ferrihydrites and its relation to adsorbed silicate. *Clay Minerals*. **17**: 471-476.
- Schwertmann, U. et Taylor, R.M. 1989. Iron oxides. Chapter 8. Dans: J.B. Dixon et S.B. Weed (Editeurs) Minerals in soil environments. SSSA Book Series: 1, Madison, Wisconsin. pp. 379-438.
- Schwertmann, U. 1991. Solubility and dissolution of iron-oxides. *Plant and Soil*. **130**(1-2): 1-25.

- Scolari, G. 1964. Etude pétrographique du niveau de base de la transgression secondaire sur la bordure NO du Morvan (Département de la Nièvre) - Rapport préliminaire. DS.64.B.26, BRGM - Département Géologie - Service de Sédimentation, Orléans. 8 pp.
- Senesi, G.S., Baldassarre, G., Senesi, N. et Radina, B. 1999. Trace element inputs into soils by anthropogenic activities and implications for human health. *Chemosphere*. **39**(2): 343-377.
- Shankar, N. et Achyuthan, H. 2007. Genesis of calcic and petrocalcic horizons from Coimbatore, Tamil Nadu: Micromorphology and geochemical studies. *Quaternary International*. **175**: 140-154.
- Sholkovitz, E.R. 1992. Chemical evolution of rare earth elements: fractionation between colloidal and solution phases of filtered river water. *Earth and Planetary Science Letters*. **114**(1): 77-84.
- Shotyk, W., Blaser, P., Grünig, A. et Cheburkin, A.K. 2000. A new approach for quantifying cumulative, anthropogenic, atmospheric lead deposition using peat cores from bogs: Pb in eight Swiss peat bog profiles. *The Science of the Total Environment*. **249**(1-3): 281-295.
- Sivakumar, M.V.K. et Stefanski, R. 2007. Climate and land degradation - an overview. Conference Information: International Workshop on Climate and Land Degradation, Dec 11-15, 2006, Arusha, Tanzania. pp. 105-135.
- Sizaret, S. 2002. Genèse du système hydrothermal à fluorine-barytine-fer de Chaillac, (Indre, France). Thèse de l'Université d'Orléans, Orléans. 255 pp.
- Smedley, P.L. 1991. The geochemistry of rare earth elements in groundwater from the Carnmenellis area, southwest England. *Geochimica et Cosmochimica Acta*. **55**(10): 2767-2779.
- Soil Survey Staff et al., 1975. Soil taxonomy. US Department of Agriculture, Agriculture Handbook, N° 436, Washington DC.
- Sommer, M., Kaczorek, D., Kuzyakov, Y. et Breuer, J. 2006. Silicon pools and fluxes in soils and landscapes - a review. *Journal of Plant Nutrition and Soil Science-Zeitschrift für Pflanzenernahrung und Bodenkunde*. **169**(3): 310-329.
- Sonke, J.E. 2006. Lanthanide-humic substances complexation. II. Calibration of humic ion-binding model V. *Environmental Science & Technology*. **40**(24): 7481-7487.
- Spark, K.M., Johnson, B.B. et Wells, J.D. 1995. Characterizing heavy-metal adsorption on oxides and oxyhydroxides. *European Journal of Soil Science*. **46**: 621-631.
- Sposito, G. 1989. The chemistry of soils. Oxford University Press. 304 pp.
- Steinmann, M. et Stille, P. 1997. Rare earth element behavior and Pb, Sr, Nd isotope systematics in a heavy metal contaminated soil. *Applied Geochemistry*. **12**(5): 607-623.
- Steinmann, P. et Shotyk, W. 1997. Geochemistry, mineralogy, and geochemical mass balance on major elements in two peat bog profiles (Jura Mountains, Switzerland). *Chemical Geology*. **138**(1-2): 25-53.

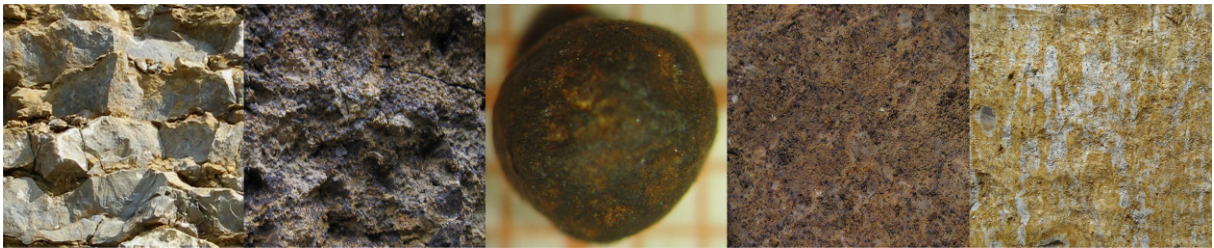
- Stipp, S.L.S., Christensen, J.T., Lakshtanov, L.Z., Baker, J.A. et Waight, T.E. 2006. Rare Earth element (REE) incorporation in natural calcite: Upper limits for actinide uptake in a secondary phase. *Radiochimica Acta*. **94**(9-11): 523-528.
- Stumm, W. et Morgan, J.J. 1981. Aquatic chemistry. 2nd edition. Wiley, New York. 780 pp.
- Tachikawa, K., Jeandel, C. et Roy-Barman, M. 1999. A new approach to the Nd residence time in the ocean: the role of atmospheric inputs. *Earth and Planetary Science Letters*. **170**(4): 433-446.
- Takahashi, Y., Shimizu, H., Usui, A., Kagi, H. et Nomura, M. 2000. Direct observation of tetravalent cerium in ferromanganese nodules and crusts by X-ray-absorption near-edge structure (XANES). *Geochimica et Cosmochimica Acta*. **64**(17): 2929-2935.
- Takahashi, Y., Sakashima, T. et Shimizu, H. 2003. Observation of tetravalent cerium in zircon and its reduction by radiation effect. *Geophysical Research Letters*. **30**(3): art. n° 1137.
- Taunton, A.E., Welch, S.A. et Banfield, J.F. 2000. Geomicrobiological controls on light rare earth element, Y and Ba distributions during granite weathering and soil formation. *Journal of Alloys and Compounds*. **303-304**: 30-36.
- Taylor, R.M. 1968. The association of manganese and cobalt in soils-further observations. *Journal of Soil Science*. **19**: 77-80.
- Taylor, S.R. et McLennan, S.M. 1985. The Continental Crust: Its composition and evolution. Blackwell Scientific Publication, Oxford. 312 pp.
- Tessier, A., Campbell, P.G.C. et Bisson, M. 1979. Sequential extraction procedure for speciation of particulate trace metals. *Analytical Chemistry*. **51**: 844-850.
- Thompson, A., Chadwick, O.A., Rancourt, D.G. et Chorover, J. 2006. Iron-oxide crystallinity increases during soil redox oscillations. *Geochimica et Cosmochimica Acta*. **70**: 1710-1727.
- Topp, S.E., Salbu, B., Roaldset, E. et Jørgensen, P. 1984. Vertical distribution of trace elements in laterite soil (Suriname). *Chemical Geology*. **47**(1-2): 159-174.
- Toutain, F. 1974. Etude écologique de l'humification dans les hêtraies acidiphiles. Thèse de l'Université de Nancy I, Nancy. 114 pp.
- Towell, D.G., Spirn, R.V. et Winchester, J.W. 1969. Europium anomalies and the genesis of basalt: A discussion. *Chemical Geology*. **4**(3-4): 461-464.
- Trolard, F., Soulier, A. et Curmi, P. 1993. The solid iron forms in acid hydromorphic environments - A partitional approach by selective dissolution. *Comptes Rendus de l'Académie des Sciences Série II*. **316**(10): 1463-1468.
- Trolard, F. et Bourrié, G. 1999. L'influence des oxydes de fer de type « rouilles vertes » sur les séquences d'oxydo-réduction dans les sols. *Comptes Rendus de l'Académie des Sciences, Sciences de la Terre et des planètes*. **329**: 801-806.
- Turner, B.F., Stallard, R.F. et Brantley, S.L. 2003. Investigation of in situ weathering of quartz diorite bedrock in the Rio Icacos basin, Luquillo Experimental Forest, Puerto Rico. *Chemical Geology*. **202**(3-4): 313-341.

- Turner, D.R., Whitfield, M. et Dickson, A.G. 1981. The equilibrium speciation of dissolved components in freshwater and sea water at 25°C and 1 atm pressure. *Geochimica et Cosmochimica Acta*. **45**(6): 855-881.
- Tyler, G. 2004a. Vertical distribution of major, minor, and rare elements in a Haplic Podzol. *Geoderma*. **119**(3-4): 277-290.
- Tyler, G. 2004b. Rare earth elements in soil and plant systems - A review. *Plant and Soil*. **267**(1-2): 191-206.
- Uygur, V. et Rimmer, D.L. 2000. Reactions of zinc with iron-oxide coated calcite surfaces at alkaline pH. *European Journal of Soil Science*. **51**(3): 511-516.
- Van Breemen, N. 1988. Effects of seasonal redox processes involving iron on the chemistry of periodically reduced soils. Dans: J.W. Stucki, B. Goodman et U. Schwertmann (Editeurs) Iron in Soils and Clay Minerals. D. Reidel Publishing Company, Dordrecht, The Netherlands. pp. 797-809.
- van der Weijden, C.H. et van der Weijden, R.D. 1995. Mobility of major, minor and some redox-sensitive trace elements and rare-earth elements during weathering of four granitoids in central Portugal. *Chemical Geology*. **125**(3-4): 149-167.
- Vasconcelos, P.M. 1999. K-Ar and $^{40}\text{Ar}/^{39}\text{Ar}$ geochronology of weathering processes. *Annual Review of Earth and Planetary Sciences*. **27**(1): 183-229.
- Vizier, J.-F. 1971. Etude de l'état d'oxydoréduction du sol et de ses conséquences sur la dynamique du fer dans les sols hydromorphes. *Cahier ORSTOM, série Pédologie*. **IX**(4): 373-397.
- Voegelin, A., Jacquat, O. et Kretzschmar, R. 2004. Long-term fate of zinc in soils in relation to soil type. Rapport du Swiss Federal Institute of Technology (ETH) Zurich, Institute of Terrestrial Ecology. 2 pp.
- Voegelin, A., Pfister, S., Scheinost, A.C., Marcus, M.A. et Kretzschmar, R. 2005. Changes in zinc speciation in field soil after contamination with zinc oxide. *Environmental Science & Technology*. **39**(17): 6616-6623.
- Volokh, A.A., Gorbunov, A.V., Gundorina, S.F., Revich, B.A., Frontasyeva, M.V. et Pal, C.S. 1990. Phosphorus-fertilizer production as a source of Rare-Earth Elements pollution of the environment. *Science of the Total Environment*. **95**: 141-148.
- Wahid, P.A., Kamalam, N.V., Prabhu, R.K., Sekhar, J.K., Vijayalakshmi, S., Mahalingam, T.R. et Kumar, C.E.A. 2003. Rare earth element fluxes in diverse soils and their absorption by coconut palm. *Journal of Plant Nutrition*. **26**(7): 1427-1438.
- Walter, A.-V. 1991. Caractérisation géochimique et minéralogique de l'altération de la carbonatite du complexe alcalin de Juquia (Brésil) - Comportement des terres rares dans les minéraux phosphates. Thèse de l'Université de Droit, d'Economie et des Sciences d'Aix-Marseille, Aix-Marseille. 247 pp.
- Wan, Y. et Liu, C. 2005. Study on adsorption of rare earth elements by kaolinite. *Journal of Rare Earths*. **23**(3): 377-381.

- Wang, L., Liang, T., Ding, L., Zhang, C., Li, G., Yan, X. et Wang, X. 2003. Geochemical characteristics of Rare Earth Elements in sewage discharge channels of Tianjin. *Journal of Rare Earths*. **21**(6): 686-690.
- Wang, L., Liang, T., Ding, S., Zhang, C., Zhang, G. et Wang, X. 2004. Biogeochemical cycle and residue of extraneous Rare Earth Elements in agricultural ecosystem. *Journal of Rare Earths*. **22**(5): 701-706.
- Wang, L., Liang, T., Hu, A., Ding, S., Zhang, C. et Yan, X. 2005. Accumulation and fractionation of Rare Earth Elements in soil-rice systems. *Journal of Rare Earths*. **23**(6): 747-752.
- Wang, Q., Huang, B., Guan, Z., Yang, L. et Li, B. 2001. Speciation of rare earth elements in soil by sequential extraction then HPLC coupled with visible and ICP-MS detection. *Fresenius Journal of Analytical Chemistry*. **370**(8): 1041-1047.
- Watson, E.B. et Green, T.H. 1981. Apatite/liquid partition coefficients for the rare earth elements and strontium. *Earth and Planetary Science Letters*. **56**: 405-421.
- Welch, S.A., Taunton, A.E. et Banfield, J.F. 2002. Effect of microorganisms and microbial metabolites on apatite dissolution. *Geomicrobiology Journal*. **19**(3): 343-367.
- Wen, B., Shan, X.-Q., Lin, J.-M., Tang, G.-G., Bai, N.-B. et Yuan, D.-A. 2002. Desorption kinetics of Yttrium, Lanthanum, and Cerium from soils. *Soil Science Society of America Journal*. **66**: 1198-1206.
- West, L.T., Drees, L.R., Wilding, L.P. et Rabenhorst, M.C. 1988. Differentiation of pedogenic and lithogenic carbonate forms in Texas. *Geoderma*. **43**(2-3): 271-287.
- White, A.F. 1995. Chemical weathering rates of silicate minerals in soils. Reviews In Mineralogy. Mineralogical Society of America, Washington. pp. 407-461.
- White, A.F., Blum, A.E., Schulz, M.S., Vivit, D.V., Stonestrom, D.A., Larsen, M., Murphy, S.F. et Eberl, D. 1998. Chemical weathering in a tropical watershed, Luquillo Mountains, Puerto Rico: I. Long-term versus short-term weathering fluxes. *Geochimica et Cosmochimica Acta*. **62**(2): 209-226.
- Wood, S.A. 1990. The aqueous geochemistry of the rare-earth elements and yttrium: 1. Review of available low-temperature data for inorganic complexes and the inorganic REE speciation of natural waters. *Chemical Geology*. **82**: 159-186.
- Wu, Q., Hendershot, W.H., Marshall, W.D. et Ge, Y. 2000. Speciation of cadmium, copper, lead, and zinc in contaminated soils. *Communications in Soil Science and Plant Analysis*. **31**(9-10): 1129-1144.
- Xing, B. et Dudas, M.J. 1993. Trace and rare earth element content of white clay soils of the Three River Plain, Heilongjiang Province, P.R. China. *Geoderma*. **58**(3-4): 181-199.
- Yaalon, D.H. et Yaron, B. 1966. Framework for man-made soil changes: an outline of metapedogenesis. *Soil Science*. **102**(4): 272-277.
- Yaalon, D.H. 1971. Soil forming processes in time and space. Dans: D.H. Yaalon (Editeur) Paleopedology: Origin, nature and dating of paleosols. ISSS and Israel Universities Press, Jerusalem. pp. 29-40.

- Yaalon, D.H. 1983. Climate, time and soil development. *Dans*: L.P. Wilding, N.E. Smeck et G.F. Hall (Editeurs) *Pedogenesis and Soil Taxonomy: I. Concepts and interactions*. Elsevier, New York. pp. 233–251.
- Yamasaki, S.-I., Takeda, A., Nanzyo, M., Taniyama, I. et Nakai, M. 2001. Background levels of trace and ultra-trace elements in soils of Japan. *Soil Science and Plant Nutrition*. **47**(4): 755-765.
- Yan, X.P., Kerrich, R. et Hendry, M.J. 1999. Sequential leachates of multiple grain size fractions from a clay-rich till, Saskatchewan, Canada: implications for controls on the rare earth element geochemistry of porewaters in an aquitard. *Chemical Geology*. **158**(1-2): 53-79.
- Yokoo, Y., Nakano, T., Nishikawa, M. et Quan, H. 2004. Mineralogical variation of Sr-Nd isotopic and elemental compositions in loess and desert sand from the central Loess Plateau in China as a provenance tracer of wet and dry deposition in the northwestern Pacific. *Chemical Geology*. **204**(1-2): 45-62.
- Yuan, F., Zhou, T. et Yue, S. 2003a. Study on mechanism of formation of volcanic rock in North Altay by using Rare Earths. *Journal of Rare Earths*. **21**(3): 387-390.
- Yuan, F., Zhou, T., Yue, S., Zhu, G. et Hou, M. 2003b. Rare Earths of magmatic rocks in Yanshanian Stage in adjacent region of Anhui and Jiangxi Provinces, Jiangnan uplift. *Journal of Rare Earths*. **21**(5): 591-594.
- Zaidel'man, F.R. et Nikiforova, A.S. 1998. Manganese-iron concretions in soils and their change under the effect of gleyification on parent materials of different genesis. *Eurasian Soil Science*. **31**(8): 817-825.
- Zapata, F. et Roy, R.N. (Editeurs). 2004. Use of Phosphate Rocks for Sustainable Agriculture. Fertilizer and Plant Nutrition, Bulletin 13. FAO Land and Water Development Division and the International Atomic Energy Agency, Rome. 172 pp.
- Zhang, F.S., Yamasaki, S. et Kimura, K. 2001. Rare earth element content in various waste ashes and the potential risk to Japanese soils. *Environment International*. **27**(5): 393-398.
- Zhang, J., Ishii, T., Yoshida, S. et Liu, C.Q. 1999. Rare earth element chemistry of rain water. *Dans*: Conference Proceedings of the 5th International Symposium on Geochemistry of the earth's surface, Reykjavik, Iceland, 15-20 August 1999. A.A. Balkema, Rotterdam Netherlands. pp. 347-350.
- Zhang, M. et Karathanasis, A.D. 1997. Characterization of iron-manganese concretions in Kentucky Alfisols with perched water tables. *Clays and Clay Minerals*. **45**(3): 428-439.
- Zhang, S.Z. et Shan, X.Q. 2001. Speciation of rare earth elements in soil and accumulation by wheat with rare earth fertilizer application. *Environmental Pollution*. **112**(3): 395-405.
- Zouita, F. 1986. Etude de la distribution des Terres Rares et des autres éléments en traces dans les roches carbonatées du district minier de Bou-Azzer-Bleïda (Anti-Atlas, Maroc): conséquences génétiques et variations à l'approche des minéralisations. Thèse de l'Université Scientifique et Médicale de Grenoble, Grenoble. 174 pp.

Annexes



Annexe 1

Description pédologique des solums échantillés

Lorsque cela est possible, les horizons sont nommés selon le Référentiel Pédologique 1995 (AFES, 1995).

Pouilly-en-Auxois

Sol complet (description par Chrétien en 1993, complétée par Cornu et Juillot en 2004)

Le solum échantillé dans l'Auxois est situé à Pouilly-en-Auxois (coordonnées Lambert II étendues 769,1 x 251,0, altitude 410 m) dans le Bois Revel, une forêt ancienne (déjà présente sur les cartes de Cassini) dont les essences principales sont le chêne et le charme. Il s'agit d'un sol complet, situé sur le replat du haut de pente et qui présente la succession d'horizons suivante (Figure 1):

- de 0 à 10/15 cm, un horizon limoneux A brun jaunâtre (10YR5/4) avec quelques petits nodules Fe-Mn millimétriques noirs ronds et durs ; horizon non carbonaté, peu compact, de faible cohésion, à structure polyédrique fine à grossière peu exprimée ; porosité structurale et biologique importante ; nombreuses racines ;
- de 10/15 à 45 cm, un horizon limono-argileux E brun jaunâtre (10YR5/6 à 4/4), avec de petits nodules Fe-Mn noirs millimétriques, plus nombreux à la base de l'horizon qu'en haut, durs et ronds ; horizon non carbonaté, faiblement compact, à cohésion faible à moyenne, et à structure polyédrique sub-angulaire fine à moyenne ; porosité moins importante que dans l'horizon LE, prédominance d'une microporosité interpédique ; moins de racines ;
- de 45 à 75/80 cm, un horizon argilo-limoneux Bgd brun-ocre (10YR4/4), irrégulièrement blanchi par glosses verticales et horizontales ondulées, avec des petits nodules Fe-Mn noirs aussi nombreux que dans l'horizon E2 mais plus friables, ronds à ovoïdes, liés entre eux par des revêtements noirs peu indurés qui recouvrent aussi les faces des agrégats, et quelques petits nodules phosphatés ; horizon non carbonaté, fortement compact, à faible cohésion avec des agrégats multi-centimétriques à structure polyédrique fine et angulaire

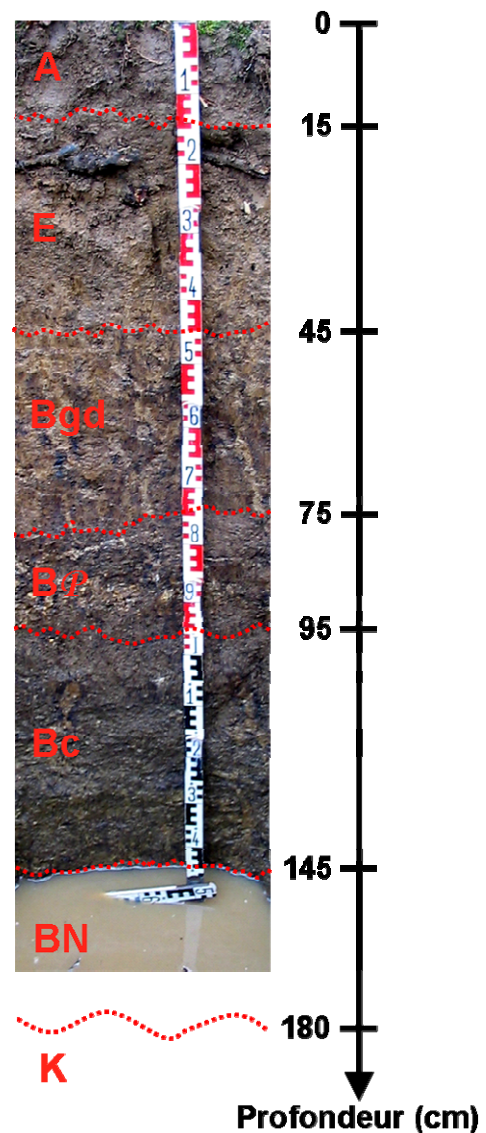


Figure 1. Photographie du profil du sol complet sous forêt de Pouilly-en-Auxois (21) avec ses différents horizons et les profondeurs associées (source Cornu 2004).

- bien exprimée ; faible porosité, principalement de la microporosité interpédique ;
- de 75/80 à 95 cm, un horizon argileux B brun à brun foncé (10YR4,5/3) très compact, avec de nombreux nodules Fe-Mn noirs, ronds et plus gros, et d'abondants nodules phosphatés jaunâtre et tendres de 1 à 2 cm disposés en lits (horizon B \mathcal{P}); matrice non carbonatée ; horizon fortement compact, à structure massive friable à débit polyédrique fine ;
 - de 95 à 145 cm, un horizon argileux B ocre (10YR4,5/4), compact, avec quelques nodules phosphatés et d'abondants nodules Fe-Mn de forme ronde à ovoïde, dur, de 0,5 à 5 m de diamètre et discordants avec la matrice de l'horizon (horizon Bc ou mâchefer) ; horizon non carbonaté, moyennement compact, à faible cohésion et à structure massive friable à débit polyédrique fin à très fin ; porosité moyenne ;
 - de 145 à 170/180 cm, un horizon C, argileux lourd, juxtaposant des volumes brun-jaunâtres (10YR5/6) à des volumes gris foncés (10YR3/1), avec de nombreux amas noirs et de rares nodules Fe-Mn, d'où son appellation d'horizon à bouillie noire BN ; horizon faiblement carbonaté, plastique et collant, moyennement compact, à faible cohérence et à structure polyédrique fine à moyenne ; porosité importante et interpédique ; horizon développé dans une nappe perchée, au contact du calcaire d'âge sinémurien qui ondule entre 170 et 180 cm.

Savigny-en-Terre-Plaine

La toposéquence est située à Savigny-en-Terre-Plaine (coordonnées Lambert II étendues 732,7 x 227,9 à 732,5 x 227,9, altitude de 256,8 à 252,9 m) dans un champ cultivé en blé, non drainé, subissant une fumure tous les deux ans (Figure 2). Ce champ est constitué de deux parcelles, auparavant séparées par une haie avant le remembrement des années soixante-dix où elles étaient alors en prairie et cultivée (Figure 2).

Dans la Terre-Plaine, les trois types de sol de la toposéquence d'érosion, d'une longueur totale de 250 m, ont été échantillonnés (Figures 2 et 3).



Figure 2. Photographies aériennes du terrain d'étude de Savigny-en-Terre-Plaine (89) : en 1968, le terrain est séparé en deux parcelles par une haie, dont une est en prairie et l'autre cultivée ; en 1983, le terrain est constitué d'une seule parcelle sous plusieurs cultures (source Institut National Géographique) ; actuellement l'ensemble de la parcelle est sous une même culture (blé).

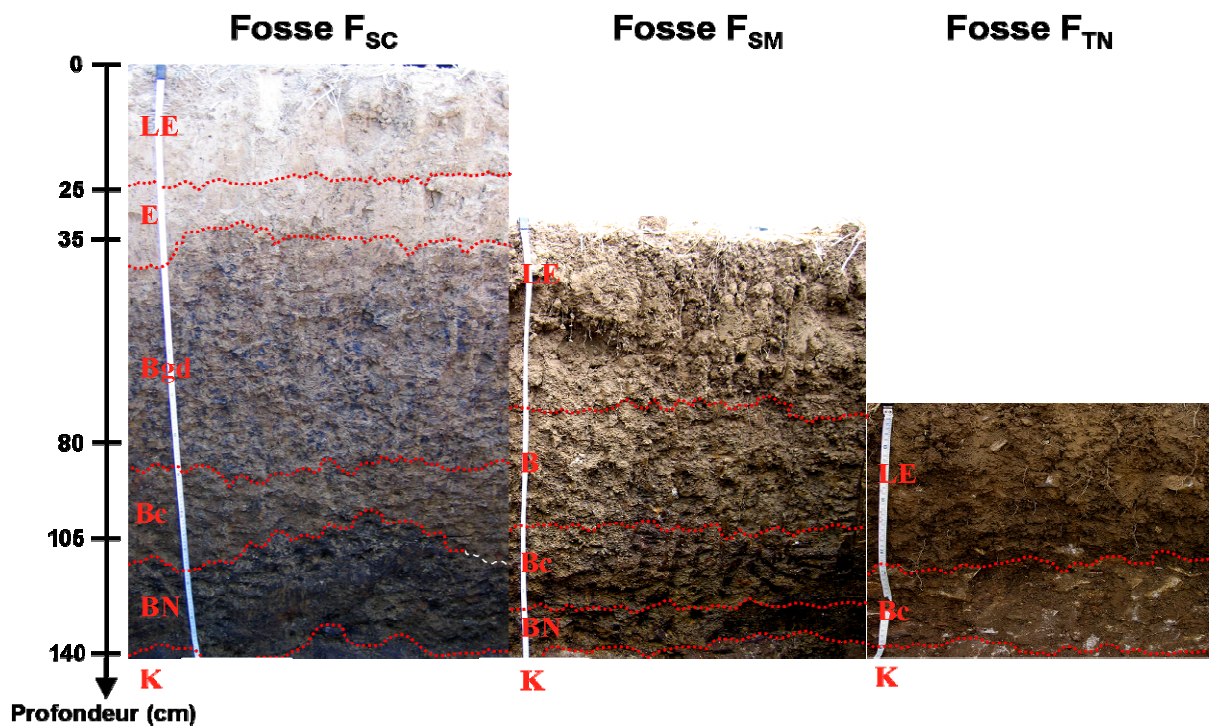


Figure 3. Photographies des trois profils des trois fosses du sol complet (F_{SC}), du sol marron (F_{SM}) et de la Terre Noire (F_{TN}) avec la délimitation de leurs horizons (source Laveuf 2006).

Sol complet (description par Cornu et Laveuf, 2006)

Le profil de la fosse du sol complet F_{SC}, située à 21 mètres en aval du haut de la toposéquence (Figure 2), présente la succession d'horizons suivante (Figure 3) :

- de 0 à 25 cm, un horizon limono-argileux cultivé LE beige (2,5Y7/4), avec quelques petits nodules Fe-Mn noirs, ronds et majoritairement durs ; horizon non carbonaté, à structure grumeleuse, agrégée, avec des agrégats prismatiques pluri-centimétriques, porosité globale abondante ; fentes verticales millimétriques à centimétriques ; activité biologique importante ;
- de 25 à 35 cm, un horizon limono-argileux E beige (2,5Y7/4), avec quelques petits nodules Fe-Mn noirs, ronds et majoritairement durs, millimétriques ; horizon non carbonaté, compact, à structure polyédrique bien marquée ; porosité globale plus faible ;
- de 35 à 80 cm, un horizon argilo-limoneux Bgd brun jaune (10YR5/4) dégradé avec la présence de glosses verticales et horizontales, de nodules Fe-Mn noirs plus nombreux, de taille plus variée, ronds à ovoïdes, plus friables et liés entre eux par des revêtements noirs peu indurés ; horizon non carbonaté, moins compact que le précédent, à structure polyédrique moins marquée avec des agrégats prismatiques pluri-centimétriques ;
- de 80 à 105 cm, un horizon argileux B brun ocre (10YR5,5/8) avec d'abondants nodules Fe-Mn noirs, de forme ronde à ovoïde, durs ou friables, de 0,5 à 5 mm de diamètre, mieux individualisés (horizon Bc ou mâchefer) ; horizon à structure polyédrique moyenne moins marquée ;
- de 105 à 140 cm, un horizon C, juxtaposant des volumes noirs (10YR2/1) à des volumes gris beiges (2,5Y6/2), argileux lourd, plastique, avec des nodules Fe-Mn noirs, durs ou friables, de forme variée, nombreux en haut de l'horizon et absent à sa base, forte humidité ; horizon non carbonaté, sauf au contact du calcaire d'âge sinémurien qui ondule vers 140 cm ; horizon à structure massive à débit polyédrique fin.

Sol marron (description par Cornu et Laveuf, 2006)

Le profil de la fosse du sol marron F_{SM}, située à 175 mètres en aval du haut de la toposéquence (Figure 2), présente la succession d'horizons suivante (Figure 3):

- de 0 à 20/25 cm, un horizon argileux cultivé LE beige (10YR5/4), avec quelques petits nodules Fe-Mn noirs, ronds et durs ; horizon non carbonaté, à structure grumeleuse avec des fentes de retrait verticales pluri-millimétriques ; porosité globale abondante et nombreuses racines ;
- de 20/25 à 40 cm, un ancien horizon LE de même caractéristique que ci-dessus, avec une structure plus compacte, des racines moins nombreuses ;
- de 35/40 à 60 cm, un horizon argileux B brun (2,5Y5/3) avec de nombreux nodules Fe-Mn noirs de diamètre variant entre 0,5 mm à 5 mm, dont certains sont soudés entre eux par des amas noirs friables ; horizon non carbonaté, à structure prismatique à débit polyédrique avec des fentes verticales pluri-millimétriques ; porosité moyenne ;
- de 65 à 85 cm, un horizon argileux B gris-beige (2,5Y6/4) avec d'abondants nodules Fe-Mn, durs, ronds, parfois cimentés entre eux par des amas noirs friables ; horizon non carbonaté, très compact, à structure massive à débit polyédrique ;

- de 85 à 100 cm, un horizon C juxtaposant des volumes noirs (10YR2/1) à des volumes gris-verdâtres (2,5Y6/2), argileux lourd, avec quelques amas noirs ronds et faiblement indurés ; horizon légèrement carbonaté par endroits, compact à structure massive.

Terre Noire (description par Cornu et Laveuf, 2006)

Le profil de la fosse de la Terre Noire F_{TN}, située à 205 mètres en aval du haut de la toposéquence (Figure 2), présente la succession d'horizons suivante (Figure 3):

- de 0 à 25 cm, un horizon argileux cultivé LE brun (10YR4/2), avec de très nombreux nodules Fe-Mn, durs, dont le diamètre varie de 0,5 mm à plus de 5 mm; horizon non carbonaté, peu compact, friable, à structure grumeleuse avec des fentes de retrait pluri-centimétriques ; présence de nombreux cailloux carbonatés pluri-centimétrique et pluri-décimétriques en surface et dans l'horizon ; porosité globale abondante et nombreuses racines ;
- de 25 à 34 cm, un ancien horizon LE de même caractéristique que ci-dessus, avec une structure polyédrique plus compacte ;
- de 30 à 50 cm, un horizon argileux B brun (10YR5/3), avec des nodules Fe-Mn très peu indurés ; horizon non carbonaté, compact à structure massive ; porosité moyenne ; racines moins nombreuses mais présentes.

Annexe 2

Pluviométrie mensuelle dans la Terre-Plaine entre mars 2006 et février 2007

Les données pluviométriques reportées dans le [Tableau 1](#) ont été relevées dans la Terre-Plaine à Saint-André en Terre-Plaine, à 3 km au Sud-Ouest du site de Savigny-en-Terre-Plaine. La période de mars 2006 à février 2007 correspond à celle de nos relevés du niveau de la nappe perchée le long de la toposéquence.

Tableau 1. Relevés pluviométriques mensuels à Saint-André-en-Terre-Plaine (89).

Mois	Pluviométrie (en mm)
Mars 2006	128
Avril 2006	38
Mai 2006	83
Juin 2006	31
Juillet 2006	19
Août 2006	129
Septembre 2006	37
Octobre 2006	149
Novembre 2006	67
Décembre 2006	32
Janvier 2007	51
Février 2007	76
Cumul annuel	840

Le cumul pluviométrique annuel entre mars 2006 et février 2007 est proche de la moyenne pluriannuelle de 880 mm calculée sur la période 1958-1970, de même que la répartition suivant les saisons ([Breton et Rouveroux, 1972](#)).

Annexe 3

Analyse des Terres Rares dans les eaux des fractionnements granulométriques

Lors des fractionnements granulométriques, le tamisage et la sédimentation se font en milieu aqueux (eau osmosée, donc faiblement acide).

Pour évaluer les quantités de Terres Rares mises en solution et leurs possibles fractionnements au cours de l'expérimentation, certaines solutions de séparations granulométriques ont été analysées en Terres Rares par ICP-MS après pré-concentration sur cartouche de résine (BRGM, Service Métrologie, Orléans, France). Les résultats de ces analyses sont reportés dans le [Tableau 1](#).

Tableau 1. Concentrations en Terres Rares (TR) dans deux solutions de séparation granulométrique et estimation du pourcentage du stock de l'échantillon mis en solution.

	Solution 1		Solution 2	
	ng L ⁻¹	% estimé mis en solution	ng L ⁻¹	% estimé mis en solution
La	0,1	7,7 10 ⁻⁶	0,2	1,5 10 ⁻⁵
Ce	0,7	4,2 10 ⁻⁵	4,3	2,6 10 ⁻⁴
Pr	0,2	7,1 10 ⁻⁵	0,4	1,4 10 ⁻⁴
Nd	1,7	1,5 10 ⁻⁴	1,7	1,5 10 ⁻⁴
Sm	1,0	4,6 10 ⁻⁴	0,8	3,7 10 ⁻⁴
Eu	0,2	4,2 10 ⁻⁴	0,2	4,2 10 ⁻⁴
Gd	1,5	7,7 10 ⁻⁴	1,4	7,2 10 ⁻⁴
Tb	0,2	6,9 10 ⁻⁴	0,2	6,9 10 ⁻⁴
Dy	1,2	7,1 10 ⁻⁴	1,1	6,5 10 ⁻⁴
Ho	0,2	5,9 10 ⁻⁴	0,2	5,9 10 ⁻⁴
Er	0,6	6,4 10 ⁻⁴	0,5	5,4 10 ⁻⁴
Tm	0,1	7,4 10 ⁻⁴⁶	0,1	7,4 10 ⁻⁴
Yb	0,5	5,6 10 ⁻⁴	0,3	3,3 10 ⁻⁴
Lu	0,1	7,3 10 ⁻⁴	0,1	7,3 10 ⁻⁴
TR	8,3	4,7 10 ⁻⁴	11,5	4,5 10 ⁻⁴

Les résultats montrent que les quantités mises en solution sont de l'ordre de la dizaine de ng L⁻¹ pour la somme des Terres Rares. Des fractionnements entre les Terres Rares se produisent lors des séparations granulométriques, les Terres Rares lourdes et moyennes étant plus mis en solution ([Figure 1](#)).

Si on considère que pour séparer 100 g d'échantillon brut, il nous faut en moyenne 5L d'eau osmosée, on peut estimer grossièrement les pourcentages du stock de Terres Rares dans l'échantillon mis en solution. Ces pourcentages sont extrêmement faibles, de l'ordre de 10⁻⁶ à 10⁻⁴% ([Tableau 1](#)), soit des quantités mises en solution au minimum de quatre ordres de grandeur inférieures aux quantités dans la phase solide.

Finalement, les pourcentages mis en solution n'influent pas significativement sur les quantités de Terres Rares et leurs fractionnements dans les échantillons solides de sol.

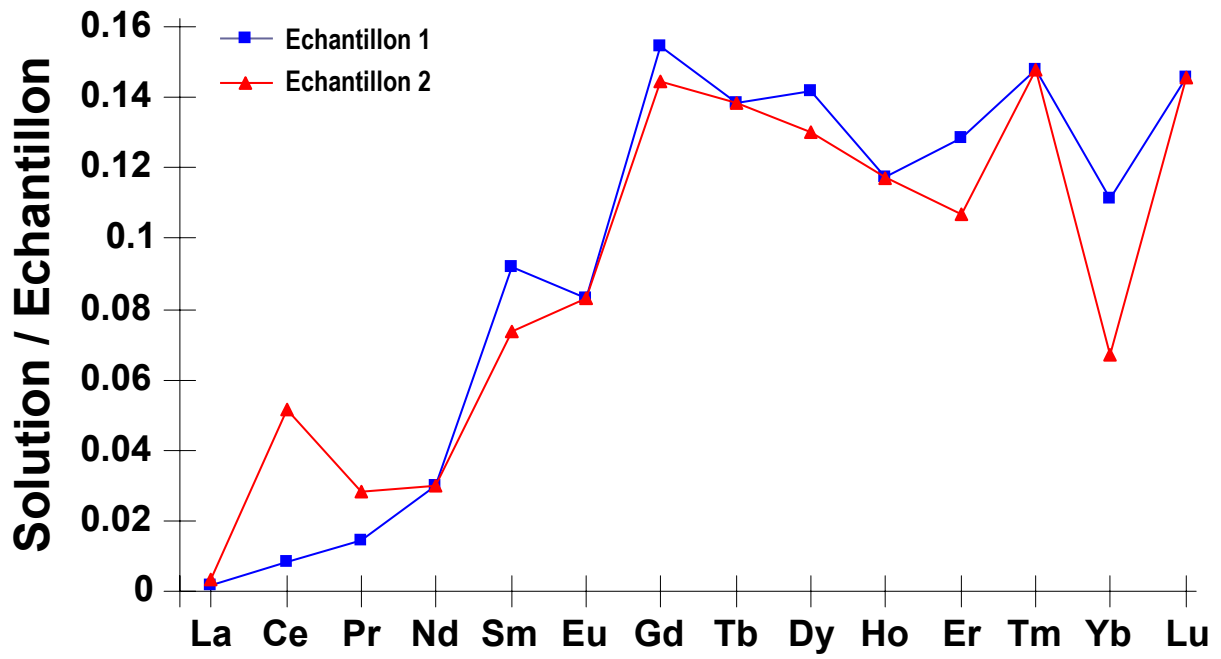


Figure 1. Spectres des concentrations en Terres Rares de deux solutions de séparations granulométriques normalisées aux concentrations en Terres Rares des deux échantillons bruts de sol correspondants.

Annexe 4

Article intitulé

Impact of redox cycles on manganese, iron, cobalt and lead in nodules

accepté pour publication dans Soil Science Society of America Journal

S. Cornu^{a§}, J.A. Cattle^{a,b}, A. Samouëlian^a, C. Laveuf^a, L.R.G. Guilherme^{a,c,d}, P. Albéric^e

- a- INRA, UR0272 Science du sol, F-45166 Olivet
- b- Ecotoxicology and Environmental Contaminants Section, Dept of Environment and Climate Change, NSW. PO Box A290, Sydney South, NSW 1232, Australia
- c- le STUDIUM Institute for Advanced Studies, 3D avenue de la Recherche scientifique, 45071 Orléans CEDEX 2, France
- d- Federal University of Lavras, Soil Science Dept., CP 3037, 37200-000 Lavras (MG), Brazil; CNPq (Brazilian Ministry of Science and Technology) Scholar
- e- ISTO UMR 6113 - CNRS/Université d'Orléans, 1A, rue de la Férollerie, 45071 Orléans CEDEX 2, France

Acknowledgments

The authors would particularly like to thank O. Josière, B. Renaux, P. Courtemanche, A. Besnault and C. Le Lay for technical support. This study was funded by the Conseil Régional of Région Centre through the METALOE project and benefited from a STUDIUM fellowship. J.Cattle is grateful to INRA, Orléans, for providing funding for this project.

Abstract

Redox processes are responsible for iron and manganese segregation as Fe-Mn oxide coatings or nodules. These nodules are also trace element scavengers in soils. Redox processes are of particular importance in seasonally saturated soil containing naturally high concentrations of trace metals. Here we report the dynamics of Fe-Mn nodules and two associated trace elements, Co and Pb, studied under controlled redox conditions in a column experiment, including 5 columns fed with mimicked topsoil solution. The obtained water was rich in Fe and Mn. This water was then percolating the nodule columns. The results show that the redox conditions reached 100 mV, which was sufficient to dissolve Mn oxides and release the associated Co, while Pb was reabsorbed onto nodule surfaces. The amounts of Mn and Co released into the water were small compared to the quantities stored in the nodules (less than 1‰ of the initial stock stored in the nodules). The redox conditions were however insufficient to allow Fe oxide dissolution. On the contrary, 70 of 90% of the Fe entering the column was fixed onto the nodules. The number of drying cycles was too small to draw a firm conclusion on their impact on the nodule fate and metal release. However, in terms of environmental threat, these results showed that Pb would not be released from soil during nodule dissolution, whereas Co, which is less toxic, would be released.

§ **Corresponding author:** Sophie Cornu

Sophie.Cornu@aix.inra.fr

INRA, UR1119 Géochimie des Sols et des Eaux, Europôle de l'Arbois, BP 80, F-13545 Aix en Provence cedex 4.

Introduction

Nodules of Mn and Fe oxides are commonly found in different soil types where they have been extensively studied (Childs and Leslie, 1977; Dawson *et al.*, 1985; Latrille *et al.*, 2001; Palumbo *et al.*, 2001; Liu *et al.*, 2002). They are generally made of both Mn and Fe oxide cements, both elements having a different spatial distribution within nodules (Dawson *et al.*, 1985; Palumbo *et al.*, 2001; Liu *et al.*, 2002), surrounding detrital grains of varying nature according to the soil context (Latrille *et al.*, 2001; Palumbo *et al.*, 2001; Liu *et al.*, 2002; Cornu *et al.*, 2005).

Iron oxides of nodules consist in goethite (Fitzpatrick, 1988) and either hematite (Herbillon and Nahon, 1988) or ferrihydrite (Cornu *et al.*, 2005) according to the soil type. Hematite is mostly found in nodules formed in tropical soils while ferrihydrite is found in those formed under temperate conditions. Manganese oxides in nodules consist mainly of birnessite and lithiophorite (Taylor, 1968; Manceau *et al.*, 2002, 2003; Neaman *et al.*, 2004).

Nodules are well-known for their high content in trace elements. Cobalt, Ni, and Zn are frequently associated with the Mn-rich parts of nodules (Childs and Leslie, 1977; Dawson *et al.*, 1985; Latrille *et al.*, 2001; Liu *et al.*, 2002; Manceau *et al.*, 2002; Neaman *et al.*, 2004, 2008), while Cr (Liu *et al.*, 2002) and Pb (Latrille *et al.*, 2001; Palumbo *et al.*, 2001; Neaman *et al.*, 2004, 2008) are associated with Fe-rich parts. McKenzie (1975), Childs and Leslie (1977), Dawson *et al.* (1985), Latrille *et al.* (2001), Palumbo *et al.* (2001) and Liu *et al.* (2002) showed that Cu and Mn partitioning between Fe and Mn oxides in nodules is variable. In some soils, nodules can even be the main trace element scavenger (Cornu *et al.*, 2005).

These nodules are formed in horizons undergoing past or present seasonal waterlogging (McKenzie, 1989 and references herein; Khan and Fenton, 1994; Zhang and Karathanasis, 1997). In environments still undergoing seasonal waterlogging, nodules are sensitive to variation in pH and Eh, and can be both source and sink of trace elements according to the intensity, and possibly also the duration, of the reduction phase (Jenne, 1968; Zaidel'man and Nikiforova, 1998; Cambier and Charlatchaka, 1999). This process is of prime importance in wetlands undergoing seasonal waterlogging periods that can last for several months (D'Amore *et al.*, 2004). Grybos *et al.* (2007) demonstrated that the fate of Fe-Mn oxides in wetlands was entirely responsible for the fate of Co and partially for that of Pb and Ni, while the impact of redox conditions on Cu and Cr was less clear.

Climate change has affected the duration of the annual waterlogging period, such that it is either reduced or increased according to the latitude (IPCC, 2001). An understanding of the dynamics and the fate of Fe and Mn in nodules, as well as their associated trace elements is of importance in predicting their environmental impact in ecosystems such as wetlands.

Several studies report the impact of redox cycles on the fate of Fe oxides (Thompson *et al.*, 2006), and Fe and Mn oxides and their associated trace elements (Quantin *et al.*, 2001, 2002; Feder *et al.*, 2005; Contin *et al.*, 2007; Grybos *et al.*, 2007). However, these oxides were dispersed into the soil matrix and, to our knowledge, no attempt was made to understand the sorption and release of trace elements from soil nodules that are the main trace element scavengers in soils (Cornu *et al.*, 2005) and have different accessibility to soil solution than the dispersed oxides.

We aim here to investigate the effect of redox cycles on the mobility of Fe and Mn in soil nodules and of the associated Co and Pb coming from temperate climate. For that an

original experimental design using nodule column experiments was designed in order to mimic natural conditions of redox cycles that occur in subsurface soil horizons.

Material and Methods

Site and soil

The study site, located on the Aigurande plateau in the Massif Central, is underlain by amphibolite and gneiss. On the footslope, Planosols (FAO, 1998) – or Albaqualfs (Soil Taxonomy, 1975) – developed on gneiss (Salvador-Blanes, 2002). The upper horizons of the Planosols are allochthonous and derived from silty, colluvial materials of amphibolitic and gneissic origin, while the deeper clayey B horizon (below 50 cm depth) and the alterite are developed in gneiss. Colluvial materials differentiate into three horizons: a sandy-loam to clay-loam organic-rich A horizon (25 to 30 cm thick) and two E horizons, one of them being rich in Fe/Mn-nodules and gravels (Cornu *et al.*, 2005). The nodule-rich horizon is a sink for Fe, Mn, Co and Pb (Table 1; Cornu *et al.*, 2005). Cornu *et al.* (2005) showed that Mn oxides preferentially scavenge Co and Pb. The E horizons are waterlogged during winter and spring due to the texture contrast with the underlying B horizon. The duration of the waterlogging period increases down the slope. This horizon is draining most of the water of a 6-ha plot.

Soil water quality was monitored on this site by Pelfrêne (2008). From the data they provided (Pelfrêne, 2008 and references herein), we estimated that the average effective rainfall for the region ranges from 200 to 300 mm.

The nodule rich E horizon and the associated top horizon were sampled from a midslope position equivalent to that of pit 2 in Cornu *et al.* (2005).

Table 1: Characteristics of the solids used in the experiment[†]

Sample name	solid density g cm ⁻³	BET Surface m ² g ⁻¹	Fe g (100g) ⁻¹	Mn g (100g) ⁻¹	Co mg kg ⁻¹	Pb mg kg ⁻¹
Surface horizon	2.43	nd	3	0.09	13	30
3-4 mm nodules	2.86 ± 0.00	66 ± 4	22 ± 1	1.45 ± 0.18	144 ± 15	59 ± 2
4-5 mm nodules	2.80 ± 0.03	60 ± 4	18 ± 1	2.02 ± 0.15	175 ± 34	48 ± 4
Quartz sand	2.56	0.57 ± 0.09	<DL	<DL	0.54	19.41

[†] When available, arithmetic mean values ± standard deviations were provided; nd = no data; DL = detection limit

Column preparation and characterisation

Nodules were sorted from the rest of the soil and carefully cleaned. They were then separated from the bulk soil matrix by wet sieving. For practical reasons, only the 2-5 mm fraction was collected and oven dried at 40°C. Nodules were manually sorted with tweezers until ~500 mL of nodules were obtained. To remove nodule clay coatings, nodules were then placed into 250-mL screw cap bottles containing ultrapure water (nodules:water 1:1 v/v). The bottles were placed on an end-over-end shaker and rotated at 100 rpm for eight hours. Water was changed after ~ four hours by tipping nodules onto a 1-mm sieve, followed by discarding and rinsing excess clay suspension through the sieve with ultrapure water. Nodules were then washed (as above) on the sieve and left covered in a tray overnight. This process was repeated for seven days. Nodules were then sieved into 3-4 mm and 4-5 mm fractions (nodules <3mm

comprised only 1.5% of the total and were not used). Each column contained equivalent amounts of each fraction. To keep the natural soil nodule particle-size distribution, 34.2 g of 3-4 mm nodules and 43.5 g of 4-5 mm nodules were weighed into each column (Table 2). We thus ensured that all the columns had the same characteristics in terms of chemistry, pore volume and surface area. A subset of nodules not used in the column experiment was kept aside for determination of BET (Brunauer, Emmett and Teller) surface area measurement, total elemental analysis by ICP-AES after triacid HF dissolution, and solid density with a pycnometer (Table 1).

Table 2: Main characteristics of the different columns

Treatment	Columns	3-4mm nodule mass g	4-5mm nodule mass g	Quartz mass g	Solid density g cm ⁻³	Pore volume of the column cm ³	Fe g/column	Mn mg/column	Co	Pb
Saturated	Quartz			96.89	2.56	24	0	0	0.05	1.9
	Nodules 1	34.27	43.53		2.83	34	15	1.4	12	4.1
	Nodules 2	34.2	43.48		2.83	34	15	1.4	12	4.1
14-day cycles	Quartz			97.145	2.56	24	0	0	0.05	1.9
	Nodule	34.24	43.51		2.83	34	15	1.4	12	4.1

Quartz sand (purchased commercially) was used as a control. It was sieved to be in the size fraction 0.4-1 mm. This size fraction was used to favour the formation of nodules around sand particles (this sand also contained small amounts of micas and feldspars as shown by X-ray diffraction; results not shown). Quartz sand was packed into the column on a volume basis matching that of the nodule columns, *i.e.* ~98 g (Table 2). A sub-sample was kept for characterisations as described for the nodules (Table 1).

Experimental setting

The experimental design is shown schematically in Figure 1. This consists in two main parts: part A designed to produce a water whose quality mimicked that of a natural one and part B that consists in the column experiment itself.

The percolating water was produced by passing ultrapure water through a topsoil monolith. A topsoil monolith of 20x13x16 cm in size was sampled from the surface A horizon directly above the sampled nodule-rich E horizon. This monolith was removed from the ground in a plastic box. The plastic box had four inlets in the surface, one outlet at the top of one side (used as a drain when necessary) and two outlets at the base on the opposite side. One of these outlets was used as the source of water to pass through the columns and the other worked as a port for sampling the inflowing column water for separate measurements. The so-produced inflow water was sampled and analysed for each sampling date (see below).

At the start of the experiment the surface horizon monolith had a moisture content of 37% (field moisture content). Prior to the experiment it was saturated from the base over a period of four hours. A total of 1700 mL of ultrapure water was required to saturate the block. Saturation continued until free water pounded on the soil surface, when the box was then connected to the columns.

Water percolated through the topsoil monolith was then pumped (via a peristaltic pump) through each of five columns. Columns were fashioned from standard syringes

(60 mL) with Teflon[®] tubing as inlet and outlet and were wrapped in Al-foil to avoid photo-oxidation. A layer of nylon mesh was placed at the base of each column to prevent fine material blocking the column outlet. A silicon stopper was used in each column to form a seal. A number of multi-feeder taps (5 taps from a single inlet; see Figure 1) linked all columns to the pump to ensure an equivalent inflow rate for each treatment. All equipment was acid-washed and blanks were performed by pumping ultrapure water through the empty system (blank readings were all below the detection limit of the analytical procedures described thereafter).

The experiment was conducted in a glove box under an oxygen-depleted atmosphere (using N₂), with treatments as follows:

- (i) nodules (in duplicate) and quartz continuously saturated for 6 months;
- (ii) nodules and quartz subjected to 14-day wetting and drying cycles. Columns undergoing drying cycles were removed from the glove box to enable exposure to oxygen.

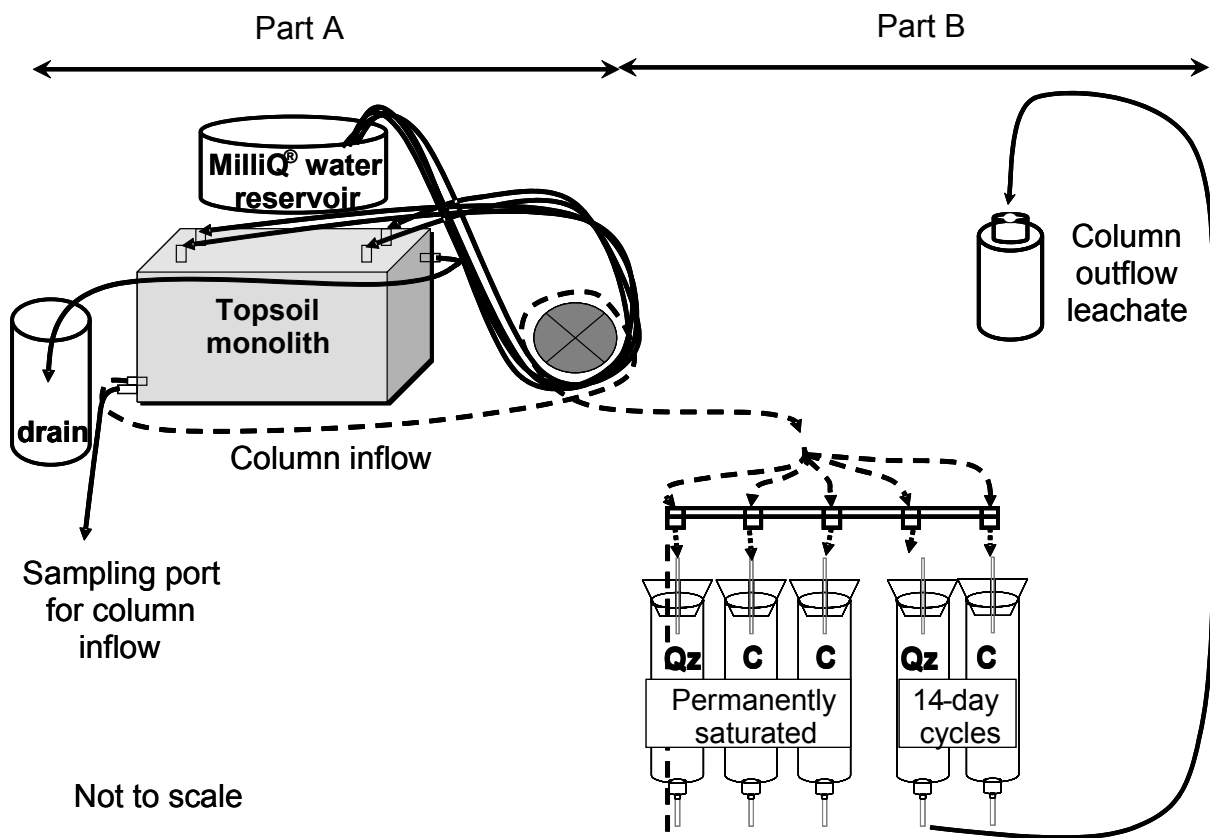


Figure 1: Schematic diagram of the experimental design. Qz refers to the quartz columns and C to the nodule ones.

Water sampling and analysis

Column leachates were collected daily over the first month of the experiment and three times a week for the rest of the experiment, which lasted over six months. Electrical conductivity (EC), pH, and redox potential (Eh) were measured immediately on sample

collection in the glove box. Redox potential was measured using an Ag/AgCl electrode and Eh measurements were then corrected to the standard hydrogen electrode, by using a correction factor depending on the temperature (Kölling, 1999):

$$Eh_{\text{corrected}} = Eh_{\text{measured}} + (207 + 0.7 (25-T))$$

where T is the temperature in °C, and $Eh_{\text{corrected}}$ is the corrected redox potential in mV. Experiments were performed at room temperature (~25°C).

As only Eh corrected values are presented in the rest of the paper they are referred as Eh for simplicity.

After collection, samples were removed from the glove box for immediate filtering (< 0.2 µm on cellulose acetate membrane). A part of the sample was then kept aside while the rest was acidified with suprapur HNO₃ for subsequent analysis by atomic absorption spectroscopy using flame for Fe and Mn, and graphite furnace for Co and Pb.

Eh-pH diagrams

Data were reported in Eh - pH stability diagrams (Brookins, 1988; McBride, 1994) for Mn and Fe species. For the manganese diagram, as no clear identification of the Mn oxides present into the nodule was available (Cornu *et al.*, 2005), the most common Mn oxides found in nodules were taken into account: birnessite (Mn⁴⁺ Mn₂³⁺ O₁₃) and lithiophorite (Al₂Mn₃⁴⁺ O₉) (Taylor, 1968; Manceau *et al.*, 2002, 2003; Neaman *et al.*, 2004). For iron diagrams, either ferrihydrite (Fe₂O₃ · 0.5(H₂O)) or goethite (FeOOH) with two possibilities γ or α forms were considered as these two last minerals are observed in the nodules by Cornu *et al.* (2005). Green rusts were also considered in the form (Fe(OH)₃) and (Fe₃(OH)₈) even if not identified as these minerals are transitory (Trolard and Bourrié, 1999; Feder *et al.*, 2005). Thermodynamic constants related to the different solids phases are reported in Table 3. Data from column outflows were plotted on Eh-pH diagrams in order to estimate the potential equilibrium or disequilibrium with minerals present in the nodules when redox conditions reached 100 mV.

Table 3: Equilibrium reactions and associated solubility constants at 25°C and 1 bar, used to construct the Eh-pH diagrams for the different minerals found in the nodules

Minerals	Reactions	log K	References
γgoethite	$\gamma\text{FeOOH} + 3\text{H}^+ + \text{e}^- \leftrightarrow \text{Fe}^{2+} + 2\text{H}_2\text{O}$	16.65	Hashimoto et Misawa (1973)
αgoethite	$\alpha\text{FeOOH} + 3\text{H}^+ + \text{e}^- \leftrightarrow \text{Fe}^{2+} + 2\text{H}_2\text{O}$	14.97	Détournay <i>et al.</i> (1975)
green rust	$\text{Fe}(\text{OH})_3 + 3\text{H}^+ + \text{e}^- \leftrightarrow \text{Fe}^{2+} + 3\text{H}_2\text{O}$	15.87	Trolard et Bourrié (1999)
green rust	$\text{Fe}_3(\text{OH})_8 + 8\text{H}^+ + 2\text{e}^- \leftrightarrow 3\text{Fe}^{2+} + 8\text{H}_2\text{O}$	46.41	Ponnamperuma <i>et al.</i> (1967)
ferrihydrite	$\text{Fe}_2\text{O}_3(0.5\text{H}_2\text{O}) + 6\text{H}^+ + 2\text{e}^- \leftrightarrow 2\text{Fe}^{2+} + 3.5\text{H}_2\text{O}$	34.778	Rabenhorst et Castenson (2005)
birnessite	$\text{Mn}_5^{4+} \text{Mn}_2^{3+} \text{O}_{13} + 26\text{H}^+ + 12\text{e}^- \leftrightarrow 7 \text{Mn}^{2+} + 13\text{H}_2\text{O}$	249.84 to 258.6	after Parc <i>et al.</i> (1989)
lithiophorite	$\text{Al}_2\text{Mn}_3^{4+} \text{O}_9 + 18\text{H}^+ + 6\text{e}^- \leftrightarrow 2\text{Al}^{3+} + 3\text{Mn}^{2+} + 9\text{H}_2\text{O}$	140.13	after Parc <i>et al.</i> (1989)

Statistic treatment

In order to determine if the discrepancies observed between the different columns were statistically significant, ANOVA tests were performed. This test was applied to the data obtained once the reduced conditions were reached. For each column, measurements were

then considered as different repetitions. One ANOVA analysis was performed for each of the studied variable: pH, Eh, Fe, Mn, Co, and Pb. The results were combined in [Tables 4 and 5](#).

Table 4: Average values for the pH and Eh values and Fe, Mn, Co and Pb concentrations according to the water type considered and Fisher's pairwise mean comparison results (ANOVA)

			pH	Eh	Fe	Mn	Co	Pb
Inflow			6.75 ^b	97 ^b	0.33 ^a	0.21 ^c	0.242 ^{cd}	0.006 ^{bc}
Outflow	Continuously saturated	Quartz	7.05 ^a	102 ^b	0.18 ^b	0.24 ^{bc}	0.275 ^{cd}	0.005 ^c
		Nodule 1	7.12 ^a	128 ^a	0.11 ^{cd}	0.25 ^b	0.592 ^b	0.005 ^c
		Nodule 2	7.07 ^a	130 ^a	0.11 ^{cd}	0.31 ^a	0.742 ^a	0.005 ^c
	14-day cycles	Quartz before drying	7.08 ^a	101 ^b	0.17 ^{bc}	0.25 ^b	0.318 ^c	0.008 ^{ab}
		Quartz after drying	7.16 ^a	133 ^a	0.07 ^d	0.11 ^d	0.146 ^d	0.006 ^{bc}
		Nodule before drying	7.05 ^a	147 ^a	0.08 ^d	0.27 ^{ab}	0.589 ^b	0.007 ^{abc}
		Nodule after drying	7.26 ^a	149 ^a	0.05 ^d	0.25 ^{bc}	0.731 ^{ab}	0.010 ^a

a, b, c, d are indicating whether the average are significantly different or not among the different samples with a confident level of 5%

Table 5: Average fraction fixed/released from the different columns for Fe, Mn and Co and Fisher's pairwise mean comparison results (ANOVA)

		Fixed Fe fraction	Released Mn fraction	Released Co fraction
Continuously saturated	Quartz	0.522 ^c	0.139 ^{bc}	0.126 ^c
	Nodule 1	0.660 ^b	0.301 ^{bc}	1.630 ^b
	Nodule 2	0.647 ^b	0.581 ^a	2.383 ^a
14-day cycles	Quartz before drying	0.440 ^c	0.158 ^{bc}	0.182 ^c
	Quartz after drying	0.800 ^{ab}	-0.186 ^c	-0.012 ^c
	Nodule before drying	0.760 ^{ab}	0.394 ^{ab}	1.417 ^b
	Nodule after drying	0.885 ^a	0.373 ^{abc}	2.864 ^a

a, b, c, d are indicating whether the average are significantly different or not among the different samples with a confident level of 5%

Results and discussion

Characteristics of the water inflow along the experiment: quality and quantity

The solution percolating through the soil monolith (column inflow) had an initial pH fluctuating from 6.60 to 6.95, increasing slightly over time to a more stable pH range of 6.85 to 6.95 ([Fig. 2a](#); average pH value of 6.75). The pH values were of the same order of magnitude as those recorded in the field by [Pelfrène \(2008\)](#), for the same site.

Redox potential decreased from values higher than 360 mV at the beginning of the experiment to values fluctuating between 90 and 120 mV after 30 days ([Fig. 2b](#)). Eh values stayed in this range (moderately reducing conditions) until the end of the experiment. The lag time needed for the re-establishment of reducing conditions in different laboratory experiments is reported to range from 100 hours ([Grybos et al., 2007](#)) to 20 days ([Quantin et al., 2001](#)). In the field, [D'Amore et al. \(2004\)](#) reported that this time ranged from a few days to three months according to the depth and the amount of rain. Our results (30 days) are in agreement with these data. In addition, these Eh values are of the same order of magnitude as

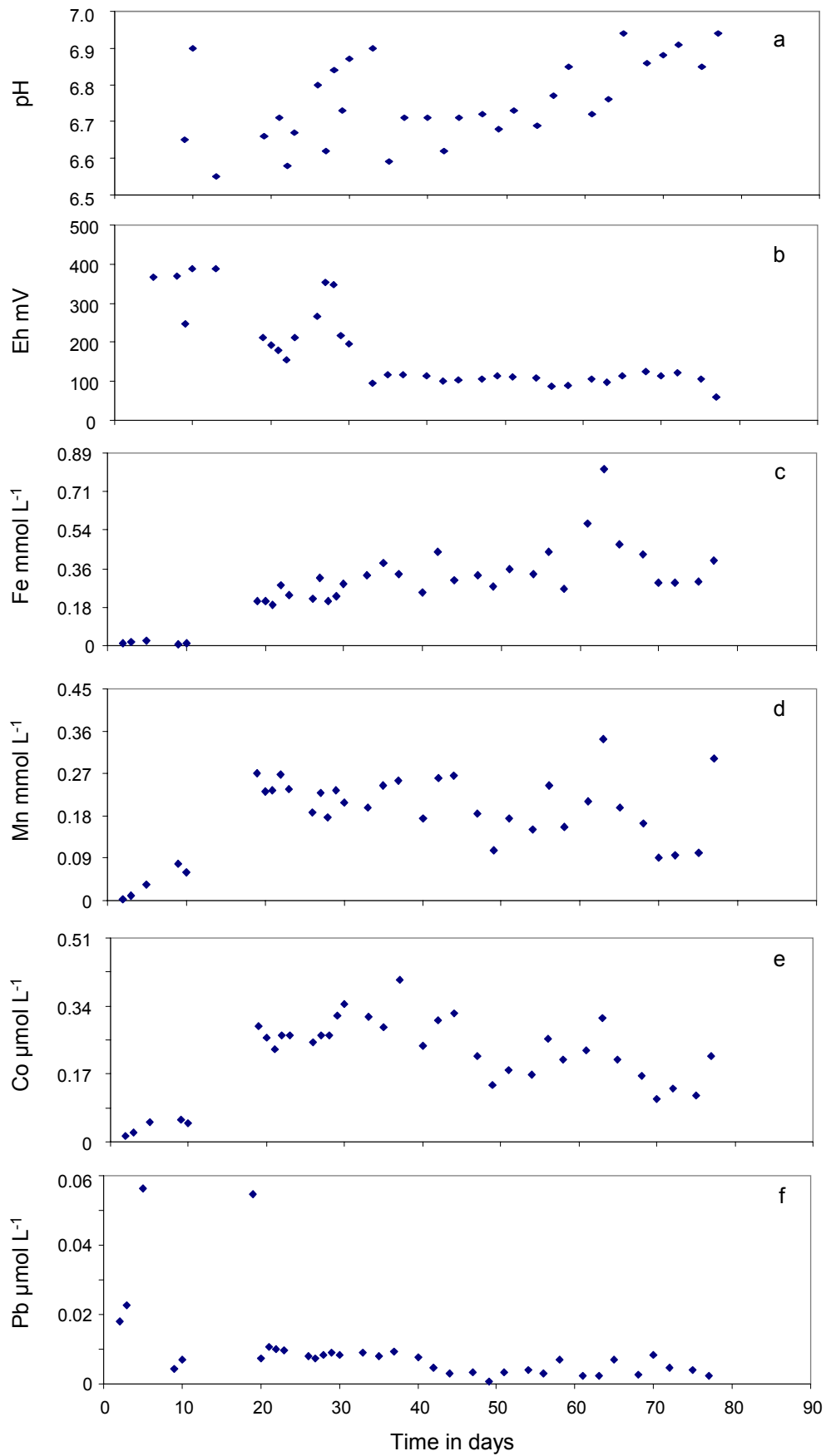


Figure 2: Characteristics of the solution percolating through the topsoil monolith as a function of time: A- pH; B- Eh; C- Fe; D- Mn; E- Co; F- Pb. Dark triangles represent the outflow, while open circles are for the inflow.

those recorded in the field by *D'Amore et al. (2004)* for wetlands, although these authors did record more reducing conditions during the wettest years. This range of Eh was also reached by *Quantin et al. (2001)* and *Thompson et al. (2006)* in their experiments, while the experiments of *Grybos et al. (2007)* reached lower redox potentials. Their Eh values were lower than the minimum value recorded in the field by *D'Amore et al. (2004)*. Unfortunately, no Eh values were recorded by *Pelfrène (2008)* for this site. *Quantin et al. (2001)* showed that an Eh decrease occurred only in biologically active samples and interpreted it as the result of biological activity.

Iron concentrations were about $\sim 0.018 \text{ mmol L}^{-1}$ over the 10 first days of the experiment, rising to $\sim 0.18 \text{ mmol L}^{-1}$ after 20 days and to 0.36 mmol L^{-1} after 35 days (*Fig. 2c*). Concentrations oscillated around this value for the duration of the experiment. *Thompson et al. (2006)* and *Quantin et al. (2001)* observed Fe oxide dissolution with comparable Eh values. Eh-pH diagrams for Fe (*Fig. 3a*) show that solutions coming out of the soil monolith are oversaturated with respect to all Fe-oxides present in the nodules.

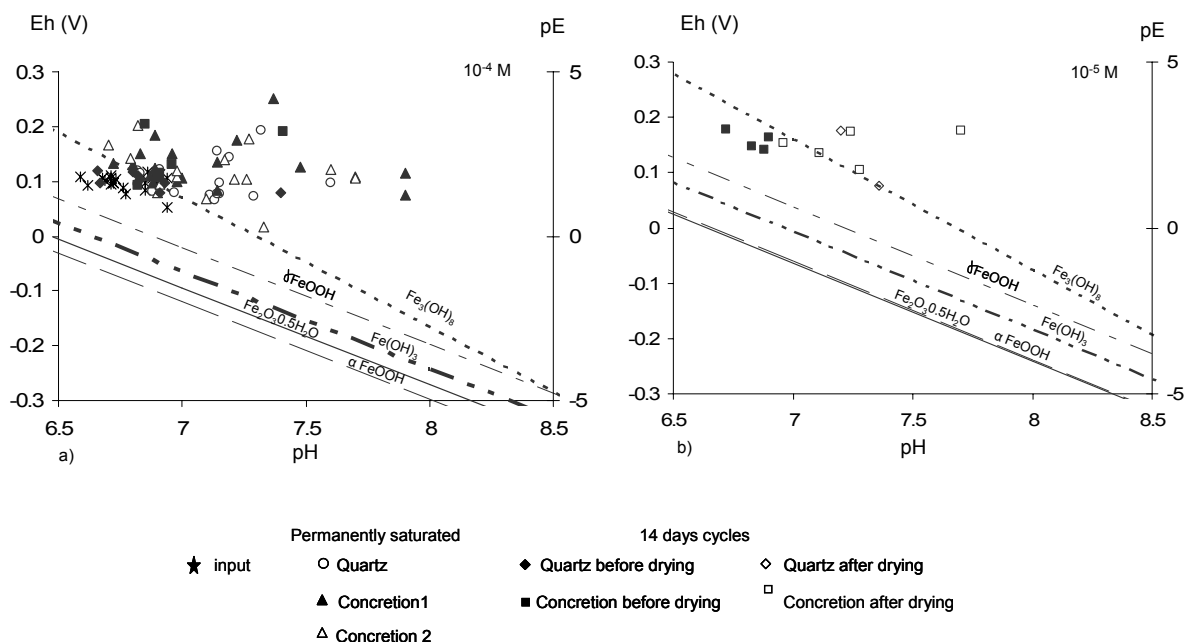


Figure 3: Eh-pH stability diagrams for Fe, considering 2 forms of goethite, 2 green rusts and ferrihydrite as Fe oxides, a) for a total Fe concentration in water at $10^{-4} \text{ mol L}^{-1}$ and b) for a total Fe concentration in water at $10^{-5} \text{ mol L}^{-1}$.

Manganese concentrations increased rapidly at the beginning of the experiment, reaching a value of 0.27 mmol L^{-1} after 20 days (*Fig. 2d*). Manganese concentrations in the soil leachates (column inflow) were of the same order of magnitude as those recorded for Fe. The inflow data (*Table 4*) revealed dissolution of Fe and Mn oxides at a molar Mn/Fe ratio of 0.61, whereas the surface horizon had a solid phase molar Mn/Fe ratio of 0.03 (ratio calculated from data in *Table 1*). This means that Mn oxides were proportionately more dissolved – about 20 folds – than Fe oxides, which is consistent with the higher sensitivity of Mn oxides to redox conditions compared with Fe oxides (*Jenne, 1968; Stumm and Morgan,*

1981) and also with data reported by Quantin *et al.* (2001). After 20 days, Mn concentrations gradually decreased to reach a value of 0.09 mmol L^{-1} at the end of the experiment. The Eh-pH diagram for Mn (Fig. 4) shows that solutions coming out of the soil monolith are undersaturated with respect to both birnessite and lithiophorite. The dissolution of these two minerals is thus probably responsible for the Mn concentrations acquired by the percolating waters.

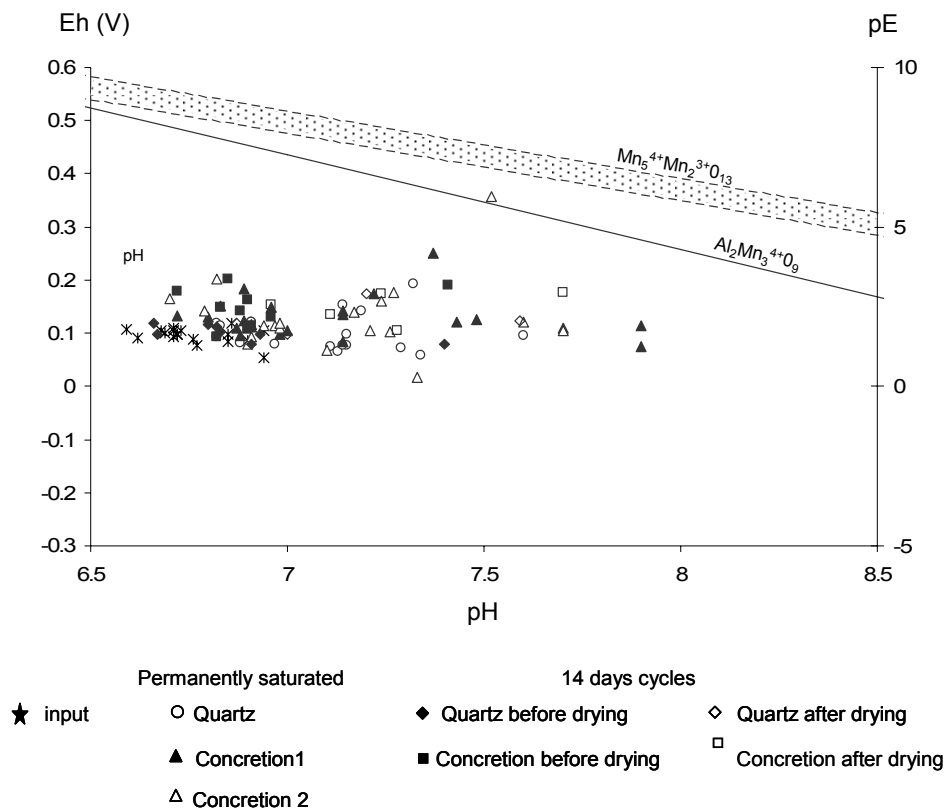


Figure 4: Eh-pH stability diagram for Mn, considering total Mn concentration in water = $10^{-4} \text{ mol L}^{-1}$ and birnessite and lithiophorite as Mn oxides. For lithiophorite, a concentration of Al in solution of $10^{-6} \text{ mol L}^{-1}$ was considered. For birnessite a range of stability constant was encountered in the literature (Table 3). The extreme values were used to calculate the stability lines for birnessite and represented as a shaded domain on the figure.

Trends observed for cobalt paralleled those described for Mn (Fig. 2e). With the exception of two high concentrations, lead concentrations decreased sharply from $0.019 \text{ } \mu\text{mol L}^{-1}$ to about $0.005 \text{ } \mu\text{mol L}^{-1}$ at 40 days and stabilised thereafter (Fig. 2f).

The obtained reducing conditions were sufficient to dissolve both iron and manganese oxides from the topsoil monolith, also observed in the experiments of Quantin *et al.* (2001) and Thompson *et al.* (2006). Patrick and Jugsujinga (1992) give lower Eh values for the reduction of Fe oxides (50 mV), while their data for Mn oxides are in agreement with results reported here.

After 80 days of the experiment the data became very noisy. The monolith structure started to collapse and had to be replaced. This change produced sample oxidation, and reducing conditions were not observed again before the end of the experiment (data not

shown). For this reason only data obtained for the 80 first days of the experiment are presented here.

Impact of the redox condition on the release of Fe, Mn and associated trace elements by nodules

As shown in [Table 6](#), the amount of water percolated through the different columns was reasonably similar despite the difficulties in regulating the water flow. The difference between the continuously saturated treatment and the 14-day wetting and drying cycle treatment was due to no solution leaching during the drying cycle. Given that the quartz and nodule columns had such different pore volumes ([Table 2](#)), percolated volumes have been expressed in terms of pore volumes hereafter to allow comparison.

Table 6: Amount of leachate collected from the different columns

Treatment	Column	Percolated volume (mL)	Percolated volume (pore volumes)	Percolated volume during the cycle (mL)
Saturated	Quartz	5704	238	987
	Nodule 1	6183	182	1440
	Nodule 2	6565	187	1411
14-day cycles	Quartz	3970	165	0
	Nodule	4225	124	0

Outflow from the columns had a significantly higher pH (around 7.1 overall; [Figs. 5a to 8a](#)) than the inflow according to an ANOVA test at a 5% confidence level ([Table 4](#)).

The outflow Eh followed the same general trend as the inflow, decreasing sharply over the first month and then stabilising ([Figs. 5b to 8b](#)). Once stabilised, the outflow Eh from the quartz column before the drying cycle was not significantly different from that of the inflow, according to an ANOVA test at a 5% confidence level ([Table 4](#)). Nodule columns had a significantly higher Eh in the outflow (ANOVA test at a 5% confidence level, [Table 4](#)), especially those undergoing drying cycles.

Iron concentrations in both column inflow and outflow increased initially, reaching a relatively stable level at about 35 days ([Figs. 5c to 8c](#)). Subsequent Fe concentrations in the outflow were significantly lower than those of the inflow (ANOVA test at a 5% confidence level, [Table 4](#)) suggesting Fe fixation within the columns. The outflow from quartz columns contained higher Fe concentrations than that from the nodule columns (ANOVA test at a 5% confidence level, [Table 4](#)). The nodule column undergoing wetting and drying cycles had the smallest outflow Fe concentrations, which could be related to the higher Eh values also recorded for this column. As inflow Fe concentrations slightly changed over time, fixation ratios were calculated to compare the fixation of Fe between the different columns as follows:

$$Fe_{\text{fixation ratio}} = ([Fe]_{\text{in}} - [Fe]_{\text{out}}) / [Fe]_{\text{in}}$$

An ANOVA test at a 5% confidence level showed that the fixation ratio of the quartz column undergoing wetting and drying cycles was the lowest before drying and the nodule column undergoing wetting and drying cycles fixed more Fe than the other nodule columns ([Table 5](#)). Thus, nodule columns were able to fix Fe more efficiently than quartz columns. Eh-pH diagrams for Fe ([Fig. 3](#)) show that column outflows are oversaturated with respect to goethite, ferrihydrite and one green rust type (Fe(OH)₃). The Fe fraction retained in the

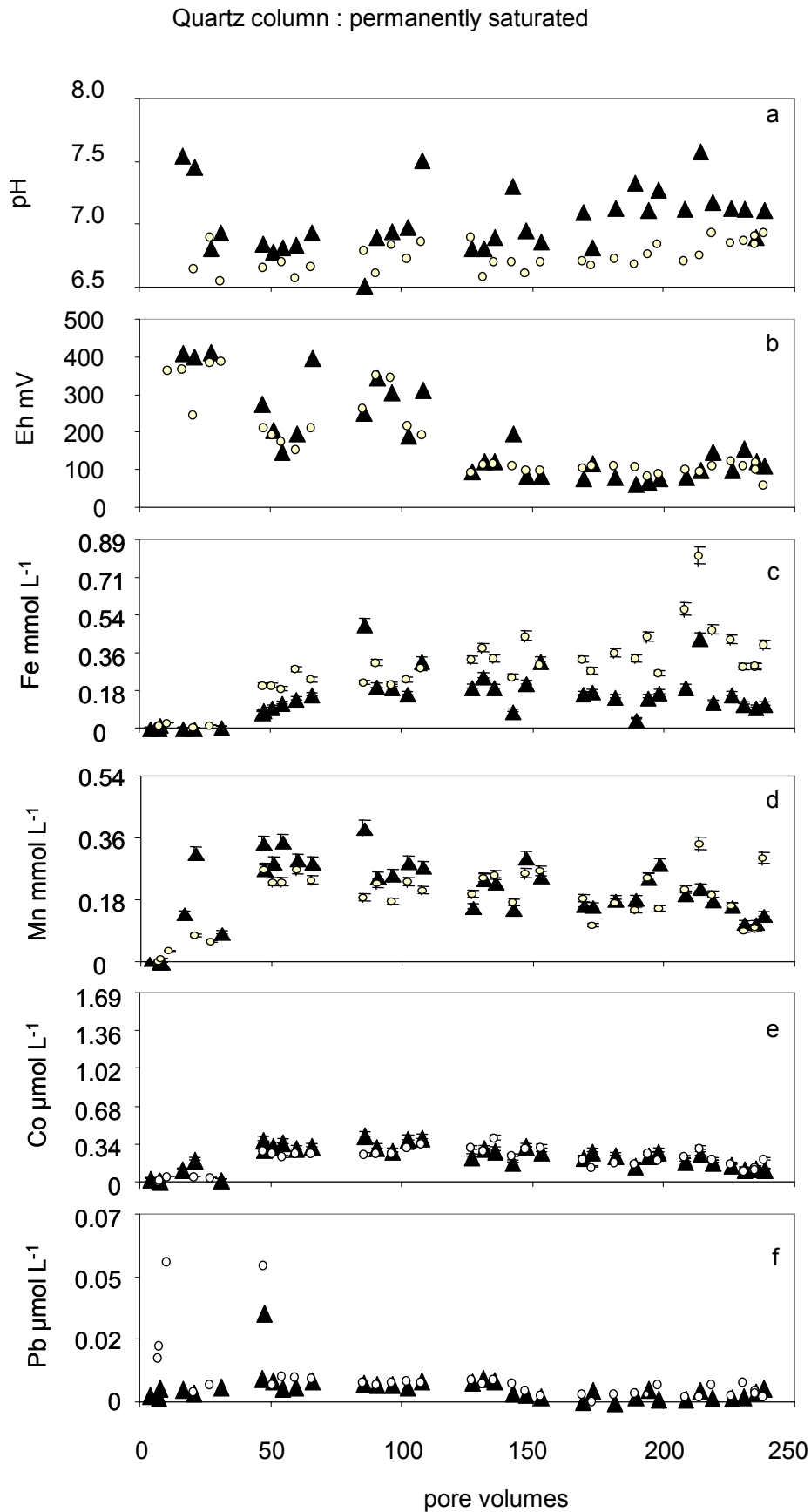


Figure 5: pH, Eh, Fe, Mn, Co and Pb concentrations as a function of the pore volume of the inflow and outflow for the quartz column undergoing permanent saturation. Dark triangles represent the outflow, while open circles are for the inflow.

Concretion columns 1 & 2 : permanently saturated

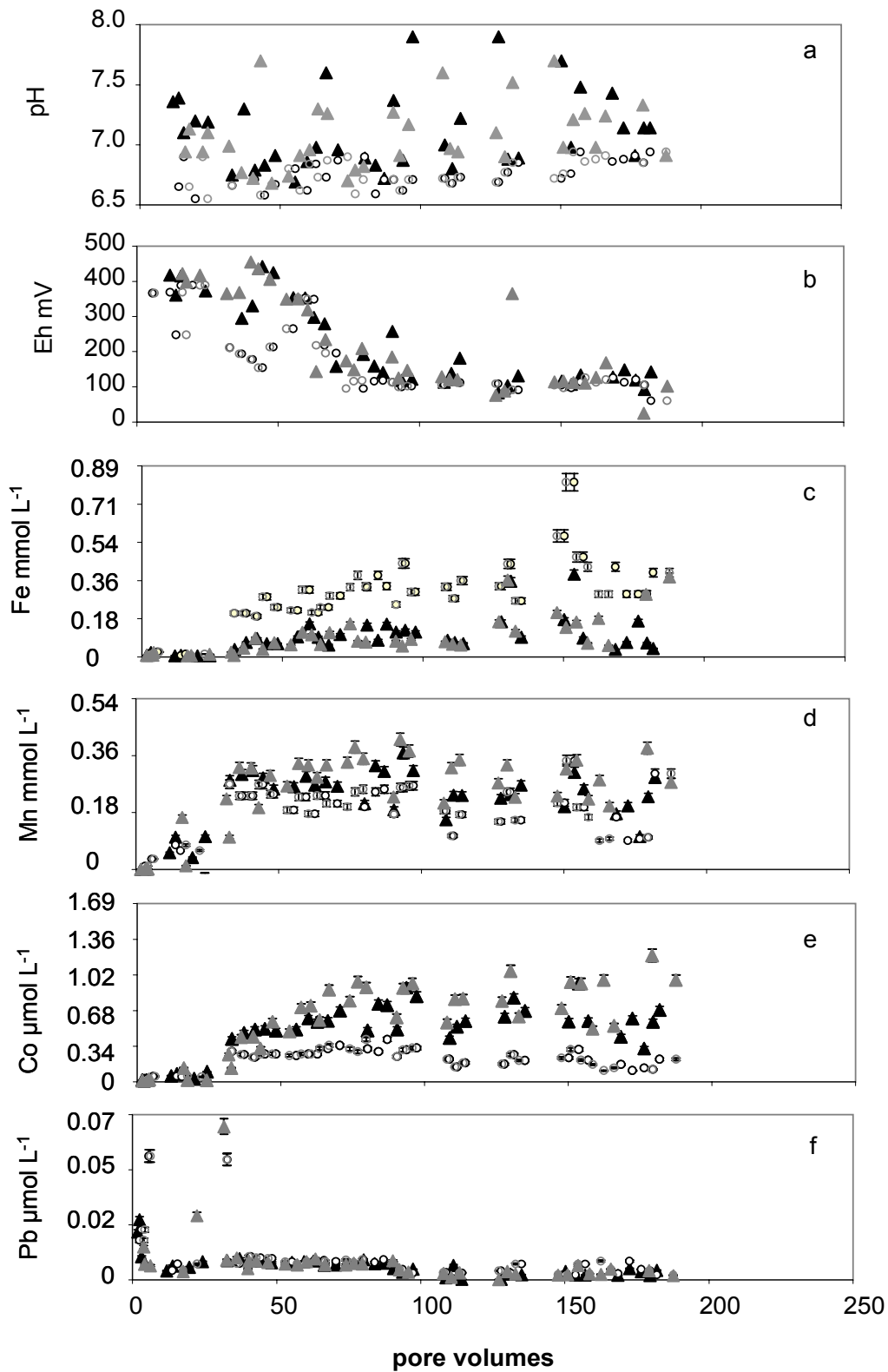


Figure 6: pH, Eh, Fe, Mn, Co and Pb concentrations as a function of the pore volume of the inflow and outflow for nodule columns 1 & 2 undergoing permanent saturation. Dark triangles represent the outflow, while open circles are for the inflow. Black symbols are for the first column, while grey ones state for the second column.

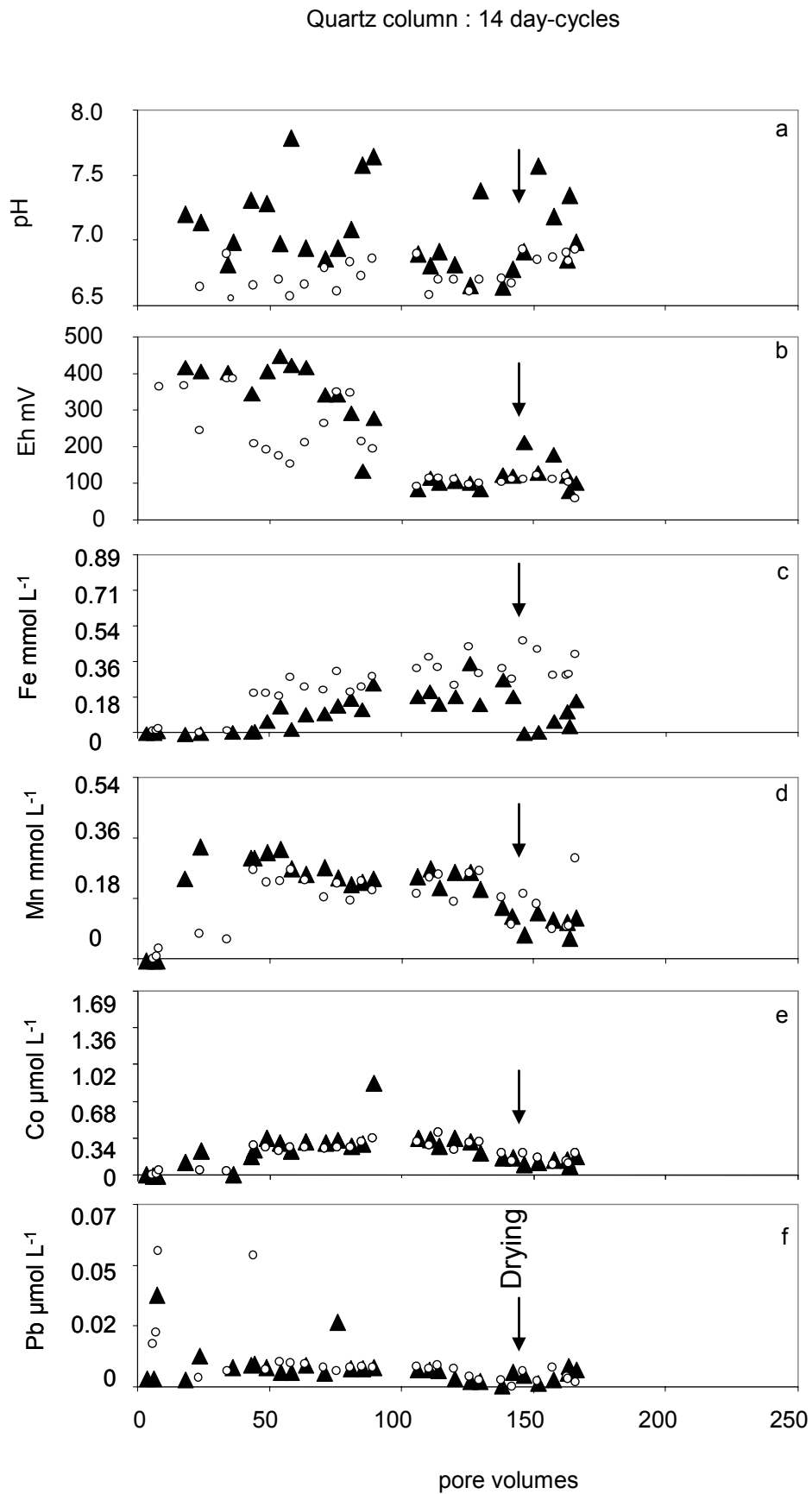


Figure 7: pH, Eh, Fe, Mn, Co and Pb concentrations as a function of the pore volume of the inflow and outflow for the quartz column undergoing 14-day cycles. Dark triangles represent the outflow, while open circles are for the inflow.

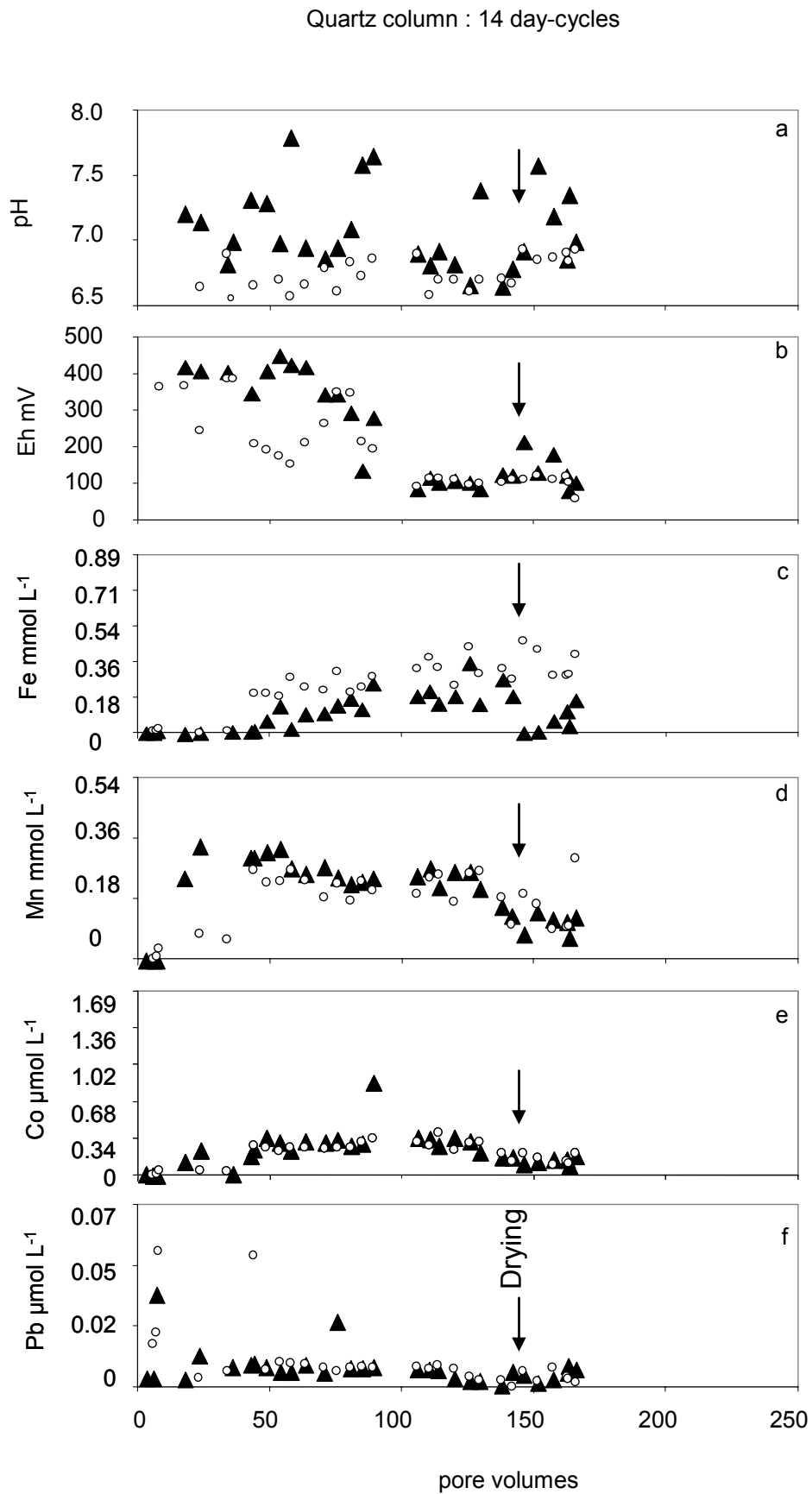


Figure 8: pH, Eh, Fe, Mn, Co and Pb concentrations as a function of the pore volume of the inflow and outflow for the nodule column undergoing 14-day cycles. Dark triangles represent the outflow, while open circles are for the inflow.

columns was thus probably precipitate as goethite, ferrihydrite and one green rust type along the experiment. Green rust, which is a transitory phase, was probably then recrystallised into goethite or ferrihydrite as 40% and 25% of the Fe contained in the nodules was into these minerals respectively (Cornu *et al.*, 2005).

Similarly to Fe, outflow Mn concentrations increased following the increase in inflow concentrations (Figs. 5d to 8d). Once stabilised, Mn concentrations in column outflows were significantly higher than column inflows (ANOVA test at a 5% confidence level, Table 4). Manganese concentrations in outflows of nodule columns were also higher than those of quartz columns, indicating a release of Mn from nodules into the water. We have expressed the Mn released from the column in terms of a release ratio to better compare the different treatments:

$$\text{Mn}_{\text{release ratio}} = ([\text{Mn}]_{\text{out}} - [\text{Mn}]_{\text{in}}) / [\text{Mn}]_{\text{in}}$$

An ANOVA test at a 5% confidence level confirmed these results (Table 5). The Eh-pH diagram for Mn shows that nearly all column outflows are undersaturated with respect to birnessite and lithiophorite (Fig. 4). As manganese oxides contained 100% of the Mn present in the nodules (Cornu *et al.*, 2005), the dissolution of these minerals is responsible for the increase in Mn concentrations in outflows from the nodule columns.

Results show that while Fe was fixed within the columns during the experiment, reduction processes released Mn. Thus, the reducing conditions were strong enough to dissolve Mn oxides but not sufficient to dissolve Fe oxides.

Cobalt concentrations in column outflows increased with those in the inflow and stabilised after 35 days (Figs. 5e to 8e). Once stabilised, inflow and outflow Co concentrations in quartz columns were not significantly different (ANOVA test at a 5% confidence level, Table 4). Outflow Co concentrations from nodule columns were significantly higher than inflow concentrations indicating a net release of Co from nodules. As for Mn we calculated a Co release ratio. The results for the Co release ratio were equivalent to those from Co concentrations (ANOVA test at a 5% confidence level, Table 5). As for Mn, 100% of the Co found in the nodules was contained in Mn oxides (Cornu *et al.*, 2005). The Co/Mn ratios of the Mn and Co released from the nodule columns were close to those of the nodules, suggesting that dissolution of Mn oxides evidenced previously is responsible for Co losses. It also suggests that readsorption does not occur within the column unless it is in the same proportion for the two elements as that originally present in the solid phases, which disagrees with results of Quantin *et al.* (2002), who showed that Co concentrations decreased over time. This was interpreted as readsorption. Such behaviour was not exhibited in our experiment.

As observed for the inflow, outflow Pb concentrations decreased sharply over time and stabilised at low values with the exception of some discrepancies (Figs. 5f to 8f). If we exclude these few very high concentrations, outflow Pb concentrations from columns undergoing wetting and drying cycles were significantly higher than those of the inflow, while those of the permanently saturated column were significantly lower (ANOVA test at a 5% confidence level, Table 4). While there was no obvious explanation for this behaviour, the overall concentrations were very low. When the ANOVA was performed with the high concentrations included no significant differences were found (ANOVA test at a 5% confidence level; results not shown). Cornu *et al.* (2005) showed that Pb was present at almost 90% in Mn nodules; however, no Pb was either added to or removed from the water suggesting that either the Mn oxides were not dissolved congruently or that the Pb was re-adsorbed on the remaining phases in the column. Indeed, McKenzie (1989) and references

herein) stated that in general Mn oxides adsorbed more Pb than Co. The same was recorded for Fe-oxides (Schwertmann and Taylor, 1989 and references herein).

Impact of the drying on the following reducing period

The drying cycle caused a slight increase in the outflow pH from the nodule column (Fig. 8a) although this difference was not significant according to an ANOVA test (Table 4). For the quartz column, the effect of the drying cycles was even smaller (Fig. 7a).

Outflow Eh values increased significantly after the drying period in the quartz column (ANOVA test at a 5% confidence level, Table 4), becoming equivalent to outflow Eh values recorded for nodule columns always saturated (Table 4). This increase of Eh upon drying was less clear for the nodule column, which already exhibited a higher outflow Eh before drying than the continuously saturated nodule columns.

Iron concentrations in outflows from the quartz column dropped significantly after drying (ANOVA test at a 5% confidence level, Table 4), however the concentrations increased quickly again (Fig. 7c). Only a slight decrease (not significant) was observed in the nodule column, possibly due to its low original Fe concentrations. The fixation ratios, show that both quartz and nodule columns fixed significantly more Fe after drying (ANOVA test at a 5% confidence level, Table 5). For these two columns, the Fe fixation ratio was closely related to Eh values of the column outflow (Fig. 9). The drying cycle clearly increased the efficiency of the nodules to fix Fe. Contin *et al.* (2007) also reported an increase in trace metal retention upon reoxidation of oxides following consecutive redox cycles. Eh-pH diagrams for Fe (Fig. 3b) show that after a drying period, column outflows are also oversaturated with respect to $\text{Fe}_3(\text{OH})_8$, which was rarely the case before the drying. Thus, more Fe oxide types are potentially responsible for the Fe uptake from the solution by the column.

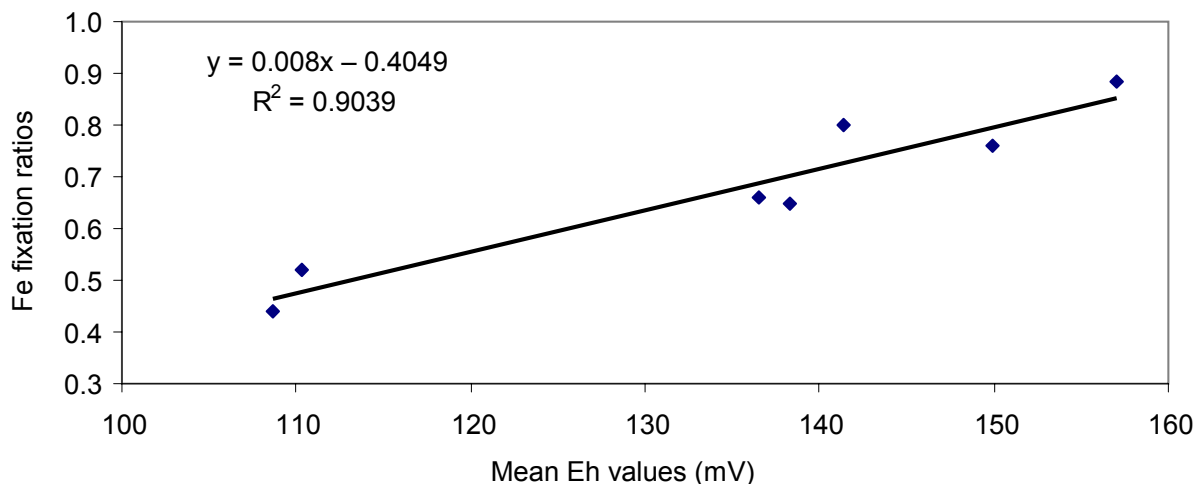


Figure 9: Iron fixation ratios versus mean Eh values for the different columns.

The drying cycles caused outflow Mn concentrations to drop significantly (ANOVA test at a 5% confidence level, Table 4). For the quartz column, the concentrations became even lower than those of the inflow, indicating Mn fixation. For the nodule column, outflow

Mn concentrations remained higher than those of the inflow, revealing Mn release. When considered in terms of the Mn release ratio, the impact of the drying cycle was smaller in nodule columns than in quartz columns (Table 5). The Eh-pH diagram for Mn (Fig. 4) did not evidence a clear difference in terms of solution equilibrium with respect to birnessite and lithiophorite before and after drying. Both types of solutions were mainly undersaturated with respect to these minerals.

The drying period provoked a net decrease in the outflow Co concentrations from the quartz column, which were significantly lower than the inflow concentrations (ANOVA test at a 5% confidence level, Table 4). This fixation of Co within the quartz column (as was seen for Mn) is small and not significant when expressed in terms of ratio (ANOVA test at a 5% confidence level, Table 5). Surprisingly, outflow Co concentrations from the nodule column increased significantly after drying, which could be better seen when expressed in terms of release ratio (ANOVA test at a 5% confidence level, Table 5).

The drying period increased the Eh within nodule columns, inducing a larger Fe fixation. The influence of these cycles on other elements was less clear. A slightly lower Mn release was recorded. Cobalt release was however found to be larger; this result was not consistent with a decrease in Mn release and Co being contained within Mn oxides. All these trends were unable to be clearly interpreted and more wetting and drying cycles should be performed in order to draw a firm conclusion.

Consequences of the redox cycles in terms of soil evolution and environmental impact

The total gains in Fe and respective losses in Mn and Co were calculated by mass balance calculation on the inflow and outflow waters and reported in Table 7. They are several orders of magnitude lower than the stocks of these elements found in the different columns (Table 2) and are thus negligible compared with the amount of these elements initially present in the nodules. This was confirmed by analyses of the solid phase at the end of the experiment, which showed no differences from analyses performed on nodules and quartz sand before the experiment (results not shown). We do not expect much of a change in the forms of Fe and Mn present in nodules, owing to the small magnitude of the gains or losses that occurred throughout the experiment. For this reason, we did not perform any sequential extractions after the experiment as was done in some other studies reporting much larger releases of Fe and/or Mn (Quantin *et al.*, 2002; Thompson *et al.*, 2006). In these studies the focus was on the fine earth soil fraction. Our results demonstrate that in the case of nodules the rate of release of these elements as a function of redox processes is slow.

Table 7: Total Fe, Mn, Co and Pb gained or lost from the different columns at the end of the experiment, calculated from mass balance calculation on the inflow and outflow waters

Treatment type	Column type	Fe mg	Mn mg	Co µg	Pb µg
Continuously saturated	Quartz	31	-8.4	8.3	1
	Nodule 1	69	-11	-102	3.7
	Nodule 2	61	-28	-169	1.4
14-day cycles	Quartz before drying	15	-6.7	-8.8	0.003
	Quartz at the end of the experiment	25	-5.5	-8.6	0.04
	Nodule before drying	27	-11	-57	0.4
	Nodule at the end of the experiment	44	-15	-85	-1.9

Reducing conditions lead to a slow increase in Fe content and dissolution of Mn oxides, which released associated Co. Lead (also contained in Mn oxides of the nodules) was not lost, as it was probably re-adsorbed on the remaining phases. Despite the over-saturation of the percolating solutions with respect to green rusts, the only Fe oxides identified in these nodules were goethite and ferrihydrite (Cornu *et al.*, 2005).

We can conclude that the nodules in the studied soils are still active but that their reactivity is very low, as shown by the low amount of Fe and Mn fixed or released with an amount of percolated water that was equivalent to 8 m. However, this study showed that nodules were very efficient Fe scavengers as they fixed 70 to 90% of the Fe initially present in the water (Table 5).

The water running out of the column experiment has concentrations ranging from 0.01 to 0.39 mmol L⁻¹ for Fe, from 0 to 0.43 mmol L⁻¹ for Mn, from 0.01 to 1.43 µmol L⁻¹ for Co and from 10⁻⁴ to 0.07 µmol L⁻¹ for Pb. This water directly runs out in a small river. However, the concentrations in Pb are very low as they never exceed the acceptable limit for drinking water of 0.048 µmol L⁻¹. This is also the case for Co concentrations, which are lower than the limit concentration for waste water release into the environment. However, Fe and Mn concentrations are generally higher, from one to several orders of magnitude, than the limit given by the European Directive – of June, 16th 1975 – for surface waters. Thus the only potential threat to the surrounding water will come from Fe and Mn and not from the trace elements. However, as Mn is very sensitive to change in redox conditions, it will precipitate easily and probably shall not reach the river. Indeed Pelfrêne (2008) gives Fe concentrations in water for this horizon that are on the same order of magnitude as the ones obtained in this study, while their Mn concentrations are one order of magnitude lower. At last, only Fe may represent a threat for the environment, as it is the only one exceeding in the soil water the limit concentration given by the European Directive of June, 16th 1976.

Conclusion

Simulating redox cycles in a laboratory experiment on soil nodules showed that redox conditions similar to those found in soils could be achieved. These conditions allow reduction of Mn oxides, while Fe oxides were still precipitated. Both the experiment and the Eh-pH diagram results were consistent with these findings. The process was relatively slow as only a very small fraction of the Mn and Fe contained in the nodules was either released or fixed. This suggested that if still active, the process of formation/dissolution of nodules in soils is slow.

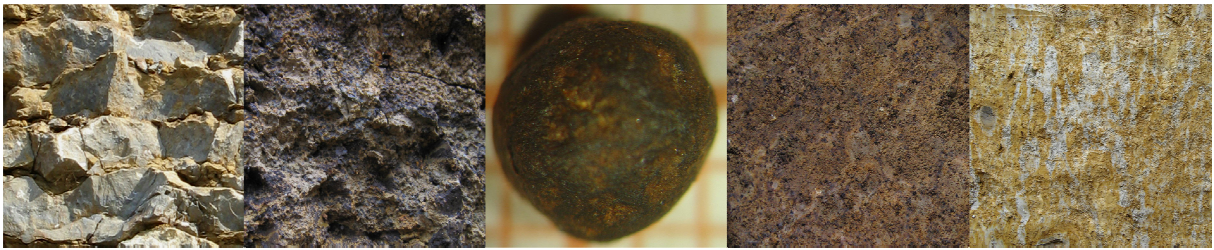
These nodules are a sink for trace elements. In this study we showed that while Co was released at the same rate as Mn, Pb also contained in Mn oxides was not released from the column and was probably re-adsorbed on nodule surfaces. This suggested that the knowledge of the trace element location as determined by sequential extraction is not sufficient to determine the fate of a trace element in the environment. Such extractions must be combined with other types of experiment.

Finally, redox cycles including a drying period would reduce the release of Co, given that Mn oxide formation would occur with concurrent adsorption of Co. Due to technical difficulties in conducting this experiment, only one complete redox cycle could be achieved. More redox cycles of different duration should be performed in order to be able to predict the

impact of waterlogging duration on nodule fate either through agricultural practices (irrigation/drainage) or due to climate change.

In terms of environmental threat this result also suggests that Pb would not be released from soil during nodule dissolution, whereas Co, which is less toxic, would be released.

Table des matières



Remerciements	2
----------------------	----------

Sommaire	6
-----------------	----------

Chapitre 1. Introduction	7
---------------------------------	----------

<i>1.1. Enjeux scientifiques et objectifs de la thèse</i>	<i>8</i>
---	----------

<i>1.2. Démarche envisagée</i>	<i>9</i>
--------------------------------	----------

<i>1.3. Choix des traceurs</i>	<i>9</i>
--------------------------------	----------

<i>1.4. Organisation de l'étude</i>	<i>10</i>
-------------------------------------	-----------

Chapitre 2. Matériels et Méthodes	12
--	-----------

<i>2.1. Genèse de la formation calcaire d'âge sinémurien et principales caractéristiques</i>	<i>14</i>
--	-----------

<i>2.2. Contexte pédologique</i>	<i>16</i>
----------------------------------	-----------

<i>2.3. Description des solums échantillonnés</i>	<i>18</i>
---	-----------

<i>2.4. Régime hydrique de la toposéquence de la Terre-Plaine</i>	<i>20</i>
---	-----------

<i>2.5. Echantillonnage</i>	<i>21</i>
-----------------------------	-----------

<i>2.6. Analyses</i>	<i>22</i>
----------------------	-----------

Chapitre 3. Potentialité du zinc comme traceur des différents processus pédogénétiques	25
---	-----------

<i>3.1. Comportement du zinc au cours de la pédogenèse</i>	<i>27</i>
--	-----------

<i>Article "Effect of Pedogenesis on Zinc Location in Soils developed from Limestones"</i>	<i>27</i>
--	-----------

ABSTRACT	27
----------	----

INTRODUCTION	28
--------------	----

MATERIALS AND METHODS	28
-----------------------	----

Studied site and samples	28
--------------------------	----

Analyses on soil samples	29
--------------------------	----

Analyses on limestone samples	31
-------------------------------	----

Mass balance calculations	31
---------------------------	----

RESULTS AND DISCUSSION	32
------------------------	----

Zinc location in the parent materials	32
---------------------------------------	----

Zinc redistribution along the solum during soil evolution	34
---	----

Impact of the different pedological processes on the redistribution of zinc	35
Validation of solid phases extracted by each extraction step and location of Zn	35
Redistribution of Zn by carbonate dissolution	37
Redistribution of Zn by primary redox processes	38
Redistribution of Zn by secondary redox processes	39
Redistribution of Zn due to the evolution of phyllosilicates and to eluviation/illuviation	39
CONCLUSIONS	41

3.2. Conclusions sur la potentialité du zinc pour tracer des processus pédogénétiques _____ **42**

Chapitre 4. Potentialité des terres rares comme traceurs des différents processus pédogénétiques	43
---	-----------

4.1. Etude bibliographique de l'impact de différents processus d'altération et de pédogenèse sur le fractionnement des terres rare _____ **45**

<i>Article "Potentiality of Rare Earth Elements as Tracers of Pedogenetic Processes: A Review"</i>	45
ABSTRACT	45
1. Introduction	46
2. Contents and origins of REEs in soils	48
3. Normalization and anomalies	49
4. Impact of weathering on REE mobilization	51
4.1 REEs in primary minerals	51
4.1.1. Minerals with high REE concentrations	51
Heavy minerals	51
Phosphates	51
4.1.2. REE-bearing minerals abundant in soils and parent materials	52
Silicate primary minerals	52
Parent carbonates	53
4.2. Impact of the properties of the different REEs in solution on their distribution within weathering profiles	54
4.3. Impact of the degree of weathering on the REE distribution into weathering profiles	54
5. Secondary mineral formation and REE immobilisation	55
5.1. Clay mineral formation	55
5.2. Fe-Mn-oxide formation	56
5.3. Formation of pedogenetic carbonates	58

6. Impact of biological recycling and organic matter on REE mobilization	59
6.1 Biological recycling of REEs and REE mobilisation	59
6.2. Complexation by organic matter and REE mobilisation	59
7. Remobilisation of secondary mineral by pedogenetic processes and REE mobilisation	60
7.1. Lessivage	60
7.2 Hydromorphy and soil degradation	61
8. Conclusions	62
9. Acknowledgments	62

4.2. Mise en point méthodologique d'utilisation des terres rares comme traceurs des processus pédogénétiques et validation de cette méthode sur un autre site _____ 63

4.2.1. Mise en point méthodologique d'utilisation des terres rares comme traceurs des processus pédogénétiques	63
--	----

Article "Rare earth elements as tracers of pedogenetic processes" _____ 63

Abstract	63
----------------	----

Résumé	64
--------------	----

1. Introduction	64
-----------------------	----

2. Materials and methods	65
--------------------------------	----

2.1. Pedological context	65
--------------------------------	----

2.2. Pedogenetic processes and pedological features	67
---	----

2.3. Samplings and experiments	67
--------------------------------------	----

3. REE pattern of the parent limestones, the limestone-phosphate nodules and the bulk soil fraction of the different horizons	68
---	----

4. Impact of the successive pedogenetic processes on REE mobilization and fractionation	71
---	----

4.1. Decarbonation	71
--------------------------	----

4.2. Redox conditions	72
-----------------------------	----

4.2.1. Primary redox conditions	72
---------------------------------------	----

4.2.2. Secondary redox conditions	73
---	----

4.3. Eluviation	74
-----------------------	----

5. Conclusion	76
---------------------	----

Acknowledgments	76
-----------------------	----

4.2.2. Validation de notre démarche méthodologique sur le site de la Terre-Plaine	77
---	----

4.2.2.1. Les méthodes de normalisation des terres rares	77
---	----

4.2.2.2. Impact des différents processus d'altération et de pédogenèse sur les stocks en terres rares	79
---	----

4.2.2.2.1. Le processus de décarbonatation	79
--	----

4.2.2.2.2. Processus redox primaires	80
--	----

4.2.2.2.3. Processus redox secondaires.....	81
4.2.2.2.4. Eluviation secondaire.....	83
4.3. Conclusions	84
<hr/>	
Chapitre 5. Reconstruction des matériaux parentaux	86
<hr/>	
5.1. Méthodologie de reconstitution des matériaux parentaux et bilan de masse	88
<hr/>	
<i>Article “Reconstruction of former parent materials and pedological behavior of major elements and Rare Earth Elements with mass balance calculations in a soil developed from a heterogeneous complex sedimentary deposit”</i>	88
Abstract.....	88
1. Introduction.....	89
2. Materials and methods.....	90
2.1. Geological context of the study site.....	90
2.2. Pedological context of the study site.....	92
2.3. Sampling strategy.....	93
2.4. Density measurements, sampling preparation and analyses.....	93
2.5. Experimental carbonate dissolution of parent materials.....	95
2.6. Errors and uncertainties on calculations.....	95
3. Results and discussion.....	95
3.1. Choice of the immobile elements.....	95
3.2. Identification of the former parent materials for each soil horizon.....	97
3.2.1. Chemical variability of the remaining sinemurian formation samples.....	97
3.2.2. Reconstruction of former parent materials.....	99
3.2.3. Former parent material thickness weathered for each soil horizon.....	103
3.3. Elemental fluxes during weathering and pedogenesis.....	105
3.3.1. Mobility of the selected immobile elements during pedogenesis.....	106
3.3.2. Mobility of major elements and REEs during weathering and pedogenesis.....	108
Weathering.....	108
Redox processes.....	108
Clay mobilization.....	112
4. Conclusion.....	112
5. Acknowledgements.....	113
5.2. Conclusions	114

Chapitre 6. Impact des processus sur la redistribution des terres rares	115
--	------------

6.1. Redistribution des terres rares au cours du processus de décarbonatation	117
--	------------

6.1.1. Matériels et méthodes	117
6.1.2. Signature en terres rares des calcaires	118
6.1.3. Mise en solution des terres rares au cours de la décarbonatation	119
6.1.4. Spéciation des éléments dans les calcaires	120
6.1.4.1. Spéciation des éléments majoritairement contenus dans les résidus de décarbonatation : Si, Al, P, Fe et K	123
6.1.4.2. Spéciation des éléments majoritairement contenus dans les carbonates : Mn et Mg	124
6.1.4.3. Spéciation des éléments contenus à la fois dans le résidu de décarbonatation et les carbonates : les terres rares	124
6.1.5. Devenir des éléments lors de la décarbonatation des calcaires	129
6.1.6. Conclusions sur le processus de décarbonatation	131

6.2. Potentiel des terres rares comme traceurs des processus redox	133
---	------------

Article "Impact of redox conditions on the mobilization of Rare Earth Elements in a soil sequence developed from limestone"	133
--	------------

Abstract	133
1. Introduction	134
2. Materials and methods	135
2.1. Geological and pedological context of the studied site	135
2.2. Sampling strategy and sample preparation	137
2.3. Sequential extractions of the different soil fractions	137
3. Results and discussion	138
3.1. Redox processes, associated pedological features and impact on the REE mobilization	138
3.2. REE signatures in the different mineral phases of the Fe-Mn nodules, of the <50 µm and <2 µm fractions	141
3.2.1. REE signature of (fluor)apatite	142
3.2.2. REE signatures of Mn-oxides	143
3.2.3. REE signatures of ferrihydrite	145
3.2.4. REE signatures of goethite	145
3.2.5. REE signatures of silicates	145
3.3 Evolution of the different mineral phases with the redox processes along the sola	146
3.3.1. Condensation in Fe-Mn nodules and subsequent dissolution	146
3.3.2. Dissolution of the oxide phases dispersed in the matrix	146

3.4. Impact of the different minerals on the signature in REEs of the pedological features: implication in terms of analysis of the processes.....	149
3.4.1. In the Fe-Mn nodules.....	149
3.4.2. In the matrix.....	152
4. Conclusion.....	154
5. Acknowledgments.....	155

6.3. Conclusions sur l'impact des processus sur la redistribution des terres rares et leur utilisation comme traceurs	156
--	------------

Chapitre 7. Conclusions générales et Perspectives	157
--	------------

7.1. Etudier le passé pour prévoir l'avenir : le choix de la démarche pédologique	158
7.2. Face à un certain nombre de points de blocage, une approche couplant une démarche pédologique classique avec des approches innovantes	158
7.3. Des résultats marquants	159
7.3.1. La reconstitution de matériaux parentaux hétérogènes.....	159
7.3.2. Le couplage de l'expérimentation au laboratoire et des bilans de masse pour quantifier l'action des différents processus pédogénétiques.....	160
7.3.3. Le zinc un traceur mitigé des processus de la pédogenèse.....	160
7.3.4. Les terres rares, des traceurs prometteurs de la pédogenèse.....	161
7.3.4.1. Une nouvelle approche de normalisation des teneurs en terres rares pour tracer les processus pédogénétiques.....	161
7.3.4.2. L'application au traçage des processus rédox.....	161
7.4. Perspectives	162

Bibliographie	163
----------------------	------------

Annexes	194
----------------	------------

Annexe 1. Description pédologique des solums échantillonnés	195
Pouilly-en-Auxois.....	195
Savigny-en-Terre-Plaine.....	196
Sol complet.....	198
Sol marron.....	198
Terre Noire.....	199

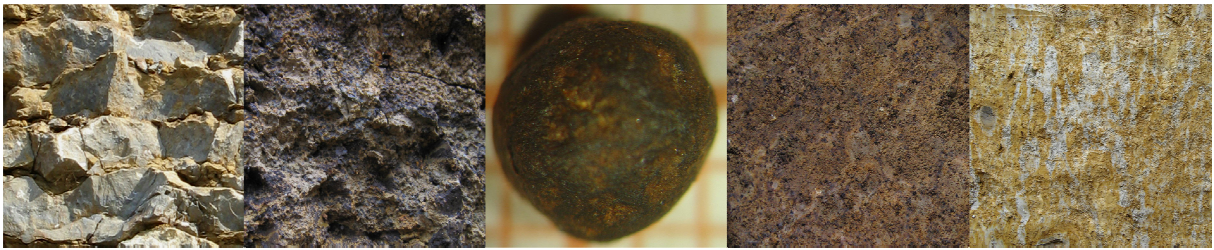
<i>Annexe 2. Pluviométrie mensuelle dans la Terre-Plaine entre mars 2006 et février 2007</i>	200
<i>Annexe 3. Analyse des terres rares dans les eaux des fractionnements granulométriques</i>	201
<i>Annexe 4. Article “Impact of redox cycles on manganese, iron, cobalt and lead in nodules”</i>	203
Acknowledgments	203
Abstract	203
Introduction	204
Material and Methods	205
Site and soil	205
Column preparation and characterisation	205
Experimental setting	206
Water sampling and analysis	207
Eh-pH diagrams	208
Statistic treatment	208
Results and discussion	209
Characteristics of the water inflow along the experiment: quality and quantity	209
Impact of the redox condition on the release of Fe, Mn and associated trace elements by nodules	213
Impact of the drying on the following reducing period	219
Consequences of the redox cycles in terms of soil evolution and environmental impact	220
Conclusion	221

Table des matières	223
---------------------------	------------

Liste des figures	231
--------------------------	------------

Liste des tableaux	242
---------------------------	------------

Liste des figures



Chapitre 1. Introduction

Chapitre 2. Matériels et Méthodes

Figure 1. _____ 13

Localisation des deux sites d'études en Bourgogne sur le pourtour liasique du Massif granitique du Morvan – Savigny-en-Terre-Plaine (Yonne) et Pouilly-en-Auxois (Côte d'Or) – ainsi que de Semur-en-Auxois, ville du stratotype de la formation d'âge sinémurien.

Figure 2. _____ 14

Coupe du calcaire d'âge sinémurien (Vic de Chassenay, Yonne), mettant en évidence l'alternance des bancs calcaires gis-bleutés et des interlits marneux ocres.

Figure 3. _____ 15

A droite, gryphées arquées (*Gryphæa arcuata*) affleurant à la surface d'un banc du calcaire d'âge sinémurien, dit calcaire à gryphées. A gauche, de bas en haut, coupe d'une gryphée arquée enchâssée dans le calcaire, photos de gryphées arquée et *cymbium* (présente dans la partie supérieure de la formation calcaire d'âge sinémurien) mettant en évidence leurs différences morphologiques.

Figure 4. _____ 15

Photographie d'un nodule phosphaté isolé de sa matrice.

Figure 5. _____ 17

Toposéquence de sols d'érosion sur les plateaux calcaires sinémuriens d'après Baize et Chrétien (1994).

Figure 6. _____ 17

Photographie d'un nodule ferro-manganique prélevé dans l'horizon Bc d'un solum complet (Pouilly-en-Auxois, Côte d'Or).

Figure 7. _____ 18

Succession d'horizons dans la toposéquence de Savigny-en-Terre-Plaine (Yonne) avec la localisation des trois fosses les plus représentatives des trois types de sols le long de la pente.

Figure 8. _____ 19

Profil des sols complets de Pouilly-en-Auxois (gauche) et de Savigny-en-Terre-Plaine (droite).

Figure 9. _____ 20

Niveaux de la nappe perchée le long de la toposéquence de Savigny-en-Terre-Plaine (89) en avril 2006, novembre 2006 et février 2007 avec les points de sondage et l'emplacement des fosses. La nappe étant absente en juillet 2006, elle n'est pas mentionnée dans la figure.

Figure 10. _____ **23**
Démarche d'analyse minéralogique et chimique des échantillons de sols sur les deux sites d'étude de Pouilly-en-Auxois et de Savigny-en-Terre-Plaine.

Chapitre 3. Potentialité du zinc comme traceur des différents processus pédogénétiques

Fig. 1 _____ **33**
Zinc particle-size distribution in the different soil horizons.

Fig. 2 _____ **33**
Particle-size distribution in the solum.

Fig. 3 _____ **34**
Scanning electron microscope pictures (in the backscattered electron mode) of the phosphate nodules of the BP-horizon and associated average concentrations of zinc and iron, analyzed by microprobe and proton induced X-ray emission (PIXE), of the fluorapatite matrix and the zones with very bright grey level. Average concentration of zinc in the phosphate nodules of the BP-horizon is 928.6 mg kg⁻¹.

Fig. 4 _____ **35**
Al, Fe and Zn stocks and fluxes in and from the different soil horizons, estimated by mass balance calculations following the method of Brimhall *et al.* (1991) modified by Egli and Fitze (2000) using Zr as invariant.

Fig. 5 _____ **36**
Quantities of Fe, Mn and Zn extracted by sequential extractions along the solum. Sequential extractions were carried out on the < 50 µm fractions for the BP- and Bc2-horizons and on the bulk samples for the other soil horizons.

Fig. 6 _____ **40**
X-ray diffraction spectra of the natural oriented slides of the 0–2 µm fractions for the different soil horizons. Intensities of (001) quartz peaks (⊙) are normalized to that of the A-horizon. Interreticular distances (in nm) are reported for main peaks.

Chapitre 4. Potentialité des terres rares comme traceurs des différents processus pédogénétiques

4.1. Etude bibliographique de l'impact de différents processus d'altération et de pédogenèse sur le fractionnement des terres rares

Fig. 1. _____ **53**
Weathering sequence of primary minerals (after Goldich, 1938).

4.2. Mise en point méthodologique d'utilisation des terres rares comme traceurs des processus pédogénétiques et validation de cette méthode sur un autre site

4.2.1. Mise en point méthodologique d'utilisation des terres rares comme traceurs des processus pédogénétiques

Fig. 1. _____ **66**
Pedogenesis of the studied solum based on the vertical transformation fronts of the successive pedogenetic processes. Processes identified by Baize and Chrétien (1994) and Laveuf *et al.* (2009; cf. Chapitre 3.1.).

Pédogenèse du solum étudié basée sur les fronts de transformation verticaux des processus pédogénétiques successifs. Les processus ont été identifiés lors d'études antérieures antérieures (Baize et Chrétien, 1994 ; Laveuf et al., 2009, cf. Chapitre 3.1.).

Fig. 2. _____ **68**
REE patterns of parent materials (limestone-phosphate nodules and Lotharingian- and Sinemurian-aged limestones) and of the soil horizons normalized to the Upper Continental Crust (U.C.C.).

Spectres de Terres rares des matériaux parentaux (nodules phosphatés du calcaire et calcaires d'âge Lotharingien et Sinémurien) et des horizons du solum normalisés à la Croûte Continentale Supérieure (U.C.C.).

Fig. 3. _____ **69**
REE patterns of the decarbonated geological parent materials (limestone-phosphate nodules and Lotharingian- and Sinemurian-aged limestones) normalized to their corresponding carbonated parent materials. The pie charts depict the stocks of LREE (La to Pr), MREE (Nd to Dy) and HREE (Ho to Lu) of the different geological materials and the striped zones represent the average percentage of REE released into solution during the experiment of decarbonation.

Spectres de Terres Rares dans les matériaux parentaux décarbonatés normalisés aux matériaux parentaux correspondants. Les graphiques à secteurs représentent les stocks de TR légères (La à Pr), moyennes (Nd à Dy) et lourdes (Ho à Lu) des différents matériaux parentaux et les zones hachurées indiquent le pourcentage moyen de TR libéré en solution au cours de l'expérience de décarbonatation.

Fig. 4. _____ **70**

REE patterns of the bulk soil fraction of each horizon normalized to the corresponding parent limestones. The A- to BP-horizons are issued from the weathering of the Lotharingian-aged limestone, while the Bc- and C-horizons are issued from the weathering of the Sinemurian-aged limestone.

Spectres de concentration des Terres Rares dans la fraction totale de chaque horizon normalisés au calcaire parental correspondant. Les horizons A à BP sont issus de l'altération du calcaire d'âge Lotharingien, tandis que les horizons Bc et C sont issus de l'altération du calcaire d'âge Sinémurien.

Fig. 5. _____ **73**

REE patterns of the Fe-Mn concretions of the Bc-horizon for different depths normalized to the bulk fraction of the C-horizon.

Spectres de Terres Rares des concrétions Fe-Mn de l'horizon Bc pour différentes profondeurs normalisés à la fraction totale de l'horizon C.

Fig. 6. _____ **74**

REE patterns of the $<2 \mu\text{m}$ particle-size fractions of each horizon normalized to the residue of extractions of the corresponding bulk soil fractions.

Spectres de Terres Rares des fractions granulométriques $<2 \mu\text{m}$ de chaque horizon normalisés au résidu d'extraction de la fraction totale correspondante.

Fig. 7. _____ **75**

REE patterns of the $<2 \mu\text{m}$ fraction of the A- and E-horizons normalized to the $<2 \mu\text{m}$ fraction of the Bgd-horizon.

Spectres de Terres Rares dans la fraction $<2 \mu\text{m}$ des horizons A et E normalisés à la fraction $<2 \mu\text{m}$ de l'horizon Bgd.

4.2.2. Validation de notre démarche méthodologique sur le site de la Terre-Plaine

Figure 1. _____ **78**

Teneurs en fraction inférieure à $2 \mu\text{m}$ en fonction de la profondeur.

Figure 2. _____ **79**

Stocks en terres rares des résidus expérimentaux de décarbonatation normalisés aux stocks en terres rares des calcaires parentaux pour les cinq strates calcaires d'âge sinémurien échantillonnées (C1 à C5).

Figure 3. _____ **80**

Stocks en terres rares des nodules Fe-Mn dans les horizons LE, Bc et C du sol complet normalisé aux stocks en terres rares de l'horizon C.

Figure 4. _____ **81**

Stocks en terres rares du résidu d'extraction de la fraction $<50 \mu\text{m}$ normalisés aux stocks en terres rares de la fraction $<50 \mu\text{m}$ du même horizon, pour les horizons LE, E, Bgd, Bc et C du sol complet.

Figure 5. _____ **82**
 Concentrations en terres rares de la fraction <50 µm normalisées aux concentrations en terres rares du résidu d'extraction de la fraction <50 µm du même horizon, pour les horizons LE, E, Bgd, Bc et C du sol complet.

Figure 6. _____ **83**
 Concentrations en terres rares du résidu d'extraction de la fraction inférieure à 2 µm de l'horizon LE normalisées à celles de l'horizon C.

Figure 7. _____ **84**
 Spectre des stocks en terres rares du résidu d'extraction de la fraction inférieure à 2 µm de l'horizon LE normalisés aux stocks en terres rares du résidu d'extraction de la fraction inférieure à 2 µm de l'horizon C.

Chapitre 5. Reconstruction des matériaux parentaux

Fig. 1. _____ **91**
(a) Location of the study site. **(b)** Studied toposequence and location of the remaining sinemurian formation samples (L1, L2, L3, L4, L5 and M). **(c)** Non-truncated profile of pit 1 and location of the soil horizons sampled (LE1, LE2, E, Bd1, Bd2, Bd3, Bd4, Bc1, Bc2, C1, C2 and C3).

Fig. 2. _____ **94**
 Formation of the different soil horizons from different former parent materials (FPMs) by pedogenetic processes. Each soil horizon results from the weathering and pedogenesis of several layers of limestones and marls, which may vary in composition and thickness.

Fig. 3. _____ **99**
 Evolution with depth of the concentration of the best candidates as immobile elements $C_{i,h}$ (plain line). This evolution can be described by a regression line starting from the upper C sample, C1, to LE1 (dotted line) and by variations along this line. The linear trend is interpreted as the result of pedogenesis and the variations around this trend are assigned to the original chemical heterogeneities of the former parent material. At each depth, $C_{i,h}^{reg}$ can be calculated thanks to the regression equations. The differences $\Delta C_{i,h}$ between $C_{i,h}$ and $C_{i,h}^{reg}$ quantify the variations in concentration of the immobile element due to the vertical heterogeneity in the composition of the parent material.

Fig. 4. _____ **101**
 Evolution with depth of the concentrations of Ti, Zr and Hf in the residues of former parent materials (calculated with equation (2) with the C1-horizon as reference). The concentrations of the residues of the remaining sinemurian formation samples – the marl (MR) and the different limestones (LR1 to LR5) – are reported on the figure as a vertical line and a vertical hachured rectangle respectively.

Fig. 5. _____ **104**
(a) Calculated volumetric strain ε (in %) along the studied solum using Zr and Hf as immobile elements. **(b)** Calculated volumetric strain normalized to the CaCO_3 contents of the corresponding former parent material reconstructed for each soil horizon.

Fig. 6. _____ **109**
 Initial stocks (\pm errors) in the former parent material of each soil horizon, actual stocks (\pm errors) in the soil horizons and mass fluxes (\pm errors and percentage of initial stock mobilized) during pedogenesis within each soil horizon for **(a)** Si, **(b)** Al, **(c)** Fe, **(d)** Mn, **(e)** REEs, **(f)** LREEs, **(g)** MREEs and **(h)** HREEs.

Fig. 7. _____ **111**
 Linear regression of the mass fluxes of Fe and Mn, within the Bd-horizon, with respect to each other **(a)**, to REEs **(b)** and **(c)**, to LREEs **(d)** and **(e)**, to MREEs **(f)** and **(g)**, and to HREEs **(h)** and **(i)**.

Chapitre 6. Impact des processus sur la redistribution des terres rares

6.1. Redistribution des terres rares au cours du processus de décarbonatation

Figure 1. _____ **118**
 Spectres des concentrations en terres rares des calcaires L1 à L5 de la Terre-Plaine et des calcaires d'âge lotharingien et sinémurien de l'Auxois normalisées à la Croûte Continentale Supérieure (UCC ; Taylor et McLennan, 1985).

Figure 2. _____ **119**
 Spectres du pourcentage du stock initial de terres rares mises en solution au cours de la décarbonatation expérimentale des différents échantillons de calcaires de la Terre-Plaine (L1 à L5) et des calcaires d'âge sinémurien et lotharingien de l'Auxois

Figure 3. _____ **122**
 Diagrammes DRX des échantillons calcaires de la Terre-Plaine (en bas de chaque figure) et de leurs résidus de décarbonatation (en haut de chaque figure). Les pics principaux des différents minéraux identifiés sont annotés selon la nomenclature suivante : Q = quartz, F = (fluor)apatite, G = goethite, Fe = ferrihydrite, B = birnessite, I = illite, K = kaolinite, In = argiles interstratifiées, C = calcite et Co = corindon (ayant servi au dopage des échantillons).

Figure 4. _____ **125**
 Espace F1-F2 des variables et des individus de l'Analyse en Composante Principale réalisée sur les concentrations des résidus de décarbonatation des calcaires de la Terre-Plaine et de l'Auxois avec les éléments majeurs (plus Ti) en variables principales et les terres rares en variables supplémentaires.

Figure 5. _____ **126**

Espace F1-F2 des variables de l'Analyse en Composante Principale réalisée sur les concentrations des résidus de décarbonatation RL1 à RL5 de la Terre-Plaine avec les éléments majeurs (plus Ti) en variables principales et les terres rares en variables supplémentaires.

Figure 6. _____ **128**

Cartographie par micro-fluorescence X de Ce, Si, Ca, P, Mn et Fe d'une zone sur une lame mince de l'échantillon calcaire L1 de la Terre-Plaine représentative des différents échantillons de calcaires analysés. La zone d'enrichissement en Ce (entourée en jaune) ne correspond à aucun enrichissement en un des autres éléments analysés.

Figure 7. _____ **131**

Diagrammes DRX de l'horizon C3 (en rouge) et du résidu de décarbonatation de l'échantillon calcaire L1 de la Terre-Plaine (en noir) au contact de l'horizon C3. Les pics principaux des différents minéraux identifiés sont annotés selon la nomenclature suivante : Q = quartz, F = (fluor)apatite, G = goethite, Fe = ferrihydrite, B = birnessite, I = illite, K = kaolinite, In = argiles interstratifiées, C = calcite et Co = corindon (ayant servi au dopage des échantillons).

6.2. Potentiel des terres rares comme traceurs des processus redox

Figure 1. _____ **136**

Localization of the studied toposequence of Savigny-en-Terre-Plaine (Yonne, France) within the geographic expansion of the Sinemurian-aged strata around the Morvan Mountain.

Figure 2. _____ **136**

Toposequence of Savigny-en-Terre-Plaine (Yonne, France) developed from the sinemurian-aged formation. Sampled pits of the non-truncated solum (NTS) and of the chestnut colored solum (CCS) are indicated.

Figure 3. _____ **139**

Patterns of stocks of REEs in the Fe-Mn nodules normalized to the residue from carbonate dissolution of their respective residues of former parent materials (RFPMs), as calculated by Laveuf *et al.* (submitted).

Figure 4. _____ **140**

Patterns of stocks of REEs in the residues from extraction of the <50 µm fractions normalized to the raw <50 µm fractions for NTS **(a)** and CCS **(b)**.

Figure 5. _____ **142**

Patterns of REE concentrations normalized to Upper Continental Crust (UCC; Taylor and McLennan, 1985) in the residues of the former parent materials (RFPMs) for each of the sampled NTS and CCS horizons.

Figure 6. _____ **142**

Concentrations of REEs in the non-magnetic >50 μm fractions as a function of their (fluor)apatite contents and Pearson's correlation coefficients of individual and groups of REEs with (fluor)apatite. Significant correlation coefficients at the threshold of $\alpha=0.05$ are reported in bold.

Figure 7. _____ **144**

REE concentrations in reconstructed (fluor)apatite, Mn-oxides, ferrihydrite, goethite, and silicates of the Fe-Mn nodules and of the <2 μm fractions normalized to the REE concentrations in the residues of former parent materials (RFPMs) of their respective soil horizons, as calculated by Laveuf *et al.* (submitted).

Figure 8. _____ **147**

Mineral stocks (g kg^{-1}) in the Fe-Mn nodules (**a**), in the <50 μm fractions (**b**) and in the <2 μm fractions (**c**) within the different soil horizons, derived from sequential extraction results (for Mn-oxides, ferrihydrite, goethite, (fluor)apatite and silicates).

Figure 9. _____ **148**

Mass fluxes (in g kg^{-1}) of Mn-oxides, ferrihydrite and goethite between the C1- and the Bc-horizon of NTS considering variations in the mineral stocks in the Fe-Mn nodules and concomitant dissolution of the Fe-Mn nodules and in the <50 μm fractions.

Figure 10. _____ **149**

Repartition of the stock of REEs between Mn-oxides, ferrihydrite, goethite, (fluor)apatite and silicates within the Fe-Mn nodules of the Bc-horizons of NTS and of CCS.

Figure 11. _____ **152**

Repartition of the stock of REEs between Mn-oxides, ferrihydrite, goethite, (fluor)apatite and silicates within the <2 μm fraction of the LE- and C1-horizons of the NTS.

Chapitre 7. Conclusions générales et Perspectives

Bibliographie

Annexes

Annexe 1. Description pédologique des solums échantillonnés

Figure 1. _____ **195**

Photographie du profil du sol complet sous forêt de Pouilly-en-Auxois (21) avec ses différents horizons et les profondeurs associées (source Cornu 2004).

Figure 2. _____ **197**

Photographies aériennes du terrain d'étude de Savigny-en-Terre-Plaine (89) : en 1968, le terrain est séparé en deux parcelles par une haie, dont une est en prairie et l'autre cultivée ; en 1983, le terrain est constitué d'une seule parcelle sous plusieurs cultures (source Institut National Géographique) ; actuellement l'ensemble de la parcelle est sous une même culture (blé).

Figure 3. _____ **197**

Photographies des trois profils des trois fosses du sol complet (F_{SC}), du sol marron (F_{SM}) et de la Terre Noire (F_{TN}) avec la délimitation de leurs horizons (source Laveuf 2006).

Annexe 2. Pluviométrie mensuelle dans la Terre-Plaine entre mars 2006 et février 2007

Annexe 3. Analyse des terres rares dans les eaux des fractionnements granulométriques

Figure 1. _____ **202**

Spectres des concentrations en Terres Rares de deux solutions de séparations granulométriques normalisées aux concentrations en Terres Rares des deux échantillons bruts de sol correspondants.

Annexe 4. Article "Impact of redox cycles on Mn, Fe, Co and Pb in nodules"

Figure 1: _____ **207**

Schematic diagram of the experimental design. Qz refers to the quartz columns and C to the nodule ones.

Figure 2: _____ **210**

Characteristics of the solution percolating through the topsoil monolith as a function of time: A- pH; B- Eh; C- Fe; D- Mn; E- Co; F- Pb. Dark triangles represent the outflow, while open circles are for the inflow.

Figure 3: _____ **211**

Eh-pH stability diagrams for Fe, considering 2 forms of goethite, 2 green rusts and ferrihydrite as Fe oxides, a) for a total Fe concentration in water at 10^{-4} mol L⁻¹ and b) for a total Fe concentration in water at 10^{-5} mol L⁻¹.

Figure 4: _____ **212**

Eh-pH stability diagram for Mn, considering total Mn concentration in water = 10^{-4} mol L⁻¹ and birnessite and lithiophorite as Mn oxides. For lithiophorite, a concentration of Al in solution of 10^{-6} mol L⁻¹ was considered. For birnessite a range of stability constant was encountered in the literature (Table 3). The extreme values were used to calculate the stability lines for birnessite and represented as a shaded domain on the figure.

Figure 5: _____ **214**
pH, Eh, Fe, Mn, Co and Pb concentrations as a function of the pore volume of the inflow and outflow for the quartz column undergoing permanent saturation. Dark triangles represent the outflow, while open circles are for the inflow.

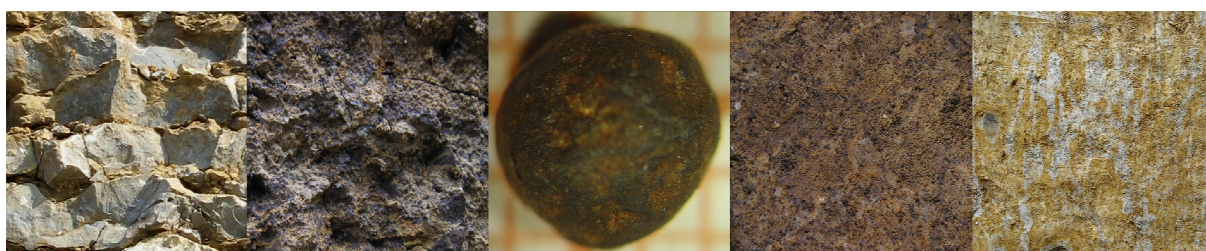
Figure 6: _____ **215**
pH, Eh, Fe, Mn, Co and Pb concentrations as a function of the pore volume of the inflow and outflow for nodule columns 1 & 2 undergoing permanent saturation. Dark triangles represent the outflow, while open circles are for the inflow. Black symbols are for the first column, while grey ones state for the second column.

Figure 7: _____ **216**
pH, Eh, Fe, Mn, Co and Pb concentrations as a function of the pore volume of the inflow and outflow for the quartz column undergoing 14-day cycles. Dark triangles represent the outflow, while open circles are for the inflow.

Figure 8: _____ **217**
pH, Eh, Fe, Mn, Co and Pb concentrations as a function of the pore volume of the inflow and outflow for the nodule column undergoing 14-day cycles. Dark triangles represent the outflow, while open circles are for the inflow.

Figure 9: _____ **219**
Iron fixation ratios versus mean Eh values for the different columns.

Liste des tableaux



Chapitre 1. Introduction

Chapitre 2. Matériels et Méthodes

Tableau 1. _____ **22**
Echantillonnage des sols et des matériaux parentaux des différents solums sur les sites de l'Auxois et de la Terre-Plaine.

Tableau 2. _____ **24**
Schéma d'extraction séquentielle des différentes fractions de sol des sites de l'Auxois et de la Terre-Plaine.

Chapitre 3. Potentialité du zinc comme traceur des différents processus pédogénétiques

TABLE I _____ **29**
Characteristics of the soil horizons (from top to bottom) in the studied solum.

TABLE II _____ **29**
Main pedological characteristics, total Fe, Mn, P and Zn concentrations and volumetric strain (ϵ) of the different soil horizons.

TABLE III _____ **32**
Chemical composition of the bulk samples of the Lotharingian and Sinemurian aged-limestones, their residues from carbonate dissolution and their estimated calcite contents derived from the previous data.

TABLE IV _____ **38**
Extraction ratios of Fe in step 6 versus step 5 and of Zn/Mn for step 3 and Zn/Fe for steps 5 and 6.

Chapitre 4. Potentialité des terres rares comme traceurs des différents processus pédogénétiques

4.1. Etude bibliographique de l'impact de différents processus d'altération et de pédogenèse sur le fractionnement des terres rares

Table 1 _____ **47**
Chemical and physical properties of REEs (after Henderson, 1984).

Table 2 _____ **47**

The coordination numbers and abundances of LREEs and HREEs in the structural sites of REE-bearing minerals; (○) and (●) are LREEs and HREEs, respectively. The size of circles shows rough abundance of REEs for each mineral class. After Kanazawa and Kamitani (2006).

Table 3 _____ **48**

Minimum, maximum and average concentrations (mg kg⁻¹) of REEs in different matrices.

Table 4 _____ **50**

REE concentrations in some classical references used for normalization.

Table 5 _____ **54**

Compartments of REEs in solution.

Table 6 _____ **56**

Comparison of the REE contents and some properties of different types of clay minerals.

4.2. Mise en point méthodologique d'utilisation des terres rares comme traceurs des processus pédogénétiques et validation de cette méthode sur un autre site

4.2.1. Mise en point méthodologique d'utilisation des terres rares comme traceurs des processus pédogénétiques

Table 1. _____ **66**

Pedogenetic processes, with their location in the solum horizons, and the derived pedological features. Normalization proposed to differentiate their respective impact on REE mobilization.

Processus pédogénétiques, avec leur localisation dans le solum, et les traits pédologiques dérivés. Normalisation proposée pour différencier leur impact respectif sur la mobilisation des Terres Rares.

Table 2. _____ **71**

Concentrations of major elements (in g/kg) in the bulk and the residues of the Lotharingian- and Sinemurian-aged limestones, with corresponding initial stock losses (in percentage) during experimental decarbonation.

Concentrations en éléments majeurs (en g/kg) des échantillons bruts et des résidus des calcaires d'âge Lotharingien et Sinémurien, avec les pertes correspondantes du stock initial (en pourcentage) durant la décarbonatation expérimentale.

Table 3. _____ **73**

Iron, manganese and cerium concentrations of the Fe-Mn concretions, of the <50 μm fraction of the Bc-horizon (115-125 cm) and of the bulk fraction of the C-horizon from which the Bc-horizon was developed.

Concentrations en fer, manganèse et cérium des concrétions Fe-Mn, de la fraction <50 µm de l'horizon Bc (115-125 cm) et de la fraction totale de l'horizon C au dépend de laquelle l'horizon Bc s'est développé.

4.2.2. Validation de notre démarche méthodologique sur le site de la Terre-Plaine

Tableau 1. _____ **77**
 Comparaison des normalisations des terres rares, *i.e.* des traits pédologiques et des matériaux de référence, pour chacun des processus sur les deux sites étudiés.

Chapitre 5. Reconstruction des matériaux parentaux

Table 1. _____ **92**
 Concentrations of major elements and REEs in the different soil horizons.

Table 2. _____ **95**
 Bulk densities of the remaining sinemurian formation samples and of soil horizons with their associated standard deviations.

Table 3. _____ **96**
 Concentrations of CaCO₃ and of some elements classically considered immobile in the different remaining sinemurian formation samples (RSFs = L1, L2, L3, L4, L5 and M), in their residues from carbonate dissolution (LR1, LR2, LR3, LR4, LR5 and MR respectively) and associated percentages of the stocks of elements released from the RSFs into solution during the experiment.

Table 4. _____ **97**
 Matrix of correlations of the concentrations of Ti, Zr, Nb, Hf and quartz in the different soil horizons. All values are significant at the threshold $\alpha = 0.050$ for the bilateral test (coefficients of Pearson).

Table 5. _____ **98**
 Concentrations of major elements and of REEs in the different remaining sinemurian formation samples (L1, L2, L3, L4, L5, M) and in their residues from carbonate dissolution (LR1, LR2, LR3, LR4, LR5).

Table 6. _____ **100**
 Calcium carbonate concentrations and abundance of the <2 µm fractions in the different soil horizons.

Table 7. _____ **100**
 Concentrations $C_{i,h}$ of the immobile elements *i* (Ti, Zr or Hf) in each soil horizon *h*.

Table 8. _____ **103**

Proportions X_{RSPM} and X_{SPM} of the different residues from carbonate dissolution of the remaining sinemurian formation samples (RRSFs) and of the different remaining sinemurian formation samples (RSFs=limestone L and marl M samples), respectively, in the weathered and non-weathered former parent materials (FPMs) of each soil horizon, respectively. The errors in the estimation of the concentration $C_{i,RFPM}$ of the immobile element i (either Zr or Hf) are calculated comparing the values estimated with the proportions X_{RSPM} to those derived from equation (3).

Table 9. _____ **105**

Thickness (in cm) of the former parent material (FPM) of each soil horizon and of the remaining sinemurian formation samples (L1, L3 and M) based on volumetric strains ε calculated with Zr.

Table 10. _____ **107**

Mass-transport function (in %) calculated for Hf, major elements and REEs in each soil horizon with Zr as immobile element.

Chapitre 6. Impact des processus sur la redistribution des terres rares

6.1. Redistribution des terres rares au cours du processus de décarbonatation

Tableau 1. _____ **121**

Concentrations en CaCO_3 (équivalentes à la perte de masse), en éléments majeurs et en terres rares des différents calcaires de la Terre-Plaine, de leurs résidus de décarbonatation respectifs, et pourcentages correspondant mis en solution.

Tableau 2. _____ **130**

Concentrations dans l'horizon C3 (en g kg^{-1} pour les éléments majeurs et en mg kg^{-1} pour les terres rares TR) et fonctions de transport de masse τ (en % du stock initial dans le matériau parental reconstitué) pour ce même horizon (Laveuf *et al.*, soumis). Les quantités repiégées correspondant au pourcentage du stock initial mis en solution et non évacué de l'horizon C3 sont calculées par différence entre les fonctions de transport de masse et les quantités mises en solution (Tableau 1).

6.2. Potentiel des terres rares comme traceurs des processus redox

Table 1. _____ **137**

Sequential extraction scheme for the $<50 \mu\text{m}$ fractions, $<2 \mu\text{m}$ fractions and Fe-Mn nodules including the extractants nature, the sample/extractant ratio (m/V ratio), the number of extractions performed per extractant and their duration.

Table 2. _____ **141**
Main soil characteristics of the NTS and of the CCS: soil horizons names and sampling depths, particle-size distribution, contents in CaCO₃, organic matter (OM), Fe and Mn of the different fractions.

Table 3. _____ **150**
Pearson's correlation matrix of the stocks of REEs in the Fe-Mn nodules normalized to their respective RFPMs (Figure 3) with the quantities of minerals in Fe-Mn nodules (Figure 8a). Significant correlation coefficients at the threshold of $\alpha=0.05$ are reported in bold.

Table 4. _____ **154**
Pearson's correlation matrix of the stocks of REEs in the residues from extraction of the <50 μm fractions normalized to the raw <50 μm fractions (Figures 4a and 4b) with the quantities of minerals in the <50 μm fractions (Figure 8b). Significant correlation coefficients at the threshold of $\alpha=0.05$ are reported in bold.

Chapitre 7. Conclusions générales et Perspectives

Bibliographie

Annexes

Annexe 1. Description pédologique des solums échantillonnés

Annexe 2. Pluviométrie mensuelle dans la Terre-Plaine entre mars 2006 et février 2007

Tableau 1. _____ **200**
Relevés pluviométriques mensuels à Saint-André-en-Terre-Plaine (89).

Annexe 3. Analyse des terres rares dans les eaux des fractionnements granulométriques

Tableau 1. _____ **201**
Concentrations en Terres Rares (TR) dans deux solutions de séparation granulométrique et estimation du pourcentage du stock de l'échantillon mis en solution.

Annexe 4. Article "Impact of redox cycles on Mn, Fe, Co and Pb in nodules"

Table 1: _____ **205**
Characteristics of the solids used in the experiment

Table 2:	206
Main characteristics of the different columns	
Table 3:	208
Equilibrium reactions and associated solubility constants at 25°C and 1 bar, used to construct the Eh-pH diagrams for the different minerals found in the nodules	
Table 4:	209
Average values for the pH and Eh values and Fe, Mn, Co and Pb concentrations according to the water type considered and Fisher's pairwise mean comparison results (ANOVA)	
Table 5:	209
Average fraction fixed/released from the different columns for Fe, Mn and Co and Fisher's pairwise mean comparison results (ANOVA)	
Table 6:	213
Amount of leachate collected from the different columns	
Table 7:	220
Total Fe, Mn, Co and Pb gained or lost from the different columns at the end of the experiment, calculated from mass balance calculation on the inflow and outflow waters.	

Cédric Laveuf

Les terres rares et le zinc comme traceurs des processus pédogénétiques : application à une séquence de sols issue de calcaires minéralisés

Résumé

Ce travail évalue le potentiel du zinc et plus particulièrement des terres rares à tracer les différents processus le long d'une catena issue d'une formation carbonatée constituée d'une succession de bancs marneux et calcaires, et ayant subi des processus de décarbonatation, des conditions redox en lien avec l'hydromorphie et de l'éluviation.

L'approche choisie repose (i) sur la spéciation des terres rares, à l'aide de méthodes physiques et chimiques, dans les traits pédologiques formés par les différents processus et des matériaux aux dépens desquels ils se sont développés, (ii) sur la quantification par bilan de masse des flux de terres rares et éléments majeurs associés.

Ce travail a nécessité deux mises aux points méthodologiques : une méthode de normalisation des terres rares, basée sur l'enfoncement des fronts de transformation afin de quantifier l'impact des processus successifs sur le fractionnement des terres rares ; une méthodologie de reconstruction des matériaux parentaux pour chacun des horizons, l'approche par bilan de masse nécessitant une connaissance des stocks initiaux.

L'impact de deux processus sur les fractionnements de terres rares est ensuite plus particulièrement abordé : la décarbonatation des matériaux parentaux et les processus d'oxydo-réduction. On montre ainsi l'importance de comparer les quantités mises en solution aux flux calculés par les bilans de masse pour prédire le devenir des éléments libérés et l'intérêt des terres rares pour quantifier les cycles de dissolution/précipitation des oxydes de fer et de manganèse.

Mots-clés : pédogenèse, oxydo-réduction, éluviation, décarbonatation, quantification, lanthanides, calcaires

Rare earth elements and zinc as tracers of pedogenetic processes: the case of soils developed from mineralized limestones

Abstract

This project aims at considering the potential of zinc and rare earth element (REEs) at quantifying pedogenetic processes along a soil sequence developed from a limestone formation consisting in a succession of marl and limestone strata which underwent carbonate dissolution, redox cycles related to soil hydromorphy and eluviation.

The chosen approach relies on (i) the speciation of rare earth elements - by a method combining sequential extractions and physical separations - in the pedological features resulting from the different processes and in the materials from which they developed; (ii) the quantification of the REE and major element fluxes by mass balance calculation.

To do so, two methodologies were developed: a methodology of normalization of REEs based on the theory of transformation fronts to quantify the impact of the processes on REE fractionations; an innovative approach of the reconstruction of the former parent material for each soil horizon as mass balance calculation requires the quantification of initial stocks in elements.

Two processes were then further studied: carbonate dissolution and redox processes. We thus point out the necessity to compare max fluxes as computed by mass balance to quantities released by carbonate dissolution in order to forecast the fate of elements released into the soil solution. We also evidenced the potential of REEs to quantify the dissolution/precipitation cycles of iron and manganese oxides.

Keywords: pedogenesis, oxidation-reduction, eluviation, carbonate dissolution, quantification, lanthanides, limestones

UNITE DE RECHERCHE DE SCIENCE DU SOL

INRA, Centre de Recherche d'Orléans

